Mechanisms of Cytotoxicity and Intracellular Trafficking for Gene Delivery Polymers

Giovanna Grandinetti

Dissertation submitted to the faculty of the Virginia Polytechnic Institute and State University in partial fulfillment of the requirements for the degree of

Doctor of Philosophy
In
Chemistry

Theresa M. Reineke, Chair
David R. Bevan
Kevin J. Edgar
Marion F. Ehrich
Hara P. Misra

June 30, 2011
Blacksburg, VA

Keywords: (Non-viral DNA delivery, polymer, toxicity, intracellular trafficking, transfection, poly(ethylenimine), poly(glycoamidoamine)s, structure-bioactivity relationship)

Mechanisms of Cytotoxicity and Intracellular Trafficking for Gene Delivery Polymers

Giovanna Grandinetti

ABSTRACT

Herein, different polymer libraries were examined to determine the effect polymer structure has on intracellular events. The effect of different polyamine lengths in copolymers on cellular uptake, the effect of modifying end groups of trehalose-containing polymers on transfection efficiency, and the effect of different linker lengths between galactose and a hepatocyte-targeted polymer on transfection efficiency were studied. Furthermore, it was demonstrated that polymers with terbium chelated in their repeat units could potentially be used for Förster resonance energy transfer (FRET) studies to monitor pDNA release from the polymer. Much of the work in this dissertation focuses on elucidating the intracellular mechanisms of linear poly(ethylenimine) (PEI) and how it compares to poly(L-tartaramidopentaethylenetetramine) (T4) and poly(galactaramidopentaethylenetetramine) (G4), two poly(glycoamidoamine)s synthesized by our group. The long-term goal of this project is to develop structure-function relationships between polymers and pDNA delivery efficacy that will result in the rational design of safe, efficient vehicles for therapeutic nucleic acid delivery.

Many polymers used as DNA delivery vehicles display high cytotoxicity. Often, the polymers with the highest transfection efficiency are the most toxic, as demonstrated herein by PEI and T4 with varying polymer lengths. Therefore, it was of interest to study how polymer structure influences mechanisms of cytotoxicity. To this end, studies on several mechanisms of cytotoxicity, including nuclear envelope permeabilization, were conducted. Longer polymers induced more cytotoxic responses than shorter ones, and it appears that hydroxyl groups in the repeat unit of polymers play a role in polyplex formation. This research has also led us to a potential link between transfection efficiency and cytotoxicity; the polymers with the highest transfection efficiency were also the most toxic, and were also able to induce the most nuclear envelope permeability. It is possible that these polymers' ability to permeabilize the nuclear envelope is what causes their high transfection efficiency and high toxicity. In addition, flow cytometry and confocal microscopy studies revealed that polymer structure plays a role in nuclear trafficking; poly(glycoamidoamine)s G4 and T4 more dependent on intracellular machinery than PEI. This research demonstrates the impact that changes in polymer structure have on intracellular mechanisms.

ACKNOWLEDGEMENTS

This dissertation would not have been possible without the help and support of many people. First, I must recognize my family, who have supported me every step of the way. My parents, Salvatore and Carolina, have taught me the importance of hard work. My siblings, Joseph, Louis, Angela and Matthew, have also supported me throughout school. I would also like to thank my husband, Daniel, for years of loving encouragement. Daniel has always been there with a "believe in yourself" and endless support whenever I have needed it, from deciding whether to pursue and M.D. or a Ph.D., to moving to Cincinnati, to moving again to Blacksburg, and for moving yet again to wherever my career brings me. I cannot thank him enough for helping me through graduate school and for listening to my practice talks, helping me with homework and T.A. duties, motivating me to keep going even when my experiments have failed, and, of course, hours and hours of computer support. There simply are not enough words to describe how much Daniel has helped and supported me these past few years.

I would also like to thank my advisor, Theresa M. Reineke, for her support and for allowing me to be independent in the laboratory. I would also like to thank my committee members, both former and current, for their guidance. To Dr. Halsall, even though we disagree on the pronunciation of the word "apoptosis", your biochemistry class has significantly influenced my understanding of how cells work, and your attention to detail in experimental design has helped me tremendously. To Dr. Tsang, you have always had insightful observations and I enjoyed our conversations about future experimental ideas. To Dr. Stalcup, it is always a pleasure discussing both science and life with you, and your career advice is greatly appreciated. To Dr. Ehrich, your

comments on my independent proposal and my seminars helped a lot, and I am glad that you agreed to be on my committee at Virginia Tech. Thank you also for making sure my data were statistically relevant. To Dr. Edgar, thank you for always offering to help whenever possible, it is very nice of you and I am happy to see such commitment from a professor. To Dr. Bevan, thank you for introducing me to VMD, and your lectures on oxidation in biochemistry during the MILES course were interesting and helpful for my research. To Dr. Misra, you always have kind words of encouragement, and I am glad to have had your input on improving not only my talks, but also my thought process in experimental design.

None of this would be possible without the help and support of my lab mates. From the lab cleanups to the lab happy hours, I have always appreciated the camaraderie the Reineke group has had. I would like to especially acknowledge Katye Fichter and Patrick McLendon, who put up with training me in the cell culture lab, and to Yemin Liu, who attempted to train me in synthesis and who has patiently answered my many questions. I would also like to acknowledge Vijay Taori, Antons Sizovs and Sneha Kelkar for all of the useful scientific discussions. Also, thanks goes to Nilesh Ingle, who stepped up and helped take care of the cell culture lab when I was finishing off my last experiments. Lastly, to everyone that has worked in the cell culture lab, thanks for putting up with my emails about lab cleanliness, and I wish all of my lab mates the best of luck and sincere thanks for always being there for everything.

Table of Contents

CHAPTER 1 : INTRODUCTION 1

1.1 Nucleic Acid Delivery 1
1.2 Polyamine-inspired Polymers as DNA Delivery Vehicles 2
1.3 Comparing the Poly(glycoamidoamine)s and PEI 4
1.4 Polyamines and Cytotoxicity 8
1.5 Goals of this Project and Dissertation Outline 9
1.6 Hypotheses by Chapter 12
1.7 References 14

CHAPTER 2 : CYTOTOXICITY OF POLY(ETHYLENIMINE) 20

2.1 Abstract 20
2.2 Introduction 21
2.3 Materials and Methods 27
2.4 Results and Discussion 32
2.5 Conclusions and Future Goals 50
2.6 References 53

CHAPTER 3 : EFFECT OF POLYMER LENGTH AND COMPOSITION ON CYTOTOXICITY 60

3.1 Abstract 60
3.2 Introduction 61
3.3 Materials and Methods 63
3.4 Results and Discussion 71
3.5 Conclusions and Future Directions 106
3.6 References 111

CHAPTER 4 : NUCLEAR IMPORT OF PDNA DURING POLYMER TRANSFECTION 116

4.1 Abstract 116
4.2 Introduction 117
4.3 Materials and Methods 119
4.4 Results and Discussion 125
4.5 Conclusions and Future Goals 148
4.6 References 153

CHAPTER 5 : MODIFICATION OF POLYMERS FOR GENE DELIVERY 157

5.1 Abstract 157
5.2 Introduction 158
5.3 Materials and Methods 166
5.4 Results and Discussion 171
5.5 Conclusions and Future Goals 195
5.6 References 198

CHAPTER 6 : CONCLUSION 201

List of Figures

FIGURE 1.1.) THE STRUCTURE OF THE POLY(GLYCOAMIDOAMINE)S (PGAAS). THE PGAAS DIFFER IN THE STEREOCHEMISTRY OF THE HYDROXYL GROUPS IN THEIR REPEAT UNITS AND, IN THE CASE OF T4, THE NUMBER OF HYDROXYL GROUPS. 4
FIGURE 2.1) PEI INDUCES APOPTOTIC EVENTS AT EARLY TIME POINTS AFTER TRANSFECTION. HELA CELLS WERE ALLOWED TO TRANSFECT FOR THE INDICATED TIME POINTS BEFORE BEING ANALYZED BY FLOW CYTOMETRY. (A) A LOSS IN MITOCHONDRIAL MEMBRANE POTENTIAL (MMP) OBSERVED BY A DECREASE IN THE FLUORESCENCE OF DIIC1(5) AND (B) AN INCREASE IN PHOSPHATIDYLSERINE EXTERNALIZATION OBSERVED BY AN INCREASE IN ANNEXIN V-ALEXA FLUOR 488 (AF488) FLUORESCENCE. DATA WERE NORMALIZED TO CELLS ONLY CONTROL. AF488 FLUORESCENCE IS PRESENTED AS A % INCREASE FROM CELLS ONLY. BARS WITH DIFFERENT LETTERS REPRESENT MEANS THAT ARE STATISTICALLY SIGNIFICANT FROM EACH OTHER ($P < 0.05$, $N = 2$) ACCORDING TO THE TUKEY-KRAMER HSD METHOD. BARS WITH MATCHING LETTERS REPRESENT MEANS THAT ARE NOT STATISTICALLY SIGNIFICANT FROM EACH OTHER. 34
FIGURE 2.2) CELLS WERE TRANSFECTED FOR THE INDICATED TIME POINTS WITH PEI AT AN N/P OF 5 AND THEN ANALYZED USING FLOW CYTOMETRY TO STUDY INCREASES IN (A) CASPASE-9 ACTIVITY AND (B) PLASMA MEMBRANE PERMEABILITY AS MEASURED BY INCREASES IN FITC AND PROPIDIUM IODIDE (PI) FLUORESCENCE, RESPECTIVELY. RESULTS WERE NORMALIZED TO A CELLS ONLY CONTROL AND DATA ARE PRESENTED AS % INCREASED FLUORESCENCE FROM CELLS ONLY. BARS WITH MATCHING LETTERS ARE NOT STATISTICALLY SIGNIFICANT FROM EACH OTHER, AND BARS WITH DIFFERENT LETTERS REPRESENT MEANS THAT ARE STATISTICALLY SIGNIFICANT FROM EACH OTHER ($P < 0.05$, $N = 2$) AS DETERMINED USING THE TUKEY-KRAMER HSD METHOD. 37
FIGURE 2.3) CONFOCAL MICROSCOPY IMAGES OF HELA CELLS TRANSFECTED WITH PEI POLYPLEXES (SHOWN AS GREEN FROM LABELED PDNA) SHOWING OVERLAP WITH MITOCHONDRIA (RED). THE CELLS WERE FIXED ONE HOUR AFTER TRANSFECTION. (A) IMAGE OF WHOLE CELLS TRANSFECTED WITH PEI POLYPLEXES. (B) HIGHLIGHTING COLOCALIZED PIXELS; MITOCHONDRIA ARE SHOWN AS RED, POLYPLEXES ARE SHOWN AS GREEN, AND COLOCALIZED PIXELS ARE SHOWN AS WHITE. THE MANDERS COEFFICIENT (M1) FOR THE AMOUNT OF GREEN OVERLAPPING RED WAS FOUND TO BE 0.349. (C) CLOSE UP VIEW FROM INSIDE THE BOX IN (B) TO FURTHER HIGHLIGHT COLOCALIZATION BETWEEN POLYPLEXES AND MITOCHONDRIA. SCALE BAR = 20 MM. 39
FIGURE 2.4) (A) CONFOCAL MICROSCOPY IMAGE OF HELA CELLS TRANSFECTED WITH PEI POLYPLEXES TWO HOURS AFTER TRANSFECTION. MITOCHONDRIA ARE SHOWN AS RED, POLYPLEXES ARE SHOWN AS GREEN. (B) HIGHLIGHTING COLOCALIZED POINTS, WHICH ARE SHOWN AS WHITE. THE MANDERS COEFFICIENT (M1) FOR THE AMOUNT OF GREEN OVERLAPPING RED IS 0.469 AT THIS TIME POINT. (C) ZOOMED-IN IMAGE OF THE AREA INDICATED BY THE BOX IN (B) TO HIGHLIGHT COLOCALIZED PIXELS. SCALE BAR = 20 MM. 40
FIGURE 2.5) FLOW CYTOMETRY RESULTS FOR PEI-TRANSFECTED HELA CELLS. CELLS WERE ANALYZED AT THE INDICATED TIME POINTS TO DETERMINE THE EFFECT OF CYCLOSPORINE *A* ON (A) MITOCHONDRIAL MEMBRANE POTENTIAL AND (B) PROPIDIUM IODIDE (PI) UPTAKE. * DENOTES STATISTICAL SIGNIFICANCE ($P < 0.05$) AS DETERMINED BY THE TUKEY-KRAMER HSD METHOD, $N = 2$. 42
FIGURE 2.6) EFFECT OF ADDING 5 MM CYCLOSPORINE A (CSA) WITH POLYPLEXES AND ADDING CSA AGAIN 1 HOUR AFTER TRANSFECTION. (A) MITOCHONDRIAL MEMBRANE POTENTIAL WAS MEASURED USING THE FLUORESCENT DYE DIIC(1)5 TWO HOURS AFTER TRANSFECTION. (B) PROPIDIUM IODIDE (PI) FLUORESCENCE WAS USED TO MONITOR PLASMA MEMBRANE INTEGRITY 2 HOURS AFTER TRANSFECTION IN PEI POLYPLEX-TREATED CELLS WITH AND WITHOUT CSA. DATA WERE NORMALIZED TO CELLS ONLY CONTROL. * INDICATES STATISTICAL SIGNIFICANCE WITH $P < 0.05$ AS DETERMINED BY THE TUKEY-KRAMER HSD METHOD, $N = 2$. ** INDICATES STATISTICAL SIGNIFICANCE WITH $P < 0.05$ AS DETERMINED BY THE TUKEY-KRAMER HSD METHOD ($N = 2$). 45
FIGURE 2.7) THE EFFECT OF DIFFERENT RESPIRATORY CHAIN INHIBITORS ON MITOCHONDRIAL MEMBRANE POTENTIAL (MMP) AT DIFFERENT TIME POINTS DURING TRANSFECTION. ROTENONE (2 MM) WAS USED TO INHIBIT COMPLEX I OF THE ELECTRON TRANSPORT CHAIN, AND OLIGOMYCIN (5 MG/ML) WAS USED

TO INHIBIT F_0F_1-ATPASE. INHIBITORS WERE ADDED EITHER (A) 4 HOURS OR (B) 6 HOURS AFTER TRANSFECTION WITH PEI POLYPLEXES AT AN N/P RATIO OF 5. CELLS WERE INCUBATED WITH INHIBITORS FOR ONE HOUR, AFTER WHICH MMP WAS MEASURED AT EITHER (A) 5 HOURS OR (B) 7 HOURS AFTER TRANSFECTION. * DENOTES DATA IS STATISTICALLY SIGNIFICANT FROM EACH OTHER ($P < 0.05$) AS DETERMINED BY THE TUKEY-KRAMER HSD METHOD ($N = 2$). ** DATA IS STATISTICALLY SIGNIFICANT FROM EACH OTHER ($P < 0.05$, $N = 2$) USING THE TUKEY-KRAMER HSD METHOD. 48
FIGURE 2.8) CONFOCAL MICROSCOPY IMAGES OF HELA CELLS FIXED 1 HOUR AFTER TRANSFECTION WITH PEI POLYPLEXES. (A) POLYPLEXES ARE ILLUSTRATED AS GREEN, AND THE ENDOPLASMIC RETICULUM IS ILLUSTRATED AS RED. (B) HIGHLIGHTING COLOCALIZED POINTS; PIXELS WITH HIGH INTENSITIES FOR BOTH THE POLYPLEX SIGNAL AND THE ER SIGNAL ARE SHOWN AS WHITE; POLYPLEXES ARE SHOWN AS GREEN; AND THE ER IS SHOWN AS RED. SCALE BAR = 20 MM FOR (A) AND (B). (C) HIGHLIGHTING COLOCALIZED POINTS, THIS IMAGE IS ZOOMED IN FROM THE BOXED PORTION OF (B)..... 49
FIGURE 2.9) EFFECT OF PENTAMIDINE (PA), AMINOGUANIDINE (AM), AND MONODANSYLCADAVERINE (MDC) ON THE CYTOTOXICITY OF BRANCHED PEI IN HELA CELLS. CELL VIABILITY WAS CALCULATED BY MEASURING PROTEIN CONTENT IN CELL LYSATES 48 HOURS AFTER TRANSFECTION. * DENOTES STATISTICAL SIGNIFICANCE ($P < 0.05$) ACCORDING TO THE TUKEY-KRAMER HSD METHOD WITH $N = 3$. 50
FIGURE 3.1) SIZE (BARS) AND ZETA POTENTIAL MEASUREMENTS (LINE) FOR POLYPLEXES FORMED WITH LINEAR PEI, $T4_6$, $T4_{12}$, $T4_{43}$, AND $A4_{42}$. PEI POLYPLEXES WERE FORMED AT AN N/P RATIO OF 5, AND THE T4 AND $A4_{42}$ POLYPLEXES WERE FORMED AT AN N/P RATIO OF 20. LETTERS ARE USED TO DENOTE STATISTICAL ANALYSIS ON SIZE MEASUREMENTS, AND ASTERISKS ARE USED TO REPRESENT STATISTICAL ANALYSIS ON ZETA POTENTIAL MEASUREMENTS. DIFFERENT LETTERS ON SIZE MEASUREMENT BARS DENOTE MEANS THAT ARE STATISTICALLY SIGNIFICANT FROM EACH OTHER ($P < 0.05$) ACCORDING TO THE TUKEY-KRAMER HSD METHOD ($N = 3$). BARS WITH MATCHING LETTERS ARE NOT STATISTICALLY SIGNIFICANT FROM EACH OTHER. FOR ZETA POTENTIAL MEASUREMENTS, MEANS WITH DIFFERENT NUMBERS OF ASTERISKS ARE STATISTICALLY SIGNIFICANT FROM EACH OTHER ($P < 0.05$) USING THE TUKEY-KRAMER HSD METHOD WITH $N = 3$. MEANS WITH THE SAME NUMBER OF ASTERISKS ARE NOT STATISTICALLY SIGNIFICANT FROM EACH OTHER. 73
FIGURE 3.2) LUCIFERASE GENE EXPRESSION AS MEASURED BY RELATIVE LIGHT UNITS (RLU) PER MILLIGRAM OF PROTEIN IN CELL LYSATES AND CELL VIABILITY AS MEASURED BY PROTEIN CONTENT IN CELL LYSATES. LUCIFERASE EXPRESSION AND CELL VIABILITY WERE MEASURED 48 HOURS AFTER TRANSFECTION IN HELA CELLS. CELLS WERE TRANSFECTED WITH JETPEI (PEI) AT AN N/P RATIO OF 5. ALL OTHER POLYMERS WERE USED AT AN N/P RATIO OF 20. ALL STATISTICAL ANALYSIS WAS DONE USING THE TUKEY-KRAMER HSD METHOD. LETTERS REPRESENT STATISTICAL ANALYSIS DONE ON TRANSFECTION EFFICIENCY DATA (BARS), AND ASTERISKS REPRESENT STATISTICAL ANALYSIS DONE ON CELL VIABILITY DATA (LINE). BARS REPRESENTING TRANSFECTION EFFICIENCY WITH DIFFERENT LETTERS ARE STATISTICALLY SIGNIFICANT FROM EACH OTHER ($P < 0.05$) ACCORDING TO THE TUKEY-KRAMER HSD METHOD, WITH $N = 6$. BARS WITH MATCHING LETTERS REPRESENT MEANS THAT ARE NOT STATISTICALLY SIGNIFICANT FROM EACH OTHER. FOR CELL VIABILITY DATA, POINTS WITH DIFFERENT NUMBERS OF ASTERISKS ARE STATISTICALLY SIGNIFICANT FROM EACH OTHER ($P < 0.05$; $N = 6$) ACCORDING TO THE TUKEY-KRAMER HSD METHOD. POINTS WITH NO ASTERISKS ARE NOT STATISTICALLY SIGNIFICANT FROM EACH OTHER. 74
FIGURE 3.3) (A) MITOCHONDRIAL MEMBRANE POTENTIAL MEASURED BY DIIC(1)5 FLUORESCENCE NORMALIZED TO THE CELLS ONLY CONTROL AND (B) PHOSPHATIDYLSERINE (PS) EXTERNALIZATION MEASURED BY ANNEXIN V BINDING ASSAY IN HELA CELLS TRANSFECTED WITH POLYPLEXES FORMED USING PEI, T4, AND $A4_{42}$. DATA IN (B) IS PRESENTED AS % INCREASED PS EXTERNALIZATION COMPARED TO THE CELLS ONLY CONTROL. BARS WITH DIFFERENT LETTERS REPRESENT MEANS THAT ARE STATISTICALLY SIGNIFICANT ($P < 0.05$) FROM EACH OTHER ($N = 3$) ACCORDING TO THE TUKEY-KRAMER HSD METHOD. BARS WITH MATCHING LETTERS ARE NOT STATISTICALLY SIGNIFICANT FROM EACH OTHER. 78
FIGURE 3.4) THE EFFECT OF EGTA, AN EXTRACELLULAR CALCIUM CHELATOR, ON (A) CELLULAR UPTAKE OF POLYPLEXES FORMED WITH THE INDICATED POLYMERS AND CY5-PDNA 2 HOURS AFTER TRANSFECTION AND (B) PLASMA MEMBRANE PERMEABILITY AS MEASURED BY % INCREASED PROPIDIUM IODIDE (PI) FLUORESCENCE COMPARED TO THE CELLS ONLY CONTROL 2 HOURS AFTER TRANSFECTION. BARS WITH DIFFERENT LETTERS ARE STATISTICALLY SIGNIFICANT ($P < 0.05$) FROM

EACH OTHER (N = 3) ACCORDING TO THE TUKEY-KRAMER HSD METHOD. BARS WITH MATCHING LETTERS ARE NOT STATISTICALLY SIGNIFICANT FROM EACH OTHER. 81
FIGURE 3.5) CONFOCAL MICROSCOPY IMAGES OF HELA CELLS 30 MINUTES AFTER BEING TRANSFECTED WITH POLYPLEXES FORMED WITH CY5-LABELED PDNA AND THE FOLLOWING POLYMERS: (A) PDNA ONLY; (B) JETPEI (PEI); (C) $T4_6$; (D) $T4_{12}$; (E) $T4_{43}$; (F) $A4_{42}$. COLORS REPRESENT THE FOLLOWING; GREEN = WGA AF488-LABELED CYTOSOL; BLUE = DAPI-LABELED NUCLEUS; MAGENTA = CY5-LABELED PDNA. SCALE BAR = 20 µM. ARROWS DENOTE SITES OF POLYPLEX INTERNALIZATION. (G) MANDERS COEFFICIENTS BETWEEN EACH POLYPLEX TYPE (FORMED WITH CY5-PDNA) AND ALEXAFLUOR-488-CONJUGATED WHEAT GERM AGGLUTININ-LABELED PLASMA MEMBRANE. BARS WITH DIFFERENT LETTERS ARE STATISTICALLY SIGNIFICANT ($P < 0.05$) FROM EACH OTHER ACCORDING TO THE TUKEY-KRAMER HSD METHOD (N = 3). BARS WITH MATCHING LETTERS REPRESENT MEANS THAT ARE NOT STATISTICALLY SIGNIFICANT FROM EACH OTHER. 83
FIGURE 3.6) DATA SHOWING % INCREASED PROPIDIUM IODIDE (PI) FLUORESCENCE COMPARED TO THE CELLS ONLY CONTROL. CELLS WERE ANALYZED FOR PI FLUORESCENCE USING FLOW CYTOMETRY AT THE INDICATED TIME POINTS AFTER TRANSFECTION. ALL POLYMERS WERE USED AT AN N/P RATIO OF 20, WITH THE EXCEPTION OF JETPEI (PEI), WHICH WAS USED AT AN N/P RATIO OF 5. DIFFERENT LETTERS ON BARS REPRESENT MEANS THAT ARE STATISTICALLY SIGNIFICANT ($P < 0.05$) FROM EACH OTHER ACCORDING TO THE TUKEY-KRAMER HSD METHOD (N = 3). BARS WITH MATCHING LETTERS REPRESENT MEANS THAT ARE NOT STATISTICALLY SIGNIFICANT FROM EACH OTHER. 85
FIGURE 3.7) HELA CELLS WERE TRANSFECTED WITH POLYPLEXES IN THE ABSENCE OR PRESENCE OF 1 MM AMINOGUANIDINE (AMG), WHICH HAS BEEN SHOWN TO INHIBIT SOME FORMS OF ROS TOXICITY. CELL VIABILITY WAS ANALYZED USING THE MTT ASSAY (A) 30 MINUTES OR (B) 4 HOURS AFTER TRANSFECTION. DATA WERE NORMALIZED TO THE CELLS ONLY CONTROL. THERE WAS NO STATISTICAL SIGNIFICANCE BETWEEN CELLS TREATED WITH POLYPLEXES VS. POLYPLEXES WITH 1 MM AMG ACCORDING TO THE TUKEY-KRAMER HSD METHOD. 88
FIGURE 3.8) HELA CELLS WERE TRANSFECTED WITH THE DIFFERENT POLYPLEXES AND H_2DCDFA FLUORESCENCE WAS MEASURED USING FLOW CYTOMETRY AT THE INDICATED TIME POINTS TO DETERMINE THE PRESENCE OF REACTIVE OXYGEN SPECIES (ROS). 100 µM OF HYDROGEN PEROXIDE (H_2O_2) WAS USED AS A POSITIVE CONTROL. BARS WITH DIFFERENT LETTERS REPRESENT MEANS THAT ARE STATISTICALLY SIGNIFICANT ($P < 0.05$, N = 3) WITH EACH OTHER ACCORDING TO THE TUKEY-KRAMER HSD METHOD. BARS WITH MATCHING LETTERS REPRESENT MEANS THAT ARE NOT STATISTICALLY SIGNIFICANT FROM EACH OTHER. 89
FIGURE 3.9) TOXICITY OF THE COMPONENTS OF THE T4 POLYMERS AS MEASURED BY MTT ASSAY. CELLS WERE TREATED WITH EITHER N6 OR L-TARTARIC ACID AT A CONCENTRATION OF 100 µG/ML FOR THE INDICATED TIME POINTS. DATA WERE NORMALIZED TO THE CELLS ONLY CONTROL. NEITHER OF THE TREATMENTS WERE STATISTICALLY SIGNIFICANT ($P < 0.05$) FROM THE CELLS ONLY CONTROL ACCORDING TO THE TUKEY-KRAMER HSD METHOD (N = 3). 90
FIGURE 3.10) NUCLEI WERE ISOLATED FROM CELLS TRANSFECTED WITH THE INDICATED POLYMERS 4 HOURS AFTER TRANSFECTION AND ANALYZED USING FLOW CYTOMETRY. (A) NUCLEAR ASSOCIATION BETWEEN POLYPLEXES AND NUCLEI MEASURED BY PERCENTAGE OF NUCLEI POSITIVE FOR CY5 AND (B) NUCLEAR MEMBRANE PERMEABILITY INDUCED BY POLYPLEXES SHOWN AS % INCREASED PROPIDIUM IODIDE (PI) POSITIVE NUCLEI COMPARED TO THE CELLS ONLY CONTROL (BARS, LEFT Y-AXIS) AND PI FLUORESCENCE INTENSITY (LINE, RIGHT Y-AXIS). BARS WITH DIFFERENT LETTERS REPRESENT MEANS THAT ARE STATISTICALLY SIGNIFICANT ($P < 0.05$) FROM EACH OTHER (N = 3) ACCORDING TO THE TUKEY-KRAMER HSD METHOD. FOR FLUORESCENCE INTENSITY, POINTS WITH DIFFERENT NUMBERS OF ASTERISKS ARE SIGNIFICANT ($P < 0.05$) FROM EACH OTHER ACCORDING TO THE TUKEY-KRAMER HSD METHOD (N = 3). 94
FIGURE 3.11) CONFOCAL MICROSCOPY IMAGES OF NUCLEI ISOLATED FROM CELLS TRANSFECTED WITH THE FOLLOWING: (A) PDNA ONLY; (B) JETPEI (PEI); (C) $T4_6$; (D) $T4_{12}$; (E) $T4_{43}$; (F) $A4_{42}$. COLORS REPRESENT THE FOLLOWING: BLUE = PROPIDIUM IODIDE-LABELED NUCLEUS; MAGENTA = CY5-LABELED PDNA. SCALE BAR = 20 µM. (G) MANDERS COEFFICIENTS BETWEEN CY5-LABELED PDNA AND PROPIDIUM IODIDE-LABELED NUCLEI TO SIGNIFY PDNA NUCLEAR IMPORT. BARS WITH DIFFERENT LETTERS REPRESENT MEANS THAT ARE STATISTICALLY SIGNIFICANT ($P < 0.05$) FROM EACH OTHER (N = 3) ACCORDING TO THE TUKEY-KRAMER HSD METHOD. BARS WITH MATCHING LETTERS REPRESENT MEANS THAT ARE NOT STATISTICALLY SIGNIFICANT FROM EACH OTHER. 96

FIGURE 3.12) COMPARISON OF CY5 AND PI FLUORESCENCE BY SLICE IN Z-STACKS OBTAINED USING CONFOCAL MICROSCOPY. NUCLEI WERE ISOLATED FROM TRANSFECTED CELLS 24 HOURS AFTER TRANSFECTION FROM HELA CELLS TRANSFECTED WITH THE FOLLOWING POLYMERS: (A) JETPEI (PEI); (B) $T4_6$; (C) $T4_{12}$; (D) $T4_{43}$; (E) $A4_{42}$. PROPIDIUM IODIDE (PI) MAXIMUM FLUORESCENCE INTENSITY WAS INTERPRETED AS THE CENTER OF THE NUCLEI FOR EACH CORRESPONDING SET OF CY5 MEASUREMENTS. POLYPLEXES WERE DEEMED TO BE IN THE CENTER OF THE NUCLEI IF THE PEAKS FOR CY5 FLUORESCENCE CORRESPONDED TO THE PEAKS FOR PI FLUORESCENCE. 99
FIGURE 3.13) CONFOCAL IMAGES OF HELA CELLS FIXED 4 HOURS AFTER TRANSFECTION. CELLS WERE TRANSFECTED WITH THE FOLLOWING: A) DNA ONLY; B) JETPEI (PEI); C) $T4_6$; D) $T4_{12}$; E) $T4_{43}$; F) $A4_{42}$. COLORS REPRESENT THE FOLLOWING; BLUE = NUCLEUS; GREEN = NUCLEAR LAMIN; MAGENTA = PDNA. SCALE BAR = 20 μM. THE WHITE ARROWS IN (B) AND (E) INDICATE SITES OF DEEP NUCLEAR INDENTATION. 100
FIGURE 3.14) CONFOCAL MICROSCOPY IMAGES OF THE NUCLEI IN WHOLE HELA CELLS TRANSFECTED WITH POLYPLEXES FORMED WITH CY5-PDNA AND (A) JETPEI (PEI); (B) $T4_6$; (C) $T4_{12}$; (D) $T4_{43}$; (E) $A4_{42}$. THE NUCLEUS IS SHOWN AS BLUE, NUCLEAR LAMIN IS SHOWN AS GREEN, AND THE POLYPLEXES ARE SHOWN AS MAGENTA. SCALE BAR = 5 μM. THESE IMAGES EMPHASIZE POLYPLEX-LAMIN COLOCALIZATION AND FURTHER SHOW NUCLEAR INDENTATIONS IN THE CASE OF (A) JETPEI AND (D) $T4_{43}$. 101
FIGURE 3.15) MANDERS COEFFICIENTS FOR THE COLOCALIZATION OF EACH POLYPLEX TYPE (FORMED WITH CY5-PDNA) WITH LAMIN ANTIBODY (AF488) FOR CONFOCAL MICROSCOPY IMAGES TAKEN OF CELLS TRANSFECTED WITH POLYPLEXES FOR 4 HOURS. HIGHER MANDERS COEFFICIENTS ARE INDICATIVE OF HIGHER COLOCALIZATION. * DENOTES STATISTICAL SIGNIFICANCE ($P < 0.05$) WITH $N = 3$ ACCORDING TO THE TUKEY-KRAMER HSD METHOD. 103
FIGURE 3.16) TRYPAN BLUE EXCLUSION ASSAY PERFORMED ON NUCLEI TREATED WITH POLYPLEXES FOR 4 HOURS. NUCLEI WERE ISOLATED FROM HELA CELLS AND TREATED WITH (A) PDNA ONLY; (B) JETPEI (PEI); (C) $T4_6$; (D) $T4_{12}$; (E) $T4_{43}$; OR (F) $A4_{42}$. SCALE BAR = 400 MM. (G) NUCLEI WERE COUNTED AND ANALYZED FOR PIXEL INTENSITY USING IMAGEJ AND THE STATISTICS WERE CALCULATED USING JMP. ROUGHLY 300 NUCLEI WERE ANALYZED FOR EACH POLYPLEX, AND THE TUKEY-KRAMER HSD METHOD REVEALS EACH SET OF DATA POINTS TO BE STATISTICALLY SIGNIFICANT ($P < 0.05$) FROM ONE ANOTHER. 104
FIGURE 3.17) LUCIFERASE EXPRESSION DATA IN THE PRESENCE OR ABSENCE OF 5 MM CAMPTOTHECIN, AN APOPTOSIS-INDUCING AGENT. TRANSFECTION EFFICIENCY WAS MEASURED 24 HOURS AFTER TRANSFECTION. * DENOTES STATISTICAL SIGNIFICANCE ($P < 0.05$, $N = 3$). ** DENOTES STATISTICAL SIGNIFICANCE ($P < 0.05$, $N = 3$). STATISTICAL SIGNIFICANCE WAS CALCULATED USING THE TUKEY-KRAMER HSD METHOD. 106
FIGURE 4.1) OVERLAYED HISTOGRAMS OF (A) CY5 FLUORESCENCE AND (B) FITC FLUORESCENCE FROM NUCLEI ISOLATED FROM HELA CELLS 24 HOURS AFTER TRANSFECTION. NUCLEI WERE ANALYZED FOR CY5 AND FITC FLUORESCENCE USING FLOW CYTOMETRY. CELLS WERE TRANSFECTED WITH POLYPLEXES MADE FROM FITC-LABELED JETPEI-FLUOF (PEI) AT AN N/P RATIO OF 5, FITC-LABELED T4 AT AN N/P RATIO OF 20, OR FITC-LABELED G4 AT AN N/P RATIO OF 20 AND CY5-LABELED PDNA. ALL POLYPLEX-TREATED NUCLEI EXHIBITED INCREASED PDNA ASSOCIATION AND POLYMER ASSOCIATION AS INDICATED BY INCREASED CY5 AND FITC FLUORESCENCE, RESPECTIVELY. (C) BAR GRAPH REPRESENTATION OF THE FLOW CYTOMETRY DATA. ONE TRIAL IS PRESENTED HERE, WE WERE UNABLE TO CARRY OUT MORE TRIALS BASED ON LIMITATIONS IN THE QUANTITY OF LABELED POLYMER. 127
FIGURE 4.2) NUCLEI ISOLATED FROM HELA CELLS 24 HOURS AFTER TRANSFECTION. CELLS WERE TRANSFECTED WITH (A) PDNA ONLY; (B) JETPEI (PEI); (C) T4, (D) GLYCOFECT (G4). COLORS REPRESENT THE FOLLOWING: MAGENTA = CY5-LABELED PDNA; BLUE = DAPI-LABELED NUCLEUS; RED = RHODAMINE-LABELED DEXTRAN. SCALE BAR = 20 MM. NUMBERS IN THE UPPER PORTION OF THE IMAGES REPRESENT THE COLOCALIZATION DATA AS DETERMINED BY MANDERS COEFFICIENTS BETWEEN RHODAMINE-LABELED DEXTRAN AND DAPI-LABELED NUCLEI. NUMBERS IN THE LOWER PORTION REPRESENT MANDERS COEFFICIENTS BETWEEN CY5-LABELED PDNA AND DAPI-LABELED NUCLEI. NOTE HOW NUCLEI ISOLATED FROM PEI-TREATED CELLS (B) EXHIBIT HIGHER RHODAMINE-DAPI AND CY5-DAPI COLOCALIZATION COMPARED TO G4 AND T4, INDICATING INCREASED NUCLEAR ENVELOPE PERMEABILITY AND INCREASED PDNA NUCLEAR IMPORT, RESPECTIVELY. 128

FIGURE 4.3) NUCLEI ISOLATED FROM TRANSFECTED HELA CELLS 24 HOURS AFTER TRANSFECTION. CELLS WERE TRANSFECTED WITH (A) T4 OR (B) G4. ARROWS INDICATE SITES OF NUCLEAR ENVELOPE RUFFLING AT SITES OF POLYPLEX-NUCLEAR INTERACTION AS DETERMINED BY DAPI FLUORESCENCE. COLORS REPRESENT THE FOLLOWING: MAGENTA = CY5-LABELED PDNA; BLUE = DAPI-LABELED NUCLEUS; RED = RHODAMINE-LABELED DEXTRAN. SCALE BAR = 20 MM. 129
FIGURE 4.4) MEAN PIXEL INTENSITIES OF ISOLATED NUCLEI TREATED WITH THE INDICATED POLYPLEXES FOR 4 HOURS AND THEN TREATED WITH TRYPAN BLUE. DARKER INTENSITIES INDICATE MORE TRYPAN BLUE PRESENT IN THE NUCLEI, INDICATING INCREASED NUCLEAR ENVELOPE PERMEABILITY. ALL MEANS ARE STATISTICALLY SIGNIFICANT FROM EACH OTHER ($P < 0.05$, $N \sim 300$) ACCORDING TO THE TUKEY-KRAMER HSD METHOD. PIXEL INTENSITIES ARE HIGHEST WITH NUCLEI TREATED WITH T4, AND THEN PIXEL INTENSITIES DECREASE IN THE ORDER PDNA (DNA) > G4 > PEI. 131
FIGURE 4.5) HELA CELLS TRANSFECTED FOR 24 HOURS WITH (A) PDNA ONLY; (B) JETPEI (PEI); (C) T4; (D) G4. POLYPLEXES WERE FORMED WITH CY5-LABELED PDNA. COLORS REPRESENT THE FOLLOWING: MAGENTA = PDNA; BLUE = NUCLEUS; RED = NUCLEOLI. SCALE BAR = 20 MM. WHITE ARROWS INDICATE POLYPLEXES APPROACHING NUCLEI AT THE SITE OF NUCLEAR DIVISION. WE OBSERVED LITTLE COLOCALIZATION BETWEEN THE POLYPLEXES (MAGENTA) AND THE NUCLEOLI (RED) AT THIS TIME POINT FOR ALL POLYMERS TESTED. 132
FIGURE 4.6) CONFOCAL IMAGES OF HELA CELLS TRANSFECTED WITH (A) T4 AND (B) G4 24 HOURS AFTER TRANSFECTION. COLORS REPRESENT THE FOLLOWING: MAGENTA = PDNA; BLUE = NUCLEUS; RED = NUCLEOLI. SCALE BAR = 20 MM. WHITE PIXELS INDICATE COLOCALIZATION BETWEEN THE POLYMERS (GREEN) AND PDNA (MAGENTA). 133
FIGURE 4.7) LUCIFERASE EXPRESSION 24 HOURS AFTER TRANSFECTION AS MEASURED BY RELATIVE LIGHT UNITS (RLU) PER MILLIGRAM OF PROTEIN IN CELL LYSATES. CELLS WERE TRANSFECTED IN THE PRESENCE OR ABSENCE OF NOCODAZOLE (NOC) OR APHIDICOLIN (APH) TO DETERMINE IF MICROTUBULE DISRUPTION OR CELL CYCLE INHIBITION AFFECTED TRANSFECTION EFFICIENCY. BARS WITH DIFFERENT LETTERS REPRESENT MEANS THAT ARE STATISTICALLY SIGNIFICANT FROM EACH OTHER ACCORDING TO THE TUKEY-KRAMER HSD METHOD ($P < 0.05$, $N = 3$). 134
FIGURE 4.8) FLOW CYTOMETRY DATA FROM NUCLEI TREATED WITH POLYPLEXES FORMED WITH DIFFERENT FITC-LABELED POLYMERS AND CY5-LABELED PLASMID DNA. NUCLEI WERE ISOLATED WITH POLYPLEXES WITH OR WITHOUT HELA CYTOSOL EXTRACT ("CYTOSOL") AND IN THE ABSENCE OR PRESENCE OF AN ATP-GENERATING SYSTEM ("ENERGY"). NUCLEI WERE ANALYZED FOR (A) CY5 FLUORESCENCE FROM THE PDNA AND (B) FITC FLUORESCENCE FROM THE POLYMERS 4 HOURS AFTER POLYPLEX TREATMENT. BARS WITH DIFFERENT LETTERS REPRESENT MEANS THAT ARE STATISTICALLY SIGNIFICANT FROM EACH OTHER ACCORDING TO THE TUKEY-KRAMER HSD METHOD ($P < 0.05$, $N = 3$). BARS WITH MATCHING LETTERS REPRESENT MEANS THAT ARE NOT STATISTICALLY SIGNIFICANT FROM EACH OTHER. 136
FIGURE 4.9) CONFOCAL IMAGES OF DIGITONIN-PERMEABILIZED HELA CELLS. AFTER PERMEABILIZATION, THE HELA NUCLEI WERE INCUBATED IN BUFFER IN THE PRESENCE OR ABSENCE OF HELA CYTOSOL EXTRACT ("CYTOSOL") AND IN THE PRESENCE OR ABSENCE OF AN ATP-GENERATING SYSTEM ("ENERGY"). THE NUCLEI WERE TREATED WITH POLYPLEXES FORMED WITH THE INDICATED POLYMERS AND CY5-LABELED PDNA FOR 4 HOURS BEFORE BEING FIXED AND IMAGED. IN THESE IMAGES, RED REPRESENTS RHODAMINE-LABELED 2 MDA DEXTRAN, BLUE REPRESENTS THE NUCLEI, AND MAGENTA REPRESENTS PDNA. SCALE BAR = 20 MM. INCREASES OF RED FLUORESCENCE IN THE NUCLEI ARE INDICATIVE OF INCREASED NUCLEAR ENVELOPE PERMEABILITY, AND INCREASES OF MAGENTA FLUORESCENCE IN THE NUCLEI ARE INDICATIVE OF INCREASED PDNA NUCLEAR IMPORT. 140
FIGURE 4.10) CONFOCAL MICROSCOPY DATA. MANDERS COEFFICIENTS WERE USED TO MEASURE COLOCALIZATION BETWEEN CY5-LABELED PLASMID DNA AND DAPI-LABELED NUCLEI. DATA IS SHOWN AS THE MEAN ± STANDARD DEVIATION FOR 10 SAMPLES. BARS WITH DIFFERENT LETTERS REPRESENT MEANS THAT ARE STATISTICALLY SIGNIFICANT FROM EACH OTHER ACCORDING TO THE TUKEY-KRAMER HSD METHOD ($P < 0.05$, $N = 10$). NO MEASUREABLE CY5 FLUORESCENCE WAS FOUND IN THE NUCLEI TREATED WITH PDNA ONLY OR IN THE CELLS ONLY CONTROLS. BARS WITH MATCHING LETTERS REPRESENT MEANS THAT ARE NOT STATISTICALLY SIGNIFICANT FROM EACH OTHER. 141
FIGURE 4.11) COLOCALIZATION DATA FOR NUCLEI TREATED WITH (A) JETPEI (PEI) POLYPLEXES; (B) T4 POLYPLEXES; (C) G4 POLYPLEXES. MANDERS COEFFICIENTS FOR CY5 AND DAPI ARE SHOWN ON THE Y-AXIS, AND MANDERS COEFFICIENTS FOR RHODAMINE (RHOD.) AND DAPI ARE SHOWN ON THE X-

axis. Data is plotted in an effort to discern trends between nuclear envelope permeability and pDNA nuclear import. In the absence of cytosol, the absence of energy results in overall lower pDNA import, unless the nuclear envelope has high permeability (as evidenced by high colocalization between rhodamine-labeled dextran and DAPI-labeled nuclei). 145
Figure 4.12) Confocal microscopy images of digitonin-permeabilized HeLa cells treated with T4 polyplexes. Cells were incubated in the following import buffers; (a) with cytosol extract and with an ATP-generating system ("energy); (b) with cytosol extract and without energy; (c) without cytosol extract and with energy; (d) without cytosol extract and without energy. Polyplexes were allowed to incubate on cells for 4 hours before cells were washed and fixed. Colors represent the following; red = rhodamine-labeled 2 MDa dextran; green = FITC-labeled T4; blue = DAPI-labeled nucleus; magenta = Cy5-labeled pDNA. Scale bar = 20 mm. Regardless of incubation conditions, polymer fluorescence (green) was present in all nuclei, predominately in the nucleoli. 147
Figure 4.13) Confocal microscopy images of digitonin-permeabilized HeLa cells treated with G4 polyplexes in the following import buffers; (a) with cytosol extract and with an ATP-generating system ("energy); (b) with cytosol extract and without energy; (c) without cytosol extract and with energy; (d) without cytosol extract and without energy. Polyplexes were allowed to incubate on cells for 4 hours before cells were washed and fixed. Colors represent the following; red = rhodamine-labeled 2 MDa dextran; green = FITC-labeled T4; blue = DAPI-labeled nucleus; magenta = Cy5-labeled pDNA. Scale bar = 20 mm. We observed diffuse polymer fluorescence throughout the nuclei, but the brightest polymer fluorescence is evident in the nucleoli. 148
Figure 5.1) Structure of a polymer scaffold incorporating galactose as a proof-of-concept targeting ligand. Polymer structures studied herein differed in the length of the linkage between the galactose and the polymer (y). The polymers were synthesized by Dr. Chen-Chang Lee, and the polymer structure illustration in this figure was provided by Dr. Chen-Chang Lee. 160
Figure 5.2) Structure of trehalose-containing polymers. Polymers Tr4-PEG-a (Tr4 A) and Tr4-PEG-b (Tr4 B) differ in the lengths of the PEG chains on the ends of the polymers. Polymers Tr4-c (Tr4 C) and Tr4-d (Tr4 D) were synthesized in order to study the effects of different polymer end groups. This figure was produced by Dr. Karina Kizjakina, and synthesis of these trehalose-containing polymers was also performed by her. 162
Figure 5.3) Schematic of polyplex formation with diblock glycopolymers and plasmid DNA. (a) The cationic charges on the AEMA block (red) allow the glycopolymer to interact with negative charges on the plasmid DNA (green). (b) Polyplex formation. The MAG block (blue) is expected to be displayed on the outside of the polyplex. (c) The polyplex is formed with the AEMA block and plasmid DNA in the inner core, and the MAG block on the outer surface. (d) Structure of the diblock polymers. The polymers differed in the lengths of the amine block; three different lengths were tested in the current work. This figure was produced by Dr. Adam E. Smith. Synthesis of these polymers was performed by Dr. Adam E. Smith and Antons Sizovs. 164
Figure 5.4) Structure of the terbium (Tb)-chelated polymers. The polymers differ in the amount of secondary amines in the repeat unit, with Tb-N4 having 4 secondary amines and Tb-N5 having 5 secondary amines. The degree of polymerization (n) is 20 for Tb-N4, and n = 23 for Tb-N5. Polymer synthesis was carried out by Sneha Kelkar. This figure was provided by Sneha Kelkar. 165
Figure 5.5) Luciferase expression data for HepG2 cells 48 hours after transfection. Cells were transfected in the presence or absence of 1 mg/mL asialofetuin (ASF) at N/P ratios of (a) 5; (b) 8; (c) 10. HepG2 cells were transfected with 0.5 mg pDNA/well. Data are presented as the mean ± standard deviation. Statistical analysis was performed on the log of the RLU/mg protein, and bars with different letters represent means that are statistically significant ($p < 0.05$) according to the Tukey-Kramer HSD method ($n = 2$). 173
Figure 5.6) Luciferase gene expression as expressed by relative light units (RLU)/mg protein in HepG2 cells 48 hours after transfection. HepG2 cells were transfected in the presence or absence of 1 mg/mL asialofetuin (ASF). Polyplexes were formed at N/P ratios of 5 for

all polymers except for G4, which was formed at an N/P ratio of 20. Cells were transfected with (A) 0.5 mg pDNA/well or (B) 1 mg pDNA/well. Data is presented as the mean ± standard deviation of three trials. Statistical analysis was performed on the log of the RLU/mg protein. Bars with different letters represent means that are statistically significant ($p < 0.05$) using the Tukey-Kramer HSD method ($n = 3$). Bars with matching letters are not statistically significant from each other. 175
Figure 5.7) Transfection efficiency in HeLa cells. Cells were transfected with 0.5 mg pDNA/well, and luciferase gene expression was assayed 48 hours after transfection. Cells were transfected in the presence or absence of 1 mg/mL asialofetuin (ASF). Statistical analysis was performed on the log of the RLU/mg protein. Bars with different letters represent means that are statistically significant ($p < 0.05$) using the Tukey-Kramer HSD method ($n = 3$). 177
Figure 5.8) Cell viability as measured by the amount of protein in cell lysates. HepG2 cells were allowed to transfect for 48 hours, after which cell viability was measured. All polymers were used at an N/P ratio of 5, with the exception of G4 that was used at an N/P ratio of 20. Cells were treated with (A) 0.5 mg of pDNA/well or (B) 1 mg of pDNA/well. * denotes means that are statistically significant ($p < 0.05$) from each other. ** denotes means that are statistically significant from each other ($p < 0.05$). Statistically analysis was performed using the Tukey-Kramer HSD method ($n = 3$). Means for cell viability data in (A) were not statistically significant from each other according to the Tukey-Kramer HSD method ($n = 3$). 179
Figure 5.9) Luciferase expression data expressed in relative light units (RLU) and RLU/mg protein. (A) RMSCs and (B) HDFn cells were transfected for 48 hours before the cell lysates were analyzed for luciferase activity. Tr4 polymers were formed at the N/P ratios indicated in parentheses. Positive controls were used according to manufacturer's instructions. Data are presented as mean ± standard deviation. Statistical analysis was performed on the log of the RLU and log of the RLU/mg protein data. Black letters represent statistical analysis for RLU data (white bars), and blue letters represent statistical analysis for RLU/mg protein (gray bars). Bars with different letters are statistically significant ($p < 0.05$) from each other according to the Tukey-Kramer HSD method ($n = 3$). 181
Figure 5.10) Green fluorescent protein (GFP) expression in RMSCs. Cells were analyzed for green GFP expression using (A) and (C) flow cytometry to determine the percentage of cells positive for green fluorescence 48 hours after transfection. Further GFP expression analysis was carried out by (B) and (D) fluorescence microscopy 48 hours after transfection. In this case, Tr6, Tr5 and Tr4 all have trityl end groups, the difference between these polymers is the number of secondary amines in their repeat units (6, 5, and 4, respectively). The trehalose polymers were used at an N/P of 20, while positive control polymers Lipofectamine 2000 (Lipo-2000), JetPEI (PEI), and Glycofect were used according to manufacturer's protocol. 183
Figure 5.11) Green fluorescent protein (GFP) expression in HDFn cells. Cells were analyzed for GFP expression using (A) and (C) flow cytometry as well as (B) and (D) fluorescence microscopy 48 hours after transfection. In this case, Tr6, Tr5 and Tr4 all have trityl end groups, the difference between these polymers is the number of secondary amines in their repeat units (6, 5, and 4, respectively). The trehalose polymers were used at an N/P of 20, while positive control polymers Lipofectamine 2000 (Lipo-2000), JetPEI (PEI), and Glycofect were used according to manufacturer's protocol. 184
Figure 5.12) Cell viability as measured by protein content present in cell lysates ("protein") and by the MTT assay in (A) RMSCs and (B) HDFn cells. Cells were transfected with the trehalose polymers at the indicated N/P ratios, and cell viability was measured 48 hours after transfection. Data are presented as mean ± standard deviation. Black letters represent statistical analysis for the MTT assay, and blue letters represent statistical analysis for the protein assay. Bars with matching letters are not statistically significant from each other, and bars with different letters represent means that are statistically significant ($p < 0.05$) from each other according to the Tukey-Kramer HSD method ($n = 3$). 186

FIGURE 5.13) PERCENTAGE OF CY5 POSITIVE HELA CELLS TRANSFECTED WITH POLYPLEXES FORMED AT N/P RATIOS 2, 5, AND 10 WITH CY5-LABELED PDNA AND P1, P2, P3 IN (A) OPTIMEM AND (B) DMEM. JETPEI AND GLYCOFECT WERE USED AS POSITIVE CONTROLS, JETPEI WAS USED AT AN N/P RATIO OF 5 AND GLYCOFECT WAS USED AT AN N/P RATIO OF 60. CY5 FLUORESCENCE WAS MEASURED 48 HOURS AFTER TRANSFECTION. THE GRAPHS WERE PROVIDED BY DR. ADAM E. SMITH. STATISTICAL ANALYSIS WAS DONE BY GIOVANNA GRANDINETTI. DATA ARE PRESENTED AS MEANS ± STANDARD DEVIATIONS. BARS WITH MATCHING LETTERS ARE NOT STATISTICALLY SIGNIFICANT FROM EACH OTHER, AND BARS WITH DIFFERENT LETTERS REPRESENT MEANS THAT ARE STATISTICALLY SIGNIFICANT FROM EACH OTHER ($P < 0.05$, $N = 3$) ACCORDING TO THE TUKEY-KRAMER HSD METHOD..... 188
FIGURE 5.14) CONFOCAL MICROSCOPY IMAGES OF HELA CELLS TRANSFECTED WITH POLYPLEXES (WHITE) FORMED BETWEEN FITC-LABELED P3 (GREEN) AND CY5-LABELED PDNA (PURPLE). NUCLEI (BLUE) WERE STAINED WITH DAPI. CELLS WERE FIXED AT (A) 4 HOURS (B) 24 HOURS AND (C) 48 HOURS AFTER TRANSFECTION. MANDERS COEFFICIENTS WERE CALCULATED USING THE SOFTWARE IMAGEJ AND ARE SHOWN IN THE COMPOSITE IMAGES FOR EACH TIME POINT. M1 = DEGREE OF OVERLAP BETWEEN CY5-LABELED PDNA WITH FITC-LABELED POLYMER; M2 = DEGREE OF OVERLAP BETWEEN FITC-LABELED POLYMER WITH CY5-LABELED PDNA. SCALE BAR = 20 MM..... 190
FIGURE 5.15) TERBIUM FLUORESCENCE AT AN EXCITATION OF 380 NM IN THE PRESENCE OR ABSENCE OF TMR-LABELED PDNA. POLYPLEXES WERE FORMED AT AN N/P RATIO OF (A) 50; (B) 20; (C) 10; OR (D) 5. LINES REPRESENT THE FOLLOWING: BLUE = POLYMER ONLY; MAGENTA = POLYPLEXES FORMED WITH UNLABELED PDNA; GREEN = POLYPLEXES FORMED WITH TMR-LABELED PDNA. (E) THE PERCENTAGE OF TERBIUM FLUORESCENCE QUENCHING AS A FUNCTION OF N/P RATIO..... 192
FIGURE 5.16) IMAGES OF HELA CELLS TREATED WITH (A) TB-N5 POLYPLEXES AT AN N/P OF 20 AND (B) TB-N5 POLYMER ONLY AT THE SAME CONCENTRATION AS THE N/P 20 POLYMER SOLUTION. THE CELLS WERE IMAGED USING FLUORESCENT MICROSCOPY 4 HOURS AFTER TRANSFECTION. ARROWS DENOTE SITES OF PUNCTUATE POLYMER FLUORESCENCE IN CELLS. SCALE BAR = 200 MM. (C) FLUORESCENCE INTENSITY FROM THE POLYMER WAS QUANTIFIED USING THE SOFTWARE IMAGEJ. MEAN PIXEL INTENSITY DATA ARE SHOWN AS MEAN ± STANDARD DEVIATION. DEAD CELLS WERE EXCLUDED FROM THESE MEASUREMENTS. *DENOTES STATISTICAL SIGNIFICANCE ($P < 0.05$, $N = 4$) ACCORDING TO ANOVA FOLLOWED BY THE STUDENT'S T-TEST. 194

List of Tables

TABLE 1.1.) SOME INTRACELLULAR FUNCTIONS OF THE NATURALLY-OCCURRING POLYAMINES SPERMINE, SPERMIDINE, AND PUTRESCINE AND POLYAMINE DERIVATIVES..... 8
TABLE 3.1) MOLECULAR WEIGHT (M_w), POLYDISPERSITY INDEX (M_w/M_N), MARK-HOUWINK-SAKURADA PARAMETER (MHS (A)), AND DEGREE OF POLYMERIZATION (N_w) FOR THE POLYMERS STUDIED. 72

List of Schemes

Scheme 1.1) How polycationic polymers deliver DNA. The positive charges along the polymer backbone allow it to interact with negative charges on the DNA backbone. The polymer condenses the DNA into a polymer-DNA complex (polyplex) which has a net positive charge. The positive charge on the polyplex allows it to interact with negatively-charged groups on the cell surface. The mechanism of polyplex uptake and DNA delivery remain largely unknown, but protein expression is observed in polymer transfection. 3

Scheme 2.1) Potential mechanisms as to how mitochondrial membrane potential (MMP) could be disrupted during PEI transfection (inhibitors of normal mitochondrial function are shown in boxes on the diagram). PEI could potentially interact with the electron transport chain or F0F1-ATPase, whose contributions to MMP can be observed using rotenone or oligomycin, respectively. The mitochondrial membrane permeability transition pore is formed during times of intracellular stress by the complexation of several proteins, including voltage-dependent anion channel (VDAC), adenine nucleotide translocase (ANT), and cyclophilin D. Cyclosporine a (CsA) is able to prevent the pore from opening and save the cell from apoptosis in certain cases. Additionally, PEI polyplexes could be directly permeabilizing the outer mitochondrial membrane, resulting in a loss of mitochondrial function. 26

Scheme 3.1) Possible routes of polymer/polyplex cytotoxicity: I.) mechanism of cellular entry *via* direct membrane permeabilization, II.) interaction with organelles or proteins during intracellular trafficking, III.) harmful products formed upon polymer degradation, IV.) mechanism of nuclear entry *via* nuclear envelope permeabilization, V.) mechanism of cellular exit..... 76

List of Abbreviations

μ: Micro

μL: Microliter

μm: Micrometer/micron

A4: Poly(adipamidopentaethylenetetramine)

AEMA : *N*-(2-aminoethyl)methacrylamide

AF488: Alexa Fluor 488

AF555: Alexa Fluor 555

ANT: Adenine nucleotide translocase

ASF: Asialofetuin

ASGPr: Asialoglycoprotein receptor

ATCC: American Type Culture Collection

ATP: Adenosine triphosphate

CMV: Cytomegalovirus

CsA: Cyclosporine a

Cy5: Cyanine dye with red emission

DAPI: 4′,6-diamidino-2-phenylindole

DMEM: Dulbecco's modified Eagle medium

DMSO: Dimethyl sulfoxide

DNA: Deoxyribonucleic acid

DiIC(1)5: 1,1′,3,3,3′,3′-hexamethylindodicarbocyanine iodide

DLS: Dynamic light scattering

DP: Degree of polymerization

EGTA: Ethylene glycol tetraacetic acid

ER: Endoplasmic reticulum

ETC: Electron transport chain

FACS: Fluorescent activated cell sorting

FBS: Fetal bovine serum

FITC: Fluorescein isithiocyanate

FRET: Förster (Fluorescence) resonance energy transfer

G4: Poly(galactaramidopentaethylenetetramine) (Glycofect)

Gal: Galactose

GFP: Green fluorescent protein

GPC: Gel permeation chromatography

GTP: Guanosine triphosphate

H_2DCDFA: 2′,7′-dichlorodihydrofluorescein diacetate

HDFn: Primary human dermal fibroblast cells neonatal

HeLa: Human cervix adenocarcinoma cell line

HepG2: Human hepatocarcinoma cell line

JetPEI: Linear poly(ethylenimine)

kDa: Kilodalton

Luc: Luciferase

M: Molar

mg: Milligram

mM: Millimolar

MAG: 2-deoxy-2-methacrylamido

Ma: Malonate

MMP: Mitochondrial membrane potential

MTOC : Microtubule organization center

N/P: Polymer protonable amines/ DNA phosphate group

NPC: Nuclear pore complex

OptiMEM: Serum-free cell culture medium

P1: P(MAG_{46}-*b*-$AEMA_{21}$)

P2: P(MAG_{46}-*b*-$AEMA_{39}$)

P3: P(MAG_{46}-*b*-$AEMA_{48}$)

PBS: Phosphate-buffered saline

pDNA: Plasmid DNA

PEG: Poly(ethyleneglycol)

PEI: Poly(ethylenimine)

PFA: Paraformaldehyde

PGAA: Poly(glycoamidoamine)

PI: Propidium iodide

PLL: Poly-L-lysine

RAFT: Reversible addition-fragmentation chain transfer

Rhod: Rhodamine

RLU: Relative light units

RMSC: Rat mesenchymal stem cells

RNA: Ribonucleic acid

ROS: Reactive oxygen species

SEC: Size-exclusion chromatography

T4: Poly(L-tartaramidopentaethylenetetramine)

Tb: Terbium

TMR: tetramehtylrhodamine

Tr: Trehalose

VDAC: Voltage-dependent anion channel

WGA: Wheat germ agglutinin

Declaration of work performed

I declare that with the exception of the items listed below, all work reported in this dissertation was performed by me.

Synthesis of the terbium-chelated polymers was performed by Sneha Kelkar. Synthesis of poly(L-tartaramidopentaethylenetetramine) with a degree of polymerization of 12 ($T4_{12}$) and poly(adipamidopentaethylenetetramine) with a degree of polymerization of 42 ($A4_{42}$) was performed by Dr. Adam E. Smith. Synthesis of poly(galactaramidopentaethylenetetramine) (G4) was performed by Dr. Joshua M. Bryson. Synthesis of the 2-deoxy-2-methacrylamido glucose (MAG) and N-(2-aminoethyl)methacrylamide (AEMA) copolymers was performed by Dr. Adam E. Smith and Antons Sizovs. Labeling of the 2-deoxy-2-methacrylamido glucose (MAG) and N-(2-aminoethyl)methacrylamide (AEMA) copolymers with FITC was performed by Antons Sizovs. The synthesis of the trehalose-containing polymers was carried out by Dr. Karina Kizjakina. Dr. Chen-Chang Lee synthesized the hepatocyte-targeted polymers. Size exclusion chromatography and viscometer measurements were carried out by Dr. Adam E. Smith. Dr. Stephen Werre assisted with the statistical analysis of the data.

Chapter 1 : Introduction

1.1 Nucleic Acid Delivery

Gene therapy has emerged as a relatively new concept for the treatment of many disorders,[1] including metastatic melanoma,[2] Duchenne muscular dystrophy,[3-4] and Severe Combined Immunodeficiency Disease (SCID).[5-6] The quest for effective treatment for these and other disorders using gene therapy is encumbered by the lack of safe, effective means for delivering the therapeutic nucleic acid to its target destination. An ideal vehicle for gene delivery must be able to bind nucleic acids, deliver them into the cell, protect the nucleic acids from degradation once inside the cell, and if carrying DNA the vehicle must be able to deliver the DNA to the nucleus, all while being non-toxic to the target cells. Choosing an ideal vehicle is not an easy task, and is currently a major issue in perfecting gene delivery for routine therapeutic use. Viruses have the innate ability to deliver genetic cargo to target cells and are currently being used in clinical trials, however, they are not ideal vehicles; they have been shown to illicit unwanted immune responses, have a small capacity for carrying nucleic acids, and are difficult to modify.[7] There are several systems being developed in response to the problems with viral vectors, including polymers, dendrimers, and lipids. Cationic polymer-based DNA vehicles have been developed to combat some of the problems associated with viral vectors[8] and are of interest due to the relative ease that they can be modified compared to viruses, allowing them to be tailored to fulfill specific needs. One example of polymer modification is adding targeting groups to facilitate uptake into certain cell types including tumor cells,[9-11] pulmonary epithelial cells[12-13] and liver cells.[14-16] Polymers can also be tailored by

altering side or end groups to enhance transfection efficiency[17-18] and improve serum stability.[19-21] Many of these polymers are able to interact with DNA to form polymer-DNA complexes (polyplexes) of 100 nm or less, allowing them to enter the cell *via* endocytic mechanisms.[8, 22] Given the wide array of possibilities for polymer modification and the polymers' ability to condense therapeutic DNA into nanoparticles, it is easy to see why the study of nanoparticles for use as delivery systems has increased steadily in recent years, and the field of nanotechnology is predicted to become a trillion dollar industry by 2015.[23] Elucidating structure-function relationships between polymers and intracellular interactions would lead to the rational design of safe, efficient polymers for therapeutic DNA delivery.

1.2 Polyamine-inspired Polymers as DNA Delivery Vehicles

Despite the recent surge in interest for the development of effective polymer therapeutics, the mechanisms of polymer DNA delivery and of polymer cytotoxicity remain largely unknown. Cationic polymer gene delivery vehicles were first suggested for use in the 1990s.[24-25] Many cationic polymers obtain their positive charge from amines that are protonated at physiological pH. The positive charge on these polymers allows them to electrostatically bind to the negatively-charged phosphate groups on DNA. Upon binding, the polymers condense DNA into a stable nanoparticle, forming a positively-charged polymer-DNA complex known as a "polyplex". The positive charge on the polyplex is due to the excess number of amines from the polymer in comparison to the phosphate groups from the DNA, forming a nitrogen-to-phosphate or "N/P" ratio greater than 1. From there, the mechanism of uptake and intracellular trafficking remains unknown and can vary depending on the polymer structure (Scheme 1.1). However,

since protein expression is observed in polyplex-treated cells it is clear that the DNA being delivered by the polymers is somehow reaching the nucleus, where it can be transcribed and translated into protein. Previous research in the Reineke group has focused on decoding the mechanism of DNA complexation,[26-27] polyplex uptake[28-29] and subsequent nuclear trafficking (unpublished results).

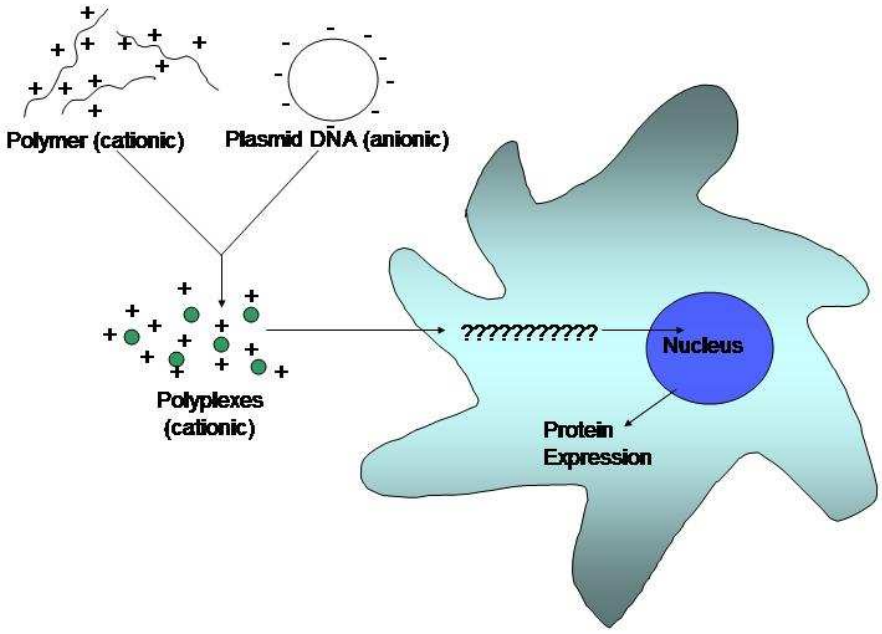

Scheme 1.1) How polycationic polymers deliver DNA. The positive charges along the polymer backbone allow it to interact with negative charges on the DNA backbone. The polymer condenses the DNA into a polymer-DNA complex (polyplex) which has a net positive charge. The positive charge on the polyplex allows it to interact with negatively-charged groups on the cell surface. The mechanism of polyplex uptake and DNA delivery remain largely unknown, but protein expression is observed in polymer transfection.

Common cationic polymers used for gene delivery are polyethylenimine (PEI) and chitosan. PEI is a polyamine initially described for use in gene therapy in 1995.[24] It is found in either a linear or a branched form, with the linear form being more efficient at gene delivery.[30-32] The amines in PEI exhibit a range in pKa's between a pH of 5 and 7, allowing them to carry a positive charge at a physiological pH.[33-34] This allows PEI to

electrostatically interact with negatively charged phosphate groups on DNA. PEI is effective at successfully delivering DNA into the nucleus of target cells; however, it is highly cytotoxic and the mechanism(s) of cytotoxicity remain largely unknown. Chitosan, another cationic polymer gene delivery vector, has also been shown to also deliver DNA into the nucleus. While not nearly as effective as PEI, chitosan has a low occurrence of cytotoxicity. In order to combine the high transfection efficiency of PEI with the low toxicity of chitosan, poly(glycoamidoamine)s (PGAAs) have been synthesized by Liu and Reineke (Figure 1.1).[35-36] They display lower cytotoxicity than PEI, but do not exhibit as much protein expression as PEI-treated cells. In order to rationally design ideal gene delivery vehicles, the mechanism of cytotoxicity along with how different polymer backbones affect intracellular trafficking and DNA delivery must be elucidated.

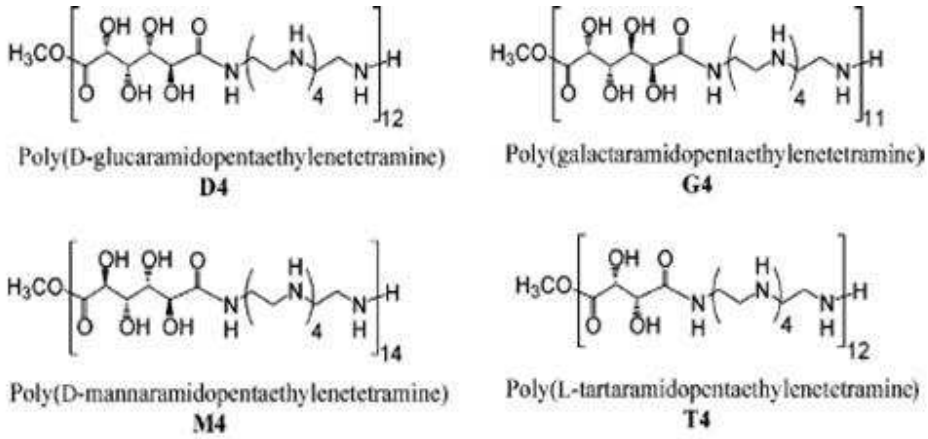

Figure 1.1.) The structure of the poly(glycoamidoamine)s (PGAAs). The PGAAs differ in the stereochemistry of the hydroxyl groups in their repeat units and, in the case of T4, the number of hydroxyl groups.

1.3 Comparing the Poly(glycoamidoamine)s and PEI

Previous research done by our group indicates that the PGAAs have a different transfection mechanism than PEI, but as of yet, this mechanism is currently unknown. It

is believed that the carbohydrate linkages on the PEI-like backbone of the PGAAs provide a more "bio-friendly" gene delivery vehicle. Both PEI and the PGAAs have a polyamine backbone that is protonated at physiological pH, giving them high cationic charge densities.[27] The amine groups may aid in endosomal buffering capacity, thus affording protection for the therapeutic nucleotide as well as a possible means of endosomal escape through the "proton sponge" mechanism.

The proton sponge theory is a hypothesis on how polyplexes escape endosomes and reach the cytoplasm. Once polyplexes and polymers are endocytosed, any non-protonated amines on the polymers can absorb protons and buffer endosomal pH. In order to compensate for the change in pH, proton pumps on the endosomal membrane pump more protons into the endosome, resulting in osmotic swelling and bursting of the endosomes. According to this theory, the higher the buffering capacity of a polymer, the more efficiently it can escape endosomes and thus polymers with high buffering capacities will yield higher protein expressions.[37-38] Contradictory to the proton sponge theory, other research has shown that when the buffering capacity of branched PEI is lowered by acetylating several amines on the polymer, transfection efficiency increases.[39] Furthermore, studies on modified PEI, β-cyclodextrin-containing polycationic polymers, and poly-L-lysine show no correlation between buffering capacity and transfection efficiency.[40] In addition, PEI has been shown to be able to directly permeabilize the plasma membrane of cells[41-43] as well as lysosomal membranes,[44] providing an alternative method of vesicle escape to the proton sponge theory. Research in our group has indicated that the PGAAs poly(L-tartaramidopentaethylenetetramine) (T4) as well as poly(galactaramidopentaethylenetetramine) (G4) are also able to induce plasma

membrane permeability, although to a lesser extent when compared with linear PEI.[28] The PGAAs T4 and G4 were also able to induce vesicle puncture when incubated with model liposomes, with T4 inducing vesicle disruption faster than G4.[28] It is possible that the PGAAs utilize different methods of endosomal escape than PEI resulting in the different cytotoxic and transfection efficiency profiles, but further work done in our group suggests that the proton sponge theory does not hold true for the PGAAs.

As mentioned previously, according to the proton sponge theory, polymers with higher buffering capacities should be able to escape from endosomes more readily, resulting in improved transfection efficiency. Previous work done in our group has shown that the buffering capacity of poly(L-tartaramidopentaethylenetetramine) (T4) decreases as the number of amines in the repeat unit increase from 1 to 4,[45] however, contradictory to the proton sponge theory, we also show an increase in transfection efficiency when 4 amines are present in the repeat unit compared to 1.[36] The main difference in structure between the PGAAs and PEI is the addition of repeat sugar units on the polyamine backbone for the PGAAs. This allows for some separation between amine groups, which may make it easier for more amines in the PGAAs to become protonated when compared to PEI due to an "intra-repeat unit interaction".[45] Within a repeat unit, when one amine becomes protonated, it electrostatically suppresses the protonation of neighboring amines. The presence of hydroxyl groups in the repeat unit of the PGAAs separates amines, and this "intra-repeat unit interaction" is seen in protonation trends for the PGAAs; for example, T1 (one amine in the repeat unit) has a higher degree of protonation at an acidic pH than T4 (four amines in the repeat unit).[45] Despite the higher protonation, T1 has a lower transfection efficiency than T4, and

despite T4's higher buffering capacity than PEI, PEI displays higher transfection efficiency,[45] further illustrating that the proton sponge theory may not apply to these polymer delivery systems. These studies also illustrate how changes in polymer structure can influence intracellular mechanisms. Research done in our group has also shown that the PGAA poly(galactaramidopentaethylenetetramine) (G4) remains in an acidic environment as long as 24 hours after transfection, while linear PEI is at a neutral pH at this time point (unpublished data), further proving that high buffering capacity does not always improve endosomal escape.

Based on our group's work comparing the different PGAAs, we show that the number of hydroxyl groups on the PGAAs as well as their stereochemistry affect cytotoxicity and transfection efficiency.[35] In addition to providing different buffering capacities, the hydroxyl groups also play a role in the degradation of the PGAAs, leading to a potential mechanism of pDNA release.[46] Also, past research has shown that the molecular weight and degree of branching for PEI play a part in cytotoxicity and transfection efficiency.[47-48] In order to provide insight on the mechanism of cytotoxicity for these polymers, the cytotoxicity of naturally occurring polyamines as well as polyamine derivatives was studied. Since we have shown that PEI is more toxic than the PGAAs, and that PGAAs with longer amine moieties are more toxic than those with shorter amine moieties, it was hypothesized that the amine moieties play a role in the mechanisms of cytotoxicity for these polymers. More specifically, we hypothesized that since PEI is a long polyamine chain, its mechanisms of cytotoxicity would be similar to that of naturally occurring polyamines. To study this further, the mechanisms of cytotoxicity for other polyamines were researched.

1.4 Polyamines and Cytotoxicity

There are naturally occurring polyamines present in all cells. They exhibit a wide range of functions (Table 1.1), including nucleic acid structure stabilization, ion channel control, and regulation of the cell cycle.[49-50] Intracellular polyamine homeostasis is closely regulated; a decrease or increase in intracellular polyamine concentration has been shown to cause apoptosis in a variety of cell lines[51-55] and polyamine deregulation has been implicated in several forms of cancer.[56-58] Furthermore, several wasp and spider toxins that target ionotropic receptors contain polyamine moieties.[59-60] Since the polymers tested herein also contain polyamine moieties, perhaps the mechanisms of toxicity for polyamine-containing toxins are similar to those of polyamine-containing polymers.

Table 1.1.) Some intracellular functions of the naturally-occurring polyamines spermine, spermidine, and putrescine and polyamine derivatives.

Intracellular Function	Mechanisms of Action
Regulation of cell cycle	Required for degradation of cyclin B1,[61] regulation of cyclin D1 and cyclin E1,[62] induction of CDK inhibitor p21[63]
Nucleic acid stabilization	Binding and compacting DNA[64-66]
Ion channel control	Spermine blocks receptor channel pores in Ca^{2+}-permeable glutamate receptors,[67] regulation of sodium and potassium channels,[55] interference with inositol-1,4,5-triphosphate binding sites[55]

Apoptosis regulation	Prevent mitochondrial permeability transition pore activation,[68] involvement in caspase cascade,[69] regulation of p53[51]

The mechanisms of cytotoxicity for naturally occurring polyamines as well as polyamine derivatives vary, depending on the specific polyamine and the cell type. Since PEI and the poly(glycoamidoamine)s have polyamine backbones, perhaps the mechanism of cytotoxicity of polyamine-based gene delivery vectors can be elucidated by studying mechanism of toxicity for the shorter, naturally-occurring polyamines and polyamine derivatives. Specifically, polyamines' harmful interactions with mitochondria[70-72] and the increase in reactive oxygen species (ROS) from the catabolism of increased intracellular polyamines[73-74] were the inspiration for several experiments described later in this work.

1.5 Goals of this Project and Dissertation Outline

Ultimately, the goals of this project have been to elucidate the mechanisms of how gene delivery polymers work and to determine structure-function relationships between gene delivery polymers and their mechanisms of action, with a focus on the mechanisms of cytotoxicity of certain polymers. Several hypotheses investigated herein are indicated in bold print in this section and are outlined by chapter in Section 1.6. In this work, different mechanisms of cytotoxicity were studied; those exhibited by naturally occurring polyamines inspired some hypotheses about cytotoxic mechanisms, while previous work done in the Reineke group incited questions about other potential mechanisms. While studying mechanisms of cytotoxicity, it was also of interest to study how polymer

function affects how polyplexes traffic to the nucleus. There have been many studies performed in the Reineke group studying mechanisms of intracellular uptake and intracellular trafficking, and the main questions the research presented in Chapter 4 attempted to answer are 1.) how polyplexes get to the nucleus and 2.) once at the nucleus, how does the plasmid DNA enter it?

The overarching hypothesis carried throughout these studies is that polymer structure influences intracellular mechanisms. Studies carried out on PEI, G4, T4, A4 and other polymers synthesized in the Reineke group illustrate this, as marked differences between cytoxicity and transfection efficiency were observed. Studies probing various potential mechanisms of cytotoxicity and nuclear trafficking/uptake were performed to elucidate these different mechanisms. Dynamic light scattering and zeta potential measurements illustrated the differences in size and charge that of polyplexes formed with different polymers. Various flow cytometric and plate reader-based assays illustrated the different cytotoxic profiles for the polymers studied, and confocal microscopy was used to determine intracellular locations at different time points for the polymers. Flow cytometric and confocal microscopy studies were performed on isolated nuclei to determine the role polymer structure has on pDNA nuclear uptake. Overall, these studies illustrate the importance of polymer structure and yield valuable information on future polymer design, which are emphasized in subsequent chapters.

Chapter 2 describes multiple studies done in an attempt to elucidate the mechanism of PEI-induced cytotoxicity. PEI is known as being toxic, and studies probing the effects PEI has on mitochondrial function as well as the effects of blocking certain routes to polyamine metabolism on PEI toxicity are illustrated. **Several hypotheses were tested**

in Chapter 2, including 1.) direct mitochondrial interaction with linear PEI causes cytotoxicity, 2.) PEI interacts with the endoplasmic reticulum (ER) during transfection and may induce apoptosis through an ER-mediated pathway, and 3.) blocking certain routes of polyamine catabolism may decrease PEI toxicity by decreasing production of harmful metabolites. Chapter 3 explores the role of polymer structure on cytotoxicity in more detail, with comparisons of cytotoxic profiles between polymers varying in molecular weight and with or without the presence of a hydroxyl moiety in their backbones. **These studies sought to determine whether higher molecular weight polymers were more efficient gene delivery vehicles, yet also more toxic due to their ability to directly permeabilize the nuclear envelope. It was our hypothesis that since polymers with hydroxyl groups in their backbone (T4) are able to degrade, they would be less toxic than non-degradable polymers (PEI and A4). Also, studies described in this chapter continue to study oxidative damage as a potential mechanism of toxicity, with the hypothesis that the presence of hydroxyl groups induced more ROS in cells during transfection.** Chapter 4 explores plasmid DNA nuclear import in more detail, and **studies were conducted to determine whether the presence and the number of hydroxyl groups present in the polymers' repeat units influenced the requirements for plasmid DNA nuclear entry.** Lastly, Chapter 5 describes studies performed on polymers tailored to yield specific characteristics, including increased hepatocyte targeting, increased colloidal stability in serum-containing media, and the ability to be tracked during transfection without the use of chemically attaching fluorescent dyes. These studies were performed in order to further illustrate how polymers have more flexibility in design than other gene delivery vehicles as well as

to determine how polymer modifications affect transfection efficiency. **It was our hypothesis that seemingly small changes in polymer structure would impact their transfection efficiency.**

1.6 Hypotheses by Chapter

Several hypotheses are tested throughout this work, and are highlighted in bold font in the previous section. In order to concisely present the hypotheses, this section lists each of the hypotheses tested in each chapter of this dissertation. As mentioned previously, the **hypothesis carried throughout this work is that polymer structure affects intracellular mechanisms.** More specific hypothesis can be found in the following chapters:

Chapter 2: This chapter focuses on elucidating the mechanism of why mitochondrial membrane potential is lowered during PEI transfection. The hypothesis tested are as follows:

1.) PEI polyplexes disrupt mitochondrial membrane potential (MMP) through direct interference with the mitochondria;
2.) MMP is lowered because PEI triggers apoptosis early in transfection, the decrease in MMP is a result of activation of the caspase cascade;
3.) MMP is lowered because PEI interferes with mitochondrial membrane pumps;
4.) MMP is lowered because PEI activates the mitochondrial permeability transition pore;
5.) Apoptosis is triggered due to PEI interfering with the endoplasmic reticulum;

6.) Apoptosis is initiated through the production of reactive oxygen species (ROS), therefore adding a ROS scavenger to PEI-treated cells will reduce toxicity.

Chapter 3: In chapter 3, the differences in cytotoxicity for several polymers were tested. The hypotheses in this chapter are:

1.) Polymers of smaller lengths are less toxic than longer polymers.

2.) The presence of hydroxyl groups is responsible for the decreased toxicity of T4 compared to PEI;

3.) Different mechanisms of cellular uptake are responsible for early toxicity (within 30 minutes of transfection);

4.) There is a link between high transfection efficiency and high toxicity with the polymers tested, this link is due to the fact that polymers with high transfection efficiency are able to directly permeabilize the nuclear envelope.

5.) The presence of hydroxyl groups leads to increased production of ROS and accounts for the different cytotoxic profiles of non-hydroxyl-containing polymers vs. polymers with hydroxyl groups.

Chapter 4: This chapter focuses on how differences in polymer structure affect how polyplexes are trafficked to the nucleus and also affect how plasmid DNA is imported into the nucleus. The hypotheses that this chapter tests are:

1.) The presence of a microtubule-disrupting agent lower the transfection efficiencies of hydroxyl-containing polymers more than PEI.

2.) Inhibiting mitosis will affect the transfection efficiencies of hydroxyl-containing polymers more than PEI.

3.) Polymer structure affects the minimal requirements for plasmid DNA nuclear import.

4.) Direct nuclear envelope permeabilization leads to higher pDNA nuclear import and therefore higher transfection efficiency.

Chapter 5: In this chapter, a variety of polymer libraries were synthesized to determine how seemingly small changes in polymer structure affect intracellular mechanisms. The hypotheses tested are as follows:

1.) The presence of galactose as a pendant group on polymers will increase receptor-mediated endocytosis for hepatocyte transfection. Furthermore, the length of the linker used to join galactose to the polymer will impact transfection efficiency.

2.) Different end groups on trehalose-containing polymers affect transfection efficiency and cytotoxicity.

3.) The length of primary amine-containing repeat units in copolymers affect intracellular uptake and pDNA release from the polyplexes.

4.) Chelating a lanthanide in the repeat unit of a polymer enables it to be used to study polymer-pDNA dissociation when used as a FRET pair with fluorescently-labeled pDNA.

1.7 References

1. Lyon, J.; Gorner, P., *Altered Fates: Gene Therapy and the Retooling of Human Life*. W.W. Norton and Company, Ltd.: New York, 1996.
2. Morgan, R. A.; Dudley, M. E.; Wunderlich, J. R.; Hughes, M. S.; Yang, J. C.; Sherry, R. M.; Royal, R. E.; Topalian, S. L.; Kammula, U. S.; Restifo, N. P.; Zheng, Z.;

Nahvi, A.; Vries, C. R. d.; Rogers-Freezer, L. J.; Mavroukakis, S. A.; Rosenberg, S. A., Cancer regression in patients after transfer of genetically engineered lymphocytes. *Science* **2006,** *314*, 126-129.
3. Webster, C.; Blau, H. M., Accelerated age-related decline in replicative life-span of Duchenne muscular dystrophy myoblasts: Implications for cell and gene therapy. *Somatic Cell and Molecular Genetics* **1990,** *16*, 557-565.
4. Denti, M. A.; Rosa, A.; D'Antona, G.; Sthandier, O.; Angelis, F. G. D.; Nicoletti, C.; Allocca, M.; Pansarasa, O.; Parente, V.; Musaro, A.; Auricchio, A.; Bottinelli, R.; Bozzoni, I., Body-wide gene therapy of Duchenne muscular dystrophy in the mdx mouse model. *Proc Natl Acad Sci U S A* **2006,** *103*, 3758-3763.
5. Cavazzana-Calvo, M.; Hacein-Bey, S.; Basile, G. d. S.; Gross, F.; Yvon, E.; Nusbaum, P.; Selz, F.; Hue, C.; Certain, S.; Casanova, J.-L.; Bousso, P.; Deist, F. L.; Fischer, A., Gene therapy of human severe combined immunodeficiency (SCID)-X1 Disease. *Science* **2000,** *288*, 669-672.
6. Blaese, R. M.; Culver, K. W.; Miller, A. D.; Carter, C. S.; Fleisher, T.; Clerici, M.; Shearer, G.; Chang, L.; Chiang, Y.; Tolstoshev, P.; Greenblatt, J. J.; Rosenberg, S. A.; Klein, H.; Berger, M.; Mullen, C. A.; Ramsey, W. J.; Muul, L.; Morgan, R. A.; Anderson, W. F., T Lymphocyte-directed gene therapy for ADA^- SCID: Initial trial results after 4 years. *Science* **1995,** *270*, 475-480.
7. Hunter, C. A., Molecular hurdles in polyfectin design and mechanistic background to polycation induced cytotoxicity. *Advanced Drug Delivery Reviews* **2006,** *58*, 1523-1531.
8. DeSmedt, S. C.; Demeester, J.; Hennink, W. E., Cationic polymer based gene delivery systems. *Pharm. Res.* **2000,** *17*, 113-126.
9. Wood, K. C.; Azarin, S. M.; Arap, W.; Pasqualini, R.; Langer, R.; Hammond, P. T., Tumor-targeted gene delivery using molecularly engineered hybrid polymers functionalized with a tumor-homing peptide. *Bioconjugate Chemistry* **2008,** *19*, 403-405.
10. Bellocq, N. C.; Pun, S. H.; Jensen, G. S.; Davis, M. E., Transferrin-containing, cyclodextrin polymer-based particles for tumor-targeted gene delivery. *Bioconjugate Chem.* **2003,** *14*, 1122-1132.
11. Blessing, T.; Kursa, M.; Holzhauser, R.; Kircheis, R.; Wagner, E., Different strategies for formation of PEGylated EGF-conjugated PEI/DNA complexes for targeted gene delivery. *Bioconjugate Chemistry* **2001,** *12*, 529-537.
12. Li, S.; Tan, Y.; Viroonchatapan, E.; Pitt, B. R.; Huang, L., Targeted gene delivery to pulmonary endothelium by anti-PECAM antibody. *American Journal of Physiology: Lung Cellular and Molecular Physiology* **1999,** *278*, L504-L511.
13. Elfinger, M.; Geiger, J.; Hasenpusch, G.; Uzgun, S.; Sieverling, N.; Aneja, M. K.; Maucksch, C.; Rudolph, C., Targeting to the β_2-adrenoceptor increases nonviral gene delivery to pulmonary epithelial cells *in vitro* and lungs *in vivo*. *Journal of Controlled Release* **2009,** *135*, 234-241.
14. Kang, J.-H.; Tachibana, Y.; Kamata, W.; Mahara, A.; Harada-Shiba, M.; Yamaoka, T., Liver-targeted siRNA delivery by polyethylenimine (PEI)-pullulan carrier. *Bioorganic and Medicinal Chemistry* **2010,** *18*, 3946-3950.
15. Zanta, M.-A.; Boussif, O.; Adib, A.; Behr, J.-P., In vitro gene delivery to hepatocytes with galactosylated polyethylenimine. *Bioconjugate Chemistry* **1997,** *8*, 839-844.

16. Lee, C.-C.; Grandinetti, G.; McLendon, P. M.; Reineke, T. M., A polycation scaffold presenting tunable "click" sites: conjugation to carbohydrate ligands and examination of hepatocyte-targeted pDNA delivery. *Macromolecular Bioscience* **2010,** *10*, 585-598.
17. Green, J. J.; Langer, R.; Anderson, D. G., A combinatorial polymer library approach yields insight into nonviral gene delivery. *Accounts of Chemical Research* **2008,** *41*, 749-759.
18. Zugates, G. T.; Peng, W.; Zumbuehl, A.; Jhunjhunwala, S.; Huang, Y.-H.; Langer, R.; Sawicki, J. A.; Anderson, D. G., Rapid optimazation of gene delivery by parallel end-modification of poly(β-amino ester)s. *Molecular Therapy* **2007,** *15*, 1306-1312.
19. Pun, S. H.; Davis, M. E., Development of a nonviral gene delivery vehicle for systemic application. *Bioconjugate Chemistry* **2002,** *13*, 630-639.
20. Dash, P. R.; Read, M. L.; Fisher, K. D.; Howard, K. A.; Wolfert, M.; Oupicky, D.; Subr, V.; Strohalm, J.; Ulbrich, K.; Seymour, L. W., Decreased binding to proteins and cells of polymeric gene delivery vectors surface modified with a multivalent hydrophilic polymer and retargeting through attachment of transferrin. *The Journal of Biological Chemistry* **2000,** *275*, 3793-3802.
21. Srinivasachari, S.; Liu, Y.; Zhang, G.; Prevette, L.; Reineke, T. M., Trehalose click polymers inhibit nanoparticle aggregation and promote pDNA delivery in serum. *Journal of the American Chemical Society* **2006,** *128*, 8176-8184.
22. Vijayanathan, V.; Thomas, T.; Thomas, T. J., DNA nanoparticles and development of DNA delivery vehicles for gene therapy. *Biochemistry* **2002,** *41*, 14085-14094.
23. Nel, A.; Xia, T.; Madler, L.; Li, N., Toxic potential of materials at the nanolevel. *Science* **2006,** *311*, 622-627.
24. Boussif, O.; Lezoualc'h, F.; Zanta, M. A.; Mergny, M. D.; Scherman, D.; Demeneix, B.; Behr, J. P., A versatile vector for gene and oligonucleotide transfer into cells in culture and in vivo: polyethylenimine. *PNAS* **1995,** *92*, 7297-7301.
25. Tomlinson, E.; Rolland, A. P., Controllable gene therapy: Pharmaceutics of non-viral gene delivery systems. *Journal of Controlled Release* **1996,** *39*, 357-372.
26. Prevette, L. E.; Lynch, M. L.; Kizjakina, K.; Reineke, T. M., Correlation of amine number and pDNA binding mechanism for trehalose-based polymers. *Langmuir* **2008,** *24*, 8090-1038.
27. Prevette, L. E.; Lynch, M. L.; Reineke, T. M., Amide spacing influences pDNA binding of poly(amidoamine)s. *Biomacromolecules* **2010,** *11*, 326-332.
28. McLendon, P. M.; Fichter, K. M.; Reineke, T. M., Poly(glycoamidoamine) vehicles promote pDNA uptake through multiple routes and efficient gene expression *via* caveolae-mediated endocytosis. *Molecular Pharmaceutics* **2010,** *7*, 738-750.
29. McLendon, P. M.; Buckwalter, D. J.; Davis, E. M.; Reineke, T. M., Interaction of poly(glycoamidoamine) DNA delivery vehicles with cell-surface glycosaminoglycans leads to polyplex internalization in a manner not soley dependent on charge. *Molecular Pharmaceutics* **2010,** *7*, 1757-1768.
30. Wiseman, J. W.; Goddard, C. A.; McLelland, D.; Colledge, W. H., A comparison of linear and branched polyethylenimine (PEI) with DCChol/DOPE liposomes for gene delivery to epithelial cells in vitro and in vivo. *Gene Therapy* **2003,** *10*, 1654-1662.

31. Wightman, L.; Kircheis, R.; Rossler, V.; Carotta, S.; Ruzicka, R.; Kursa, M.; Wagner, E., Different behavior of branched and linear polyethylenimine for gene delivery in vitro and in vivo. *Journal of Gene Medicine* **2001,** *3*, 362-372.
32. Uduehi, A. N.; Stammberger, U.; Frese, S.; Schmid, R. A., Efficiency of non-viral gene delivery systems to rat lungs. *European Journal of Cardio-thoracic surgery* **2001,** *20*, 159-163.
33. Han, J.; Kim, S. K.; Cho, T.-S.; Lee, J.-C.; Joung, H. S., Polyplex formation of calf thymus DNA with branched and linear polyethyleneimine. *Macromolecular Research* **2004,** *12*, 501-506.
34. Utsuno, K.; Uludag, H., Thermodynamics of polyethylenimine-DNA binding and DNA condensation. *Biophysical Journal* **2010,** *99*, 201-207.
35. Liu, Y.; Reineke, T. M., Hydroxyl stereochemistry and amine number within poly(glycoamidoamine)s affect intracellular delivery. *JACS* **2005,** *127*, 3004-3015.
36. Liu, Y., Wenning, L., Lynch, M., and Reineke, T.M., Gene delivery with novel poly(L-tartaramidoamine)s In *Polymeric Drug Delivery Volume I - Particulate Drug Carriers*, Svenson, S., Ed. American Chemical Society: Washington, D.C., 2005.
37. Akinc, A.; Thomas, M.; Klibanov, A. M.; Langer, R., Exploring polyethylenimine-mediated DNA transfection and the proton sponge hypothesis. *The Journal of Gene Medicine* **2005,** *7*, 657-663.
38. Kichler, A.; Leborgne, C.; Coeytaux, E.; Danos, O., Polyethylenimine-mediated gene delivery: A mechanistic study. *The Journal of Gene Medicine* **2001,** *3*, 135-144.
39. Forrest, M. L.; Meister, G. E.; Koerber, J. T.; Pack, D. W., Partial acetylation of polyethylenimine enhances *in vitro* gene delivery. *Pharm. Res.* **2004,** *21*, 365-371.
40. Kulkarni, R. P.; Mishra, S.; Fraser, S. E.; Davis, M. E., Single cell kinetics of intracellular, nonviral, nucleic acid delivery vehicle acidification and trafficking. *Bioconjugate Chem.* **2005,** *16*, 986-994.
41. Chen, J.; Hessler, J. A.; Putchakayala, K.; Panama, B. K.; Khan, D. P.; Hong, S.; Mullen, D. G.; DiMaggio, S. C.; Som, A.; Tew, G. N.; Lopatin, A. N.; Baker, J. R.; Holl, M. M. B.; Orr, B. G., Cationic nanoparticles induce nanoscale disruption in living cell plasma membranes. *J. Phys. Chem. B* **2009,** *113*, 11179-11185.
42. Hong, S.; Hessler, J. A.; Banaszak Holl, M. M.; Leroueil, P.; Mecke, A.; Orr, B. G., Physical interactions of nanoparticles with biological membranes: The observation of nanoscale hole formation. *Bioconjugate Chemistry* **2006,** *17*, 728-734.
43. Hong, S.; Leroueil, P. R.; Janus, E. K.; Peters, J. L.; Kober, M.-M.; Islam, M. T.; Orr, B. G.; Baker, J. R.; Holl, M. M. B., Interaction of polycationic polymers with supported lipid bilayers and cells: Nanoscale hole formation and enhanced membrane permeability. *Bioconjugate Chemistry* **2006,** *17*, 728-734.
44. Klemm, A. R.; Young, D.; Lloyd, J. B., Effects of polyethyleneimine on endocytosis and lysosome stability. *Biochem. Pharmacol.* **1998,** *56*, 41-46.
45. Liu, Y.; Reineke, T. M., Poly(glycoamidoamine)s for gene delivery. Structural effects on cellular internalization, buffering capacity, and gene expression. *Bioconjugate Chemistry* **2007,** *18*, 19-30.
46. Liu, Y.; Reineke, T. M., Degradation of poly(glycoamidoamine) DNA delivery vehicles: Polyamide hydrolysis at physiological conditions promotes DNA release. *Biomacromolecules* **2010,** *11*, 316-325.

47. Godbey, W. T.; Wu, K. K.; Mikos, A. G., Size matters: Molecular weight affects the efficiency of poly(ethylenimine) as a gene delivery vehicle. *J. Biomed. Mater. Res.* **1999,** *45*, 268-275.
48. Godbey, W. T.; Wu, K. K.; Mikos, A. G., Poly(ethyelimine)-mediated gene delivery affects endothelial cell function and viability. *Biomaterials* **2001,** *22*, 471-480.
49. Algranati, I. D.; Goldemberg, S. H., Polyamines and their role in protein synthesis. *Trends in Biochemical Sciences* **1977,** *2*, 272-274.
50. Hunter, A. R.; Farrell, P. J.; Jackson, R. J.; Hunt, T., The role of polyamines in cell-free protein synthesis in the wheat-germ system. *European Journal of Biochemistry* **1977,** *75*, 149-157.
51. Schipper, R. G.; Penning, L. C.; Verhofstad, A. A. J., Involvement of polyamines in apoptosis. Facts and controversies: effectors or protectors? *Seminars in Cancer Biology* **2000,** *10*, 55-68.
52. Hu, R.-H.; Pegg, A. E., Rapid induction of apoptosis by deragulated uptake of polyamine analogues. *Biochem. J.* **1997,** *328*, 307-316.
53. El-Salahy, E. M., Correlation between polyamines and apoptosis among Egyptian breast cancer patients. *Clinical Biochemistry* **2002,** *35*, 555-560.
54. Seiler, N.; Raul, F., Polyamines and apoptosis. *J. Cell. Mol. Med.* **2005,** *9*, 623-642.
55. Seiler, N., Pharmacological aspects of cytotoxic polyamine analogues and derivatives for cancer therapy. *Pharmacology and Therapeutics* **2005,** *107*, 99-119.
56. Gerner, E. W.; Meyskens, F. L., Polyamines and cancer: old molecules, new understanding. *Nature Reviews Cancer* **2004,** *4*, 781-792.
57. Bachrach, U., Polyamines and cancer: Minireview Article. *Amino Acids* **2004,** *26*, 307-309.
58. Verma, A. K., Polyamines and Cancer. In *Polyamine Cell Signaling*, Wang, J.-Y.; Casero, R. A., Eds. Humana Press: 2006; pp 313-328.
59. Mellor, I. R.; Usherwood, P. N. R., Targeting ionotropic receptors with polyamine-containing toxins. *Toxicon* **2004,** *43*, 493-508.
60. Stromgaard, K.; Jensen, L. S.; Vogenson, S. B., Polyamine toxins: Development of selective ligands for ionotropic receptors. *Toxicon* **2005,** *45*, 249-254.
61. Thomas, T.; Thomas, T. J., Regulation of cyclin B1 by estradiol and polyamines in MCF-7 breast cancer cells. *Cancer Res* **1994,** *54*, 1077-1084.
62. Thomas, T.; Thomas, T. J., Polyamines in cell growth and cell death: molecular mechanisms and therapeutic applications. *Cell. Mol. Life Sci.* **2001,** *58*, 244-258.
63. Kramer, D. L.; Vujcic, S.; Diegelman, P.; Alderfer, J.; Miller, J. T.; Black, J. D.; Bergeron, R. J.; Porter, C. W., Polyamine analogue induction of the p53-p21$^{WAF1/CIP1}$-Rb pathway and G_1 arrest in human melanoma cells. *Cancer Res* **1999,** *59*, 1278-1286.
64. Deng, H.; Bloomfield, V. A.; Benevides, J. M.; Thomas, G. J., Structural basis of polyamine-DNA recognition: spermidine and spermine interactions with genomic B-DNAs of different GC content probed by Raman spectroscopy. *Nucleic Acids Research* **2000,** *28*, 3379-3385.
65. Hou, M.-H.; Lin, S.-B.; Yuann, J.-M. P.; Lin, W.-C.; Wang, A. H.-J.; Kan, L.-S., Effects of polyamines on the thermal stability and formation kinetics of DNA duplexes with abnormal structure. *Nucleic Acids Research* **2001,** *29*, 5121-5128.

66. Esposito, D.; Vecchio, P. D.; Barone, G., Interactions with natural polyamines and thermal stability of DNA: A DSC study and a theoretical reconsideration. *Journal of the American Chemical Society* **1997,** *119*, 2606-2613.
67. Williams, K., Interactions of polyamines with ion channels. *Biochem. J.* **1997,** *325*, 289-297.
68. Tassani, V.; Biban, C.; Toninello, A.; Siliprandi, D., Inhibition of mitochondrial permeability transition by polyamines and magnesium: Importance of the number and distribution of electric charges. *Biochemical and Biophysical Research Communications* **1995,** *207*, 661-667.
69. Ray, R. M.; Viar, M. J.; Yuan, Q.; Johnson, L. R., Polyamine depletion delays apoptosis of rat intenstinal epithelial cells. *Am. J. Physiol. Cell Physiol.* **1999,** *278*, 480-489.
70. Salvi, M.; Toninello, A., Effects of polyamines on mitochondrial Ca^{2+} transport. *Biochimica et Biophysica Acta* **2004,** *1661*, 113-124.
71. Snyder, R. D.; Beach, D. C.; Loudy, D. E., Anti-mitochondrial effects of bisethyl polyamines in mammalian cells. *Anticancer Research* **1994,** *14*, 347-356.
72. Rilo, M. C.; Stoppani, A. O., Effect of polyamines on mitochondrial F-ATPase from Crithidia fasciculata and Trypanosoma cruzi. *Biochem. Mol. Biol. Int.* **1993,** *29*, 131-139.
73. Babbar, N.; Murray-Stewart, T.; Casero, R. A., Inflammation and polyamine catabolism: the good, the bad and the ugly. *Biochem. Soc. Trans.* **2007,** *35*, 300-304.
74. Seiler, N., Catabolism of polyamines. *Amino Acids* **2004,** *26*, 217-233.

Chapter 2 : Cytotoxicity of Poly(ethylenimine)

Based on the manuscript “Interaction of Poly(ethylenimine)-DNA Complexes with Mitochondria: Implications for Mechanisms of Cytotoxicity” from Grandinetti, G.; Ingle, N.P.; Reineke, T.M. *Molecular Pharmaceutics*, accepted.

2.1 Abstract

Poly(ethylenimine) (PEI) and PEI-based systems have been widely studied for use as nucleic acid delivery vehicles. However, many of these vehicles display high cytotoxicity, rendering them unfit for therapeutic use. By exploring the mechanisms that cause cytotoxicity, and through understanding structure-function relationships between polymers and intracellular interactions, nucleic acid delivery vehicles with precise intracellular properties can be tailored for specific function. Previous research has shown that PEI is able to depolarize mitochondria, but the exact mechanism as to how depolarization is induced remains elusive and therefore is the focus of the current study. Potential mechanisms for mitochondrial depolarization include direct mitochondrial membrane permeabilization by PEI or PEI polyplexes, activation of the mitochondrial permeability transition pore, and interference with mitochondrial membrane proton pumps, specifically Complex I of the electron transport chain and F_0F_1-ATPase. Herein, confocal microscopy and live cell imaging showed that PEI polyplexes do colocalize to some degree with mitochondria early in transfection, and the degree of colocalization increases over time. Cyclosporine *a* was used to prevent activation of the mitochondrial membrane permeability transition pore, and it was found that early in transfection

cyclosporine a was unable to prevent the loss of mitochondrial membrane potential. Further studies done using rotenone and oligomycin to inhibit Complex I of the electron transport chain and F_0F_1-ATPase, respectively, indicate that both of these mitochondrial proton pumps are functioning during PEI transfection. Overall, we conclude that direct interaction between polyplexes and mitochondria may be the reason why mitochondrial function is impaired during PEI transfection. Furthermore, this chapter presents data illustrating PEI polyplex-endoplasmic reticulum colocalization and the effect of inhibiting certain forms of polyamine metabolism on the toxicity of branched PEI.

2.2 Introduction

The delivery of nucleic acids has great potential for advancing biomedical and therapeutic research; however, the field has faced several obstacles that are mostly related to the lack of effective delivery methods. In response to the problems associated with viral vectors,[1] several research groups have developed polycation-based delivery vehicles. While some systems are effective, generally, the vehicles with the highest efficacy have been shown to display a cytotoxic response, and the mechanisms that cause cytotoxicity remain unclear. In particular, polyethylenimine (PEI) has been widely studied over the last decade as it is very efficient at delivering various types of nucleic acids into a wide variety of cell types.[2-8] Yet, the high cytotoxicity associated with this material has prevented it from being used clinically.[1, 9-12] Gaining a better understanding of the mechanisms associated with toxicity and the role that polymer structure plays in transfection will enhance the ability of researchers to design vehicles with the ideal combination of low toxicity and high delivery efficiency. Herein, we aim to further

advance the knowledge of how synthetic materials interact with and adversely affect cellular function by examining the specific effect of linear PEI on mitochondrial function, which is responsible for regulating cell cycle, differentiation, energy, signaling, growth, and cell death. To this end, we chose to use a commercially available linear PEI (JetPEI, Polyplus-transfection Inc.) due to its widespread use as a transfection reagent.

Currently, the mechanisms involved in the cytotoxic response of common delivery agents such as PEI are beginning to be uncovered but currently remain unclear. One study indicated altered gene expression in cells treated with branched 25 kDa PEI, with an increase in genes specific for oxidative stress, inflammation and cytotoxicity evident six hours after transfection.[13] Further studies by Godbey *et al*. on branched PEI indicate that cell death appears to occur in two phases; one at 2 hours characterized by altered cell morphology and cell detachment and a later phase occurring between seven and nine hours after transfection.[2] The later phase was characterized by increased secretion of the gene products tissue-type plasminogen activator (tPA), plasminogen activator inhibitor type 1 (PAI-1), and von Willebrand Factor (vWF). Increased levels of these gene products are linked to endothelial cellular stress responses.[14-17] Another study has found that 25 kDa branched PEI and 750 kDa linear PEI both induce toxicity in two phases; a necrotic-like cell death at 30 minutes of transfection and a mitochondrial-mediated apoptotic cell death at 24 hours after transfection.[12] The first involves an early necrotic-like toxicity due to membrane damage, characterized by lactate dehydrogenase (LDH) release in cells treated with PEI. It is interesting to note that in that study, phosphatidylserine externalization, a sign of apoptosis, was evident in cells treated with high concentrations of PEI within 30 minutes of transfection. However, the authors

mention that the early phosphatidylserine externalization could be due to necrotic-like damage as well as apoptosis, since the phosphatidylserine externalization occurred at the same time as LDH release.[12] The second mechanism involves a late, apoptotic-like cell death 24 hours after transfection.[12] Moghimi *et al.* concluded that the apoptotic-like cell death was a result of mitochondrial-mediated cell death pathways due to an increase in caspase 3 activation and loss of mitochondrial membrane potential 24 hours after transfection. Furthermore, Moghimi *et. al.* conducted additional studies to determine the mechanism of mitochondrial depolarization; isolated mitochondria were treated with either branched or linear PEI and cytochrome c release was measured, and it was found that branched PEI was able to induce more cytochrome c release than linear PEI. It was also found that there was no mitochondrial swelling or change in respiration during cytochrome c release, indicating that the mitochondrial permeability transition pore was not involved in PEI-induced cytochrome c release from isolated mitochondria.[12] The means by which mitochondrial membrane potential (MMP) is reduced during PEI transfection remains unknown; therefore, we chose to further investigate the interaction between polyplexes formed with linear PEI and mitochondria by performing several *in vitro* studies.

The effects of inhibiting the formation of the mitochondrial permeability transition pore were studied during PEI transfection to determine if our studies done within intact cells support the conclusions from the previous studies done in isolated mitochondria. In times of intracellular stress, the voltage-dependent anion channel (VDAC), adenine nucleotide translocase (ANT), and cyclophilin D come together to form a pore in the mitochondrial membrane known as the mitochondrial permeability transition pore

(MPTP). The opening of this pore results in the release of pro-apoptotic factors from the intermembrane space and loss of mitochondrial membrane potential.[18] Cyclosporine *a* (CsA) is able to stop this pore from opening by preventing cyclophilin D from complexing with the other proteins to form the pore;[19-20] this inhibits the loss of MMP and can prevent apoptosis in certain situations.[21-23]

In addition to MPTP activation, another possible reason for the loss of MMP could potentially be interference with membrane pumps.[10] Polyamines found in nature, such as spermine, putrescine, and spermidine,[24-26] along with polyamine analogues[27] such as pentaethylenehexamine, a small 232 Da linear PEI,[28] have also been found to bind to mitochondria and subsequently interfere with normal mitochondrial function. Natural polyamines and polyamine analogues have been shown to decrease mitochondrial protein synthesis,[29] induce the release of cytochrome c,[30] and interfere with calcium transport across the mitochondrial membrane.[24, 27-28] Given how a variety of polyamines are able to induce mitochondrial cytotoxicity,[31] it was of interest to us to study mitochondrial membrane pump disruption as a potential mechanism for how mitochondrial membrane potential is lost during PEI transfection. MMP is normally maintained by proton pumping *via* the electron transport chain (ETC) and F_0F_1-ATPase.[32] Complex I of the ETC can be inhibited by rotenone, and F_0F_1-ATPase can be inhibited by oligomycin, which are useful tools to examine the effects of these signaling pathways on toxicity mechanisms.[32] These inhibitors were used during PEI transfection to determine the contribution to MMP by these two mitochondrial membrane pumps.

Another possible reason for the loss of MMP during PEI transfection is that the PEI polyplexes could directly disrupt the mitochondrial membrane, allowing for release of

pro-apoptotic factors and eventual cell death. There has been work showing that branched 78 kDa PEI is capable of disrupting lipid membranes.[33-35] Indeed, if PEI is able to disrupt lipid membranes, it is possible that the observed loss of MMP is due to PEI disrupting the mitochondrial membrane. Researchers have previously suggested that one route to mitochondrial depolarization is the direct permeabilization of the outer mitochondrial membrane, allowing cytochrome c to escape the intermembrane space, leading to the activation of caspases and apoptosis.[12, 36] Since polyamines are capable of binding to mitochondria,[24] and given the ability of PEI to negatively impact MMP, it was of interest to us to further study these effects and, more specifically, examine the related outcomes of PEI polyplex interactions with the mitochondria as a function of time. Due to the negative impact of PEI on isolated mitochondrial function found in previous studies, it was of interest to us to study PEI polyplex-mitochondria interactions *in vitro*. Activation of the MPTP, inhibition of mitochondrial membrane pumps, and direct polyplex interaction with the mitochondrial membrane along with certain inhibitors used in the current study are illustrated in Scheme 2.1.

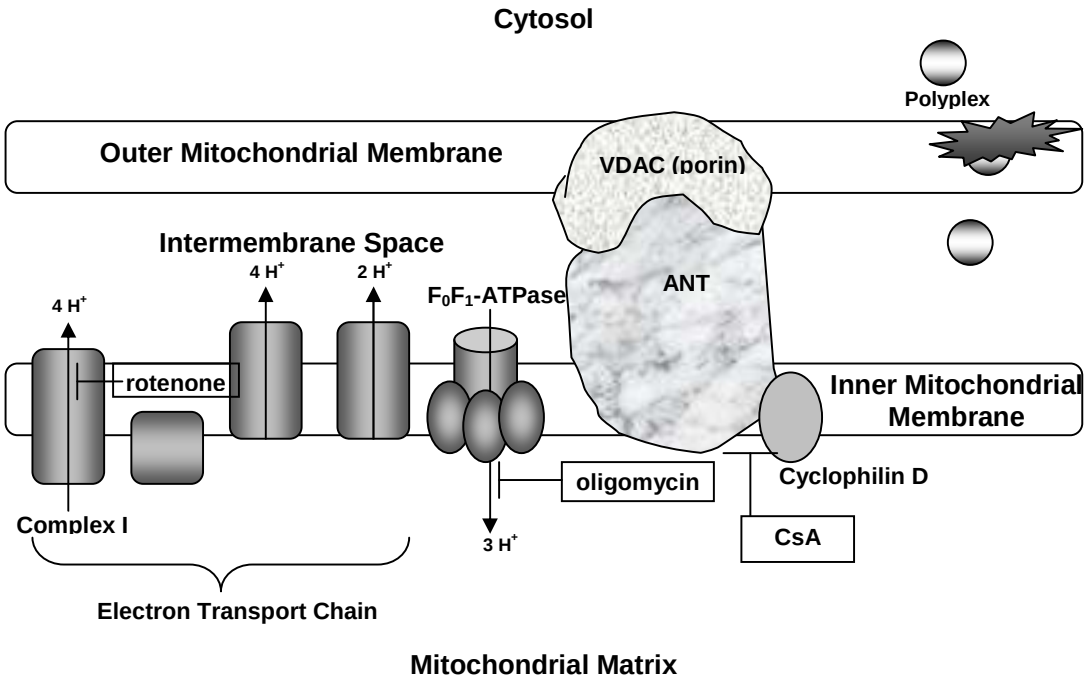

Scheme 2.1) Potential mechanisms as to how mitochondrial membrane potential (MMP) could be disrupted during PEI transfection (inhibitors of normal mitochondrial function are shown in boxes on the diagram). PEI could potentially interact with the electron transport chain or F0F1-ATPase, whose contributions to MMP can be observed using rotenone or oligomycin, respectively. The mitochondrial membrane permeability transition pore is formed during times of intracellular stress by the complexation of several proteins, including voltage-dependent anion channel (VDAC), adenine nucleotide translocase (ANT), and cyclophilin D. Cyclosporine a (CsA) is able to prevent the pore from opening and save the cell from apoptosis in certain cases. Additionally, PEI polyplexes could be directly permeabilizing the outer mitochondrial membrane, resulting in a loss of mitochondrial function.

Based on our results, we propose that the early toxicity of linear PEI is neither due to the opening of the mitochondrial permeability transition pore, nor because of direct interference with mitochondrial pumps. We also show that PEI is able to induce apoptosis early during transfection. In fact, we observe an increase in caspase-9 activity and mitochondrial membrane depolarization within one hour. Our data also indicate increasing colocalization between polyplexes and mitochondria over time. Thus, our data indicates the possibility of linear PEI initiating caspase activation by direct mitochondrial permeabilization, which ultimately leads to toxicity and cell death. Other mechanisms

for toxicity, including interaction with the endoplasmic reticulum and the possibility of harmful metabolites being formed during PEI transfection, are also investigated.

Endoplasmic reticulum (ER) stress has also been implicated in apoptosis.[37-40] Previous studies show that PEI may be trafficking through cells *via* a caveolae-mediated pathway,[41-43] which may provide a pathway for PEI polyplexes to reach the ER.[43-45] Therefore, ER stress pathways may also be implicated in the mechanism of cytotoxicity for PEI as well as the mitochondria. Also, as mentioned in Chapter 1, polyamine catabolism can lead to apoptosis, so it was of interest to us to determine if inhibiting polyamine catabolism would have any effect on the toxicity of PEI. We illustrate colocalization with PEI polyplexes and the endoplasmic reticulum within one hour after transfection, and no effect on the cytotoxicity or transfection efficiency of branched PEI in the presence of certain inhibitors of polyamine metabolism.

2.3 Materials and Methods

Cell culture media and supplements were purchased from Gibco (Carlsbad, CA). HeLa cells were purchased from ATCC (Rockville, MD). Cyclosporine *a* and oligomycin were obtained from CalBioChem (San Diego, CA). The mitochondrial membrane potential probe 1,1′,3,3,3′,3-hexamethylindodicarbocyanine iodide (DiIC(1)5), 4′,6-diamidino-2-phenylindole (DAPI), phosphatidylserine externalization probe Annexin V-Alexa Fluor 488, secondary goat anti-rabbit antibody, and viability probe Propidium Iodide were purchased from Molecular Probes (Eugene, OR) and used according to manufacturer's protocol. Linear PEI (JetPEI) was purchased from PolyPlus Transfections (Illkirch, France) and used according to manufacturer's protocol.

Rotenone, aminoguanidine, pentamidine, and monodansylcadaverine were purchased from Sigma (St. Louis, MO). Plasmid DNA (pCMV-luc) was purchased from Plasmidfactory (Bielefeld, Germany).

Polyplex formation: Jet-PEI (PEI) was added to a 0.02 μg/μL solution of plasmid DNA (pDNA) according to manufacturer's protocol to make a solution with a nitrogen-to-phosphate (N/P) ratio of 5. Polyplexes were allowed to incubate at room temperature for one hour prior to transfection. Where indicated, branched PEI (Sigma Aldrich) was used at the indicated N/P ratios. For the confocal microscopy studies, pDNA was labeled with Cy5 using a Cy5 *Label*IT® Nucleic Acid Labeling Kit from Mirus Bio, LLC (Madison, WI) according to manufacturer's protocol, which covalently links Cy5 to pDNA, and the Cy5-labeled pDNA was used to form polyplexes.

Mitochondrial membrane potential: HeLa cells were seeded at a density of 250,000 cells/well in a 6-well plate in Dulbecco's Modified Eagle Medium (DMEM) substituted with 10 % fetal bovine serum, 100 μg/mL streptomycin, 0.25 μg/mL amphotericin, and 100 units/mg penicillin. The cells were incubated at 37 °C and 5 % CO_2 for 24 hours. After 23 hours, polyplexes were formed at an N/P of 5 and using 5 μg of plasmid DNA per well. The final volume of each N/P 5 solution was 500 μL (250 μL of JetPEI solution added to 250 μL of plasmid DNA at a concentration of 0.02 μg/mL). Polyplexes were incubated for one hour at room temperature, after which 1 mL of serum-free OptiMEM was added to each 500 μL polyplex solution to form the transfection solution. Twenty-four hours after the cells were plated, the DMEM was aspirated from the cells, the cells were washed with 1mL of phosphate-buffered saline (PBS) per well, and 1.5 mL of transfection solution was added to each well. Transfections were performed in duplicate.

Cells were allowed to transfect for the indicated times, then transfection media was aspirated off, cells were washed twice with 1 mL of PBS/well and pelleted. The mitochondrial membrane potential-sensitive dye DiIC(1)5 was used according to manufacturer's protocol. The dye Annexin V-Alexa Fluor 488 was added to cells where indicated according to manufacturer's protocol to detect phosphatidylserine externalization. This dye binds only to cells with exposed phosphatidylserine, so an increase in Alexa Fluor 488 (AF488) fluorescence indicates an increase in phosphatidylserine externalization. The viability dye propidium iodide was used according to manufacturer's protocol. Flow cytometry was done on a BD FACSCanto II (Becton Dickinson Biosciences, San Jose, CA). A minimum of 50,000 events was collected for each sample.

Mitochondrial permeability transition pore inhibition. In order to study the role that the mitochondrial membrane permeability transition pore (MPTP) has on maintaining mitochondrial membrane potential during PEI transfection, the opening of the pore was inhibited using the drug cyclosporine *a*. HeLa cells were plated in 6 well plates and transfected as described above. At the indicated time points, cyclosporine *a* was dissolved in dimethyl sulfoxide (DMSO), then added to DMEM substituted with 10 % FBS to give a final concentration of 5 µM cyclosporine *a*. Then, 4 mLs of DMEM with or without cyclosporine *a* were added to each well. The cyclosporine *a* was allowed to incubate on the cells for one hour, after which MMP was measured using flow cytometry as described above using the dye DiIC(1)5.

Complex I and F_0F_1-ATPase inhibition. In order to determine whether the respiratory chain in the mitochondrial membrane were contributing to MMP in PEI-

treated cells, inhibitors of these pumps were used on PEI-transfected cells to see if MMP would be affected. To inhibit Complex I of the electron transport chain, 2 µM of rotenone was used as described previously.[46] To inhibit F_0F_1-ATPase, 5 µg/mL (6.3 µM) of oligomycin was used as described previously.[47] Briefly, the inhibitors were added at the indicated concentrations at 4 hours after transfection or 6 hours after transfection in order to determine if respiratory chain inhibition was the cause of the sudden loss of MMP observed at these time points. The inhibitors were allowed to incubate on the cells for one hour, and then MMP was analyzed using flow cytometry as described above.

Confocal microscopy: Previous work done on isolated mitochondria showed that polyplexes formed with 25 kDa PEI at a PEI/DNA weight ratio of 0.8/1 (roughly N/P ratio ~3) did not have strong mitochondrial interactions.[48] For our studies, we wanted to determine if linear PEI used at typical transfection conditions (N/P = 5) interacted with mitochondria in whole cells during transfection. HeLa cells were seeded onto poly-L-lysine (PLL)-coated 12 mm diameter round thickness No. 1 coverslips (Fisher Scientific, Pittsburgh, PA) in 12 well plates at a density of 15,000 cells per well. The cells were grown on coverslips for 48 hours in conditions described above (37 °C, 5 % CO_2, supplemented DMEM). Polyplexes were formed by adding 50 µL of PEI N/P = 5 solution to 50 µL of 0.02 mg/mL Cy5-labeled pDNA solution and allowing the polyplex solution to incubate for 1 hour at room temperature. Cells were transfected with 100 µL of polyplex solution diluted with 1 mL of OptiMEM for a total of 1 µg of pDNA per well. Cells were fixed at the indicated time points after transfection and all microscopy preparation was carried out in the dark at room temperature unless otherwise noted. Cells were fixed by incubating with 1 mL of 4 % paraformaldehyde (Sigma, St. Louis, MO)

per well for 15 minutes and permeabilized by incubating each well with 1 mL of 0.25 % Triton X-100 solution for 15 minutes. After permeabilization, cells were washed three times with 1 mL of PBS per well (cells were incubated in PBS for 5 minutes each wash) and blocked using 1 mL of 1 % bovine serum albumin (BSA) in PBS for 45 minutes. After blocking, cells were incubated with 1 mL of a 1:3000 dilution of rabbit monoclonal COX IV primary antibody (Cell Signaling Technologies, Danvers, MA) to label the mitochondria or a 1:200 dilution of rabbit polyclonal GRP78 BiP primary antibody (Abcam, Cambridge, United Kingdom) to label the endoplasmic reticulum for one hour. Cells were washed with 1 mL of PBS for each well, 5 minutes each wash, and then coverslips were placed face down in 100 µL of a 5 µg/mL goat anti-rabbit secondary antibody conjugated to Alexa Fluor 555 or Alexa Fluor 488 (Molecular Probes, Eugene, OR) in a humidified chamber for one hour. Cells were washed three times with PBS as described previously, and coverslips were placed cells-side-down in 300 µL of a 300 nm solution of DAPI (Molecular Probes, Eugene, OR) for five minutes to stain the nuclei. Coverslips were washed again with PBS as described above and mounted onto slides using 12 µL of Prolong Antifade Gold Reagent (Molecular Probes, Eugene, OR) per coverslip. Coverslips were sealed with clear nail polish after 24 hours. Cells were imaged on a Zeiss LSM 510 META confocal microscope (Carl Zeiss, Thornwood, NY) and colocalization analyses on fixed cells was performed using the software ImageJ.[49]

Inhibition of polyamine metabolism. The main routes to catabolize polyamines in cells are acetylation, oxidation, and cross-linking.[50] HeLa cells were plated into 24 well plates at a density of 50,000 cells/well in media containing either 1mM aminoguanidine to inhibit polyamine oxidase (oxidation),[51-52] 90 µM monodansylcadaverine to inhibit

transglutaminase (cross-linking),[50, 53] or 20 μM of pentamidine to inhibit polyamine oxidase and spermidine/spermine N-1 acetyltransferase (SSAT) (oxidation and acetylation).[54-55] The cells were incubated for 24 hours, after which cells were transfected in OptiMEM with branched PEI at the indicated N/P ratios (1 μg pDNA/well) as previously described.[56] Four hours after transfection, 800 μL of fresh 10 % FBS DMEM was added to each well. Twenty-four hours after transfection, cell viability was assayed by measuring the amount of protein in cell lysates using Bio-Rad's DC Protein Assay (Hercules, CA) as previously described[57] and transfection efficiency was analyzed using Promega's luciferase assay reagent (Madison, WI) as previously described.[56]

Statistical analysis: All data are presented as mean ± standard deviation. For statistical analysis of data, the JMP software was used (S.A.S. Institute Inc., Cary, NC) and means were compared using ANOVA followed by the Tukey-Kramer HSD method, with $p < 0.05$ being considered as statistically significant.

2.4 Results and Discussion

Due to the integral role of the mitochondria in cytotoxicity and apoptosis, we have explored in detail the mitochondrial interaction of a linear, 22 kDa PEI (JetPEI, Polyplus-transfection Inc.), due to its widespread use in the literature and its utility as a transfection reagent.[58-59] To study PEI polyplex-mitochondrial interactions, flow cytometry assays, confocal microscopy, and live cell imaging techniques were used to study the interaction of polyplexes and mitochondria over time to further delineate the role of this organelle in PEI-induced cytoxicity and cell death. The effects of cyclosporine *a* (mitochondrial permeability transition pore inhibitor), rotenone (inhibitor

of Complex I), and oligomycin, (F_0F_1-ATPase inhibitor) on the mitochondrial membrane potential of transfected cells were also studied to better understand mechanisms of mitochondrial depolarization during PEI transfection.

Onset of apoptosis. There are several distinct steps in apoptosis, including a decrease in mitochondrial membrane potential (mitochondrial depolarization) and phosphatidylserine externalization, two early signs of apoptosis.[60-63] To gauge the approximate time points when mitochondria start to become depolarized, studies probing the effect of PEI polyplex exposure early on in the transfection time course were performed using the mitochondrial membrane potential-sensitive cyanine dye DiIC(1)5 (Molecular Probes®, Invitrogen Corp., Eugene, OR). Here, we found about a 20 % decrease in DiIC1(5) fluorescence in PEI polyplex-treated cells one hour after transfection when compared to the cells only control, indicating a decrease in MMP (Figure 2.1, a). To monitor phosphatidylserine externalization, the dye Annexin V-Alexa Fluor 488 was used. Annexin V is able to bind to exposed phosphatidylserine, then fluorescence from the conjugated fluorescent dye Alexa Fluor 488 can be measured using flow cytometry to distinguish cells with externalized phosphatidylserine (apoptotic cells). A ~75 % increase in Annexin V-Alexa Fluor 488 fluorescence was found in cells transfected with PEI polyplexes compared to the cells only control after 30 minutes (Figure 2.1, b). Increased Annexin V fluorescence was also observed in PEI polyplex-treated cells compared to cells only one hour after transfection (Figure 2.1, b). The results confirmed that PEI polyplexes are able to induce an appreciable loss ($p < 0.05$) of mitochondrial membrane potential and increased phosphatidylserine externalization

within one hour post-transfection compared to pDNA only, signifying that cells are experiencing apoptosis signals at early time points in transfection process.

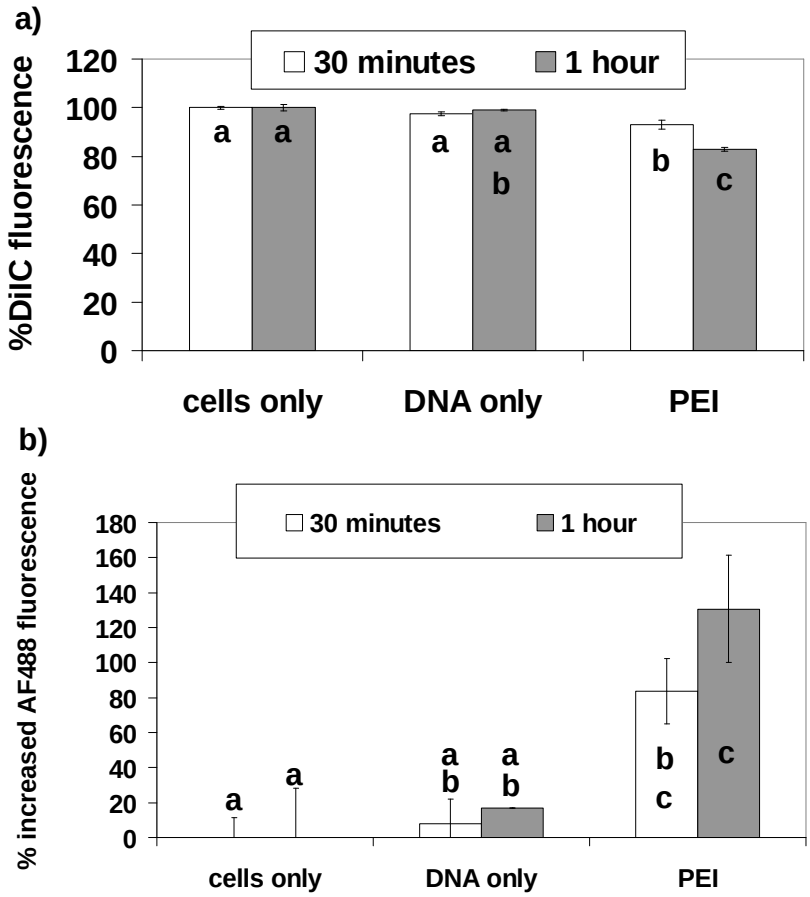

Figure 2.1) PEI induces apoptotic events at early time points after transfection. HeLa cells were allowed to transfect for the indicated time points before being analyzed by flow cytometry. (a) A loss in mitochondrial membrane potential (MMP) observed by a decrease in the fluorescence of DiIC1(5) and (b) an increase in phosphatidylserine externalization observed by an increase in Annexin V-Alexa Fluor 488 (AF488) fluorescence. Data were normalized to cells only control. AF488 fluorescence is presented as a % increase from cells only. Bars with different letters represent means that are statistically significant from each other ($p < 0.05$, $n = 2$) according to the Tukey-Kramer HSD method. Bars with matching letters represent means that are not statistically significant from each other.

Caspase-9 activation. To further understand and determine the point during the time course of transfection when cells are committed to apoptosis, the activation of the caspase cascade was studied. It should be noted that Moghimi *et al.* have studied the activation of caspase 3, an executioner caspase, 24 hours after treatment with free 25 kDa branched

PEI or 750 kDa linear PEI.[12] To further elucidate when apoptosis is first initiated during transfection, we have chosen to examine the time point of caspase-9 activation, an initiator caspase, early in linear PEI transfection. Caspase-9 is linked to mitochondrial-mediated apoptosis, and is activated upon release of cytochrome c. After this, apoptotic protease activating factor 1 (Apaf-1) is released from the mitochondria into the cytosol.[64-67] Upon release, cytochrome c and Apaf-1 combine to form a complex known as the apoptosome. The apoptosome then recruits procaspase-9, activating it into its proteolytic form of caspase-9.[64, 68-70] Caspase-9 then activates caspase-3, which goes on to cleave a variety of substrates and hastens the cell on its course to death.[71] To study caspase-9 activation, we utilized a carboxyfluorescein (FAM) linked *fl*uorochrome *i*nhibitor of *ca*spases (FLICA) specific for caspase-9 (Neuromics, Inc., Edina, MN). The FAM-FLICA reagent only binds to active caspase-9, any unbound reagent diffuses out of the cells. Once bound to active caspases, the fluorescence from the fluorochrome on the caspase inhibitor can be measured and used to observe caspase activation; in this case, an increase in fluorescence indicates an increase in caspase-9 activation. As shown in Figure 2.2, cells were transfected with linear PEI for the indicated time points. We chose to examine caspase-9 activation one hour after transfection because that is when we observed significant ($p < 0.05$) changes in mitochondrial membrane potential (Figure 2.1 a) and phosphatidylserine externalization (Figure 2.1 b). Our results reveal a ~300 % increase in caspase-9 activation as early as one hour after transfection (Figure 2.2 a), which corresponds to the observed loss of mitochondrial membrane potential and phosphatidylserine externalization previously shown (Figure 2.1). These results confirm that apoptosis is induced early during linear PEI polyplex transfection, although the exact

trigger for caspase-9 release remains unclear. It is possible that direct interaction of linear PEI with the mitochondria triggers this signaling cascade. Likewise, linear PEI could also initiate apoptosis elsewhere in the cell and that the release of caspase-9 is downstream from that event. Propidium iodide (PI) (Molecular Probes®, Eugene, OR) was used as a viability dye according to manufacturer's instructions; increased PI fluorescence indicates an increase in plasma membrane disruption. In this experiment, we found a ~250 % increase in PI fluorescence in PEI polyplex-treated cells one hour after transfection (Figure 2.2 b), indicating the plasma membrane integrity of these cells is also compromised at this early time point. PI is also used as a live/dead stain, so this increase in PI indicates cell death at this time point.

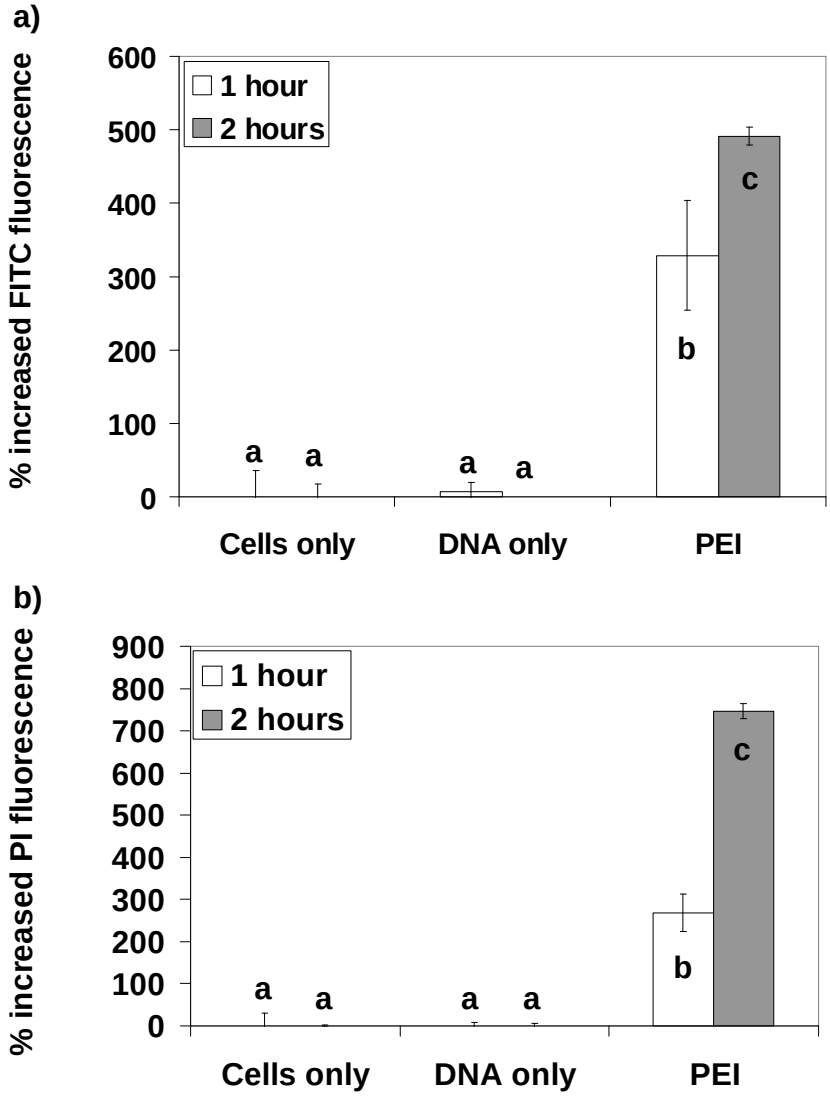

Figure 2.2) Cells were transfected for the indicated time points with PEI at an N/P of 5 and then analyzed using flow cytometry to study increases in (a) caspase-9 activity and (b) plasma membrane permeability as measured by increases in FITC and propidium iodide (PI) fluorescence, respectively. Results were normalized to a cells only control and data are presented as % increased fluorescence from cells only. Bars with matching letters are not statistically significant from each other, and bars with different letters represent means that are statistically significant from each other ($p < 0.05$, $n = 2$) as determined using the Tukey-Kramer HSD method.

Colocalization analysis between polyplexes and mitochondria over time. Data in Figures 2.1 and 2.2 indicate that apoptosis is signaled early on in the transfection process with linear PEI, which has further prompted us to investigate possible direct interaction

between PEI polyplexes and the mitochondria. Colocalization between mitochondria and Cy5-pDNA as observed in fixed HeLa cells at one hour and two hours post-transfection was measured. Microscopy images were taken using a slice thickness of 0.8 µM using a Zeiss LSM 510 META microscope and Zeiss ZEN 2009 software, and images were processed using ImageJ software to calculate the degree of colocalization between polyplexes and mitochondria. To observe colocalization, overlap between the channel representing mitochondria fluorescence and the channel representing pDNA fluorescence was calculated according to the method described by Manders *et. al.*[72-73] The degree of channel overlap can be represented as Manders coefficients, which range from 0 to 1 with 0 being no channel overlap and 1 being 100 % channel overlap. The Manders coefficients calculating the degree of channel overlap between the Cy5-labeled pDNA with antibody-labeled mitochondria were calculated at one hour post-transfection (Figure 2.3) and at two hours post-transfection (Figure 2.4); colocalized pixels are shown as white in both of these figures. At one hour after transfection, the Manders coefficient M1 (overlap of Cy5 fluorescence with secondary antibody fluorescence) was 0.349, indicating low colocalization (Figure 2.3). The degree of colocalization increased with time, as evidenced by the fact that the M1 result was 0.469 two hours after transfection (Figure 2.4).

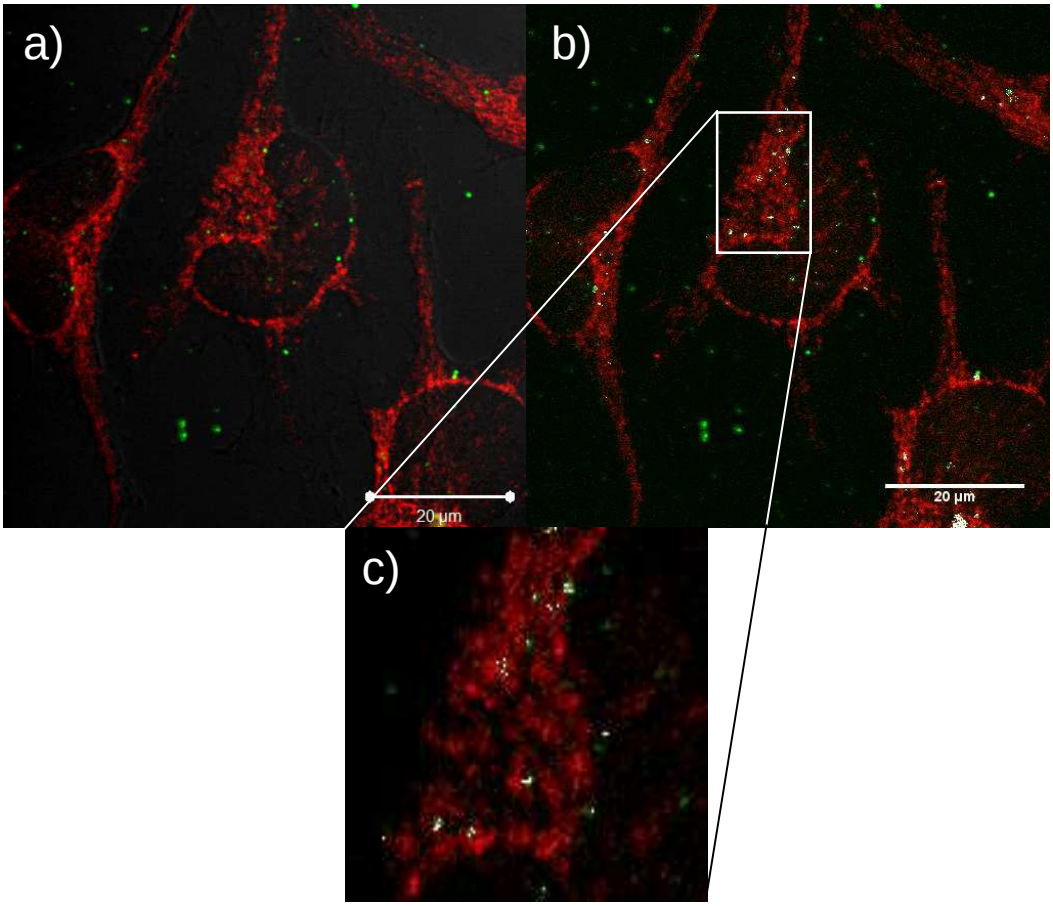

Figure 2.3) Confocal microscopy images of HeLa cells transfected with PEI polyplexes (shown as green from labeled pDNA) showing overlap with mitochondria (red). The cells were fixed one hour after transfection. (a) Image of whole cells transfected with PEI polyplexes. (b) Highlighting colocalized pixels; mitochondria are shown as red, polyplexes are shown as green, and colocalized pixels are shown as white. The Manders coefficient (M1) for the amount of green overlapping red was found to be 0.349. (c) Close up view from inside the box in (b) to further highlight colocalization between polyplexes and mitochondria. Scale bar = 20 µm.

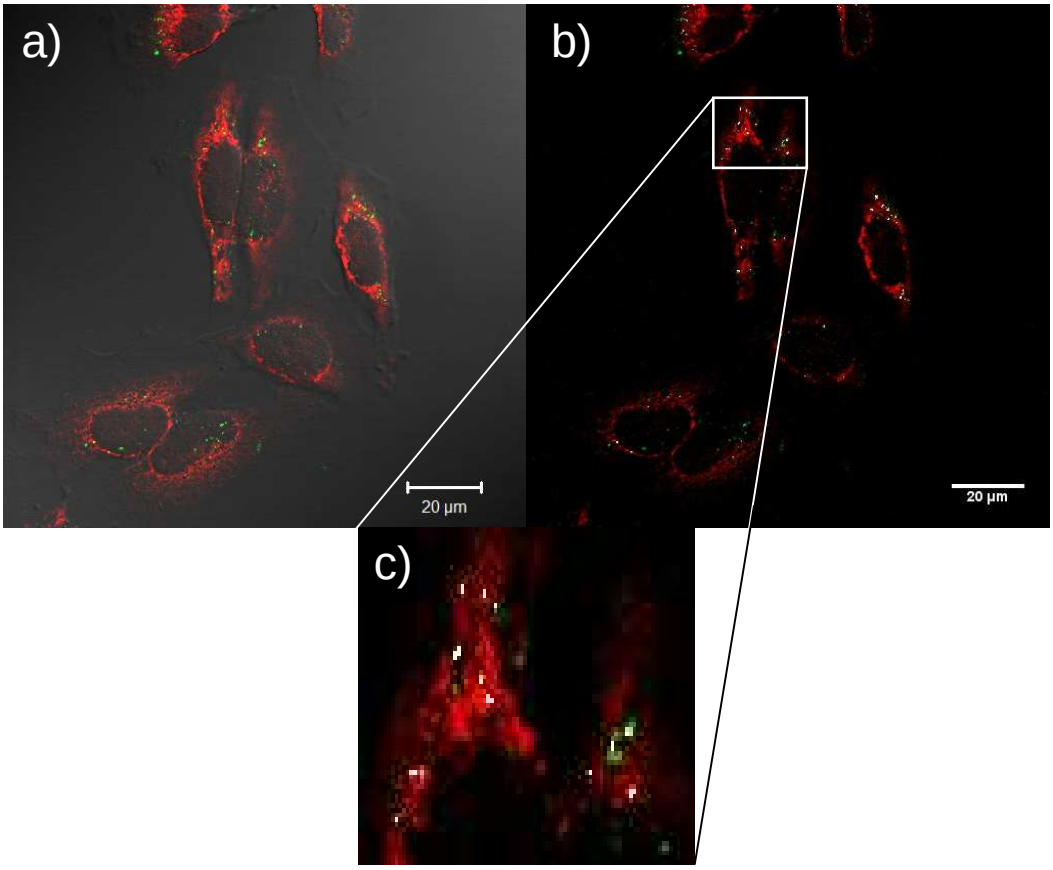

Figure 2.4) (a) Confocal microscopy image of HeLa cells transfected with PEI polyplexes two hours after transfection. Mitochondria are shown as red, polyplexes are shown as green. (b) Highlighting colocalized points, which are shown as white. The Manders coefficient (M1) for the amount of green overlapping red is 0.469 at this time point. (c) Zoomed-in image of the area indicated by the box in (b) to highlight colocalized pixels. Scale bar = 20 µm.

The apparent overlap of linear PEI-delivered pDNA with the mitochondria (Figures 2.3 and 2.4) prompted us to examine the possibility that the interaction of linear PEI with the mitochondria was responsible for the reduced mitochondrial function observed in transfected cells. Specifically, studies were carried out to understand the involvement of linear PEI with the mitochondrial permeability transition pore, Complex I of the electron transport chain, and the F_0F_1-ATPase pump and determine the roles of these pathways in the loss of mitochondrial membrane potential during PEI-mediated pDNA delivery.

Effect of cyclosporine *a* on PEI toxicity. One important factor in some forms of mitochondrial-induced apoptosis, as well as necrosis, is the mitochondrial permeability transition pore (MPTP), which is a high conductance channel that opens in times of cellular stress.[74] Opening of this pore causes mitochondrial swelling and loss of mitochondrial membrane potential.[75-76] The addition of the immunosuppressive drug, cyclosporine *a*, however, has been shown to prevent MPTP induction and cell death in cases of oxidative stress, hypoxia and the addition of chemical toxins.[75,32]

To investigate whether prohibiting the MPTP from opening would impede the loss of mitochondrial membrane potential and cell death, the drug cyclosporine *a* (CsA) was added to cells at various times after PEI transfection. In each case, the CsA was allowed to incubate on the cells for 1 hour, after which MMP was measured using flow cytometry. The data revealed that there was no effect of MPTP inhibition on the loss of mitochondrial membrane potential two hours after transfection (Figure 2.5 a). Next, in order to determine whether the MPTP contributed to loss of mitochondrial membrane potential at later time points, CsA was added to PEI-treated cells at indicated time points after transfection, allowed to incubate on cells for 1 hour, and then mitochondrial membrane potential was analyzed using flow cytometry. When measuring mitochondrial membrane potential 3 hours after transfection, we observed a sharp decrease in MMP in PEI polyplex-treated cells. PEI polyplex-treated cells with cyclosporine *a* added two hours after transfection were able to retain slightly higher ($p < 0.05$) mitochondrial membrane potential, but the loss of MMP was not completely prevented (Figure 2.5 a). Again, similar results were obtained when CsA was added 4 hours after transfection and MMP was measured 5 hours after transfection (Figure 2.5 a).

Although there was some slight recovery of MMP in PEI-treated cells in the presence of CsA, inhibiting the mitochondrial membrane permeability transition pore did not completely prevent or restore the loss of MMP.

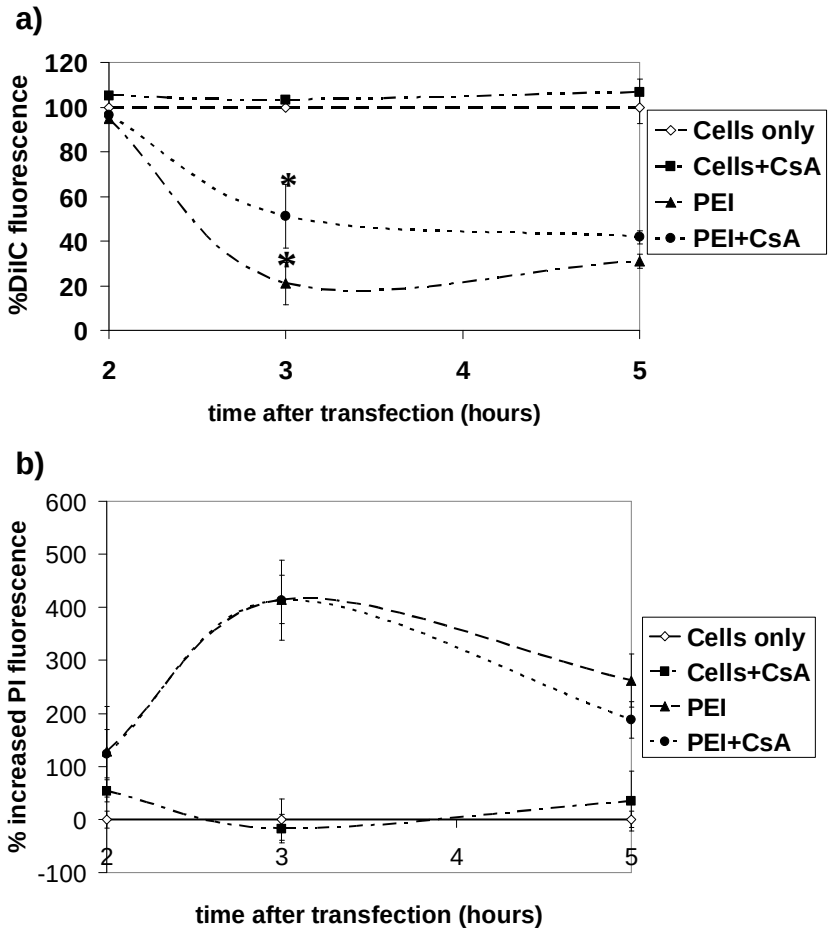

Figure 2.5) Flow cytometry results for PEI-transfected HeLa cells. Cells were analyzed at the indicated time points to determine the effect of cyclosporine *a* on (a) mitochondrial membrane potential and (b) propidium iodide (PI) uptake. * denotes statistical significance ($p < 0.05$) as determined by the Tukey-Kramer HSD method, n = 2.

Our results suggest that after two hours, even though mitochondrial membrane potential is lowered in PEI polyplex-treated cells, inhibiting the MPTP does not prevent the decrease in MMP. Our data also shows CsA to have no effect on MMP in PEI-treated

cells at 30 minutes and 1 hour after transfection (results not shown). However, at three hours post-transfection, a sharp decrease in MMP was observed, which is the point at which CsA begins to have an effect ($p < 0.05$) on MMP (Figure 2.5 a). It is possible that the early lowering (within 2 hours of transfection) of MMP is due to PEI polyplexes' direct mitochondrial interaction or interaction with other organelles, thus initiating apoptosis and stimulating the MPTP to form. As we noted, MMP was slightly ($p < 0.05$) less affected at the three-hour point in the presence of CsA, indicating that some of the loss of MMP can be attributed to the opening of the MPTP. A similar result occurred when CsA was added 4 hours after transfection and MMP was measured 5 hours post-transfection; there was a slight increase in MMP when cells were treated with cyclosporine *a* (Figure 2.5 a). Cyclosporine *a* had no dramatic effect on cell death, as indicated by propidium iodide fluorescence (Figure 2.5 b). From these data, we concluded that the decrease in MMP at the 3 hour time point was due in part to MPTP was being induced, which should not be considered the principal reason for the loss of mitochondrial membrane potential because MMP was already lowered previous to this time point (Figure 2.1). While the degree of MMP loss was slightly decreased in the presence of CsA, cell death was not prevented (Figure 2.5 b). This outcome further substantiates that loss of MMP may be a result, rather than the cause, of PEI polyplex-induced cytotoxicity. Rather, the observed reduction in MMP was more likely induced in response to cellular stress at these time points. Also, adding CsA with polyplexes and maintaining 5 µM CsA in transfected HeLa cells for two hours had no significant effect on MMP compared to cells treated with PEI polyplexes only (Figure 2.6 a), although we did observe an increase in PI positive cells when CsA was added with PEI polyplexes

(Figure 2.6 b). Instead, we believe this is a downstream occurrence of apoptosis that was initiated elsewhere in the cell. This conclusion is also supported by the caspase-9 data, which indicated that caspase-9 was being activated before the MPTP during PEI transfection (Figure 2.2). It is possible, therefore, that apoptotic signals such as caspase activation are responsible for inducing the opening of the mitochondrial permeability transition pore, as opposed to it being directly impacted by PEI. These data support previous research done using 25 kDa branched and 750 kDa linear PEI on isolated mitochondria, which has also found little involvement of the MPTP in PEI-induced mitochondrial depolarization.[12]

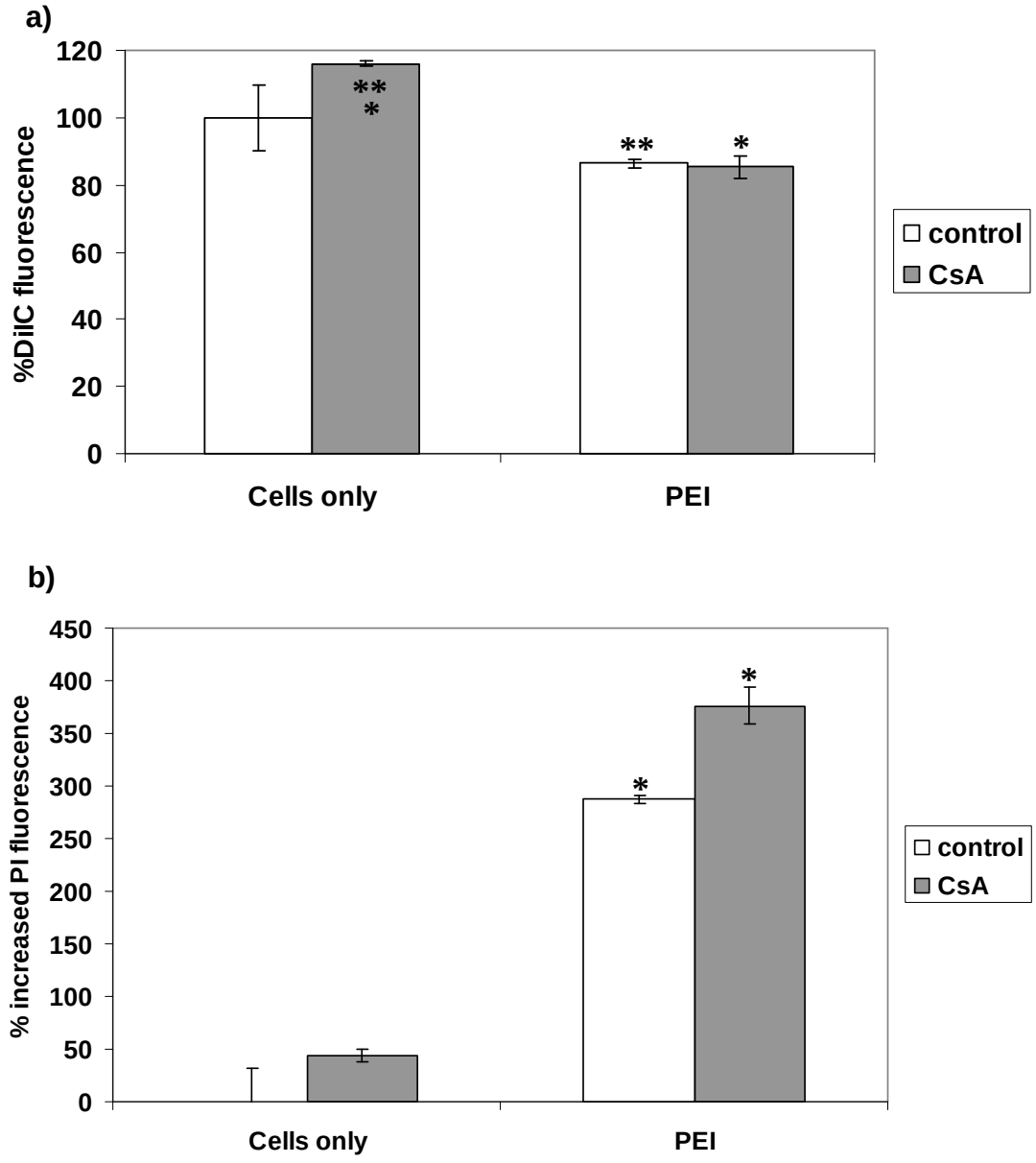

Figure 2.6) Effect of adding 5 μM cyclosporine a (CsA) with polyplexes and adding CsA again 1 hour after transfection. (a) Mitochondrial membrane potential was measured using the fluorescent dye DiIC(1)5 two hours after transfection. (b) Propidium iodide (PI) fluorescence was used to monitor plasma membrane integrity 2 hours after transfection in PEI polyplex-treated cells with and without CsA. Data were normalized to cells only control. * indicates statistical significance with $p < 0.05$ as determined by the Tukey-Kramer HSD method, n = 2. ** indicates statistical significance with $p < 0.05$ as determined by the Tukey-Kramer HSD method (n = 2).

Effect of PEI on mitochondrial respiratory chain function. Another possible mechanism associated with the loss of mitochondrial membrane potential is the direct

interaction of PEI and/or PEI polyplexes interact directly with mitochondrial membrane pumps. Normally, proton pumps found in the mitochondrial electron transport chain maintain membrane potential. However, if the pumps are inhibited, the electron transport chain will be inhibited, decreasing mitochondrial membrane potential. In order to maintain homeostasis, F_0F_1-ATPase pumps in the mitochondrial membrane can pump protons to maintain MMP in the presence of ATP.[46, 77] To study this further, we chose to inhibit Complex I of the electron transport chain, which is able to maintain MMP by pumping protons into the intermembrane space of mitochondria and forming a proton gradient. In the current study, rotenone was used as an inhibitor for Complex I.[46, 78] If Complex I is inhibited, there should be no observable change in mitochondrial membrane potential for the cells only control, since the F_0F_1-ATPase pump will be activated and be able to maintain MMP as long as ATP is present. However, if a decrease in MMP is observed in rotenone-treated cells, it would indicate that the F_0F_1-ATPase is inhibited, either through direct pump interference or *via* lack of ATP. Similarly, adding oligomycin, an F_0F_1-ATPase inhibitor,[46-47, 79] to cells should not affect MMP as long as the respiratory chain is functioning; if MMP is lowered in the presence of oligomycin it is indicative of an impaired respiratory chain or that the mitochondrial inner membrane is leaking protons.[80] We observed that neither rotenone nor oligomycin had an effect on mitochondrial membrane potential in the cells only controls (Figure 2.7). This is to be expected, since in the case of rotenone addition F_0F_1-ATPase would maintain MMP as long as ATP is present and in the case of oligomycin addition Complex I and the electron transport chain would still be functional and able to maintain MMP.[46] However, when rotenone was added to PEI polyplex-treated cells four hours after transfection, a decrease

in MMP was observed compared to cells treated with PEI only ($p < 0.05$, Figure 2.7 a). This indicates that the F_0F_1-ATPase is not properly functioning and is unable to compensate for the decrease in MMP for cells transfected with PEI, and by inhibiting Complex I it hastens the depolarization of mitochondria. The results also show that Complex I is still contributing to mitochondrial membrane potential at this time point; if it was dysfunctional prior to rotenone treatment, then the rotenone should have no further effect on the loss of MMP. Interestingly, a decrease in oligomycin-treated cells also results in a further decrease of MMP than in cells treated with PEI polyplexes only at this time point ($p < 0.05$, Figure 2.7 a). The results indicate that F_0F_1-ATPase is contributing to mitochondrial membrane potential, but one would expect this to be occurring only if the electron transport chain is inhibited or if the mitochondrial membrane is leaking protons.[46, 80] However, since the rotenone results suggest that the electron transport chain is functional at this time point, these results could indicate that PEI is inducing changes in MMP in other ways not involving mitochondrial respiratory chain inhibition, such as by inserting a channel into the mitochondrial membrane thus creating a "leaky proton" scenario. At 7 hours after transfection, neither rotenone nor oligomycin had a significant ($p < 0.05$) effect on MMP in PEI-polyplex treated cells (Figure 2.7 b), indicating that neither of these pumps were functional at this time point in PEI polyplex-treated cells. This is likely a result of activation of executioner caspases at this time, which disrupt mitochondrial function by cleaving Complex I of the electron transport chain. [1]

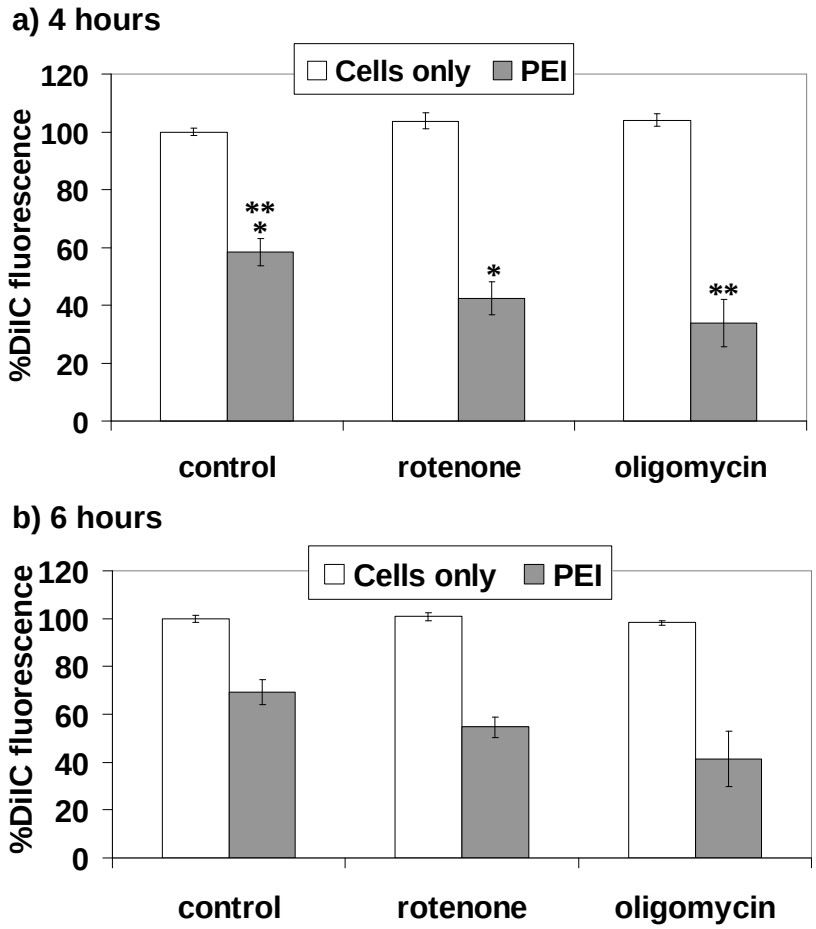

Figure 2.7) The effect of different respiratory chain inhibitors on mitochondrial membrane potential (MMP) at different time points during transfection. Rotenone (2 μM) was used to inhibit Complex I of the electron transport chain, and oligomycin (5 μg/mL) was used to inhibit F_0F_1-ATPase. Inhibitors were added either (a) 4 hours or (b) 6 hours after transfection with PEI polyplexes at an N/P ratio of 5. Cells were incubated with inhibitors for one hour, after which MMP was measured at either (a) 5 hours or (b) 7 hours after transfection. * denotes data is statistically significant from each other ($p < 0.05$) as determined by the Tukey-Kramer HSD method ($n = 2$). ** data is statistically significant from each other ($p < 0.05$, $n = 2$) using the Tukey-Kramer HSD method.

Colocalization between PEI polyplexes and the endoplasmic reticulum. It has previously been suggested that the endoplasmic reticulum (ER) may play a role in PEI polyplex trafficking.[42] Indeed, the ER has been implicated in several forms of apoptosis. Here, HeLa cells were transfected for one hour. We do show colocalization between the PEI polyplexes and the ER (Figure 2.8), supporting previous studies that PEI trafficks through a caveolae-mediated pathway.

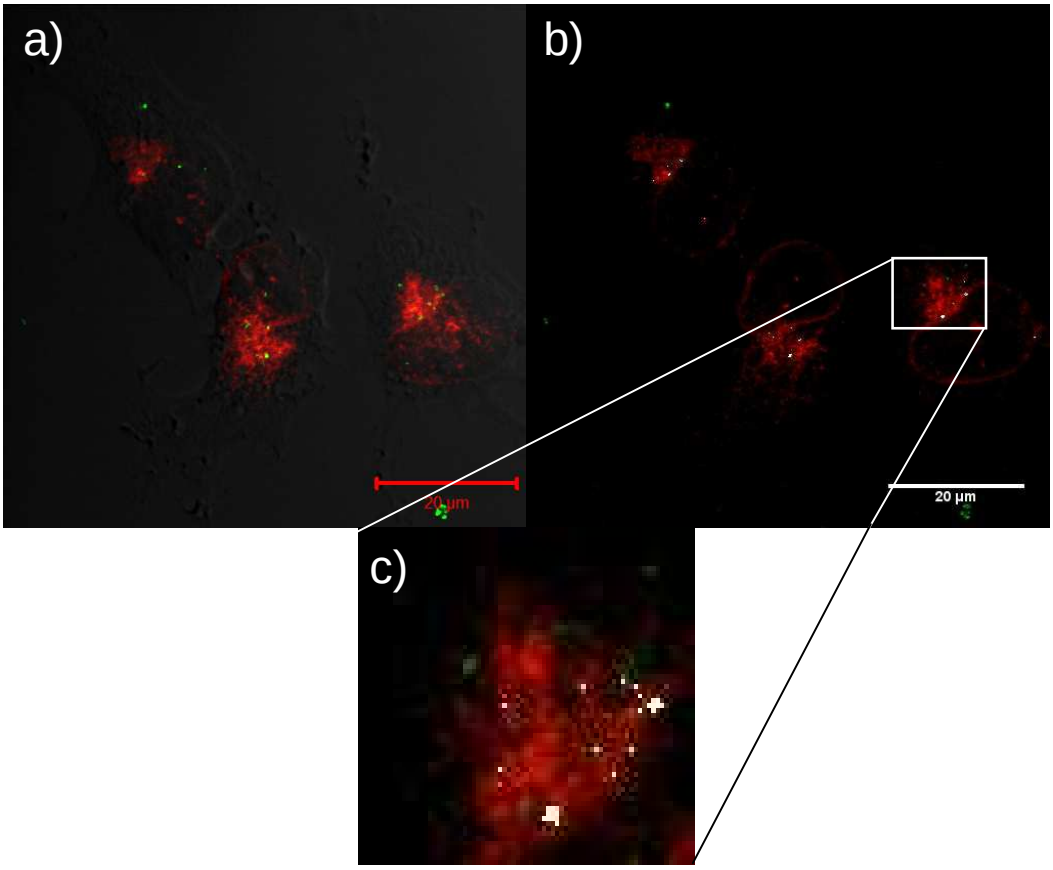

Figure 2.8) Confocal microscopy images of HeLa cells fixed 1 hour after transfection with PEI polyplexes. (a) Polyplexes are illustrated as green, and the endoplasmic reticulum is illustrated as red. (b) Highlighting colocalized points; pixels with high intensities for both the polyplex signal and the ER signal are shown as white; polyplexes are shown as green; and the ER is shown as red. Scale bar = 20 µM for (a) and (b). (c) Highlighting colocalized points, this image is zoomed in from the boxed portion of (b).

Effect of the inhibition of polyamine metabolism on branched PEI cytotoxicity. An increase in polyamine degradation products, particularly ROS, can cause apoptosis in a variety of cell lines.[54, 81] Previous research has shown that blocking polyamine catabolism can prevent apoptosis in certain cases. However, many of the chemicals used have other mechanisms of action in addition to inhibiting polyamine catabolism. For example, aminoguanidine has been shown to inhibit polyamine oxidase, but it can also inhibit other forms of oxidative-induced death.[82-83] The studies presented in this section

represent preliminary work to probe the effects of blocking certain intracellular pathways on branched PEI toxicity. The results of inhibiting polyamine oxidase/oxidative damage with aminoguanidine, inhibiting polyamine oxidase and SSAT with pentamidine, and the effects of inhibiting the enzyme transglutaminase with monodansylcadaverine are shown in Figure 2.9.

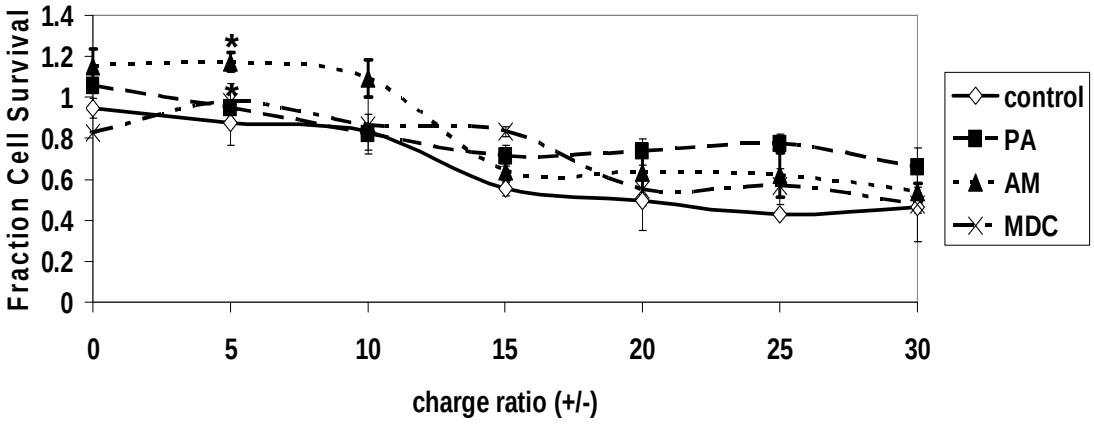

Figure 2.9) Effect of pentamidine (PA), aminoguanidine (AM), and monodansylcadaverine (MDC) on the cytotoxicity of branched PEI in HeLa cells. Cell viability was calculated by measuring protein content in cell lysates 48 hours after transfection. * denotes statistical significance ($p < 0.05$) according to the Tukey-Kramer HSD method with n = 3.

In order to be more relevant, these studies should be redone with JetPEI and using the different flow cytometric methods outlined above to study cytotoxicity. However, based on the results it would seem that none of these inhibitors dramatically alter cell viability during transfection. These data indicate that only aminoguanidine is able to slightly ($p < 0.05$) decrease the toxicity of branched PEI at an N/P ratio of 5. Further research probing the effects of aminoguanidine on polymer cytotoxicity is discussed in Chapter 3.

2.5 Conclusions and Future Goals

There are multiple toxicity pathways present in cells, and PEI has been implicated in several of these.[13] Indeed, there are likely multiple interactions between PEI and various intracellular components that could result in an array of cytotoxic events. Another consideration associated with cytotoxicity is the intracellular trafficking of free polymer versus polyplex. In this present study the focus has been on polyplexes; however, the free PEI polymer could also be initiating a wide variety of cytotoxic cell responses. The research described herein confirmed that PEI polyplexes do colocalize with mitochondria and the endoplasmic reticulum within one hour of transfection. Increased caspase-9 activity and phosphatidylserine externalization at one hour post-transfection were also evident, indicating that apoptosis was initiated early in transfection.

The colocalization between PEI polyplexes and mitochondria increase over time. Polyamines found in nature have been shown to bind to mitochondria and influence their activity. As discussed, previous research done on PEI has shown that mitochondrial membrane potential is lowered during transfection—the goal of this research was to elucidate the mechanisms that contribute to this reduction. Some possible explanations for mitochondrial depolarization include activation of the MPTP and interference with mitochondrial membrane pumps, neither of which proved to be factors early in transfection. However, our results do indicate some small involvement of the MPTP at later time points in transfection (after 3 hours), supporting the notion of a multiphase mechanism involved in the cytotoxic response with PEI-based polyplexes.[12-13] When performing studies on the contribution of Complex I and F_0F_1-ATPase to mitochondrial membrane potential, we have found that inhibition of either of these pumps results in a decrease in MMP in PEI polyplex-treated cells, indicating that these pumps are still

functional during PEI transfection. Had PEI or PEI polyplexes inhibited these pumps, the addition of rotenone or oligomycin should have no further effect on mitochondrial membrane potential. This outcome is similar to the one found when studying the mechanism of mitochondrial depolarization induced by P24, a cytotoxic adenine dinucleotide.[46]

The results show increased caspase-9 activity, decreased mitochondrial membrane potential, and increased phosphatidylserine externalization as early as one hour after treatments with PEI polyplexes at an N/P ratio of 5. Taken together, these data indicate that apoptosis is signaled very early on by polyplexes containing PEI. Even though colocalization between PEI polyplexes with the mitochondria is observed one hour after transfection, it is possible that PEI polyplexes or free PEI are interacting with other organelles in the cell and initiating apoptosis elsewhere, and that the decrease in MMP over time is a result of apoptosis initiation and the caspase cascade activation. One hypothesis was that PEI polyplexes could be interfering with the endoplasmic reticulum, and our confocal microscopy results confirm this. However, more studies need to be done to further elucidate the endoplasmic reticulum's contribution to PEI-induced apoptosis. A decrease in MMP over time was also observed, which correlated with an increase in PEI polyplex-mitochondria colocalization over time. While direct interaction and permeabilization of mitochondria with PEI remains a possibility, our results suggest that MTP activation and mitochondrial membrane pump dysfunction are not implicated as reasons for early MMP loss. Investigation into PEI and PEI polyplex interactions with other organelles resulting in various mechanisms of cytotoxicity is ongoing in our lab and will be reported in due course.

In addition to endoplasmic reticulum-mediated apoptosis, another possibility is oxidative damage formed from harmful metabolites of PEI, as is the case with several naturally occurring polyamines. The studies presented in Figure 2.9 represent preliminary data meant to act as a screening for potential agents for the inhibition of PEI cytotoxicity. We have found that only aminoguanidine was able to slightly increase cell survival when cells were transfected with PEI at an N/P of 5. For future work, different assays to monitor cytotoxicity as well as tests on linear PEI and other amine-containing polymers should be carried out.

Overall, data presented in this chapter provides an in-depth look at the interactions between PEI and mitochondria, and indicates some directions in which to take future cytotoxicity studies, namely the study of endoplasmic reticulum-mediated toxicity, and toxicity caused by potentially harmful byproducts of PEI catabolism, particularly ROS. These studies may serve as a guide for future endeavors in the study of PEI-mediated cytotoxicity. Furthermore, performing a microarray analysis and comparing RNA expression between control and PEI-treated cells may indicate certain toxicity pathways that can further elucidate the mechanism of PEI cytotoxicity.

2.6 References

1. Hunter, C. A., Molecular hurdles in polyfectin design and mechanistic background to polycation induced cytotoxicity. *Adv. Drug Delivery Rev.* **2006,** *58*, 1523-1531.
2. Godbey, W. T.; Wu, K. K.; Mikos, A. G., Poly(ethylenimine)-mediated gene delivery affects endothelial cell function and viability. *Biomaterials* **2001,** *22*, 471-480.
3. Rudolph, C.; Oritz, A.; Schillinger, U.; Jauernig, J.; Plank, C.; Rosenecker, J., Methodological optimization of polyethylenimine (PEI)-based gene delivery to the lungs of mice via aerosol applications. *The Journal of Gene Medicine* **2005,** *7*, 59-66.

4. Boussif, O.; Lezoualc'h, F.; Zanta, M. A.; Mergny, M. D.; Scherman, D.; Demeneix, B.; Behr, J. P., A versatile vector for gene and oligonucleotide transfer into cells in culture and in vivo: polyethylenimine. *PNAS* **1995,** *92*, 7297-7301.
5. Wightman, L.; Kircheis, R.; Rossler, V.; Carotta, S.; Ruzicka, R.; Kursa, M.; Wagner, E., Different behavior of branched and linear polyethylenimine for gene delivery *in vitro* and *in vivo*. *The Journal of Gene Medicine* **2001,** *3*, 362-372.
6. DiGioia, S.; Conese, M., Polyethylenimine-mediated gene delivery to the lung and therapeutic applications. *Drug Design, Development and Therapy* **2008,** *2*, 163-188.
7. Godbey, W. T.; Wu, K. K.; Mikos, A. G., Size matters: Molecular weight affects the efficiency of poly(ethylenimine) as a gene delivery vehicle. *J. Biomed. Mater. Res.* **1999,** *45*, 268-275.
8. Akinc, A.; Thomas, M.; Klibanov, A. M.; Langer, R., Exploring polyethylenimine-mediated DNA transfection and the proton sponge hypothesis. *The Journal of Gene Medicine* **2005,** *7*, 657-663.
9. Godbey, W. T.; Wu, K. K.; Mikos, A. G., Poly(ethyelimine)-mediated gene delivery affects endothelial cell function and viability. *Biomaterials* **2001,** *22*, 471-480.
10. Ira, Y., Mely, Y., and Krishnamoorthy, G., DNA vector polyethyleneimine affects cell pH and membrane potential: A time-resolved fluorescence microscopy study. *Journal of Fluorescence* **2003,** *13*, 339-347.
11. Lv, H., Zhang, S., Wang, B., Cui, S., and Yan, J., Toxicity of cationic lipids and cationic polymers in gene delivery. *J. Controlled Release* **2006,** *114*, 100-109.
12. Moghimi, S. M., Symonds, P., Murray, J.C., Hunter, A.C., Debska, G., and Szewczyk, A., A two-stage poly(ethyleneimine)-mediated cytotoxicity: implications for gene transfer/therapy. *Molecular Therapy* **2005,** *11*, 990-995.
13. Beyerle, A.; Irmler, M.; Beckers, J.; Kissel, T.; Stoeger, T., Toxicity pathway focused gene expression profiling of PEI-based polymers for pulmonary applications. *Mol. Pharmaceutics* **2010,** *7*, 727-737.
14. S.L. Diamond; Sharefkin, J. B.; Dieffenbach, C.; Frasier-Scott, K.; McIntire, L. V.; Eskin, S. G., Tissue plasminogen activator messenger RNA levels increase in cultured human endothelial cells exposed to laminar shear stress. *Journal of Cellular Phsyiology* **1990,** *143*, 364-371.
15. Wojta, J.; Holzer, M.; Hufnagl, P.; Christ, G.; Hoover, R. L.; Binder, B. R., Hyperthermia stimulates plasminogen activator inhibitor type 1 expression in human umbilical vein endothelial cells in vitro. *American Journal of Pathology* **1991,** *139*, 911-919.
16. Huber, D.; Cramer, E. M.; Kaufmann, J. E.; Meda, P.; Masse, J.-M.; Kruithof, E. K. O.; Vischer, U. M., Tissue-type plasminogen activator (t-PA) is stored in Weibel-Palade bodies in human endothelial cells both in vitro and in vivo. *Blood* **2002,** *99*, 3637-3645.
17. Cines, D. B.; Pollack, E. S.; Buck, C. A.; Loscalzo, J.; Zimmerman, G. A.; McEver, R. P.; Pober, J. S.; Wick, T. M.; Konkle, B. A.; Schwartz, B. S.; Barnathan, E. S.; McCrae, K. R.; Hug, B. A.; Schmidt, A.-M.; Stern, D. M., Endothelial cells in physiology and in the pathophysiology of vascular disorders. *Blood* **1998,** *91*, 3527-3561.
18. Crompton, M., The mitochondrial permeability transition pore and its role in cell death. *Biochem. J.* **1999,** *341*, 233-249.

19. Crompton, M.; Virji, S.; Ward, J. M., Cyclophilin-D binds strongly to complexes of the voltage-dependent anion channel and the adenine nucleotide translocase to form the permeability transition pore. *Eur. J. Biochem.* **1998,** *258*, 729-735.
20. Halestrap, A. P.; McStay, G. P.; Clarke, S. J., The permeability transition pore complex: another view. *Biochimie* **2002,** *84*, 153-166.
21. Griffiths, E. J.; Halestrap, A. P., Further evidence that cyclosporin A protects mitochondria from calcium overload by inhibiting a matrix peptidyl-prolyl *cis-trans* isomerase: Implications for the immunosuppressive and toxic effects of cyclosporin. *Biochem. J.* **1991,** *274*, 611-614.
22. Halestrap, A. P.; McStay, G. P.; Clarke, S. J., The permeability transition pore complex: another view. *Biochimie* **2002,** *84*, 153-166.
23. Weissig, V.; Cheng, S.-M.; D'Souza, G. G. M., Mitochondrial pharmaceutics. *Mitochondrion* **2004,** *3*, 229-244.
24. Salvi, M.; Toninello, A., Effects of polyamines on Ca^{2+} transport. *Biochimica et Biophysica Acta* **2004,** *1661*, 113-124.
25. Schuber, F., Influence of polyamines on membrane functions. *Biochem. J.* **1989,** *260*, 1-10.
26. Toninello, A.; Via, L. D.; Siliprandi, D.; Garlid, K. D., Evidence that spermine, spermidine and putrescine are transported electrophoretically in mitochondria by a specific polyamine uniporter. *J. of Biol. Chem* **1992,** *267*, 18393-18397.
27. Rustenbeck, I., Loptein, D., Fricke, K., Lenzen, S., and Reiter, H., Polyamine modulation of mitochondrial calcium transport. II. Inhibition of mitochondrial permeability transition by aliphatic polyamines but not by aminoglucosides. *Biochemical Pharmacology* **1998,** *56*, 987-995.
28. Rustenbeck, I.; Eggers, G.; Reitzer, H.; Munster, W.; Lenzen, S., Polyamine modulation of mitochondrial calcium transport I: Stimulatory and inhibitory effects of aliphatic polyamines, aminoglucosides and other polyamine analogues on mitochondrial calcium uptake. *Biochemical Pharmacology* **1998,** *56*, 977-885.
29. He, Y.; Suzuki, T.; Kashiwagi, K.; Kusama-Eguchi, K.; Shirahata, A.; Igarashi, K., Correlation between the inhibition of cell growth by bis(ethyl)polyamine analogues and the decrease in the function of mitochondria. *European Journal of Biochemistry* **1994,** *221*, 391-398.
30. Stefanelli, C.; Stanic, I.; Zini, M.; Bonavita, F.; Flamigni, F.; Zambonin, L.; Landi, L.; Pignatti, C.; Guarnieri, C.; Caldarera, C. M., Polyamines directly induce release of cytochrome c from heart mitochondria. *Biochem. J.* **2000,** *347*, 875-880.
31. Seiler, N., Pharmacological aspects of cytotoxic polyamine analogues and derivatives for cancer therapy. *Pharmacology and Therapeutics* **2005,** *107*, 99-119.
32. Bruzzone, S., Dodini, G., Kaludercic, N., Basile, G., Millo, E., DeFlora, A., DiLisa, F., and Zocchi, E., Mitochondrial dysfunction induced by cytotoxic adenine dinucleotide produced by ADP-ribosoyl cyclases from cADPR. *J. of Biol. Chem.* **2007,** *282*, 5045-5052.
33. Hong, S.; Hessler, J. A.; Banaszak Holl, M. M.; Leroueil, P.; Mecke, A.; Orr, B. G., Physical interactions of nanoparticles with biological membranes: The observation of nanoscale hole formation. *Bioconjugate Chem.* **2006,** *17*, 728-734.

34. Prevette, L. E., Mullen, D.G., and Banaszak Holl, M.M., Polycation-induced cell membrane permeability does not enhance cellular uptake or expression efficiency of delivered DNA. *Mol. Pharmaceutics* **2010,** *7*, 870-883.
35. Hong, S.; Leroueil, P. R.; Janus, E. K.; Peters, J. L.; Kober, M.-M.; Islam, M. T.; Orr, B. G.; Baker, J. R.; Holl, M. M. B., Interaction of polycationic polymers with supported lipid bilayers and cells: Nanoscale hole formation and enhanced membrane permeability. *Bioconjugate Chem.* **2006,** *17*, 728-734.
36. Ferri, K. F.; Kroemer, G., Organelle-specific initiation of cell death pathways. *Nature Cell Biol.* **2001,** *3*, 255-263.
37. Hu, Q.; Chang, J.; Tao, L.; Yan, G.; Xie, M.; Wang, Z., Endoplasmic reticulum mediated necrosis -like apoptosis of HeLa cells induced by Ca^{2+} oscillation. *Journal of Biochemistry and Molecular Biology* **2005,** *38*, 709-716.
38. Hussain, S. G.; Ramaiah, K. V. A., Endoplasmic reticulum: Stress, signalling and apoptosis. *Current Science* **2007,** *93*, 1684-1696.
39. Li, J.; Lee, B.; Lee, A. S., Endoplasmic reticulum stress-induced apoptosis. *The Journal of Biological Chemistry* **2006,** *281*, 7260-7270.
40. Xu, C.; Bailly-Maitre, B.; Reed, J. C., Endoplasmic reticulum stress: Cell life and death decisions. *The Journal of Clinical Investigation* **2005,** *115*, 2656-2664.
41. Aa, M. A. E. M. v. d.; Huth, U. S.; Hafele, S. Y.; Schubert, R.; Oosting, R. S.; Mastrobattista, E.; Hennick, W. E.; Peschka-Suss, R.; Koning, G. A.; Crommelin, D. J. A., Cellular uptake of cationic polymer-DNA complexes via caveolae plays a pivotal role in gene transfection in COS-7 cells. *Pharmaceutical Research* **2007,** *24*, 1590-1598.
42. McLendon, P. M.; Fichter, K. M.; Reineke, T. M., Poly(glycoamidoamine) vehicles promote pDNA uptake through multiple routes and efficient gene expression *via* caveolae-mediated endocytosis. *Molecular Pharmaceutics* **2010,** *7*, 738-750.
43. Grosse, S.; Aron, Y.; Thevenot, G.; Francois, D.; Monsigny, M.; Fajac, I., Potocytosis and cellular exit of complexes as cellular pathways for gene delivery by polycations. *The Journal of Gene Medicine* **2005,** *7*, 1275-1286.
44. Le, P. U.; Nabi, I. R., Distinct caveolae-mediated endocytic pathways target the Golgi apparatus and the endoplasmic reticulum. *Journal of Cell Science* **2003,** *116*, 1059-1071.
45. Pelkmans, L.; Kartenbeck, J.; Helenius, A., Caveolar endocytosis of simian virus 40 reveals a new two-step vesicular-transport pathway to the ER. *Nature Cell Biology* **2001,** *3*, 473-483.
46. Bruzzone, S.; Dodini, G.; Kaludercic, N.; Basile, G.; Millo, E.; DeFlora, A.; DiLisa, F.; Zocchi, E., Mitochondrial dysfunction induced by cytotoxic adenine dinucleotide produced by ADP-ribosoyl cyclases from cADPR. *J. of Biol. Chem.* **2007,** *282*, 5045-5052.
47. Shchepina, L. A.; Pletjushkina, O. Y.; Avetisyan, A. V.; Bakeeva, L. E.; Fetisova, E. K.; Izyumov, D. S.; Saprunova, V. B.; Vyssokikh, M. Y.; Chernyak, B. V.; Skulachev, V. P., Oligomycin, inhibitor of the F_0 part of H+-ATP-synthase, suppres the TNF-induced apoptosis. *Oncogene* **2002,** *21*, 8149-8157.
48. Choi, J. S.; Choi, M. J.; Ko, K. S.; Rhee, B. D.; Pak, Y. K.; Bang, I. S.; Lee, M., Low molecular weight polyethylenimine-mitochondrial leader peptide conjugate for DNA delivery to mitochondria. *Bull. Korean Chem. Soc.* **2006,** *27*, 1335-13340.

49. Rasband, W. S. *ImageJ*, U.S. National Institutes of Health: Bethseda, MA, 1997-2009.
50. Facchiano, F.; D'Arcangelo, D.; Riccomi, A.; Lentini, A.; Berninati, S.; Capogrossi, M. C., Transglutaminase activity in polyamine-induced programmed cell death. *Experimental Cell Research* **2001,** *271*, 118-129.
51. Wu, F.; Gehring, H., Structural requirements for novel coenzyme-substrate derivatives to inhibit intracellular ornithine decarboxylase and cell proliferation. *The FASEB Journal* **2009,** *23*, 565-574.
52. Takano, K.; Ogura, M.; Yoneda, Y.; Nakamura, Y., Oxidative metabolites are involved in polyamine-induced microglial cell death. *Neuroscience* **2005,** *134*, 1123-1131.
53. Yamaguchi, H.; Wang, H.-G., Tissue transglutaminase serves as an inhibitor of apoptosis by cross-linking caspase 3 in thapsigargin-treated cells. *Molecular and Cellular Biochemistry* **2006,** *26*, 569-579.
54. Wallace, H. M., Fraser, A.V., and Hughes, A., A perspective of polyamine metabolism. *Biochem. J.* **2003,** *376*, 1-14.
55. Libby, P. R.; Porter, C. W., Inhibition of enzymes of polyamine back-conversion by pentamidine and berenil. *Biochemical Pharmacology* **1992,** *44*, 830-832.
56. Liu, Y.; Reineke, T. M., Hydroxyl stereochemistry and amine number within poly(glycoamidoamine)s affect intracellular delivery. *JACS* **2005,** *127*, 3004-3015.
57. Liu, Y., Wenning, L., Lynch, M., and Reineke, T.M., Gene delivery with novel poly(L-tartaramidoamine)s In *Polymeric Drug Delivery Volume I - Particulate Drug Carriers*, Svenson, S., Ed. American Chemical Society: Washington, D.C., 2005.
58. Beyerle, A.; Hobel, S.; Czubayko, F.; Shulz, H.; Kissel, T.; Aigner, A.; Stoeger, T., In vitro cytotoxic and immunomodulatory profiling of low molecular weight polyethylenimines for pulmonary application. *Toxicology in Vitro* **2009,** *23*, 500-508.
59. Ohana, P.; Gofrit, O.; Ayesh, S.; Al-Sharef, W.; Mizrahi, A.; Birman, T.; Schneider, T.; Matouk, I.; Groot, N. d.; Tavdy, E.; Sidi, A. A.; Hochberg, A., Regulatory sequences of the H19 gene in DNA based therapy of bladder cancer. *Gene Ther Mol Biol* **2004,** *8*, 181-192.
60. Martin, S. J.; Reutelingsperger, C. P.; McGahon, A. J.; Rader, J. A.; Schie, R. C. v.; LaFace, D. M.; Green, D. R., Early redistrubution of plasma membrane phosphatidylserine is a general feature of apoptosis regardless of the initiating stimulus: inhibition by overexpression of Bcl-2 and Abl. *The Journal of Experimental Medicine* **1995,** *182*, 1545-1556.
61. Fabbri, F.; Carloni, S.; Brigliadori, G.; Zoli, W.; Lapalombella, R.; Marini, M., Sequential events of apoptosis involving docetaxel, a microtubule-interfering agent: A cytometric study. *BMC Cell Biology* **2006,** *7*, 6.
62. Engeland, M. v.; Nieland, L. J. W.; Ramaekers, F. C. S.; Shutte, B.; Reutelingsperger, C. P. M., Annexin V-affinity assay: A review on an apoptosis detection system based on phosphatidylserine exposure. *Cytometry* **1998,** *31*, 1-9.
63. Engeland, M. v.; Nieland, L. J. W.; Ramaekers, F. C. S.; Shutte, B.; Reutelingsperger, C. P. M., Annexin V-affinity assay: a review on apoptosis detection based on phosphatidylserine exposure. *Cytometry* **1998,** *31*, 1-9.
64. Shi, Y., A structural view of mitochondria-mediated apoptosis. *Nature Structural Biology* **2001,** *8*, 394-401.

65. Schimmer, A. D.; Hedley, D. W.; Penn, L. Z.; Minden, M. D., Receptor- and mitochondrial-mediated apoptosis in acute leukemia: a translational view. *Blood* **2001,** *98*, 3541-3553.
66. Kluck, R. M.; Bossy-Wetzel, E.; Green, D. R.; Newmeyer, D. D., The release of cytochrome c from mitochondria: a primary site for Bcl-2 regulation of apoptosis. *Science* **1997,** *275*, 1132-1136.
67. Desagher, S.; Osen-Sand, A.; Nichols, A.; Eskes, R.; Montessuit, S.; Lauper, S.; Maundrell, K.; Antonsson, B.; Martinou, J.-C., Bid-induced conformational change of Bax is responsible for mitochondrial cytochrome c release during apoptosis. *Journal of Cell Biology* **1998,** *144*, 891-901.
68. Shi, Y., Apoptosome: The cellular engine for the activation of caspase-9. *Structure* **2002,** *10*, 285-288.
69. Pop, C.; Timmer, J.; Sperandio, S.; Salvesen, G. S., The apoptosome activates caspase-9 by dimerization. *Molecular Cell* **2006,** *22*, 269-275.
70. Renatus, M.; Stennicke, H. R.; Scott, F. L.; Liddington, R. C.; Salvesen, G. S., Dimer formation drives the activation of the cell death protease caspase 9. *PNAS* **2001,** *98*, 14250-14255.
71. Slee, E. A.; Harte, M. T.; Kluck, R. M.; Wolf, B. B.; Casiano, C. A.; Newmeyer, D. D.; Wang, H.-G.; Reed, J. C.; Nicholson, D. W.; Alnemri, E. S.; Green, D. R.; Martin, S. J., Ordering the cytochrome c-initiated caspase cascade: hierarchichal activation of caspases-2, -3, -6, -7, -8, and -10 in a caspase-9-dependent manner. *Journal of Cell biology* **1999,** *144*, 281-292.
72. Manders, E. M. M.; Stap, J.; Brakenhoff, G. J.; Driel, R. V.; Aten, J. A., Dynamics of three-dimensional replication patterns during the S-phase, analysed by double labelling of DNA and confocal microscopy. *Journal of Cell Science* **1992,** *103*, 857-862.
73. Manders, E. M. M.; Verbeek, F. J.; Aten, J. A., Measurement of co-localizatin of objects in dual-colour confocal images. *Journal of Microscopy* **1993,** *169*, 375-382.
74. Kroemer, G.; Dallaporta, B.; Resche-Rigon, M., The mitochondrial death/life regulator in apoptosis and necrosis. *Annual Reviews in Physiology* **1998,** *60*, 619-642.
75. Lemasters, J. J., Nieminen, A., Qian, T., Trost, L.C., and Herman, B., The mitochondrial permeability transition in toxic, hypoxic and repurfustion injury. *Molecular and Cellular Biochemistry* **1997,** *174*, 159-165.
76. Zamzami, N.; Marchetti, P.; Castedo, M.; Hirsch, T.; Susin, S. A.; Masse, B.; Kroemer, G., Inhibitors of permeability transition interfere with the disruption of the mitochondrial transmembrane potential during apoptosis. *FEBS Letters* **1996,** *384*, 53-57.
77. Rego, A. C.; Vesce, S.; Nicholls, D. G., The mechanism of mitochondrial membrane potential retention following release of cytochrome c in apoptotic GT1-7 neural cells. *Cell Death and Differentiation* **2001,** *8*, 995-1003.
78. Li, N.; Ragheb, K.; Lawler, G.; Sturgis, J.; Rajwa, B.; Melendez, J. A.; Robinson, J. P., Mitochondrial complex I inhibitor rotenone induces apoptosis through enhancing mitochondrial reactive oxygen species production. *J. of Biol. Chem.* **2003,** *278*, 8516-8525.
79. Penefsky, H. S., Mechanism of inhibition of mitochondrial adenosine triphosphatase by dicyclohexylcarbodiimide and oligomycin: Relationship to ATP synthesis. *PNAS* **1985,** *82*, 1589-1593.

80. Rego, A. C.; Vesce, S.; Nicholls, D. G., The mechanism of mitochondrial membrane potential retention following release of cytochrome c in apoptotic GT1-7 neural cells. *Cell Death and Differentiation* **2001,** *8*, 995-1003.
81. Seiler, N., Catabolism of polyamines. *Amino Acids* **2004,** *26*, 217-233.
82. Nilsson, B. O., Biological effects of aminoguanidine: An update. *Inflammation Research* **1999,** *48*, 509-515.
83. Wolff, D. J.; Lubeskie, A., Aminoguanidine is an isoform-selective, mechanism-based inactivator of nitric oxide synthase. *Arch. Biochem. Biophys.* **1995,** *316*, 290-301.

Chapter 3 : Effect of Polymer Length and Composition on Cytotoxicity

Based on the manuscript "Direct Nuclear Permeabilization by Polymeric pDNA Vehicles: Efficient Method for Gene Delivery or Mechanism of Cytotoxicity?" from Grandinetti, G.; Smith, A.E.; Reineke, T.M. in preparation.

3.1 Abstract

The aim of this study is to compare the cytotoxicity mechanisms of linear PEI to those of two analogous polymers synthesized by our group: a hydroxyl-containing poly(L-tartaramidopentaethylenetetramine) (T4) and a version containing an alkyl chain spacer poly(adipamidopentaethylenetetramine) (A4) by studying the cellular responses to polymer transfection. We have also synthesized analogues of T4 with different molecular weights (degrees of polymerization of 6, 12, and 43) to examine the role of molecular weight on the cytotoxicity mechanism. Several other mechanisms of polymer-induced cytotoxicity are investigated, including plasma membrane permeabilization, the formation of potentially harmful polymer degradation products during transfection including reactive oxygen species, and nuclear membrane permeabilization. We hypothesized that since cationic polymers are capable of disrupting the plasma membrane, they may also be capable of disrupting the nuclear envelope, which would be a potential mechanism for delivery of plasmid DNA (pDNA) into the nucleus (as opposed to nuclear envelope breakdown during mitosis). Using flow cytometry and confocal microscopy, we show that the polymers with the highest transfection efficiency and toxicity, PEI and $T4_{43}$, are capable of inducing nuclear membrane permeability. This finding is important for the field of nucleic acid delivery in that not only could

permeabilization of the nucleus be a mechanism for pDNA nuclear import but also a potential mechanism of cytotoxicity and cell death.

3.2 Introduction

The delivery of nucleic acids has great potential to alleviate many disorders, but finding a safe and effective vehicle has proven to be a challenge. Viruses have the innate ability to deliver genetic cargo to target cells and are currently being used in clinical trials, however, they are not ideal vehicles; they have been shown to elicit unwanted immune responses, have a limited capacity, are not versatile for carrying a variety of nucleic acid forms, and are difficult to modify.[1] Cationic polymer-based DNA vehicles have been developed to combat some of the problems associated with viral vectors;[2] many of these polymers are able to interact with DNA to form polymer-DNA complexes (polyplexes) of 100 nm diameters or less.[3] The study of nanosystems for use as delivery vehicles has increased steadily in recent years, and the field of nanotechnology is predicted to become a trillion dollar industry by 2015.[4] Despite the recent surge in interest for the development of effective polymer therapeutics, the mechanisms of polymer-mediated DNA delivery and particularly of their cytotoxicity remain largely unknown.

Polyethylenimine (PEI) and PEI-based systems have undergone extensive study for their use as DNA delivery vehicles.[5-7] PEI is able to deliver its cargo DNA effectively, but its high cytotoxicity has hampered its use *in vivo*.[8-10] In an effort to create a safe and efficient cationic polymer vehicle for DNA delivery, our group has synthesized a series of poly(glycoamidoamine)s (PGAAs), which contain carbohydrate moieties along with

short PEI-like polyamines repeated along the backbone.[11-14] These polymers display significantly lower toxicity than PEI, and previous research in our group has shown that these PGAAs are taken into cells and trafficked internally by different mechanisms.[15-16] Further studies performed by our group show the presence of a carbohydrate moiety within the backbone of these polyamides facilitates their rapid degradation at physiological conditions.[17] Although less toxic than PEI, a small fraction of cell death still occurs with PGAA-transfected cells.

The aim of this study is to examine the role that polymer structure plays in transfection and toxicity during the polyplex transfection process. In particular, to yield insight into the mechanisms of toxicity for this class of polymers, we have focused on comparing one PGAA structure, T4, consisting of an L-tartarate monomer copolymerized with pentaethylenehexamine to an analogous model lacking hydroxyls that contains methylenes only, $A4_{42}$, which does not degrade. We also investigate the influence of T4 polymer length on the biological properties and utilize linear PEI as a control in these experiments. Understanding the differences in the mechanism of toxicity between these three vehicle structures is important to the general field of drug and nucleic acid delivery to enable rational vehicle design for high transfection and low toxicity. To this end, cells were transfected with five different polymer structures: a commercially available linear PEI (JetPEI), three different lengths of polymer T4 ($T4_6$, $T4_{12}$, and $T4_{43}$; subscript corresponding to the degree of polymerization), and polymer $A4_{42}$, which had a comparable degree of polymerization and molecular weight to $T4_{43}$. This study allowed us to examine the role of polymer molecular weight and the presence of hydroxyl groups have on polyplex toxicity and transfection efficiency with HeLa cells. Herein, it is

demonstrated that the presence or absence of hydroxyl groups as well as polymer length influence polyplex cytotoxicity significantly. Furthermore, we show that polymers with the highest transfection efficiency are also able to induce the most nuclear envelope permeability, thus providing a link between high cytotoxicity and high transfection efficiency observed in many polymer delivery systems.

3.3 Materials and Methods

Cell culture media and supplements were purchased from Gibco (Carlsbad, CA). Human cervix adenocarcinoma (HeLa) cells were purchased from ATCC (Rockville, MD). The mitochondrial membrane potential probe 1,1′,3,3,3′,3′-hexamethylindodicarbocyanine iodide (DiIC(1)5), phosphatidylserine externalization probe Annexin V-Alexa Fluor 488, nuclear stain 4′,6-diamidino-2-phenylindole (DAPI) and viability probe propidium iodide were purchased from Molecular Probes (Eugene, OR) and used according to manufacturer's protocol. Linear PEI (JetPEI) was purchased from PolyPlus Transfections (Illkirch, France) and used according to manufacturer's protocol.

Synthesis and characterization of polymers. To study the effect of polymer length on cytotoxicity for the T4 analogues, three different molecular weight polymers were synthesized by varying polymerization reaction times. The T4 was synthesized as described by Liu *et. al.*[13] except with some modifications; to create short T4 with a degree of polymerization of 6 ($T4_6$), the monomers were reacted for 4 days, and to synthesize the intermediate-sized T4 with a degree of polymerization of 12 ($T4_{12}$), the polymerization was carried out for 6 days, and in order to synthesize the longer T4

polymers with a degree of polymerization >40 ($T4_{43}$) the monomers were polymerized for 8 days. $A4_{42}$ (degree of polymerization of 42) was synthesized as previously described.[17] Gel permeation chromatography (GPC) was used to determine the average molecular weight (M_n) and polydispersity indices (PDIs) for the T4 and $A4_{42}$ polymers using an aqueous eluent of 1.0 wt% acetic acid/0.1 M Na_2SO_4. A flow rate of 0.3 mL/min, Eprogen Inc. (Downers Grove, IL) columns [CATSEC1000 (7μ, 50×4.6), CATSEC100 (5μ, 250×4.6), CATSEC300 (5μ, 250×4.6), and CATSEC1000 (7μ, 250×4.6)], a Wyatt HELEOS II light scattering detector (λ = 662 nm), a ViscoStar II differential viscometer, and an Optilab rEX refractometer (λ = 658 nm) were used. Astra V (version 5.3.4.18, Wyatt Technologies) was used for the determination of M_w, PDI, Mark-Houwink-Sakurada profile, and d*n*/dc of the polymers.

Polyplex characterization. Polyplexes were formed by adding 150 μL of polymer solution to 150 μL of plasmid DNA (pDNA) (0.02 μg/μL) at an N/P ratio of 20 for the PGAAs. Polyplexes formed with PEI were formed the same way except an N/P ratio of 5 was used. Polyplexes were incubated for one hour at room temperature, then diluted with 600 μL of water prior to size and charge measurements. Polyplex size was measured on a Zetasizer (Nano ZS) (Malvern Instruments, Malvern, UK) at 37 °C using dynamic light scattering with a laser wavelength of 633 nm. Zeta potentials of the polyplexes were subsequently measured on the same instrument. Three polyplex solutions were used for each measurement; data are presented as means ± standard deviations.

Transfection efficiency. Transfection efficiency was measured using a luciferase reporter gene assay 48 hours after transfection as previously described.[11] Briefly, HeLa cells were seeded at a density of 50,000 cells/well in a 24 well plate. Polyplexes were

formed as described above for the polyplex characterization studies, except 600 µL of serum-free media (OptiMEM, Gibco, Carlsbad, CA) was added to each polyplex solution instead of water. Cells were transfected using 1 µg of pDNA per well. Transfections were performed in triplicate, and the results of two separate experiments (n = 6) are presented herein. Where indicated, 5 µM of camptothecin (Sigma, St. Louis, MO) was added to cells with polyplexes for 4 hours, then the camptothecin-containing media was aspirated off, cells were washed with phosphate-buffered saline (PBS), and 1 mL of 10 % FBS DMEM was added to each well. For the camptothecin studies, cells were transfected in triplicate, and the transfection efficiency was measured 24 hours after transfection.

Flow cytometry. HeLa cells were seeded at a density of 250,000 cells/well in a 6 well plate in Dulbecco's Modified Eagle Medium (DMEM) substituted with 10 % fetal bovine serum, 100 µg/mL streptomycin, 0.25 µg/mL amphotericin, and 100 units/mg penicillin. The cells were incubated at 37 °C and 5 % CO_2 for 24 hours. After the 24 hour cell incubation, 500 µL of each polyplex solution was made by adding 250 µL of polymer solution at indicated N/P ratios to 250 µL of 0.02 µg/µL pDNA solution. The polyplex solution was allowed to incubate for one hour at room temperature. After one hour, 1 mL of serum-free media (OptiMEM) was added to the 500 µL polyplex solutions. Cells were washed with PBS (1 mL/well), and 1.5 mL of transfection solution was added to each well (5 µg of pDNA/well). The cells were transfected in triplicate. Cells were allowed to transfect for indicated time periods, then transfection media was aspirated off, cells were washed twice with PBS, trypsinized, and pelleted at 200 x g for 10 minutes. Cells were resuspended in 1 mL of PBS, pelleted, and resuspended in 500 µL PBS and

analyzed using a BD FACSCanto II (Becton-Dickenson, San Jose, California) flow cytometer.

Apoptosis detection. The dyes DiIC(1)5 and Annexin V conjugated to Alexa Fluor 488 were used to monitor mitochondrial membrane potential and phosphatidylserine externalization, respectively, according to manufacturer's protocol. Propidium iodide was added to cells prior to flow cytometry analysis to study plasma membrane permeability according to manufacturer's protocol. Transfections were done in triplicate. A minimum of 20,000 events was collected for each sample.

Cellular uptake. For cellular uptake experiments, polyplexes were formed using Cy5-labeled pDNA and the increase in Cy5 fluorescence in HeLa cells was measured two hours after transfection using flow cytometry. Cells were transfected in the presence or absence of 0.9 mM ethylene glycol tetraacetic acid (EGTA) to chelate extracellular calcium, and cells were transfected in triplicate. Cells were pelleted as described above (200 x g for 10 minutes) and resuspended in 0.5 mL of PBS prior to flow cytometry analysis. A minimum of 10,000 events was collected for each sample.

MTT assay. Cells were plated at a density of 50,000 cells/well in a 24 well plate. The cells were grown on the plate for 24 hours prior to transfection. Polyplexes were formed using the same procedure as that used for the transfection efficiency experiments. Cells were transfected in triplicate with 1 µg of plasmid DNA added to each well. At the indicated time points, polyplex solutions were aspirated off, cells were washed with 0.5 mL of PBS per well, and 1 mL of DMEM containing 10 % FBS and 0.5 mg/mL of 3-(4,5-dimethylthiazol-2-yl)-2,5-diphenyltetrazolium bromide (MTT) reagent (Molecular Probes, Eugene, OR) was added to cells. Cells were incubated with the MTT-containing

media for 1 hour at 37 °C, then the media was aspirated off, cells were washed with PBS as described above, and 600 µL of dimethyl sulfoxide (DMSO) was added to each well. Cells were incubated on a shaker for 15 minutes to ensure even distribution of the purple formazan. After the shaking incubation, 200 µL was pipetted out of each well and into a clear 96 well plate, and then analyzed for absorbance at 570 nm using a Tecan GENios Pro plate reader (Tecan U.S., Research Triangle Park, N.C.).

ROS detection. Intracellular reactive oxygen species (ROS) was detected using the fluorescent dye 2′,7′-dichlorodihydrofluorescein diacetate (H_2DCDFA) (Molecular Probes, Eugene, OR) according to manufacturer's protocol. HeLa cells were plated on 6 well plates at a density of 250,000 cells/well. Cells were transfected in 6 well plates as described above. At the indicated time points, polyplexes were aspirated off, cells were washed with PBS, and 1 mL of a 10 µM solution of H_2DFDFA in PBS was added to each well. Hydrogen peroxide (H_2O_2) was used at a concentration of 100 µM as a positive control and was added with the dye. Cells were incubated with the dye at 37°C for 30 minutes. After the incubation, the dye was aspirated off, cells were washed with PBS, and trypsinized using phenol-red free trypsin. Cells were pelleted at 200 x g, 4 °C for 10 minutes and each sample was resuspended in 500 µL of PBS. H_2DCDFA fluorescence was measured using flow cytometry, and a minimum of 20,000 events was collected for each sample

Nucleus isolation. HeLa cells were seeded and transfected in 6 well plates as described above. Four hours after transfection, each sample was pelleted and resuspended in 500 µL of OptiMEM containing 2 mM DL-dithiothreitol (DTT), 40 µg/mL digitonin, and 1 µg/mL protease inhibitor cocktail (Sigma Aldrich, St. Louis,

MO). Cells were incubated on ice for 5 minutes. After incubation, nuclei were pelleted *via* centrifugation at 2000 x g, 4 °C for 10 minutes. Nuclei were resuspended in 500 µL OptiMEM containing 2 mM DTT and incubated on ice for 10 minutes to ensure complete isolation of the nuclei and separation from the cytosolic components. After the 10 minute incubation, nuclei were pelleted at 2000 x g as described above and resuspended in 500 µL of PBS for flow cytometric analysis.

Nuclear uptake. After nuclear isolation, the nuclei were analyzed for Cy5 and propidium iodide fluorescence *via* flow cytometry as described above. Briefly, after isolation, nuclei were pelleted and resuspended in 500 µL of PBS before flow cytometry analysis. To determine whether polyplexes were inside the nuclei or adhered to the surfaces of the nuclei, confocal microscopy was then performed on the samples analyzed by flow cytometry. The nuclei were re-pelleted after flow cytometric analysis and resuspended in 1 mL of 4 % paraformaldehyde solution. Nuclei were fixed for 15 minutes at room temperature, after which nuclei were pelleted, resuspended in 1 mL of PBS, and deposited onto poly-L-lysine (PLL)-coated coverslips. Nuclei were allowed to incubate on coverslips for 12 hours at 4 °C before being mounted on microscopy slides using ProLong Gold Antifade reagent (Molecular Probes, Eugene, OR) according to the manufacturer's protocol. Nuclei were analyzed on a Zeiss LSM 510 META confocal microscope. Z-stacks of each image were collected using overlapping 0.39 µM slice thicknesses and Zeiss Zen 2009 software. Fluorescence for each z-stack slice in the microscopy images was quantified using the software ImageJ.[18]

Confocal microscopy. HeLa cells were grown on PLL-coated coverslips in a 12 well plate for 48 hours before being transfected. The cells were seeded at 15,000 cells/well.

After the 48 hour incubation, the media was aspirated off, cells were washed with 1 mL of PBS per well, and 1 mL OptiMEM was added to each well. Polyplexes were formed as described in the polyplex characterization section except 50 µL of polymer solution was added to 50 µL of 0.02 µg/µL Cy5-labeled plasmid DNA solution, giving a total of 100 µL of transfection solution per well (1 µg of pDNA/well). The 100 µL of transfection solution was added on top of the 1 mL of OptiMEM in each well, the plate was swirled to give even distribution of polyplexes, and the cells were incubated at 37 °C and 5 % CO_2 for 30 minutes. After transfecting for 30 minutes, the polyplex-containing OptiMEM was aspirated off, wells were washed with 1 mL of PBS, and 1 mL of 10 µg/mL Alexa Fluor 488 wheat germ agglutinin (WGA) (Molecular Probes, Eugene, OR) in Hank's Buffered Salt Solution (HBSS) was added to each well. Cells were incubated with the labeled WGA for 15 minutes at room temperature, after which time the WGA was aspirated off, cells were washed twice with 1 mL of PBS in each well, and fixed using 4 % paraformaldehyde at room temperature for 15 minutes. After fixation, cells were washed three times with PBS and nuclei were stained using 4',6-diamidino-2-phenylindole, dilactate (DAPI) (Molecular Probes, Eugene, OR) and mounted using ProLong Gold Antifade Reagent (Molecular Probes, Eugene, OR) according to the manufacturer's protocol. The slides were dried overnight in the dark before being sealed with clear nail polish and imaged using confocal microscopy.

Immunostaining of lamin A. HeLa cells were grown on coverslips and transfected as described above. Four hours after transfection, cells were fixed in 4 % paraformaldehyde at room temperature for 15 minutes. After fixation, cells were washed three times with PBS (1 mL of PBS per well each wash) and permeabilized using 0.25 %

Triton X-100 for 15 minutes at room temperature. Cells were then washed with PBS three times, leaving the PBS in the wells for five minutes for each wash. The cells were then blocked using a 1 % bovine serum albumin (BSA) solution in PBS for 45 minutes at room temperature. After blocking, a 1:2000 solution of rabbit polyclonal lamin A antibody (Abcam, Cambridge, MA) in 1 % BSA/PBS was added to the cells. Cells were incubated with the primary antibody for one hour at room temperature, after which time the antibody solution was aspirated off, and a 5 µg/mL solution of goat anti-rabbit secondary antibody conjugated to Alexa Fluor 488 (Molecular Probes, Eugene, OR) in 1 % BSA/PBS was added to coverslips in a humidified chamber. After incubating with the secondary antibody for one hour at room temperature, coverslips were washed three times with 1 mL of PBS/well, and the PBS was allowed to stay on coverslips for 5 minutes each wash. After the third PBS wash, coverslips were stained with DAPI (Molecular Probes, Eugene, OR) to stain the nuclei according to the manufacturer's protocol. Coverslips were then washed twice with 600 µL of PBS and mounted on to microscopy slides using ProLong Antifade Gold reagent (Molecular Probes, Eugene, OR) according to manufacturer's protocol. The microscopy slides were allowed to dry horizontally overnight in the dark before being sealed with clear nail polish and imaged using confocal microscopy.

Nuclear envelope permeability in a cell-free system. Nuclei were isolated from HeLa cells as described above and added to a 12 well plate at a density of 50,000 nuclei/well. Polyplexes were formed as described above (50 µL of polymer solution was added to 50 µL of 0.02 µg/µL Cy5-labeled plasmid DNA solution) and added to the nuclei in 1 mL of OptiMEM. The nuclei were incubated at 37 °C and 5 % CO_2 for 4

hours, after which 200 μL of a 0.4 % trypan blue solution (Gibco, Carlsbad, CA). The nuclei were then imaged using an EVOS fl digital inverted fluorescence microscope (Advanced Microscopy Group, Bothell, WA). Mean pixel intensity for the nuclei was characterized using the software ImageJ, and ~300 nuclei were analyzed for each polyplex.

Statistical analysis. All data are presented as means ± standard deviations with n = 3 unless otherwise noted. For statistical analysis of data, the software JMP was used (S.A.S. Institute Inc., Cary, NC) and means were compared using ANOVA followed by the Tukey-Kramer HSD method, with $p < .05$ being considered as statistically significant.

3.4 Results and Discussion

Synthesis and characterization of T4 polymers. To examine the role that polymer length has on cytotoxicity, three different degrees of polymerization (DPs) of T4 were synthesized by varying their polymerization reaction times from 4 days to 8 days using previously published method.[11] GPC with a triple detection system (viscometry, static light scattering, and refractive index) was used to analyze each of the polymers for molecular weight, polydispersity, and polymer solution structure (MHS parameter between 0.6-0.8 denotes a linear randomly-coiled polymer structure).[19] The results are shown in Table 3.1.

Table 3.1) Molecular weight (M_w), polydispersity index (M_w/M_n), Mark-Houwink-Sakurada parameter (MHS (α)), and degree of polymerization (n_w) for the polymers studied.

Polymer	M_w (kDa)	M_w/M_n	MHS (α)	n_w
$T4_6$	2.2	1.3	0.600	6
$T4_{12}$	4.3	1.1	0.814	12
$T4_{43}$	14.8	1.7	0.760	43
$A4_{42}$	14.4	1.2	0.643	42

Size and charge of polyplexes. Polyplexes were formulated according to our previously published protocol[11] and the polyplexes formed with linear PEI, $T4_6$, $T4_{12}$, $T4_{43}$, and $A4_{42}$ were examined *via* dynamic light scattering and zeta potential to understand how the differences in polymer chemistry and molecular weight influenced the physical properties of the polyplexes. It was found that polyplexes formulated with $A4_{42}$ and pDNA yielded the highest Zeta potential (+35.1 ± 5.9 mV), significantly higher than the charges of the other polyplexes ($p < 0.05$) (Figure 3.1). Despite changing the molecular weight, there was no significant difference in zeta potential values when comparing the three T4 analogues, however, the shorter polymer, $T4_6$, formed significantly ($p < 0.05$) larger polyplexes (about 250 nm) than the longer vehicle analogues $T4_{12}$ and $T4_{43}$, which were around 80 nm (Figure 3.1). Polyplexes formed with linear PEI were similar in size to $T4_{12}$ and $T4_{43}$, however, the zeta potential was lower and is likely due to the fact that PEI polyplexes were formed at an N/P ratio of 5 rather than 20, as recommended by the manufacturer for transfection.

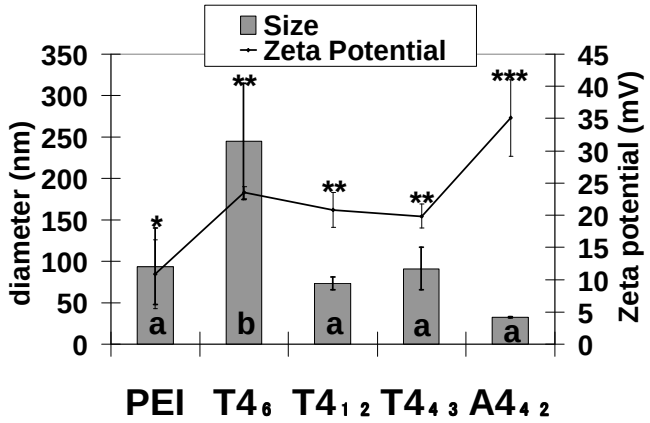

Figure 3.1) Size (bars) and zeta potential measurements (line) for polyplexes formed with linear PEI, $T4_6$, $T4_{12}$, $T4_{43}$, and $A4_{42}$. PEI polyplexes were formed at an N/P ratio of 5, and the T4 and $A4_{42}$ polyplexes were formed at an N/P ratio of 20. Letters are used to denote statistical analysis on size measurements, and asterisks are used to represent statistical analysis on zeta potential measurements. Different letters on size measurement bars denote means that are statistically significant from each other ($p < 0.05$) according to the Tukey-Kramer HSD method ($n = 3$). Bars with matching letters are not statistically significant from each other. For zeta potential measurements, means with different numbers of asterisks are statistically significant from each other ($p < 0.05$) using the Tukey-Kramer HSD method with $n = 3$. Means with the same number of asterisks are not statistically significant from each other.

Based on these data, it appears that the polymer structure plays a role in how plasmid DNA is complexed. The absence of hydroxyls on the $A4_{42}$ polymer seemed to result in a slightly smaller, yet significantly ($p < 0.05$) more positively charged polyplex. However, linear PEI, which also lacks hydroxyl groups, forms polyplexes similar in size to $T4_{12}$ and $T4_{43}$ and the size and charge data for these three polymers is not statistically different. $T4_6$, however, forms particles double in size compared to all other polymers, indicating that the lower molecular weight analogue forms looser complexes with pDNA. Prior research in our group has indicated that T4 exhibits significant hydrogen bonding when complexing with plasmid DNA.[20-21] The different binding mechanism of the hydroxyl-containing T4 analogues vs. $A4_{42}$ may account for their difference in polyplex charge.[17, 20]

Transfection efficiency. To study how polymer molecular weight and structure affect transfection efficiency, HeLa cells were transfected with polyplexes formed with each of the five different polymers and luciferase expression was measured after 48 hours (Figure 3.2). JetPEI at an N/P ratio of 5 along with $T4_{43}$ and $A4_{42}$ at N/P ratios of 20 yielded significantly higher transfection efficiency ($p < 0.05$) compared to the lower molecular weight polymers $T4_6$ and $T4_{12}$. Interestingly, the transfection efficiency of polyplexes created with pDNA and the T4 derivatives increases with increasing molecular weight by four orders of magnitude going from $T4_6$ to $T4_{43}$.

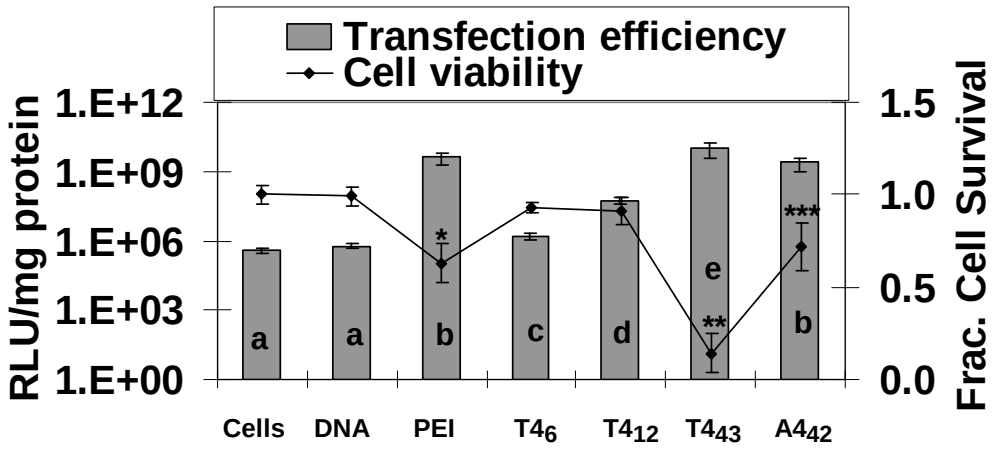

Figure 3.2) Luciferase gene expression as measured by relative light units (RLU) per milligram of protein in cell lysates and cell viability as measured by protein content in cell lysates. Luciferase expression and cell viability were measured 48 hours after transfection in HeLa cells. Cells were transfected with JetPEI (PEI) at an N/P ratio of 5. All other polymers were used at an N/P ratio of 20. All statistical analysis was done using the Tukey-Kramer HSD method. Letters represent statistical analysis done on transfection efficiency data (bars), and asterisks represent statistical analysis done on cell viability data (line). Bars representing transfection efficiency with different letters are statistically significant from each other ($p < 0.05$) according to the Tukey-Kramer HSD method, with $n = 6$. Bars with matching letters represent means that are not statistically significant from each other. For cell viability data, points with different numbers of asterisks are statistically significant from each other ($p < 0.05$; $n = 6$) according to the Tukey-Kramer HSD method. Points with no asterisks are not statistically significant from each other.

Previous work in our group has shown that A4 with a degree of polymerization (DP) of 12 exhibits lower transfection efficiency when compared to T4 with a similar molecular

weight (DP of 14).[17] This trend is also seen here when studying the transfection efficiency of the higher molecular weight derivatives of these polymers. It is likely that the higher transfection efficiency of $T4_{43}$ (as compared to $A4_{42}$) results from its ability to degrade, thus providing a mechanism for plasmid DNA release from the polyplex.[17] $T4_{43}$ also exhibits statistically higher ($p < 0.05$) transfection efficiency than PEI (Figure 3.2). When comparing the cytotoxicity of the polymers, it was found that high transfection efficiency also correlated with high cytotoxicity and cell death. We were also surprised to find that despite the degradability of $T4_{43}$, it actually appeared to exhibit a statistically ($p < 0.05$) higher toxicity profile than $A4_{42}$ and PEI, which do not degrade. The cell viability data for polymers $T4_{12}$ and $T4_{6}$ were not statistically significant ($p > 0.05$) from the cells only and pDNA only controls (Figure 3.2); it appears that the polymers with the highest transfection efficiency (PEI, $T4_{43}$ and $A4_{42}$) also exhibited the highest cytotoxicity (Figure 3.2). To this end, we were interested in the further investigation of the timing and mechanisms of toxicity with these polymeric vehicles, and how the polymer structure influences the cellular mechanisms related to apoptosis.

Induction of apoptosis. Cationic polymers utilized for the delivery of polynucleotides may elicit toxicity that results in apoptosis in a number of ways. Previous studies implicate that both 25 kDa branched[22-23] and 750 kDa linear[23] PEI have two distinct toxicity pathways; one exhibited early in transfection and another occurring after DNA release from the polymer-DNA complex (polyplex) several hours after transfection. The current study focuses on several potential mechanisms of toxicity in order to understand how the polymer structure affects the cytotoxic pathways of these gene delivery vehicles. There are several possible sites for apoptosis initiation during

transfection (Scheme 3.1). The effect of polymer structure (with or without hydroxyls in the backbone) and molecular weight on several potential mechanisms of cytotoxicity were tested in the current study. These include plasma membrane permeabilization (Scheme 3.1, I), the effects of reactive oxygen species (ROS) (Scheme 3.1, III), and the mechanism of how polymer-DNA complexes (polyplexes) enter the nucleus (Scheme 3.1, IV).

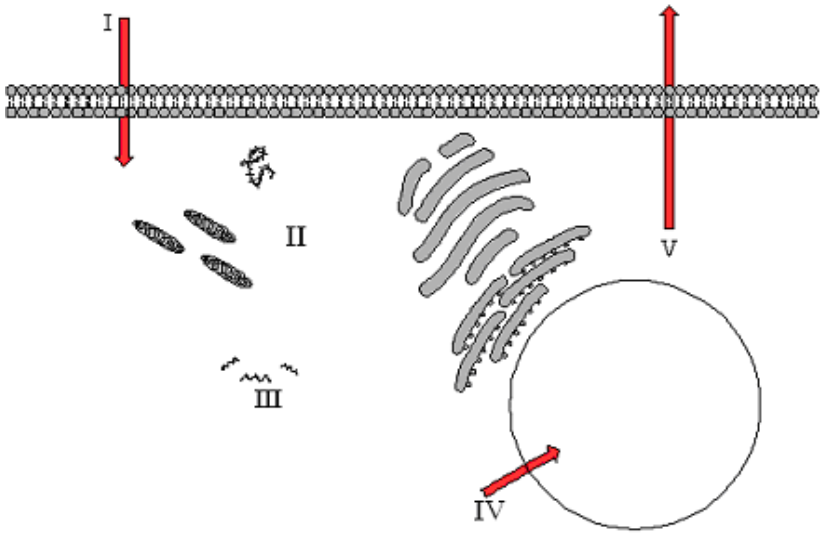

Scheme 3.1) Possible routes of polymer/polyplex cytotoxicity: I.) mechanism of cellular entry *via* direct membrane permeabilization, II.) interaction with organelles or proteins during intracellular trafficking, III.) harmful products formed upon polymer degradation, IV.) mechanism of nuclear entry *via* nuclear envelope permeabilization, V.) mechanism of cellular exit.

Changes in mitochondrial membrane potential as well as phosphatidylserine externalization (markers of apoptosis) were initially used to gauge the timing of apoptosis initiation. All polymers were able to depolarize mitochondrial membrane potential as evidenced by a decrease in DiIC(1)5 fluorescence (Figure 3.3, a) as well as induce phosphatidylserine externalization as evidenced by an increase in Annexin V-FITC fluorescence (Figure 3.3, b), within half an hour into the transfection (Figure 3.3). There

was no statistically significant difference in the amount of mitochondrial membrane potential reduction or the amount of phosphatidylserine increase between the T4 polymers and the structures lacking hydroxyl groups ($A4_{42}$ and linear PEI polymers) at this early time point, however, four hours after transfection, a dramatic difference in apoptotic signals was found. Polyplexes formed with linear PEI, $T4_{43}$, and $A4_{42}$, the longest polymers, reduced mitochondrial membrane potential and increased phosphatidylserine externalization to a greater extent ($p < 0.05$) when compared to the data from $T4_6$ and $T4_{12}$. This result indicates that the longer polymers induce apoptosis and lead to cell death faster than shorter structures. Interestingly, polyplexes formed with the carbohydrate-containing $T4_{43}$ induced the most phosphatidylserine externalization and mitochondrial membrane depolarization, indicating that the hydroxyls in the $T4_{43}$ backbone could contribute to toxicity at longer degrees of polymerization. Both $T4_{43}$ and $A4_{42}$ induced significantly more phosphatidylserine externalization ($p < 0.05$) than PEI and $T4_{12}$ 4 hours after transfection (Figure 3.3 b). These data agree with the lower viability data observed for $T4_{43}$ in the previous transfection experiment (Figure 3.2). It is interesting to note that the polymer structures responsible for inducing apoptotic signals (Figure 3.3) are the same structures with the highest transfection efficiency (Figure 3.2).

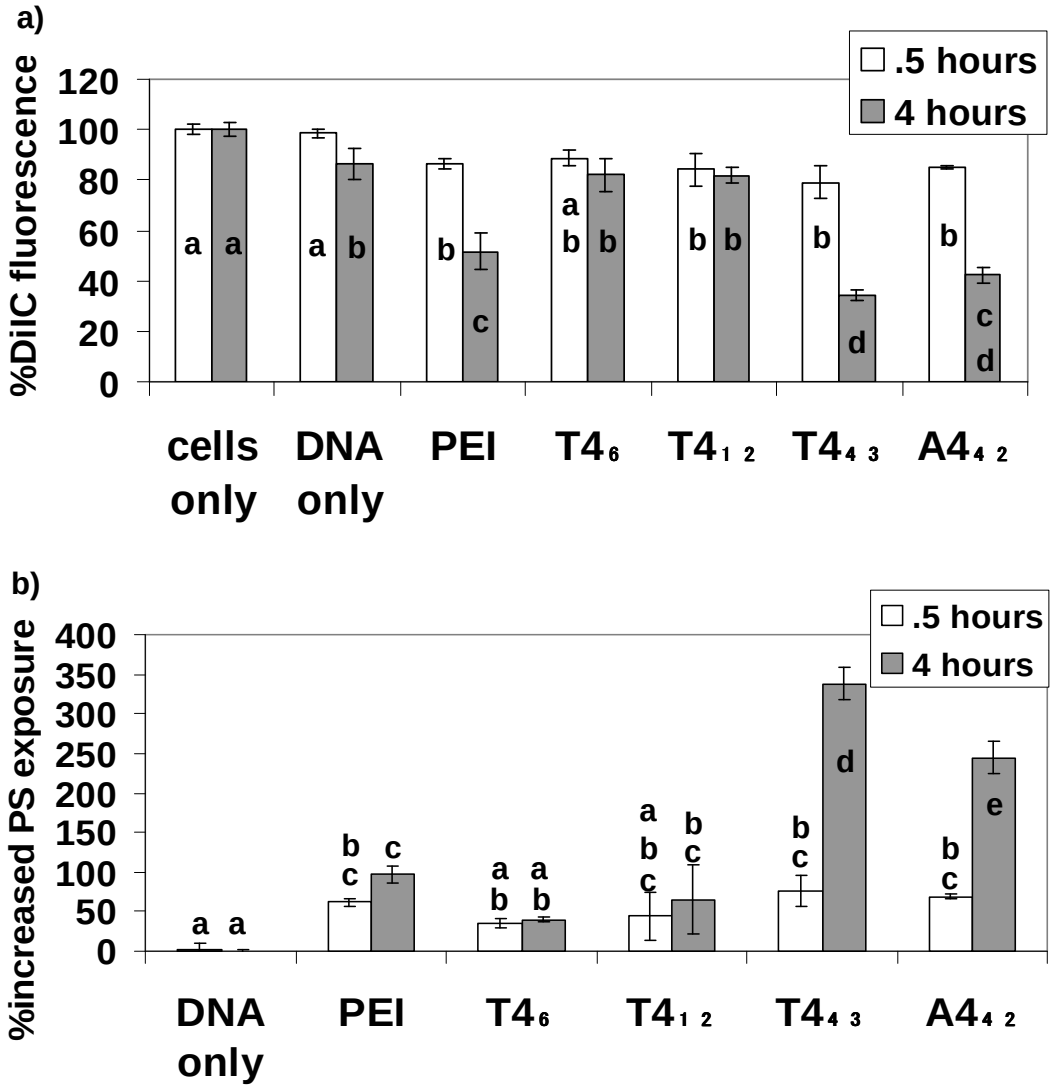

Figure 3.3) (a) Mitochondrial membrane potential measured by DiIC(1)5 fluorescence normalized to the cells only control and (b) phosphatidylserine (PS) externalization measured by Annexin V binding assay in HeLa cells transfected with polyplexes formed using PEI, T4, and $A4_{42.}$ Data in (b) is presented as % increased PS externalization compared to the cells only control. Bars with different letters represent means that are statistically significant ($p < 0.05$) from each other ($n = 3$) according to the Tukey-Kramer HSD method. Bars with matching letters are not statistically significant from each other.

Plasma membrane interactions. The plasma membrane is the first barrier polyplexes encounter during transfection, and prior studies have indicated that cationic polymers are able to disrupt and induce hole formation in the plasma membrane of the cells.[24-26] However, it is currently unclear in our field whether disruption of the plasma

membrane results in cell death or whether the cell can recover from such damage. Previous research on these systems completed by our group has shown that polyplexes formed with JetPEI and T4 enter the cell in different ways, and this could cause different interactions leading to or preventing toxicity.[15] Also of significance, previous work by other groups has shown that direct permeabilization of the plasma membrane is observed by branched and linear PEI, and this permeabilization is implicated as a potential mechanism of cytotoxicity.[1, 9, 27] It is possible that the different cytotoxic profiles observed for linear PEI vs. the PGAAs are a result of their different mechanisms of cellular entry.[15]

To further support previous studies showing that the T4 polymer and PEI enter the cell *via* different routes,[15] cells were transfected in the presence or absence of EGTA, an extracellular calcium chelator. EGTA has been shown to disrupt cell-cell junctions and expose basolateral surfaces of endothelial cells,[28] which can result in increased cellular binding and transfection efficiency of several non-viral DNA delivery vehicles.[28-30] We found that chelating extracellular calcium resulted in a statistically significant ($p < 0.05$) increase in cellular internalization for polyplexes formed with linear PEI two hours after transfection. Conversely, the removal of extracellular calcium with EGTA had an inhibitory effect ($p < 0.05$) on the internalization of the $T4_{12}$ and $T4_{43}$, and did not effect on the uptake of $A4_{42}$ (Figure 3.4 a). $T4_6$ polyplex uptake was slightly inhibited by EGTA, but the uptake of the T46 polyplexes was significantly lower ($p < 0.05$) than that of the other polyplexes, which could be the reason for the observed decreased effect of EGTA when compared to the other T4 analogues. Extracellular calcium is required to maintain membrane fluidity,[31] and without it cells are not able to recover as well after

membrane penetration.[32-34] Since cells without extracellular calcium exhibited improved polyplex uptake in the case of PEI, it appears that membrane fluidity could influence PEI transfection. Interestingly, the cells did not exhibit a significant increase ($p < 0.05$) in propidium iodide permeability in the presence of EGTA (Figure 3.4 b), thus discounting the idea that membrane permeability aids polyplex internalization in the cells. Supporting this observation, a recent study by Prevette *et al.* indicates that membrane permeability does not play a role in PEI transfection.[35] Collectively considering the current and published results, we hypothesize that a more likely toxicity mechanism is that the increased basolateral surface of the cells could play a role in PEI uptake, and that the different mechanisms of cellular uptake of PEI vs. T4 polyplexes may play a role in early cytotoxicity (< 30 minutes after transfection). EGTA had a slight inhibitory effect ($p < 0.05$) on $T4_{12}$ and $T4_{43}$ uptake, further illustrating that the poly(glycoamidoamine)s are entering the cell *via* different endocytic mechanisms than PEI.[15] The inhibitory effect of EGTA on the uptake of $T4_{12}$ and $T4_{43}$ is similar to results obtained for several lipid-DNA complexes.[36-37] The exact mechanism by which decreasing extracellular Ca^{+2} decreases the intracellular uptake of certain gene delivery vehicles while enhancing others remains unknown, but it is speculated that chelation of extracellular calcium could decrease rates of endocytosis.[36, 38-39] Collectively, these studies support previous findings that structure of the polymers influence their endocytic routes.[15] Furthermore, it supports the conclusion that polymer structure influences plasma membrane interactions; the T4 analogues may take a different endocytic route than linear PEI or $A4_{42}$ that involves calcium-mediated endocytosis. The difference in intracellular uptake mechanisms could contribute to the different toxicity profiles for these polymers.

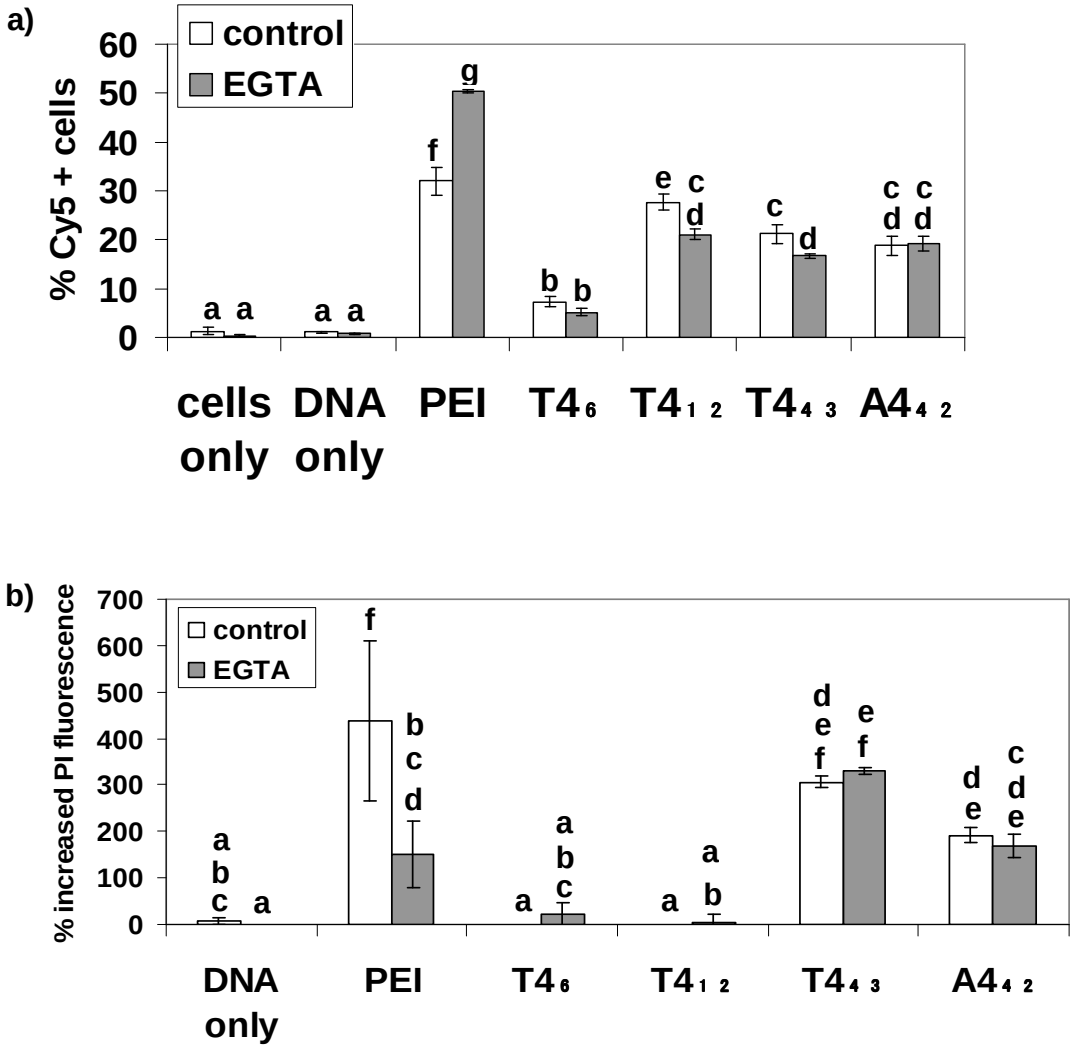

Figure 3.4) The effect of EGTA, an extracellular calcium chelator, on (a) cellular uptake of polyplexes formed with the indicated polymers and Cy5-pDNA 2 hours after transfection and (b) plasma membrane permeability as measured by % increased propidium iodide (PI) fluorescence compared to the cells only control 2 hours after transfection. Bars with different letters are statistically significant ($p < 0.05$) from each other ($n = 3$) according to the Tukey-Kramer HSD method. Bars with matching letters are not statistically significant from each other.

To further study how polymer length and structure influence the interaction of polyplexes with the plasma membrane and the mechanism of cellular uptake, confocal

microscopy was used to monitor colocalization of polyplexes and the plasma membrane 30 minutes after transfection. AlexaFluor-488-conjugated wheat germ agglutinin, a lectin that binds to N-acetylglucosamine and sialic acid residues,[40-41] was used to label the plasma membrane. The software ImageJ[18] was used to calculate Manders coefficients for polyplexes formed with Cy5-labeled pDNA and the wheat germ agglutinin on the plasma membrane as a measure of colocalization.[42-43]

Z-stacks of HeLa cells were taken using slice thicknesses of 0.39 µM/slice and colocalization was analyzed throughout the entire stack. The images shown in Figure 6 represent one slice of the z-stack. Based on the confocal images and Manders coefficients (Figure 3.5), we conclude that all polyplexes have some interaction with the plasma membrane as early as 30 minutes after transfection, and the data reveals that $T4_{12}$, $T4_{43}$, $A4_{42}$, and PEI all have a similar degree of interaction with the cell membrane. It was noticed that polymer $T4_6$ had the lowest interaction with cells and internalization when compared with the other polymers (Figure 3.5) and these results correlate with the previous observation that $T4_6$ has the lowest transfection efficiency. The other polymers exhibit significant polyplex internalization. Several internalized polyplexes are denoted by the white arrows in Figure 3.5, with polyplexes for PEI (Figure 3.5 b), $T4_{12}$ (Figure 3.5 d), $T4_{43}$ (Figure 3.5 e), and $A4_{42}$ (Figure 3.5 f) all illustrating more polyplex internalization ($p < 0.05$) than $T4_6$ (Figure 3.5 c). To determine whether there was a difference in plasma membrane permeability at this time point, a propidium iodide exclusion assay was performed.

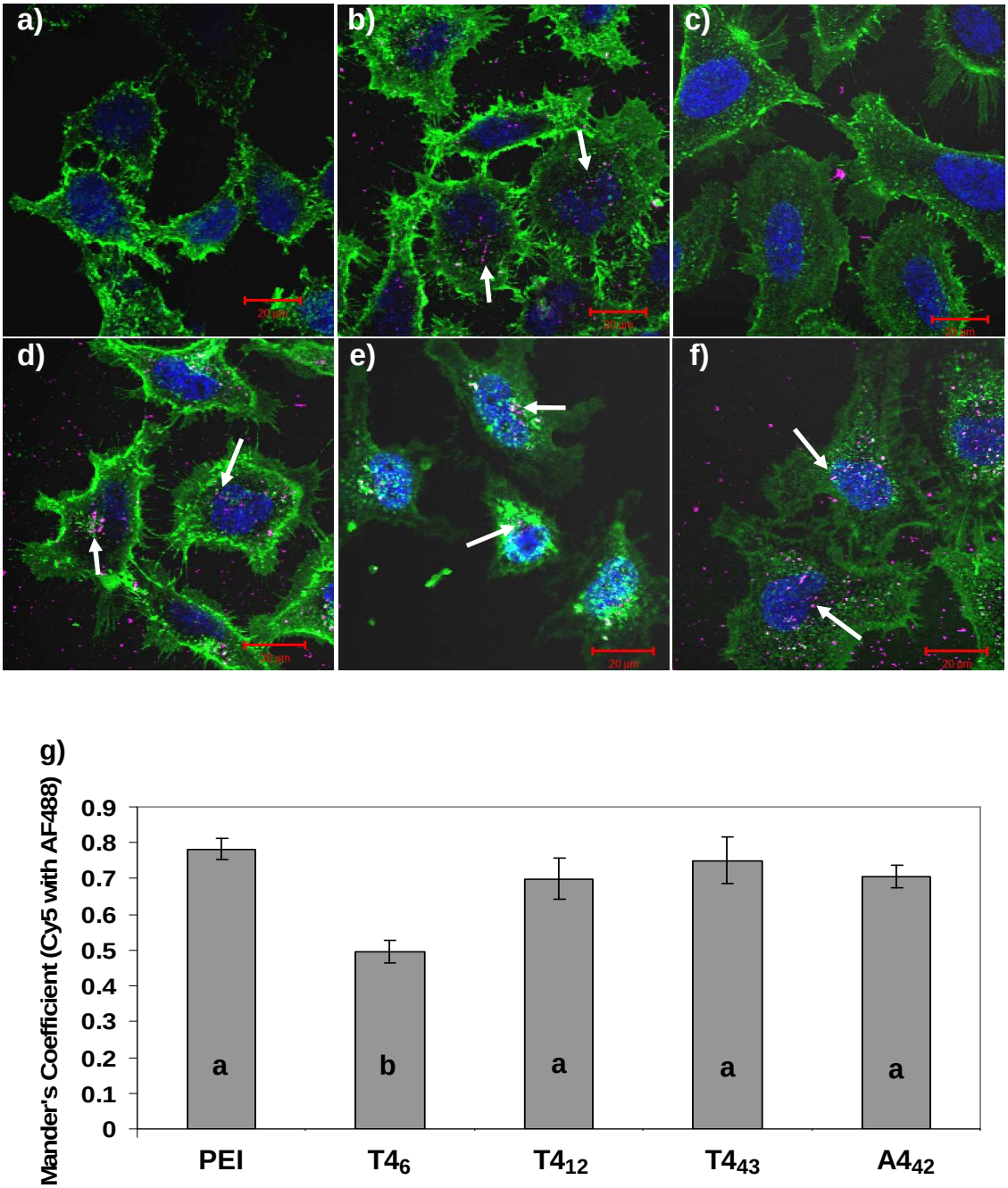

Figure 3.5) Confocal microscopy images of HeLa cells 30 minutes after being transfected with polyplexes formed with Cy5-labeled pDNA and the following polymers: (a) pDNA only; (b) JetPEI (PEI); (c) $T4_6$; (d) $T4_{12}$; (e) $T4_{43}$; (f) $A4_{42}$. Colors represent the following; green = WGA AF488-labeled cytosol; blue = DAPI-labeled nucleus; magenta = Cy5-labeled pDNA. Scale bar = 20 µm. Arrows denote sites of polyplex internalization. (g) Manders coefficients between each polyplex type (formed with Cy5-pDNA) and AlexaFluor-488-conjugated Wheat Germ Agglutinin-labeled plasma membrane. Bars with different letters are statistically significant ($p < 0.05$) from each other

according to the Tukey-Kramer HSD method (n = 3). Bars with matching letters represent means that are not statistically significant from each other.

Plasma membrane permeability. Propidium iodide (PI) is a small molecule that has a diameter of ~1 nm[35] and is normally excluded from cells with an intact plasma membrane but can penetrate cells in which the plasma membrane has been disrupted (and is also commonly used as a marker of dead cells). PI fluorescence was used as a measure of plasma membrane permeability at 30 minutes and 4 hours after transfection. It is apparent that $T4_{43}$ induces the most membrane disruption 4 hours after transfection and the polymers with the highest transfection efficiency are also the structures inducing the most plasma membrane permeability according to these PI assays (Figure 3.6). As observed in the mitochondrial membrane potential and phosphatidylserine externalization assays (Figure 3.3), there is no significant difference in the degree of membrane permeability induced by the polyplexes 30 minutes after transfection, the time point where polyplexes were shown to interact with the plasma membrane (Figure 3.5). However, 4 hours after transfection, we see a dramatic increase ($p < 0.05$) in membrane permeability, indicative of cell death, in cells treated with linear PEI, $T4_{43}$, and $A4_{42}$ compared to the cells only control. Indeed, it is evident that the three polymers with the highest transfection efficiency are able to induce the most plasma membrane damage. Prevette *et. al.* have shown that plasma membrane permeability plays no role in transfection efficiency,[35] but perhaps if these polymers are able to induce plasma membrane permeability, they are able to induce membrane permeability in other organelles, including the nucleus. Based on these studies, it is difficult to tell whether the plasma membrane permeability is induced directly by the polymers, or is a consequence of apoptosis activation at this time point as evidenced by the mitochondrial membrane

potential and phosphatidylserine externalization assays (Figure 3.3). We observe an increase in PI fluorescence (Figure 3.6), a decrease in mitochondrial membrane potential (Figure 3.3 a), and an increase in phosphatidylserine externalization (Figure 3.3 b) within 30 minutes of transfection, indicating that cells are dying at this early time point. We do notice a trend in both the apoptosis studies (Figure 3.3) and the PI study (Figure 3.6). It seems that in each of the different assays, 30 minutes after transfection there are no dramatic differences between the polymers. However, 4 hours after transfection, cells transfected with PEI, $T4_{43}$, and $A4_{42}$ exhibit significantly more ($p < 0.05$) mitochondrial depolarization (Figure 3.3 a), phosphatidylserine externalization (Figure 3.3 b), and PI fluorescence (Figure 3.6) when compared to $T4_6$ and $T4_{12}$. Furthermore, it appears that $T4_{43}$ induces significantly more ($p < 0.05$) cellular disruption based on these studies when compared to the other polymers. Based on the dramatic changes in toxicity profiles between the polymers 4 hours after transfection, it was of interest to us to perform further studies to determine the cause of apoptosis initiation.

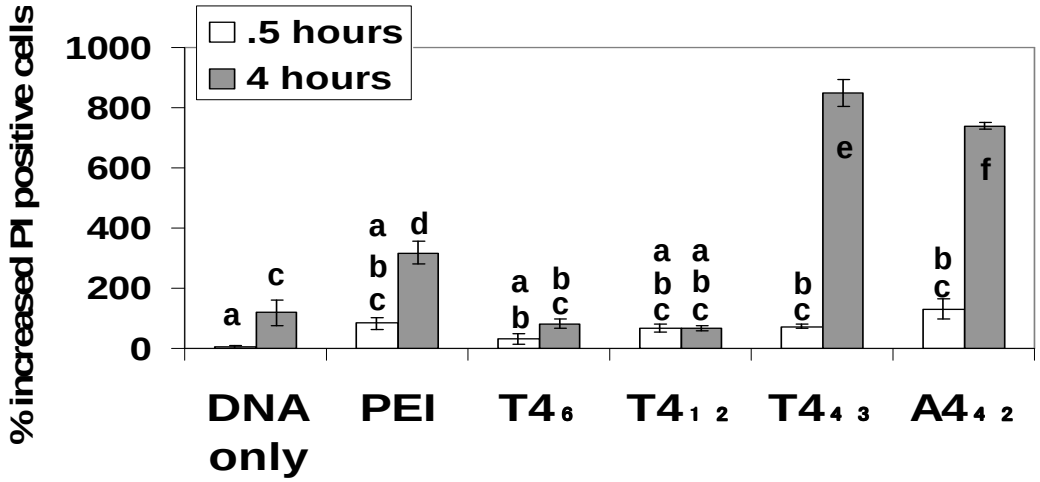

Figure 3.6) Data showing % increased propidium iodide (PI) fluorescence compared to the cells only control. Cells were analyzed for PI fluorescence using flow cytometry at the indicated time points

after transfection. All polymers were used at an N/P ratio of 20, with the exception of JetPEI (PEI), which was used at an N/P ratio of 5. Different letters on bars represent means that are statistically significant ($p < 0.05$) from each other according to the Tukey-Kramer HSD method ($n = 3$). Bars with matching letters represent means that are not statistically significant from each other.

Toxicity of potential polymer degradation products. It has been previously shown in several previous studies in the field of nucleic acid delivery that the molecular weight of polymeric delivery vehicles influences their cytotoxicity profile to a large degree; higher molecular weight polymers generally induce more toxic effects and cell death.[6, 44-47] Based on previous studies in our group, one main difference between the T4 structures examined herein as compared to polymers $A4_{42}$ and linear PEI is that the T4 polymers (and our class of PGAAs) are degradable.[17] It is possible that the T4 structures degrade into lower molecular weight polymers or by-products that may or may not affect the cell viability. However, the mechanism of polymer degradation once in cells is not currently understood. It is possible that, depending on the degradation mechanism, there could be toxic by-products that lead to apoptosis, as is the case with naturally-occurring polyamines found in cells.[48-51] Specifically, intracellular catabolism of natural polyamines that are similar in structure to the monomer used to synthesize the T4 structures, such as spermine and spermidine, causes a rise in hydrogen peroxide, leading to oxidative damage and apoptosis initiation.[49] Thus, the degradation products could lead to increased toxicity. Also, previous studies have revealed that polymer vehicles can elicit oxidative stress; interestingly, cells transfected with chitosan[52] and a PEGylated branched PEI polymer[53] show upregulated oxidative stress genes when compared to 25 kDa branched PEI-treated cells. In the case of the PEGylated branched PEI, the PEGylated polymer induced higher upregulation of oxidative stress genes than non-PEGylated branched PEI within 6 hours of transfection, and it was suggested that this

resulted from the higher molecular weight of the PEGylated PEI-based polymers compared to the branched PEI.[53] In light of this previous data, it was of interest to us to study oxidative damage as a potential mechanism of cytotoxicity for the PGAAs. Cells were transfected with the polymers in the presence or absence of aminoguanidine, an inhibitor of several forms of oxidative-induced apoptosis.[54-55] Aminoguanidine was unable to prevent any cell death from the polyplexes 30 minutes (Figure 3.7 a) or 4 hours after transfection (Figure 3.7 b); there was no statistical significance ($p < 0.05$) in cells treated with polyplexes vs. polyplexes with aminoguanidine. Furthermore, no increase in reactive oxygen species (ROS) in PGAA-treated cells was found compared to the cells only control (Figure 3.8). In fact, we observed a significant ($p < 0.05$) decrease in ROS in cells treated with all polymers except for $T4_6$. This is most likely because cells produce ROS normally through metabolic processes; as cells die, there would be a decrease in metabolism leading to a decrease in ROS. Taken together, these results reveal that oxidative damage is not a major mechanism of toxicity for the gene delivery polymers tested, as was earlier hypothesized based on the mechanisms of cytotoxicity for other polyamines discussed in Chapters 1 and 2.

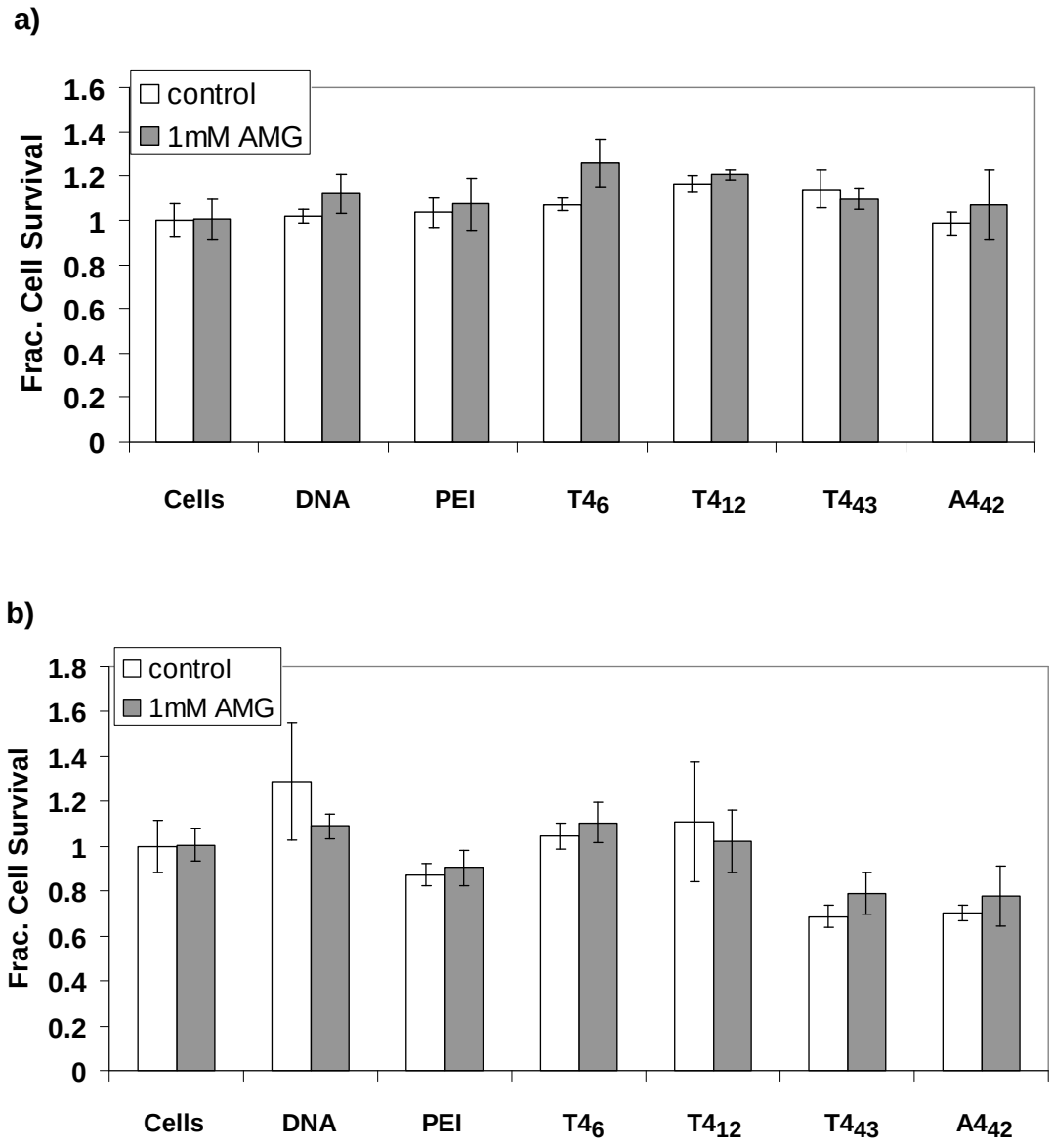

Figure 3.7) HeLa cells were transfected with polyplexes in the absence or presence of 1 mM aminoguanidine (AMG), which has been shown to inhibit some forms of ROS toxicity. Cell viability was analyzed using the MTT assay (a) 30 minutes or (b) 4 hours after transfection. Data were normalized to the cells only control. There was no statistical significance between cells treated with polyplexes vs. polyplexes with 1 mM AMG according to the Tukey-Kramer HSD method.

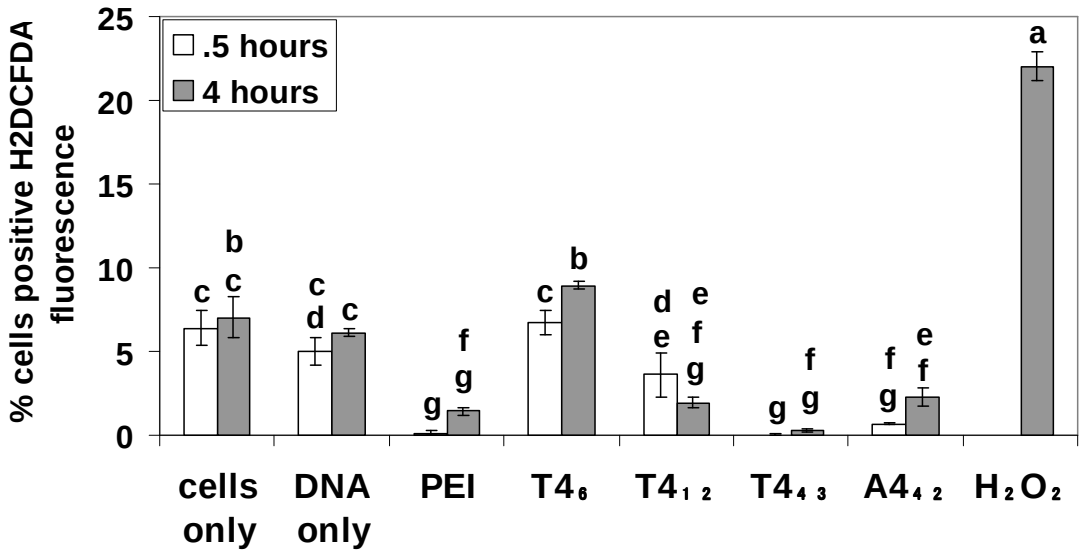

Figure 3.8) HeLa cells were transfected with the different polyplexes and H_2DCDFA fluorescence was measured using flow cytometry at the indicated time points to determine the presence of reactive oxygen species (ROS). 100 µM of hydrogen peroxide (H_2O_2) was used as a positive control. Bars with different letters represent means that are statistically significant ($p < 0.05$, $n = 3$) with each other according to the Tukey-Kramer HSD method. Bars with matching letters represent means that are not statistically significant from each other.

To further examine the role of degradation product toxicity in the T4 polymer series, the toxicity of L-tartaric acid and pentaethylenehexamine hexahydrochloride (N6), the monomers used to synthesize the T4 polymers and suspected degradation by-products, was examined *via* MTT assay. The cells were treated for 4 hours and 24 hours with the L-tartaric acid and N6 at concentrations of 100 µg/mL. We saw no significant cytotoxic responses induced in the cells at either of these time points (Figure 3.9).

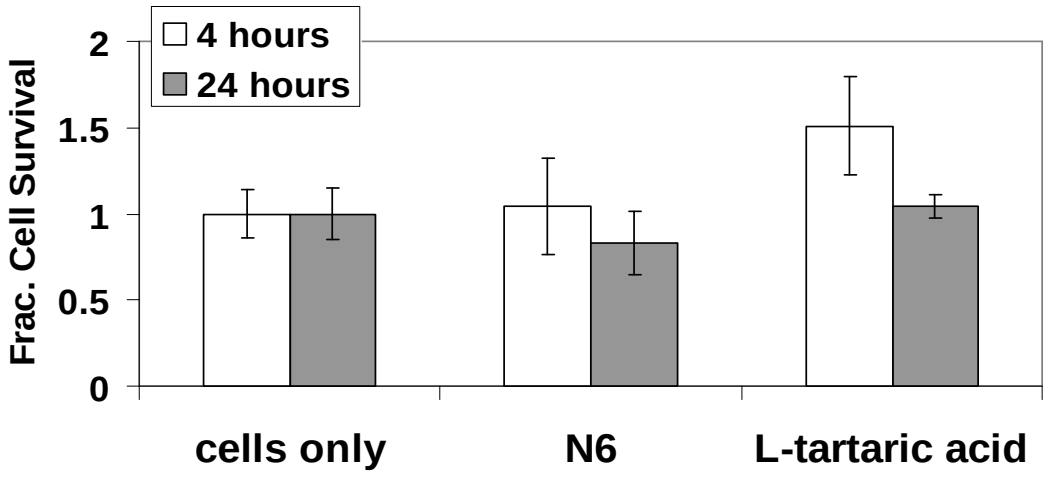

Figure 3.9) Toxicity of the components of the T4 polymers as measured by MTT assay. Cells were treated with either N6 or L-tartaric acid at a concentration of 100 µg/mL for the indicated time points. Data were normalized to the cells only control. Neither of the treatments were statistically significant ($p < 0.05$) from the cells only control according to the Tukey-Kramer HSD method ($n = 3$).

It is possible that once in the cell, the polymers are catabolized by other means besides hydrolysis and the higher molecular weight polymers create higher oxidative stress over time, however, studies to examine this effect are beyond the scope of the current manuscript. Based on these data, the polymers that are shorter in length are certainly less toxic than the same structures that are longer in length. Furthermore, the individual components of the T4 polymers (L-tartaric acid and N6) do not elicit any cytotoxic responses within 4 hours (Figure 3.9), so the apoptotic signals elicited by the polyplexes at this time point (Figure 3.3) may not be a result of polymer degradation products.

Nuclear membrane permeabilization. Polymer gene delivery vehicles are able to deliver pDNA to the nucleus of their target cells, but the mechanism by which the pDNA from the polyplex is transported across the nuclear membrane for transcription is currently unknown. While previous studies indicate that polyplexes are able to induce plasma membrane damage that contributes to cytoxicity, we were interested to examine

the role of nuclear membrane damage in the increase of transfection efficiency, toxicity, and cell death. The nuclear membrane, being a double bilayer membrane, is more resistant to permeabilization than the plasma membrane. However, it is unknown whether polyplexes could disrupt the nuclear membrane as a potential mechanism of nuclear entry. Prior studies indicate that polyplexes are able to deliver their DNA cargo into the nucleus when the nuclear envelope degrades in preparation for cell division.[56-59] This is a likely mechanism, as higher transfection efficiency is often observed in rapidly dividing cells. However, this hypothesis does not explain transfection in non-dividing or slowly dividing cells. Other studies show that in order to deliver the plasmid DNA into the nucleus, intracellular nuclear import machinery must be utilized.[59-61] The mechanisms by which polyplexes are able to utilize this remain uncertain, but research shows that the sequence of the plasmid DNA plays a role. Certain DNA sequences are able to bind to transcription factors. The incorporation of binding sequences for transcription factors, such as Nf-κB,[62-64] has been used as a strategy to increase transfection efficiency. Once bound to the transcription factors, plasmid DNA is able to achieve nuclear entry *via* the nuclear pore complexes (NPCs).[65-66] Another strategy to increase nuclear entry is to use nuclear localization signals.[67] Direct nuclear permeabilization by polyplexes, however, is a mechanism of nuclear entry that has not been thoroughly studied. It should be noted here that the polymers used in the current study do not contain a nuclear localization signal. Also, the plasmid DNA used in this study contains a CMV promoter, and previous work has shown that plasmids with this promoter are not actively trafficked by the cell to the nucleus when injected into the cytosol of smooth muscle cells.[68-70] Our studies show that the polymers with the highest transfection efficiency (Figure 3.2) also induce the

most plasma membrane permeability (Figure 3.6). Based on these data, we hypothesized that the polymers able to induce plasma membrane permeability may be capable of delivering pDNA to the nucleus *via* direct nuclear permeabilization; thus yielding a mechanism for possible cytotoxicity and polymer-based DNA nuclear delivery other than nuclear envelope breakdown during mitosis. To examine this, polyplexes were formed with Cy5-labeled plasmid DNA, and HeLa cells were transfected with each polyplex type for 4 hours, the time point at which differences in the induced apoptotic signals between the polyplexes were apparent (Figure 3.3). After 4 hours, the nuclei from the transfected cells were removed, and Cy5 fluorescence and PI fluorescence were measured using flow cytometry (Figure 3.10). Nuclear isolation was confirmed using microscopy, dynamic light scattering, and static light scattering (results not shown). It should be mentioned here that using this flow cytometric method, we were unable to determine whether the Cy5-labeled plasmid DNA was actually inside the nucleus, or attached to the nuclear membrane; it is likely a combination of both, and we arbitrarily name this "nuclear association". We found an astounding trend; polymer length does seem to affect nuclear interactions, and when considering polymer molecular weight, the shorter the polymer, the higher the pDNA association with the nucleus. These data surprised us because they are the opposite of the transfection efficiency trend; polymers with lower molecular weights exhibited the lowest transfection efficiency, yet had significantly higher ($p < 0.05$) nuclear interaction than polyplexes with higher transfection efficiency (Figure 3.10 a). This is evidenced by the significantly higher ($p < 0.05$) percentage of nuclei positive for Cy5 fluorescence in nuclei isolated from cells transfected with lower molecular weight polymers compared with nuclei isolated from cells transfected with polyplexes

formed with higher molecular weight polymers (Figure 3.10 a). The nuclei from cells transfected with polyplexes formed with the higher molecular weight polymers PEI and $T4_{43}$ show a significant ($p < 0.05$) increase in propidium iodide (PI) fluorescence, indicating an increase in nuclear membrane permeability (Figure 3.10 b). These trends are interesting, because although pDNA delivered with $T4_6$ displayed higher nuclear association, it also has the lowest transfection efficiency of the polyplexes tested (Figure 3.2). Also, the higher molecular weight polymers PEI, $T4_{43}$, and $A4_{42}$ display lower nuclear association than $T4_6$, but higher transfection efficiency. This higher transfection efficiency also correlates with increased PI fluorescence both in whole cells (Figure 3.6) and in isolated nuclei (Figure 3.10 b).

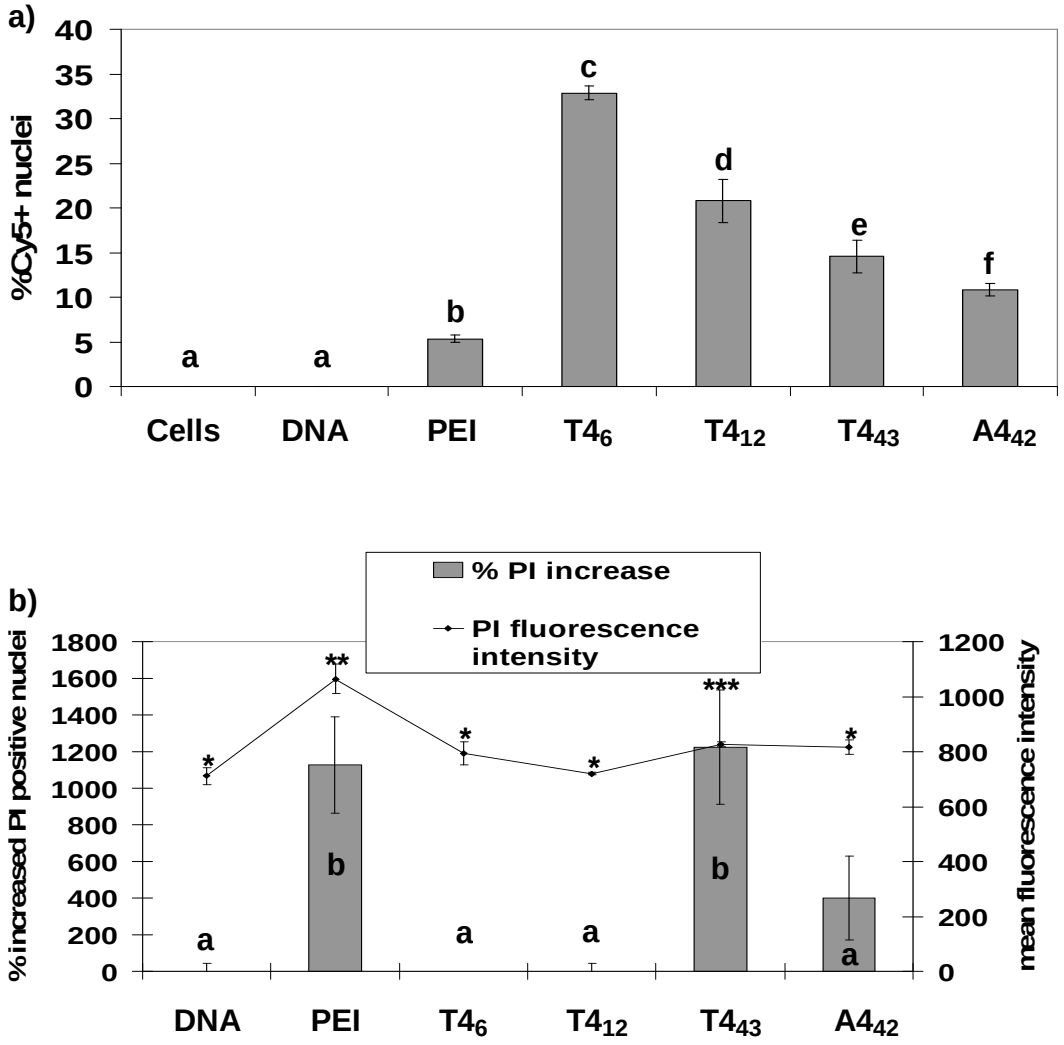

Figure 3.10) Nuclei were isolated from cells transfected with the indicated polymers 4 hours after transfection and analyzed using flow cytometry. (a) Nuclear association between polyplexes and nuclei measured by percentage of nuclei positive for Cy5 and (b) nuclear membrane permeability induced by polyplexes shown as % increased propidium iodide (PI) positive nuclei compared to the cells only control (bars, left y-axis) and PI fluorescence intensity (line, right y-axis). Bars with different letters represent means that are statistically significant ($p < 0.05$) from each other ($n = 3$) according to the Tukey-Kramer HSD method. For fluorescence intensity, points with different numbers of asterisks are significant ($p < 0.05$) from each other according to the Tukey-Kramer HSD method ($n = 3$).

It was our hypothesis that although $T4_6$ was able to get pDNA to the nuclear membrane, it was unable to enter the nucleus since $T4_6$ polyplexes did not induce as much membrane permeability as the polymers with higher transfection efficiency (Figure

3.6). It is likely that the increased Cy5 fluorescence observed in $T4_6$-transfected nuclei was due to polyplexes binding to the nuclear surface. In order to determine this, the nuclei from the isolated cells used for the flow cytometry experiments were fixed and deposited on to coverslips, and were then imaged using confocal microscopy. The confocal microscopy results supported our hypothesis; $T4_6$ polyplexes were found on the periphery of the nuclear membranes, while polyplexes formed with linear PEI, $T4_{43}$ and $A4_{42}$ were found inside the nuclei (Figure 3.11).

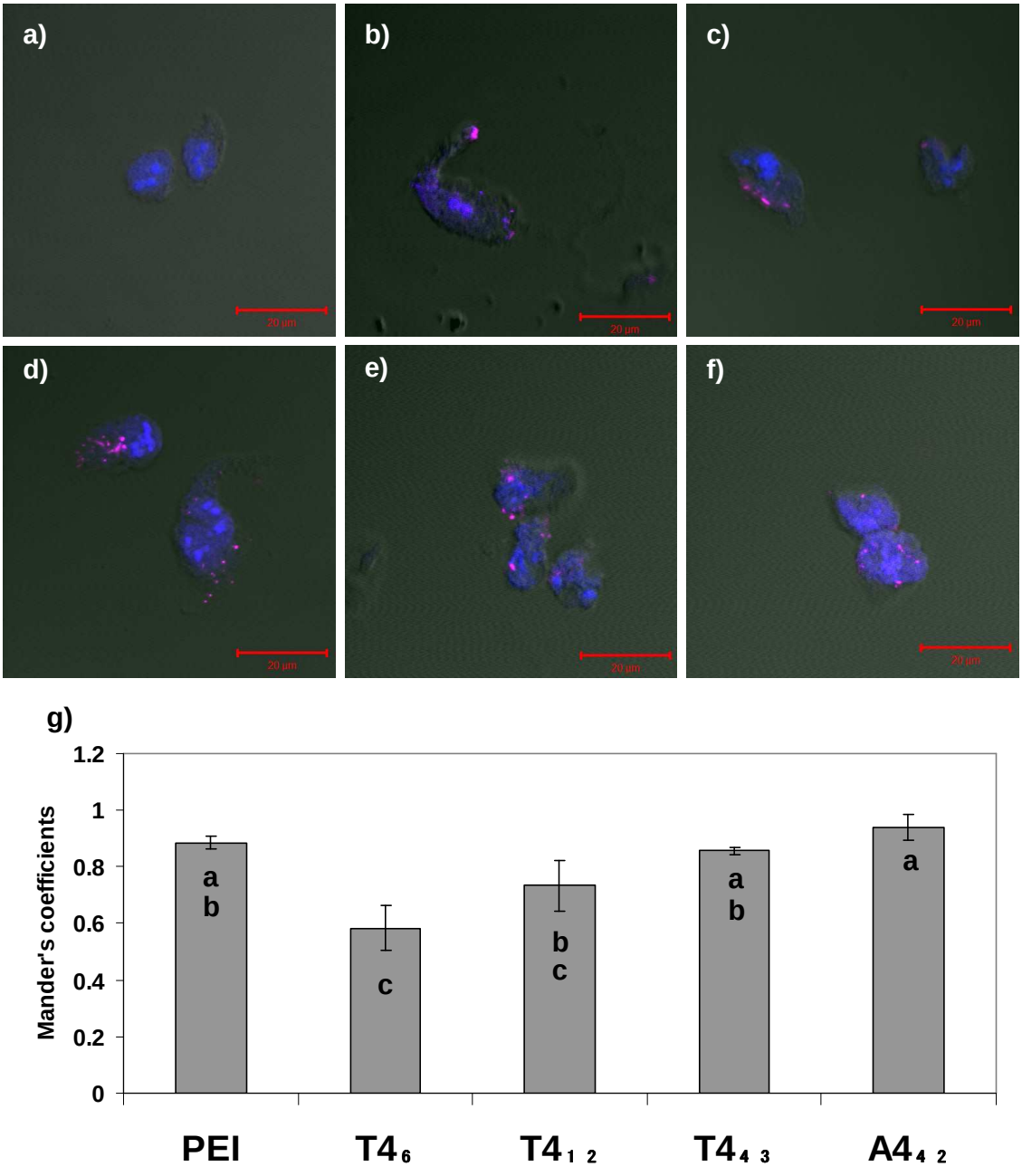

Figure 3.11) Confocal microscopy images of nuclei isolated from cells transfected with the following: (a) pDNA only; (b) JetPEI (PEI); (c) $T4_6$; (d) $T4_{12}$; (e) $T4_{43}$; (f) $A4_{42}$. Colors represent the following: Blue = Propidium iodide-labeled nucleus; magenta = Cy5-labeled pDNA. Scale bar = 20 µm. (g) Manders coefficients between Cy5-labeled pDNA and propidium iodide-labeled nuclei to signify pDNA nuclear import. Bars with different letters represent means that are statistically significant ($p < 0.05$) from each other ($n = 3$) according to the Tukey-Kramer HSD method. Bars with matching letters represent means that are not statistically significant from each other.

Polyplexes formed with $T4_{12}$ were found both on the periphery of the nuclei and inside of the nuclei, but to a lesser extent than polyplexes formed with the higher molecular weight polymers. To further confirm this, Z-stacks of each image were taken and fluorescence was quantified for each slice using the software ImageJ (Figure 3.12). The peak of PI fluorescence was used to determine where the center of the nucleus was. Indeed, $T4_6$-treated nuclei exhibited higher Cy5 fluorescence near the surface of the nuclei, while PEI, $T4_{43}$ and $A4_{42}$-treated nuclei exhibited Cy5 fluorescence from the inside of the nuclei.

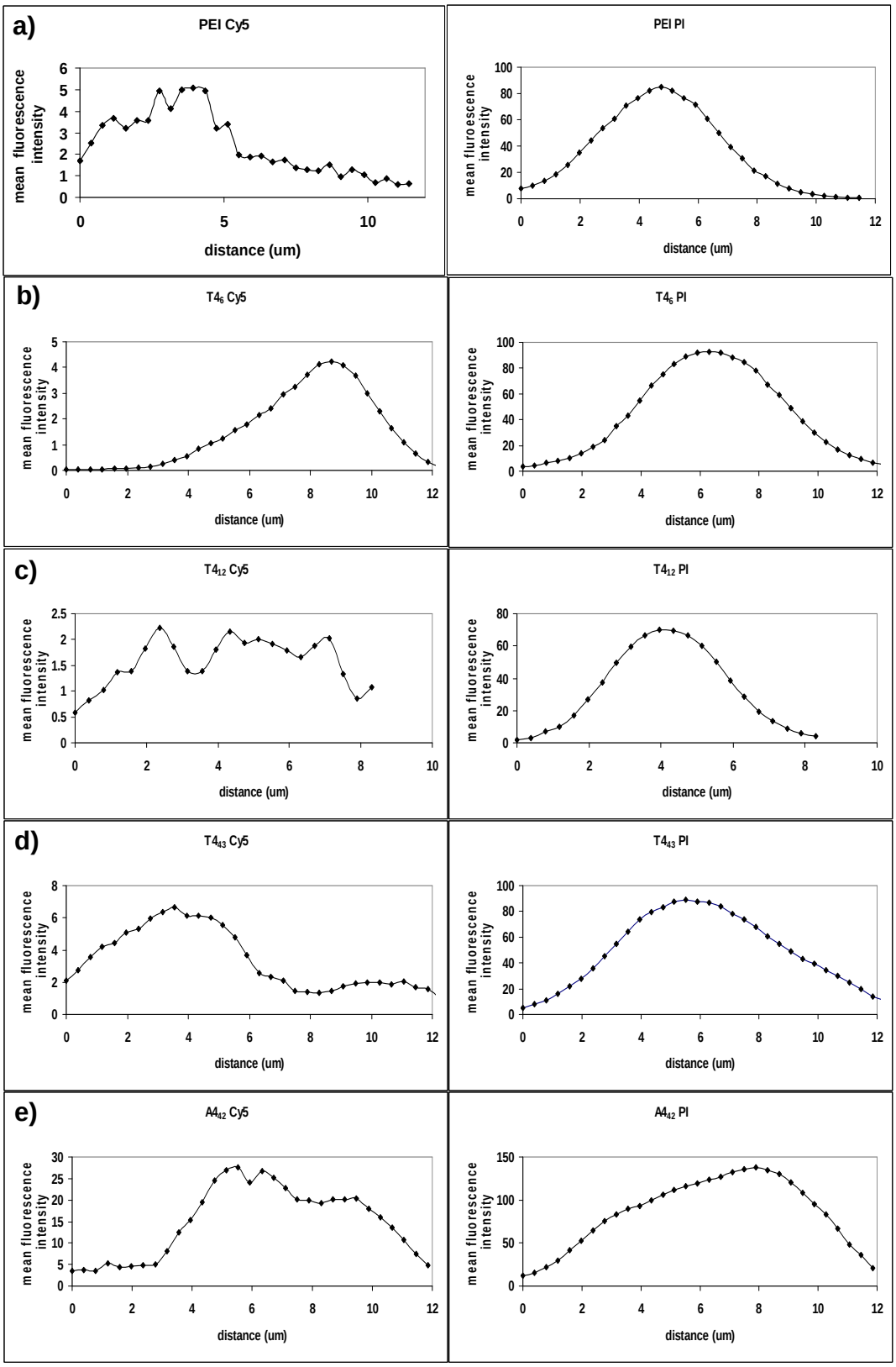
a)
PEI Cy5
mean fluorescence intensity
distance (um)
PEI PI
mean fluorescence intensity
distance (um)
b)
T4$_6$ Cy5
mean fluorescence intensity
distance (um)
T4$_6$ PI
mean fluorescence intensity
distance (um)
c)
T4$_{12}$ Cy5
mean fluorescence intensity
distance (um)
T4$_{12}$ PI
mean fluorescence intensity
distance (um)
d)
T4$_{43}$ Cy5
mean fluorescence intensity
distance (um)
T4$_{43}$ PI
mean fluorescence intensity
distance (um)
e)
A4$_{42}$ Cy5
mean fluorescence intensity
distance (um)
A4$_{42}$ PI
mean fluorescence intensity
distance (um)

Figure 3.12) Comparison of Cy5 and PI fluorescence by slice in Z-stacks obtained using confocal microscopy. Nuclei were isolated from transfected cells 24 hours after transfection from HeLa cells transfected with the following polymers: (a) JetPEI (PEI); (b) $T4_6$; (c) $T4_{12}$; (d) $T4_{43}$; (e) $A4_{42}$. Propidium iodide (PI) maximum fluorescence intensity was interpreted as the center of the nuclei for each corresponding set of Cy5 measurements. Polyplexes were deemed to be in the center of the nuclei if the peaks for Cy5 fluorescence corresponded to the peaks for PI fluorescence.

Furthermore, Manders coefficients were measured to observe colocalization between Cy5-labeled pDNA and propidium iodide in the nucleus to verify which polymers were able to induce nuclear import of the pDNA. The trends observed with transfection efficiency (Figure 3.2), plasma membrane disruption (Figure 3.6), and nuclear membrane permeability (Figure 3.10 b) were also evident when studying nuclear pDNA import; polymers with the highest transfection efficiency exhibited the most colocalization between pDNA and propidium iodide, with PEI, $T4_{43}$ and $A4_{42}$ exhibiting significantly ($p < 0.05$) more colocalization than $T4_6$ (Figure 3.11 g).

It is possible that the observed increase in PI fluorescence was not due to direct nuclear envelope permeabilization by the polymers, but rather a result of apoptosis being initiated at this time point. During apoptosis, nuclear envelope integrity breaks down, which may be why high transfection efficiency is also accompanied by high cytotoxicity in the polymers examined herein. To further study this, we wanted to observe whether the polyplexes were at the nuclear membrane 4 hours after transfection.

Nuclear interactions. The flow cytometry results indicated that $T4_6$ had higher nuclear interactions than the other polymers 4 hours after transfection, and the degree of nuclear interaction decreased with an increase in polymer length (Figure 3.10 a). To confirm that polyplexes were in fact reaching the nuclear membrane 4 hours after transfection, HeLa cells were transfected as described above for 4 hours, then the cells were fixed in 4 % paraformaldehyde, immunostained to label the nuclear lamin, and

imaged using confocal microscopy. Images of the whole cells with the differential interference contrast (DiC) images are shown in Figure 3.13, illustrating that all polyplexes are able to enter the cells and reach the nucleus 4 hours after transfection. The nuclei of the transfected cells are the focus of the confocal images shown in Figure 3.14 to further illustrate nuclear membrane ruffling at the site of polyplex-nuclear association and colocalization of the polyplexes with the nuclear lamin.

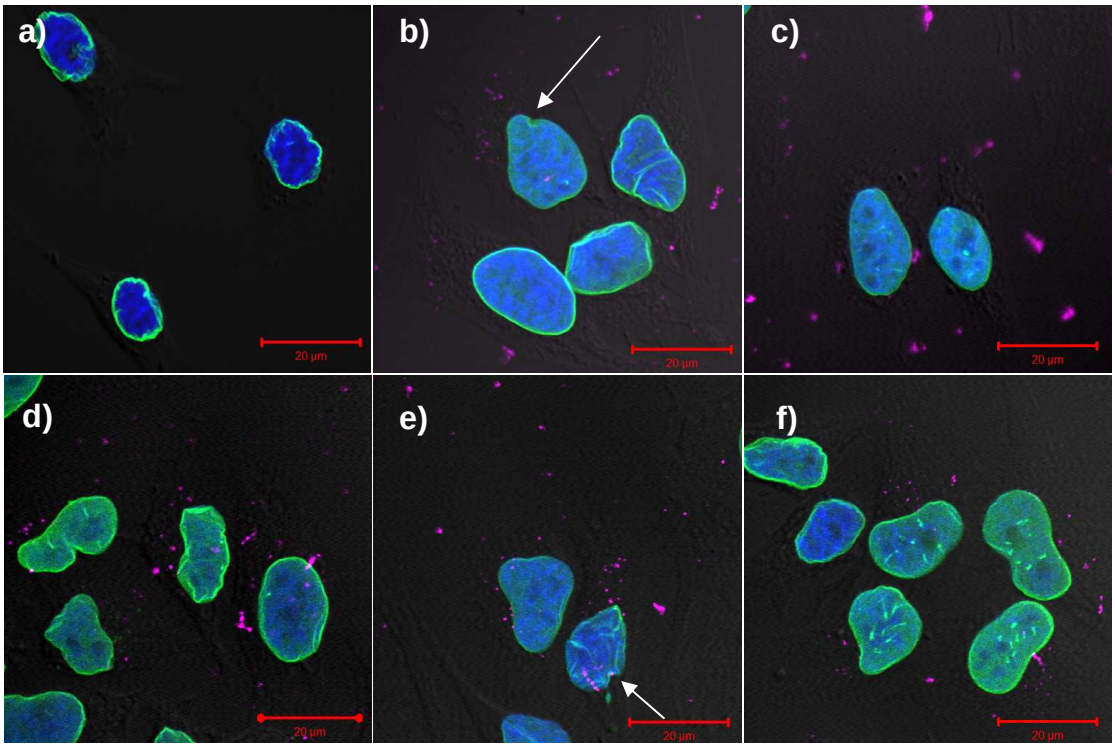

Figure 3.13) Confocal images of HeLa cells fixed 4 hours after transfection. Cells were transfected with the following: a) DNA only; b) JetPEI (PEI); c) $T4_6$; d) $T4_{12}$; e) $T4_{43}$; f) $A4_{42}$. Colors represent the following; blue = nucleus; green = nuclear lamin; magenta = pDNA. Scale bar = 20 µm. The white arrows in (b) and (e) indicate sites of deep nuclear indentation.

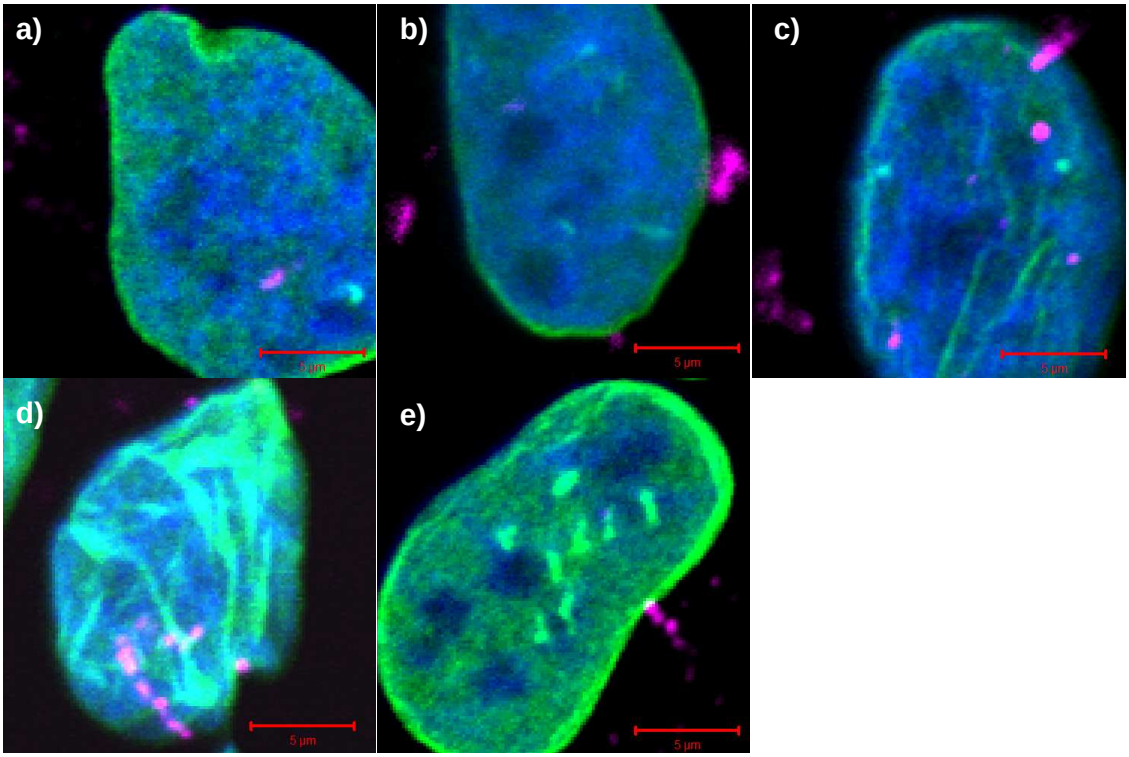

Figure 3.14) Confocal microscopy images of the nuclei in whole HeLa cells transfected with polyplexes formed with Cy5-pDNA and (a) JetPEI (PEI); (b) $T4_6$; (c) $T4_{12}$; (d) $T4_{43}$; (e) $A4_{42}$. The nucleus is shown as blue, nuclear lamin is shown as green, and the polyplexes are shown as magenta. Scale bar = 5 µm. These images emphasize polyplex-lamin colocalization and further show nuclear indentations in the case of (a) JetPEI and (d) $T4_{43}$.

Nuclear envelope ruffling was evident in all nuclei to some extent, but we see deeper indentations from cells treated with JetPEI (Figure 3.14 a) and $T4_{43}$ (Figure 3.14 d) as evidenced by the white arrows. This membrane ruffling could be caused by apoptosis, but the image for $T4_{43}$ is especially striking. In the case of $T4_{43}$, there is evidence of nuclear membrane disruption at the site of polyplex contact (Figure 3.14 d). The images in Figure 3.13 indicate that all polyplexes are able to reach the nuclear membrane within 4 hours of transfection. To verify this result, Manders coefficients were calculated to determine colocalization between the polyplexes and the nuclear lamin using the software ImageJ. Z-stacks of each image were taken using overlapping slices of 0.39 µm, and Manders coefficients were calculated using the entire z-stack. We observed slight

differences in the degree of colocalization between the different polymers, and these results confirm that the polyplexes were in fact reaching the nuclear envelope at this time point (Figure 3.15). Our results indicate that polyplexes formed with $T4_{43}$ had higher colocalization with the nuclear lamin 4 hours after transfection compared to PEI, $T4_{12}$ and $A4_{42}$ and had similar colocalization compared to $T4_6$. $T4_6$, despite having lower transfection efficiency than PEI, displayed significantly higher ($p < 0.05$) colocalization with the nuclear lamin when compared to PEI, and these results support the flow cytometry data. Because $T4_6$ is able to reach the nucleus to the same extent as the higher transfection efficiency polymers, we conclude that reaching the nucleus is not a limiting factor for pDNA delivery with these polymers. Rather, successful nuclear import of pDNA leads to efficient transfection. As seen in Figure 3.11 g, $T4_6$ has the lowest incidence of colocalization between pDNA and propidium iodide, indicating lower nuclear import. The trends between nuclear interactions and nuclear envelope permeability (Figure 3.10), colocalization with the inner nucleus (Figure 3.11 g) and transfection efficiency (Figure 3.2) are apparent. However, it is still unclear whether the polyplexes are directly permeabilizing the nuclear envelope or if the increased nuclear permeability is a result of apoptosis initiation. To test whether polyplexes alone could induce nuclear envelope permeability, studies on isolated nuclei were conducted.

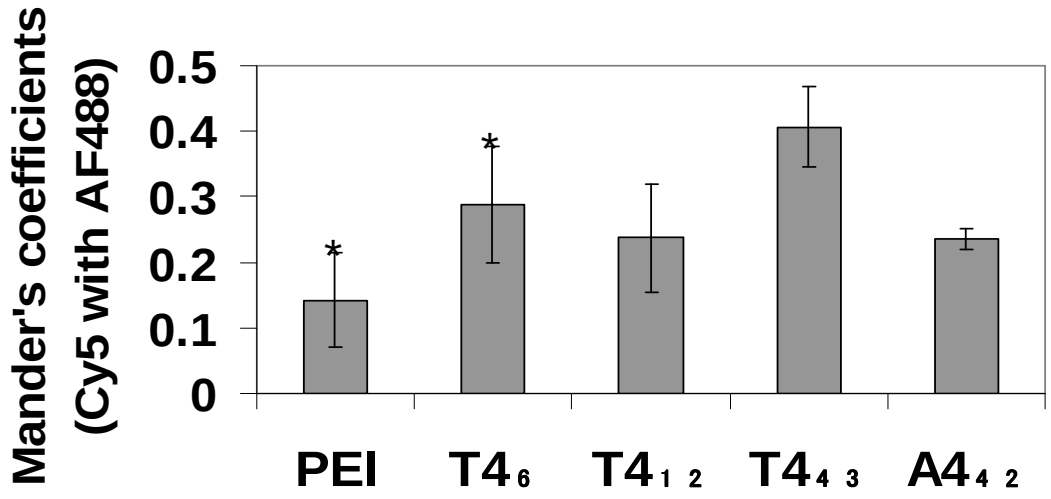

Figure 3.15) Manders coefficients for the colocalization of each polyplex type (formed with Cy5-pDNA) with lamin antibody (AF488) for confocal microscopy images taken of cells transfected with polyplexes for 4 hours. Higher Manders coefficients are indicative of higher colocalization. * denotes statistical significance ($p < 0.05$) with n = 3 according to the Tukey-Kramer HSD method.

Nuclear envelope permeability in isolated nuclei. As mentioned previously, the increased nuclear envelope permeability observed as increased PI fluorescence (Figure 3.10) could be a result of apoptosis initiation and not necessarily caused by direct polyplex interaction. To determine whether polyplexes could induce nuclear envelope permeability in a cell-free system, nuclei were isolated from HeLa cells and treated with polyplexes for 4 hours. The results are shown in Figure 3.16.

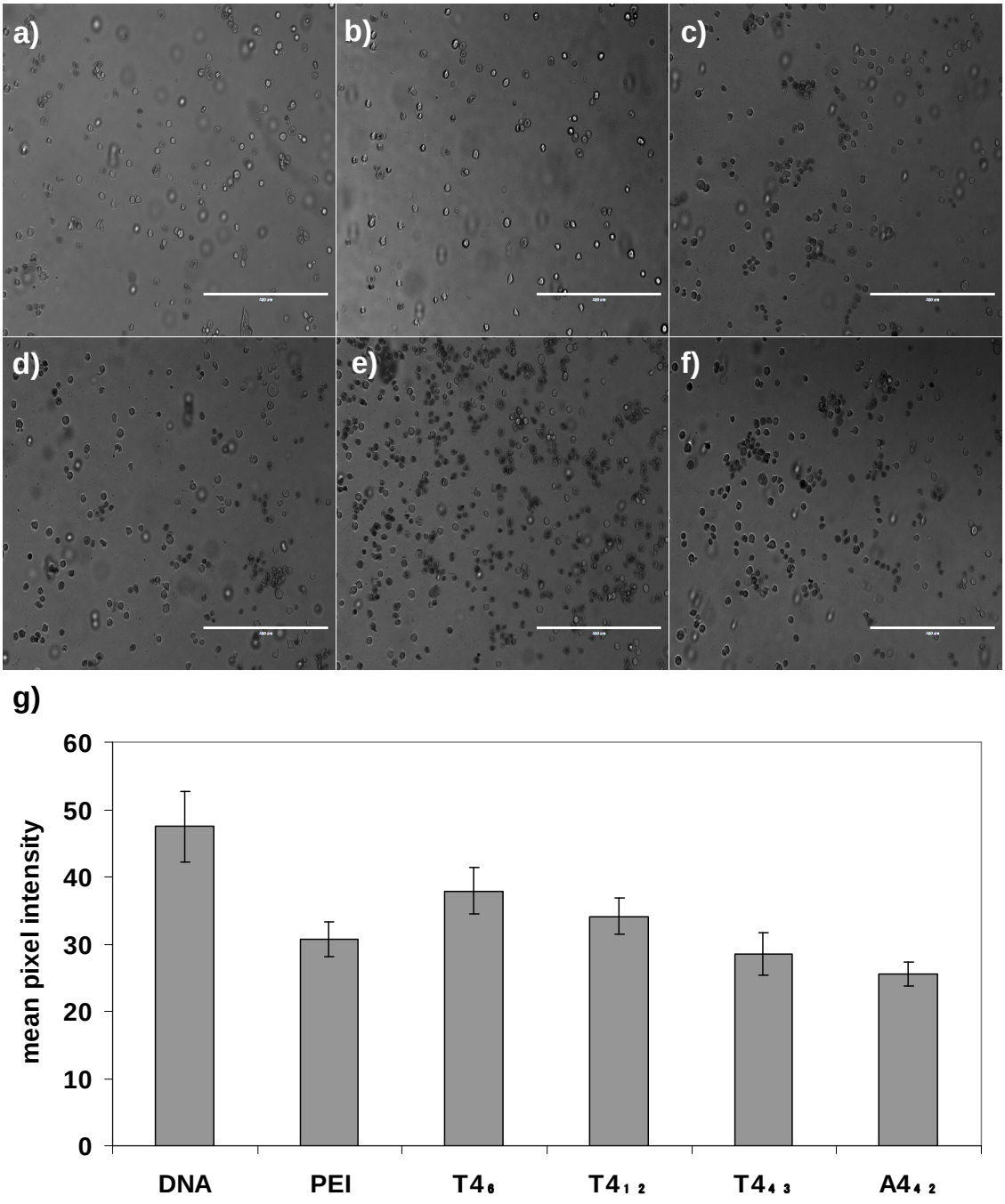

Figure 3.16) Trypan blue exclusion assay performed on nuclei treated with polyplexes for 4 hours. Nuclei were isolated from HeLa cells and treated with (a) pDNA only; (b) JetPEI (PEI); (c) $T4_6$; (d) $T4_{12}$; (e) $T4_{43}$; or (f) $A4_{42}$. Scale bar = 400 µm. (g) Nuclei were counted and analyzed for pixel intensity using ImageJ and the statistics were calculated using JMP. Roughly 300 nuclei were analyzed for each polyplex, and the Tukey-Kramer HSD method reveals each set of data points to be statistically significant ($p < 0.05$) from one another.

Trypan blue is a small molecule and is able to diffuse through the nuclear pore complex, so we would expect to see trypan blue staining in all nuclei to some extent, similar to propidium iodide exclusion. However, when observing the isolated nuclei under the microscope, we notice that nuclei treated with PEI (Figure 3.16 c), $T4_{12}$ (Figure 3.16 d), $T4_{43}$ (Figure 3.16 e), and $A4_{42}$ (Figure 3.16 d) all exhibited darker trypan blue staining compared to nuclei treated with pDNA only (Figure 3.16 a) and $T4_6$ (Figure 3.16 b). To further compare these images, image analysis was conducted to calculate the mean pixel intensity of each nuclei present in the images using ImageJ. We found that nuclei treated with the polymers all exhibited darker fluorescence intensity ($p < 0.05$) compared to the nuclei treated with pDNA only (Figure 3.16 g), with PEI, $T4_{43}$ and $A4_{42}$ exhibiting the darkest intensities, indicating that these polymers are able to induce the most trypan blue inclusion. Furthermore, we also wanted to test whether inducing apoptosis would increase transfection efficiency due to the aforementioned apoptosis-induced nuclear envelope permeability.

Transfection efficiency in apoptotic cells. To test whether the induction of apoptosis would cause increased plasma membrane permeability and nuclear envelope permeability leading to increased transfection efficiency, cells were treated with camptothecin along with the polyplexes for the first 4 hours of transfection. We saw no significant increase in transfection efficiency in transfected cells treated with 5 μM camptothecin, an apoptosis-inducing agent, compared to control cells (Figure 3.17).

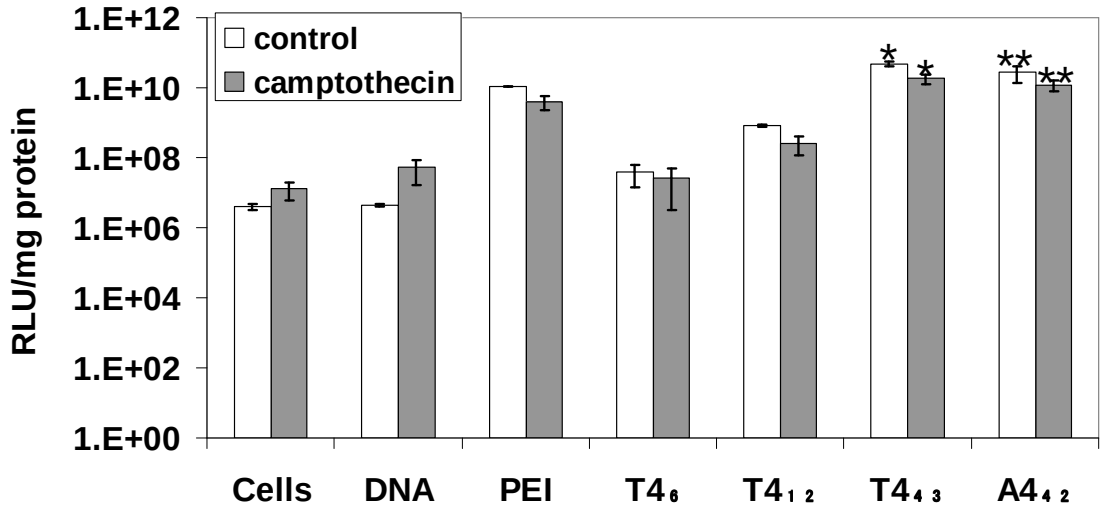

Figure 3.17) Luciferase expression data in the presence or absence of 5 μM camptothecin, an apoptosis-inducing agent. Transfection efficiency was measured 24 hours after transfection. * denotes statistical significance ($p < 0.05$, $n = 3$). ** denotes statistical significance ($p < 0.05$, $n = 3$). Statistical significance was calculated using the Tukey-Kramer HSD method.

Camptothecin had an inhibitory effect ($p < 0.05$) on $T4_{43}$ and $A4_{42}$, and did not increase the transfection efficiency of any of the polymers tested. This indicates that the induction of apoptosis is not necessary for efficient polymer-based transfection.

3.5 Conclusions and Future Directions

In the current study, we investigated several potential mechanisms of cytotoxicity for five different polymeric gene delivery vehicles, linear PEI, $T4_6$, $T4_{12}$, $T4_{43}$, and $A4_{42}$. These polymeric delivery vehicles vary in their structure (containing or lacking hydroxyls) and molecular weight. The goal of this study was to understand the role of these structural parameters on the biological behavior during pDNA delivery. These behaviors include polyplex size and charge, transfection efficiency, potential harmful interactions with the plasma membrane, ability to induce apoptosis, their ability to

generate ROS, and whether polyplexes were capable of directly permeabilizing the nuclear envelope. Herein, it was found that the length of the polymer as well as the composition of the polymer influence cytotoxicity and cell interactions to a large degree.

The first noticeable difference between the different polymers was their interactions with pDNA. We observed the polymer with the lowest molecular weight resulted in the polyplex with the largest hydrodynamic radius. Also, when comparing polymers of similar molecular weight ($T4_{43}$ and $A4_{42}$), we observe that the hydroxyl-containing $T4_{43}$ formed polyplexes of larger size and lower charge (Figure 3.1), indicating that the hydroxyls do play a role in the complexation of pDNA. We also observed differences in transfection efficiency between these two polymers, with $T4_{43}$ having slightly higher transfection efficiency than $A4_{42}$ (Figure 3.2). Previous studies in our group indicate that the hydroxyl groups present in T4 may contribute to pDNA release and therefore result in higher transfection efficiency than non-hydroxyl containing polymers.[17] To further investigate the influence of polymer structure on biological behaviors, we tested the effect of molecular weight and structure on cytotoxicity.

These polymers are able to induce apoptosis within 30 minutes of transfection as indicated by decreases in mitochondrial membrane potential and phosphatidylserine externalization (Figure 3.3). Therefore, it is prudent to study the mechanisms of cellular uptake for these polymers since the cell membrane is the first obstacle to polymer-based gene delivery and could present the first negative interaction leading to toxic effects. We did find that the higher molecular weight polymers were able to induce membrane permeability/cell death (Figure 3.6) and apoptosis (Figure 3.3) to a larger extent than the lower molecular weight polymers within 4 hours of transfection. The higher molecular

weight polymers also had higher interactions with the plasma membrane within 30 minutes of transfection when compared to the shorter polymers (Figure 3.5). It is possible that since the higher molecular weight polymers are able to condense plasmid DNA into smaller polyplexes than the lower molecular weight polymers, the mechanism of uptake for the smaller polyplexes will be altered, resulting in different cytotoxic profiles. To further investigate this, intracellular uptake of the polyplexes was studied in the presence of EGTA to determine the role of extracellular calcium. We observed that chelating extracellular calcium resulted in increased uptake of PEI polyplexes, but resulted in slight inhibition of uptake for the hydroxyl-containing T4 analogues. It is possible that the hydroxyl groups influence the mechanism of endocytosis, as EGTA had no effect on the non-hydroxyl containing $A4_{42}$. Also, direct plasma membrane permeabilization may be a mechanism of uptake and of cytotoxicity for the higher molecular weight polymers, as evidenced by the increase in membrane permeability. However, although some cytotoxic responses are evident 30 minutes after transfection, the time point where colocalization of polyplexes with the plasma membrane is observed (Figure 3.5), we find that the cytotoxic profiles of the polymers tested become more apparent 4 hours after transfection, prompting us to investigate other mechanisms of polymer-induced cytotoxicity.

Previous research in our group has shown that the PGAAs are able to degrade in water and other biologically relevant buffers.[17] Here, we examined whether the different cytotoxic profiles exhibited by the polymers tested were a result of T4's ability to degrade into non-toxic byproducts. To this end, we have synthesized T4 of different molecular weights to observe the influence of molecular weight upon on T4 toxicity. We

do find that the higher molecular weight T4 shows higher cytotoxicity and transfection efficiency than its lower molecular weight counterparts, indicating that if T4 does in fact possess the ability to degrade into lower molecular weight polymers once inside the cell, it could alleviate some of the toxicity observed during polymer-based DNA delivery. We have also tested the toxicity of model T4 degradation products and have found that they do not exhibit cytoxicity 24 hours after treatment at a concentration of 100 µg/mL. Naturally occurring polyamines such as spermine and spermidine are able to induce cytotoxicity at high concentrations. One mechanism of polyamine-induced cytotoxicity is that they form harmful reactive oxygen species (ROS) when they are catabolized by cells. This was also investigated and our data show that ROS is not increased polymer-transfected cells (Figure 3.8) compared to the cells only control. In addition, aminoguanidine, which is able to prevent certain forms of oxidatively-induced cell death, did not fully prevent polyplex cytotoxicity in HeLa cells (Figure 3.7). These results lead us to believe that the main mechanism of cytotoxicity for these polymers is not from toxic by-products of their degradation.

Another potential mechanism of cytotoxicity investigated in the current work is nuclear membrane permeabilization. If the polyplexes are able to induce plasma membrane permeability, we hypothesized that they may also be able to induce nuclear membrane permeability and thus provide a mechanism of nuclear entry for their plasmid DNA cargo. We do see polyplex-nucleus interactions 4 hours after transfection, the same time point where we see drastic differences in the cytotoxic profiles of the polymers. Our data show increased propidium iodide fluorescence in nuclei isolated from PEI, $T4_{43}$, and $A4_{42}$-treated cells, indicating increased membrane permeability (Figure 3.10 b). Not only

do these three polymers exhibit the most cytotoxic responses four hours after transfection (Figures 3.3 and 3.6), but these polymers also have the highest transfection efficiency (Figure 3.2). It is possible that their high transfection efficiency correlates with their ability to permeabilize the plasma membrane; if this is the case, then these three polymers do not need to wait for nuclear envelope breakdown during mitosis to deliver their plasmid DNA into the nucleus. It is also possible that their ability to induce apoptosis (Figure 3.3) is the reason for the increased nuclear envelope permeability (Figure 3.10), and that this nuclear envelope breakdown during apoptosis allows pDNA delivered by these polyplexes to enter the nucleus. Studies performed on isolated nuclei (Figure 3.16) confirmed that polyplexes themselves are able to induce nuclear envelope permeability in a cell-free system, and studies conducted in the presence or absence of camptothecin, an apoptosis-inducing agent, indicated that the induction of apoptosis does not increase transfection efficiency for the polymers tested (Figure 3.17).

Overall, we conclude that early cytotoxicity (within 30 minutes of transfection) is due to plasma membrane permeabilization, and that toxicity four hours after transfection is due in part to nuclear membrane permeabilization. We do notice colocalization between polyplexes and the nuclear envelope at this time point, and polyplexes are able to increase nuclear envelope permeability in isolated nuclei as well as in nuclei isolated from transfected cells. If these polymers are in fact able to permeabilize the nuclear membrane, then it is possible that they are able to permeabilize the membrane of different organelles. Further study on polyplex interaction with other organelles is necessary to make definite conclusions on this matter, since polyplexes are present throughout cells 4 hours after transfection (Figure 3.13) and could potentially interact with a myriad of

intracellular processes. Although we predict that nuclear membrane permeabilization may be a mechanism of toxicity, a polymer's ability to permeabilize the nuclear membrane may be desirable for efficient transfection.

3.6 References

1. Hunter, C. A., Molecular hurdles in polyfectin design and mechanistic background to polycation induced cytotoxicity. *Adv. Drug Delivery Rev.* **2006,** *58*, 1523-1531.
2. DeSmedt, S. C.; Demeester, J.; Hennink, W. E., Cationic polymer based gene delivery systems. *Pharm. Res.* **2000,** *17*, 113-126.
3. Vijayanathan, V.; Thomas, T.; Thomas, T. J., DNA nanoparticles and development of DNA delivery vehicles for gene therapy. *Biochemistry* **2002,** *41*, 14085-14094.
4. Nel, A.; Xia, T.; Madler, L.; Li, N., Toxic potential of materials at the nanolevel. *Science* **2006,** *311*, 622-627.
5. Boussif, O.; Lezoualc'h, F.; Zanta, M. A.; Mergny, M. D.; Scherman, D.; Demeneix, B.; Behr, J. P., A versatile vector for gene and oligonucleotide transfer into cells in culture and in vivo: polyethylenimine. *PNAS* **1995,** *92*, 7297-7301.
6. Godbey, W. T.; Wu, K. K.; Mikos, A. G., Size matters: Molecular weight affects the efficiency of poly(ethylenimine) as a gene delivery vehicle. *J. Biomed. Mater. Res.* **1999,** *45*, 268-275.
7. Bieber, T.; Meissner, W.; Kostin, S.; Niemann, A.; Elsasser, H.-P., Intracellular route and transcriptional competence of polyethylenimine-DNA complexes. *J. Controlled Release* **2002,** *82*, 441-454.
8. Moghimi, S. M., Symonds, P., Murray, J.C., Hunter, A.C., Debska, G., and Szewczyk, A., A two-stage poly(ethyleneimine)-mediated cytotoxicity: implications for gene transfer/therapy. *Molecular Therapy* **2005,** *11*, 990-995.
9. Godbey, W. T., Wu, K.K., and Mikos, A.G., Poly(ethylenimine)-mediated gene delivery affects endothelial cell function and viability. *Biomaterials* **2001,** *22*, 471-480.
10. Lv, H., Zhang, S., Wang, B., Cui, S., and Yan, J., Toxicity of cationic lipids and cationic polymers in gene delivery. *J. Controlled Release* **2006,** *114*, 100-109.
11. Liu, Y., Wenning, L., Lynch, M., and Reineke, T.M., Gene delivery with novel poly(L-tartaramidoamine)s In *Polymeric Drug Delivery Volume I - Particulate Drug Carriers*, Svenson, S., Ed. American Chemical Society: Washington, D.C., 2005.
12. Lee, C. C., Liu, Y., and Reineke, T.M., General structure-activity relationship for poly(glycoamidoamine)s: The effect of amine density on cytotoxicity and DNA delivery efficiency. *Bioconjugate Chem.* **2008,** *19*, 428-440.
13. Liu, Y., Wenning, L., Lynch, M., and Reineke, T.M., Gene delivery with novel poly(L-tartaraminoamine)s. In *Polymeric Drug Delivery Volume I - Particulate Drug Carriers*, Svenson, S., Ed. American Chemical Society: Washington, D.C., 2006; Vol. 923, pp 217-227.

14. Liu, Y., and Reineke, T.M., Poly(glycoamidoamine)s for gene delivery: Stability of polyplexes and efficacy with cardiomyoblast cells. *Bioconjugate Chem.* **2006,** *17*, 101-108.
15. McLendon, P. M.; Fichter, K. M.; Reineke, T. M., Poly(glycoamidoamine) vehicles promote pDNA uptake through multiple routes and efficient gene expression *via* caveolae-mediated endocytosis. *Mol. Pharmaceutics* **2010,** *7*, 738-750.
16. McLendon, P. M.; Buckwalter, D. J.; Davis, E. M.; Reineke, T. M., Interaction of poly(glycoamidoamine) DNA delivery vehicles with cell-surface glycosaminoglycans leads to polyplex internalization in a manner not soley dependent on charge. *Mol. Pharmaceutics* **2010,** *7*, 1757-1768.
17. Liu, Y.; Reineke, T. M., Degradation of poly(glycoamidoamine) DNA delivery vehicles: Polyamide hydrolysis at physiological conditions promotes DNA release. *Biomacromolecules* **2010,** *11*, 316-325.
18. Rasband, W. S. *ImageJ*, U.S. National Institutes of Health: Bethseda, MA, 1997-2009.
19. Stevens, M. P., *Polymer Chemistry: An Introduction*. 3 ed.; Oxford University Press: New York, 1999.
20. Prevette, L. E.; Lynch, M. L.; Reineke, T. M., Amide spacing influences pDNA binding of poly(amidoamine)s. *Biomacromolecules* **2010,** *11*, 326-332.
21. Prevette, L. E.; Kodger, T. E.; Reineke, T. M.; Lynch, M. L., Deciphering the role of hydrogen bonding in enhancing pDNA-polycation interactions. *Langmuir* **2007,** *23*, 9773-9784.
22. Godbey, W. T.; Wu, K. K.; Mikos, A. G., Poly(ethyelimine)-mediated gene delivery affects endothelial cell function and viability. *Biomaterials* **2001,** *22*, 471-480.
23. Moghimi, S. M.; Symonds, P.; Murray, J. C.; Hunter, A. C.; Debska, G.; Szewczyk, A., A two-stage poly(ethyleneimine)-mediated cytotoxicity: implications for gene transfer/therapy. *Molecular Therapy* **2005,** *11*, 990-995.
24. Mecke, A.; Majoros, I. J.; Patri, A. K.; Baker, J. R.; Holl, M. M. B.; Orr, B. G., Lipid bilayer disruption by polycationic polymers: The role of size and chemical functional group. *Langmuir* **2005,** *21*, 10348-10354.
25. Chen, J.; Hessler, J. A.; Putchakayala, K.; Panama, B. K.; Khan, D. P.; Hong, S.; Mullen, D. G.; DiMaggio, S. C.; Som, A.; Tew, G. N.; Lopatin, A. N.; Baker, J. R.; Holl, M. M. B.; Orr, B. G., Cationic nanoparticles induce nanoscale disruption in living cell plasma membranes. *J. Phys. Chem. B* **2009,** *113*, 11179-11185.
26. Hong, S.; Leroueil, P. R.; Janus, E. K.; Peters, J. L.; Kober, M.-M.; Islam, M. T.; Orr, B. G.; Baker, J. R.; Holl, M. M. B., Interaction of polycationic polymers with supported lipid bilayers and cells: Nanoscale hole formation and enhanced membrane permeability. *Bioconjugate Chem.* **2006,** *17*, 728-734.
27. Hong, S.; Hessler, J. A.; Banaszak Holl, M. M.; Leroueil, P.; Mecke, A.; Orr, B. G., Physical interactions of nanoparticles with biological membranes: The observation of nanoscale hole formation. *Bioconjugate Chem.* **2006,** *17*, 728-734.
28. Zuhorn, I. S.; Kalicharan, D.; Robillard, G. T.; Hoekstra, D., Adhesion receptors mediate efficient non-viral gene delivery. *Molecular Therapy* **2007,** *15*, 946-953.
29. DiGioia, S.; Conese, M., Polyethylenimine-mediated gene delivery to the lung and therapeutic applications. *Drug Design, Development and Therapy* **2008,** *2*, 163-188.

30. Meng, Q.-H.; Robinson, D.; Jenkins, R. G.; McAnulty, R. J.; Hart, S. L., Efficient transfection of non-proliferating human airway epithelial cells with a synthetic vector system. *J. Gene Med.* **2004,** *6*, 210-221.
31. Orlov, S. N., Aksentsev, S.L., Kotelevtsev, S.V., Extracellular calcium is required for the maintenance of plasma membrane integrity in nucleated cells. *Cell Calcium* **2005,** *38*, 53-57.
32. Zhou, Y., Shi, J., Cui, J., and Deng, C.X., Effects of extracellular calcium on cell membrane resealing in sonoporation. *J. Controlled Release* **2008,** *126*, 34-43.
33. Reddy, A.; Caler, E. V.; Andrews, N. W., Plasma membrane repair is mediated by Ca+2-regulated exocytosis of lysosomes. *Cell* **2001,** *106*, 157-169.
34. McNeil, P. L.; Kirchausen, T., An emergency response team for membrane repair. *Nat. Rev. Mol. Cell Biol.* **2005,** *6*, 499-505.
35. Prevette, L. E., Mullen, D.G., and Banaszak Holl, M.M., Polycation-induced cell membrane permeability does not enhance cellular uptake or expression efficiency of delivered DNA. *Mol. Pharmaceutics* **2010,** *7*, 870-883.
36. Lam, A. M. I.; Cullis, P. R., Calcium enhances the transfection potency of plasmid DNA-cationic liposome complexes. *Biochim. Biophys. Acta* **2000,** *1463*, 279-290.
37. Mozafari, M. R.; Omri, A., Importance of divalent cations in nanolipoplex gene delivery. *Journal of Phamaceutical Sciences* **2007,** *96*, 1955-1966.
38. Sun, Y.; Zeng, X.-R.; Wenger, L.; Cheung, H. S., Basic calcium phosphate cyrstals stimulate the endocytic activity of cells--inhibition by anti-calcification agents. *Biochem. Biophys. Res. Commun.* **2003,** *312*, 1053-1059.
39. Kulkarni, V. I.; Shenoy, V. S.; Dodiya, S. S.; Rajyaguru, T. H.; Murthy, R. R., Role of calcium in gene delivery. *Expert Opinion on Drug Delivery* **2006,** *3*, 235-245.
40. Jett, M.; Jamieson, G. A., Comparison of binding sites for wheat germ agglutinin on Raji lymphoblastoid cells and their isolated nuclei and plasma membranes. *Biochemistry* **1981,** *20*, 5221-5226.
41. Peters, B. P.; Ebisu, S.; Goldstein, I. J.; Flashner, M., Interaction of wheat germ agglutinin with sialic acid. *Biochemistry* **1979,** *18*, 5505-5511.
42. Manders, E. M. M.; Stap, J.; Brakenhoff, G. J.; Driel, R. V.; Aten, J. A., Dynamics of three-dimensional replication patterns during the S-phase, analysed by double labelling of DNA and confocal microscopy. *J. Cell Sci.* **1992,** *103*, 857-862.
43. Manders, E. M. M.; Verbeek, F. J.; Aten, J. A., Measurement of co-localizatin of objects in dual-colour confocal images. *J. Microsc.* **1993,** *169*, 375-382.
44. DeWolf, H. K.; DeRaad, M.; Snel, C.; Steenbergen, M. J. v.; Fens, M. H. A. M.; Storm, G.; Hennink, W. E., Biodegradable poly(2-dimethylamino ethylamino)phosphazene for gene delivery to tumor cells. Effect of polymer molecular weight. *Pharm. Res.* **2007,** *24*, 1572-1580.
45. Symonds, P.; Murray, J. C.; Hunter, A. C.; Debska, G.; Szewczyk, A.; Moghimi, S. M., Low and high molecular weight poly(L-lysine)s/poly(L-lysine)-DNA complexes initiate mitochondrial-mediated apoptosis differently. *FEBS Lett.* **2005,** *579*, 6191-6198.
46. Shin, J.-Y.; Suh, D.; Kim, J. M.; Choi, H.-G.; Kim, J. A.; Ko, J. J.; Lee, Y. B.; Kim, J.-S.; Oh, Y.-K., Low molecular weight polyethylenimine for efficient transfection of human hematopoietic and umbilical cord blood-derived $CD34^+$ cells. *Biochimica et Biophysica Acta* **2005,** *1725*, 377-384.

47. Sundaram, S.; Lee, L. K.; Roth, C. M., Interplay of polyethyleneimine molecular weight and oligonucleotide backbone chemistry in the dynamics of antisense activity. *Nucleic Acids Res.* **2007,** *35*, 4396-4408.
48. Henle, K. J.; Moss, A. J.; Nagle, W. A., Mechanism of spermidine cytotoxicity at 37 degrees C and 43 degrees C in chinese hamster ovary cells. *Cancer Res.* **1986,** *46*, 175-182.
49. Wallace, H. M., Fraser, A.V., and Hughes, A., A perspective of polyamine metabolism. *Biochem. J.* **2003,** *376*, 1-14.
50. Seiler, N., Catabolism of polyamines. *Amino Acids* **2004,** *26*, 217-233.
51. Seiler, N., Pharmacological aspects of cytotoxic polyamine analogues and derivatives for cancer therapy. *Pharmacology and Therapeutics* **2005,** *107*, 99-119.
52. Regnestrom, K.; Ragnarsson, E. G. E.; Fryknas, M.; Koping-Hoggard, M.; Artursson, P., Gene expression profiles in mouse lung tissue after administration of two cationic polymers used for nonviral gene delivery. *Pharm. Res.* **2006,** *23*, 475-482.
53. Beyerle, A.; Irmler, M.; Beckers, J.; Kissel, T.; Stoeger, T., Toxicity pathway focused gene expression profiling of PEI-based polymers for pulmonary applications. *Mol. Pharmaceutics* **2010,** *7*, 727-737.
54. Nilsson, B. O., Biological effects of aminoguanidine: An update. *Inflamm. Res.* **1999,** *48*, 509-515.
55. Takano, K.; Ogura, M.; Yoneda, Y.; Nakamura, Y., Oxidative metabolites are involved in polyamine-induced microglial cell death. *Neuroscience* **2005,** *134*, 1123-1131.
56. Brunner, S.; Sauer, T.; Carotta, S.; Cotten, M.; Saltik, M.; Wagner, E., Cell cycle dependence of gene transfer by lipoplex, polyplex and recombinant adenovirus *Gene Therapy* **2000,** *7*, 401-407.
57. Tait, A. S.; Brown, C. J.; Galbraith, D. J.; Hines, M. J.; Hoare, M.; Birch, J. R.; James, D. C., Transient production of recombinant proteins by chinese hamster ovary cells using polyethyleneimine/DNA complexes in combination with microtubule disrupting anti-mitotic agents. *Biotechnology and Bioengineering* **2004,** *88*, 707-721.
58. Pack, D. W.; Hoffman, A. S.; Pun, S.; Stayton, P. S., Design and development of polymers for gene delivery. *Nature Reviews Drug Discovery* **2005,** *4*, 581-593.
59. Ogris, M.; Wagner, E., Targeting tumors with non-viral gene delivery systems. *Drug Discovery Today* **2002,** *7*, 479-485.
60. Dean, D. A.; Strong, D. D.; Zimmer, W. E., Nuclear entry of nonviral vectors. *Gene Therapy* **2005,** *12*, 881-890.
61. Lam, A. P.; Dean, D. A., Progress and prospects: nuclear import of nonviral vectors. *Gene Therapy* **2010,** *17*, 439-447.
62. Thanaketpaisarn, O.; Nishikawa, M.; Okabe, T.; Yamashita, F.; Hashida, M., Insertion of nuclear factor-κB binding sequence into plasmid DNA for increased transgene expression in colon carcinoma cells. *Journal of Biotechnology* **2008,** *133*, 36-41.
63. Munkonge, F. M.; Amin, V.; Hyde, S. C.; Green, A.-M.; Pringle, I. A.; Gill, D. R.; Smith, J. W. S.; Hooley, R. P.; Xenariou, S.; Ward, M. A.; Leeds, N.; Leung, K.-Y.; Chan, M.; Hillery, E.; Geddes, D. M.; Griesenbach, U.; Postel, E. H.; Dean, D. A.; Dunn, M. J.; Alton, E. W. F. W., Identification and functional characterization of cytoplasmic

determinants of plasmid DNA nuclear import. *Journal of Biological Chemistry* **2009,** *284*, 26978-26987.
64. Breuzard, G.; Tertil, M.; Goncalves, C.; Cheradame, H.; Geguan, P.; Pichon, C.; Midoux, P., Nuclear delivery of NfκB-assisted DNA/polymer complexes: plasmid DNA quantification by confocal laser scanning microscopy and evidence of nuclear polyplexes by FRET imaging. *Nucleic Acids Research* **2008,** *36*, e71.
65. Dean, D. A., Import of plasmid DNA into the nucleus is sequence specific. *Experimental Cell Research* **1997,** *230*, 293-302.
66. Munkonge, F. M.; Dean, D. A.; Hillery, E.; Griesenbach, U., Emerging significance of plasmid DNA nuclear import in gene therapy. *Advanced Drug Delivery Reviews* **2003,** *55*, 749-760.
67. Hebert, E., Improvement of exogenous DNA nuclear importation by nuclear localization signal-bearing vectors: a promising way for non-viral gene therapy? *Biology of the Cell* **2003,** *95*, 59-68.
68. Dean, D. A.; Dean, B. S.; Muller, S.; Smith, L. C., Sequence requirements for plasmid nuclear transport. *Experimental Cell Research* **1999,** *253*, 713-722.
69. Miller, A. M.; Dean, D. A., Tissue-specific and transcription factor-mediated nuclear entry of DNA. *Advanced Drug Delivery Reviews* **2009,** *61*, 603-613.
70. Vacik, J.; Dean, B. S.; Zimmer, W. E.; Dean, D. A., Cell-specific nuclear import of plasmid DNA. *Gene Therapy* **1999,** *6*, 1006-1014.

Chapter 4 : Nuclear Import of pDNA During Polymer Transfection

Based on the manuscript “Mechanisms of pDNA Nuclear Import in Polymer-based DNA Delivery” from Grandinetti, G.; and Reineke, T.M., in preparation.

4.1 Abstract

Cationic polymers are commonly used to transfect mammalian cells, but their exact mechanism of DNA delivery is unknown. This study seeks to decipher the mechanism by which plasmid DNA delivered by cationic polymers trafficks to and enters the nucleus. Studies have been done to elucidate the mechanism by which naked plasmid DNA (pDNA) is imported into the nuclei of mammalian cells, but our goal was to determine how polymer complexation affects pDNA nuclear import. To this end, we have performed studies in whole cells and in isolated nuclei using flow cytometry and confocal microscopy to determine the mechanism by which polymer-DNA complexes (polyplexes) are able to deliver their DNA cargo to the nuclei of their target cells. The polymers tested herein include linear poly(ethylenimine) (PEI), and two poly(glycoamidoamine)s synthesized by the Reineke group. Our results indicate that the presence of intracellular machinery has less of an impact on PEI-mediated pDNA delivery when compared to poly(glycoamidoamine)s. However, the amount of pDNA import into the nucleus increases in the presence of cytosolic extract when pDNA is delivered by PEI, thus indicating that intracellular machinery plays a role in pDNA nuclear import for all polymers tested.

4.2 Introduction

Cationic polymer-based gene delivery systems are able to successfully compact plasmid DNA into polymer-DNA complexes (polyplexes) and deliver them to cells, but they are less efficient than viruses and many exhibit high cytotoxicity.[1-3] One well-studied cationic gene delivery polymer is poly(ethylenimine) (PEI).[4-7] Although PEI is able to deliver DNA, its high toxicity prevents it from being an ideal transfection agent. In response to the high cytotoxicity, several groups have developed cationic gene delivery polymers based on PEI [8-10] in order to create a safe yet efficient gene delivery vehicle. The Reineke group has created a library of poly(glycoamidoamine)s (PGAAs), which include a PEI-like amine moiety as well as a sugar moiety in the polymer repeat unit to improve biocompatibility.[11-14] While not as efficient at plasmid DNA delivery as PEI, the PGAAs exhibit vastly different cytotoxicity profiles, with PEI-treated cells having low cell survival rates when a low charge ratio (N/P ratio) of 5 and the PGAAs achieving >80% cell survival rates even when used at the higher N/P ratio of 20.[11] Elucidating the mechanism of intracellular trafficking for these sugar-containing cationic gene delivery polymers will yield more rational design of safe, effective vehicles. Recent studies in our group indicate that the intracellular trafficking mechanisms of PEI and the PGAAs vary greatly.[15] Ultimately, the goal for these polymers is to deliver their DNA cargo to the nucleus. Herein, the effects of polymer structure on plasmid DNA nuclear import are studied using the commercially-available JetPEI (Illkirch, France), poly(galactaramidopentaethylenetetramine) (G4) (Techulon, Blacksburg, VA) and poly(L-tartaramidopentaethylenetetramine) (T4).

Previous research has shown that the sequence of the DNA significantly impacts its mechanism of nuclear entry.[16] The DNA used in these studies contains a human cytomegalovirus (CMV) early promoter sequence. The CMV promoter has no known DNA nuclear targeting signal (DTS)[17] and inclusion of a DTS in the sequence greatly enhances the transfection efficiency of CMV plasmids.[18-20] However, CMV plasmids complexed with polymers are able to efficiently transfect cells, even without a DTS, indicating that polyplexes may go through different nuclear uptake pathways than naked plasmid DNA. It is unclear whether polymer-mediated pDNA delivery utilizes intracellular machinery such as the classic nuclear localization signal (NLS) pathway which employs the nuclear pore complexes (NPCs), or a different pathway, as is the case for glycosylated proteins that utilize a sugar-dependent mechanism for nuclear import.[21]

The structure of the polymer itself can greatly affect intracellular events during pDNA delivery. Previous work has shown that PEI is capable of disrupting plasma membranes.[22] The addition of carbohydrate moieties to gene delivery polymers can also affect nuclear trafficking and uptake when the carbohydrates are used as pendant groups from polymer backbone.[23-25] In order to study the effects of including both a carbohydrate moiety and amine moieties in the polymer backbone, our group compared how the presence or absence of a carbohydrate moiety affects cytotoxicity and nuclear uptake. This research has indicated direct nuclear permeabilization as a possible mechanism of polyplex nuclear import (unpublished results). In order to further determine whether the type of carbohydrate moieties present in the PGAAs affects their mechanisms of transfection, specifically nuclear import of pDNA, studies were performed using polyplexes formed with JetPEI (PEI), G4, or T4 in isolated nuclei and whole cells.

4.3 Materials and Methods

Materials. PEI (JetPEI) was purchased from Polyplus Transfection, Inc. (Illkirch, France). The polymer G4 (Glycofect) was a generous gift from Techulon Inc. (Blacksburg, VA). The polymer T4 was synthesized as previously described.[11] The plasmid DNA used for the flow cytometry and confocal microscopy studies was pCMV-luc from PlasmidFactory (Bielfield, Germany) and labeled with Cy5 using a LabelIT kit (Mirus, Madison, WI), and the plasmid DNA used for luciferase activity assays was gWiz-luc (Aldevron, Fargo, ND). Dithiothreitol (DTT), 4-(2-hydroxyethyl)-1-piperazineethanesulfonic acid (HEPES), ethylene glycol tetraacetic acid (EGTA), potassium acetate, sucrose, magnesium acetate, protease inhibitor cocktail, digitonin, ATP, GTP, creatine phosphokinase, and creatine phosphate were from Sigma (St. Louis, MO).

Cell culture. Cell culture media and supplements were purchased from Gibco (Carlsbad, CA). Human cervical adenocarcinoma (HeLa) cells were purchased from ATCC (Rockville, MD) and cultured according to the manufacturer's specified conditions. Cells were maintained in Dulbecco's modified Eagle medium (DMEM) supplemented with 10 % fetal bovine serum (FBS), 100 μg/mL streptomycin, 0.25 μg/mL amphotericin, and 100 units/mg penicillin. Transfections were performed in serum-free medium (OptiMEM).

Transfection efficiency. Luciferase activity was measured as previously described.[26] Briefly, polyplexes were formed by adding 150 μL of polymer solution diluted to the appropriate N/P ratio to 150 μL of a 0.02 mg/mL solution of gWiz-Luc pDNA (Aldevron,

Fargo, ND). Polyplexes were incubated for 1 hour at room temperature prior to transfection. Forty-eight hours after transfection, luminescence was measured using Promega's luciferase substrate (Madison, WI) on a plate reader (GENios Pro, Tecan, Research Triangle Park, NC). Cells were transfected in triplicate and the average luminescence was used to calculate transfection efficiency based on luciferase activity. Where indicated, cells were transfected in the presence of 0.006 mg/mL (20 μM) of nocodazole for the first 4 hours of transfection to disrupt microtubules or 10 μg/mL (30 μM) of aphidicolin for 24 hours during transfection to halt the cell cycle. Transfection efficiency in the presence/absence of nocodazole and the presence/absence of aphidicolin was measured 24 hours after transfection.

Labeling polymers. Fluorescently-labeled JetPEI (JetPEI-FluoF) was purchased from Polyplus Transfections (Illkirch, France). In order to label T4 and G4, the polymers were dissolved in methanol at a concentration of 1 mM for T4 and 0.5 mM for G4. FITC-isothiocyanate (Sigma, St. Louis, MO) was dissolved in methanol and added dropwise to the polymer solution while stirring to reach a final molar ratio of 3:1 FITC: polymer. The polymer and FITC were reacted for 48 hours in the dark at room temperature with continuous stirring. Excess dye was separated from the polymer using dialysis with a 1000 MWCO membrane.

Isolation of HeLa nuclei for flow cytometry. HeLa cells were pelleted at 200 x g at 4 °C for 10 minutes and resuspended in 2 mLs of ice-cold phosphate-buffered saline (PBS) containing 2 mM DTT, 1 μg/mL protease inhibitor cocktail and 40 μg/mL digitonin. The cells were incubated on ice for 5 minutes as described previously[27] to permeabilize the cells. Nuclei from the permeabilized cells were then pelleted at 2,000 x

g at 4 °C for 10 minutes and resuspended in 2 mLs of ice-cold PBS containing 2 mM DTT and 1 μg/mL protease inhibitor cocktail and incubated on ice for 5 minutes. Nuclei were pelleted as described above and resuspended in 500 μL of PBS prior to flow cytometry analysis. Flow cytometry was performed on a BD FACSCanto II flow cytometer (BD Biosciences, San Jose, CA).

Nuclear association in transfected cells. In order to determine nuclear uptake, cells were plated in 6 well plates at a density of 250,000 cells/well and incubated at 37 °C and 5 % CO_2 for 24 hours. Polyplexes were formed by adding 250 μL of FITC-labeled polymer diluted to the appropriate N/P ratio to 250 μL of a 0.02 mg/mL Cy5-labeled pDNA solution. The 500 μL of polyplex solution was allowed to incubate for 1 hour at room temperature before being diluted with 1 mL of serum-free medium (OptiMEM) and added to cells. Cells were washed with 1 mL of PBS/well before being transfected, and cells were transfected with 5 μg pDNA/well. Four hours after transfection, the polyplex-containing OptiMEM was aspirated off, cells were washed with 1 mL of PBS/well, and 5 mLs of supplemented DMEM was added to each well. Twenty-four hours after transfection, nuclei were isolated using the procedure described in the previous section. Nuclei were pelleted and resuspended in 500 μL PBS before being analyzed for FITC and Cy5 fluorescence using flow cytometry. A minimum of 20,000 events was collected for each sample. To further study the nuclear interactions of the polyplexes, nuclei from the flow cytometry experiment were pelleted at 2,000 x g, 4 °C for 10 minutes and resuspended 1 mL of PBS containing 100 μg/mL of 2 MDa rhodamine-labeled dextran (Molecular Probes, Eugene, OR). The nuclei were incubated in the dextran-containing PBS for 15 minutes, and then pelleted at 2,000 x g in the conditions described above and

resuspended in 1 mL of 4 % paraformaldehyde (PFA) solution. The nuclei were fixed in the PFA solution for 15 minutes at room temperature. After that, nuclei were pelleted, washed in PBS and deposited on poly-L-lysine (PLL)-coated coverslips. The nuclei incubated on the coverslips overnight at 4 °C before being mounted onto microscopy slides and analyzed *via* confocal microscopy. The degree of pixel overlap between two fluorescence channels was calculated using Manders coefficients to determine colocalization.[28-29] Manders coefficients were calculated using the software ImageJ.[30]

Isolation of soluble HeLa cytosolic proteins. Nuclei were isolated from HeLa cells as described in the previous section. After pelleting the nuclei, the supernatant was collected. Ice-cold acetone (4 x supernatant volume) was added to the supernatant, and the mixture stirred on ice for 1 hour. The mixture was distributed into 1.5 mL Eppendorf tubes, and the proteins were pelleted out by centrifuging at 14,000 x g for 10 minutes. The supernatant was discarded and the pellets were resuspended in sterile import buffer (20 mM HEPES, 0.25 M sucrose, 100 mM potassium acetate, 2 mM magnesium acetate, and 1 mM EGTA), and protein concentrations were quantified using a Bio-Rad DC Protein Assay (Hercules, CA) according to manufacturer's protocol.

Nuclear association in a cell-free system. In order to design a high-throughput method to determine the minimal requirements for pDNA-nuclear association, nuclei were isolated from HeLa cells *via* digitonin permeabilization and centrifugation as described above and deposited into 6 well plates at a concentration of 250,000 nuclei/well. The nuclei were incubated in a buffer solution consisting of 20 mM HEPES, 0.25 M sucrose, 100 mM potassium acetate, 2 mM magnesium acetate, and 1 mM EGTA as previously described by Munkonge *et. al*.[31] The buffer solution was added with or

without 50 μg HeLa cytosolic protein and with or without the ATP-generating system. Nuclei were also incubated in the presence or absence of HeLa cytosol extract and the presence or absence of an ATP-generating system (0.5 mM ATP, 0.2 mM GTP, 5 mM creatine phosphate, and 1 Unit creatine phosphokinase) as previously described by Hagstrom *et. al.*[32] Polyplexes were formed as described above and added to the nuclei. After incubating for 4 hours at 37 °C and 5 % CO_2, nuclei were pelleted, resuspended in 1 mL PBS to wash away unbound polyplexes/polymers, pelleted again, and resuspended in 500 μL of PBS before being analyzed by flow cytometry.

Confocal microscopy in a cell-free system. HeLa cells were seeded onto uncoated coverslips at a density of 50,000 cells/coverslip and allowed to incubate at 37 °C and 5 % CO_2 for 24 hours. After incubation, media was aspirated off the cells, and then the cells were washed with 1 mL of PBS/well, and 1 mL of ice-cold PBS containing 2 mM DTT, 1 μg/mL protease inhibitor cocktail and 40 μg/mL digitonin. After 5 minutes, this solution was aspirated off and 1 mL of ice-cold PBS containing 2 mM DTT and 1 μg/mL protease inhibitor cocktail was added to each well. The cells incubated in this solution for 5 minutes, after which this solution was aspirated off, the permeabilized cells were washed with PBS, and 1 mL of the aforementioned buffer solutions (20 mM HEPES, 0.25 M sucrose, 100 mM potassium acetate, 2 mM magnesium acetate, and 1 mM EGTA with/without 50 μg HeLa cytosolic protein and with/without an ATP-generating system) was added to each well. Polyplexes were formed by adding 50 μL of FITC-labeled polymer solution diluted to the appropriate N/P ratio to 50 μL of 0.02 mg/mL Cy5-labeled pDNA solution and allowed to incubate at room temperature for 1 hour. After one hour, the 100 μL of polyplex solution was added to the permeabilized cells (1 μg

pDNA/well). After 4 hours, the polyplex solution was aspirated off, the cells were washed with 1 mL of PBS/well, and cells were fixed in 4 % paraformaldehyde for 15 minutes at room temperature. Coverslips were mounted onto microscopy slides using ProLong Gold Antifade Reagent (Molecular Probes, Eugene, OR) according to manufacturer's protocol. The slides were allowed to dry overnight in the dark before being sealed with clear nail polish and imaged on a Zeiss LSM 510 META confocal microscope (Carl Zeiss MicroImaging, LLC, Thornwood, NY). Images were taken using a slice thickness of 0.8 μm. Manders coefficients were used to calculate the amount of overlap between two channels to monitor colocalization.[28-29] Manders coefficients were calculated using the software ImageJ.[30]

Confocal microscopy in whole cells. HeLa cells were seeded onto poly-L-lysine (PLL)-coated coverslips at a density of 15,000 cells/coverslip and allowed to incubate under the aforementioned conditions for 48 hours. Cells were then transfected using JetPEI-FluoF at an N/P ratio of 5 according to manufacturer's protocol and FITC-labeled T4 and FITC-labeled G4 were used at an N/P of 20. A 0.02 mg/mL Cy5-labeled pDNA solution was used to make the polyplexes, and cells were transfected with a total of 1 μg of pDNA per coverslip. Transfection was carried out in serum-free media (OptiMEM), with 1 mL of OptiMEM/well. At the indicated time points, the cells were washed with PBS and fixed using 4 % paraformaldehyde. Cells were immunostained using a 1:200 dilution of anti-fibrillarin rabbit monoclonal antibody (Cell Signaling Technologies, Inc.) and Alexa Fluor 555 goat anti-rabbit secondary antibody (Molecular Probes, Eugene, OR) as previously described.[15] Manders coefficients were used to calculate

colocalization between polyplexes and the nucleoli, and Manders coefficients were calculated using the software ImageJ as described above.

Nuclear envelope permeability in a cell-free system. HeLa cells were grown to confluency and then trypsinized and pelleted at 200 x g, 4 °C for 10 minutes. Nuclei were isolated from HeLa cells as described above and added to a 12 well plate at a density of 50,000 nuclei/well. Polyplexes were formed as described above (50 µL of polymer solution was added to 50 µL of 0.02 mg/mL plasmid DNA solution) and added to the nuclei in 1 mL of OptiMEM. The nuclei were incubated at 37 °C and 5 % CO_2 for 4 hours, after which 200 µL of a 0.4 % trypan blue solution (Gibco, Carlsbad, CA) was added to each well. The nuclei were then imaged using an EVOS fl digital inverted fluorescence microscope (Advanced Microscopy Group, Bothell, WA). The mean pixel intensity for individual nuclei was calculated using the software ImageJ.[30]

Statistical analysis. Histograms are representative of a minimum of 10,000 events from flow cytometry experiments. Data in bar graphs are presented as means ± standard deviations. For statistical analysis of data, JMP software was used (SAS Institute Inc., Cary, NC) and means were compared using ANOVA followed by the Tukey-Kramer HSD method, with $p < 0.05$ being considered as statistically significant.

4.4 Results and Discussion

Nuclear association. In order to determine whether pDNA and the polymers were associated with the nuclei, HeLa cells were transfected and their nuclei were isolated 24 hours after transfection. The nuclei were analyzed *via* flow cytometry, and histograms of Cy5-positive and FITC-positive nuclei are shown in Figure 4.1. Based on these data, we

are unable to tell whether the pDNA/polymers were bound to the surface of the nuclei or whether the fluorescent signals were coming from inside of the nuclei, so we arbitrarily call these signals “nucleus association”. Increased Cy5 fluorescence indicates increased pDNA-nucleus association, while increased FITC fluorescence indicates increased polymer-nucleus association.

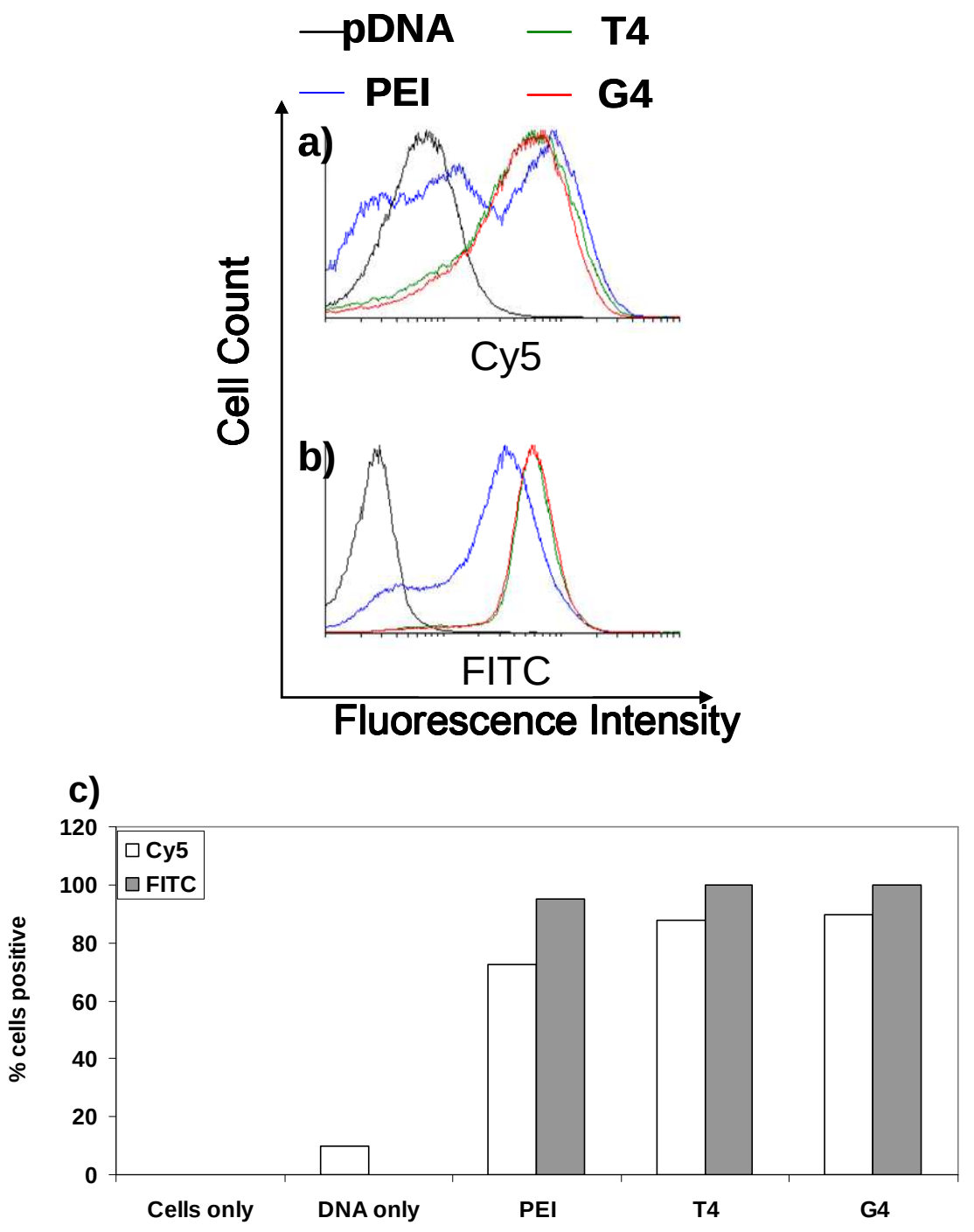

Figure 4.1) Overlayed histograms of (a) Cy5 fluorescence and (b) FITC fluorescence from nuclei isolated from HeLa cells 24 hours after transfection. Nuclei were analyzed for Cy5 and FITC fluorescence using flow cytometry. Cells were transfected with polyplexes made from FITC-labeled JetPEI-FluoF (PEI) at an N/P ratio of 5, FITC-labeled T4 at an N/P ratio of 20, or FITC-labeled G4 at an N/P ratio of 20 and Cy5-labeled pDNA. All polyplex-treated nuclei exhibited increased pDNA association and polymer association as indicated by increased Cy5 and FITC fluorescence,

respectively. (c) Bar graph representation of the flow cytometry data. One trial is presented here, we were unable to carry out more trials based on limitations in the quantity of labeled polymer.

Using this flow cytometry method, we were unable to tell whether the pDNA and the polymers were inside of the nuclei or localized to the nuclear membrane. We also wanted to determine nuclear envelope permeability by incubating the isolated nuclei with 2 MDa rhodamine-labeled dextran. After the dextran incubation, nuclei were fixed and deposited onto coverslips, followed by confocal microscopy analysis. Dextran colocalization with the DAPI-stained nuclei was used as a measure of nuclei permeability. The confocal images and colocalization data are shown in Figure 4.2.

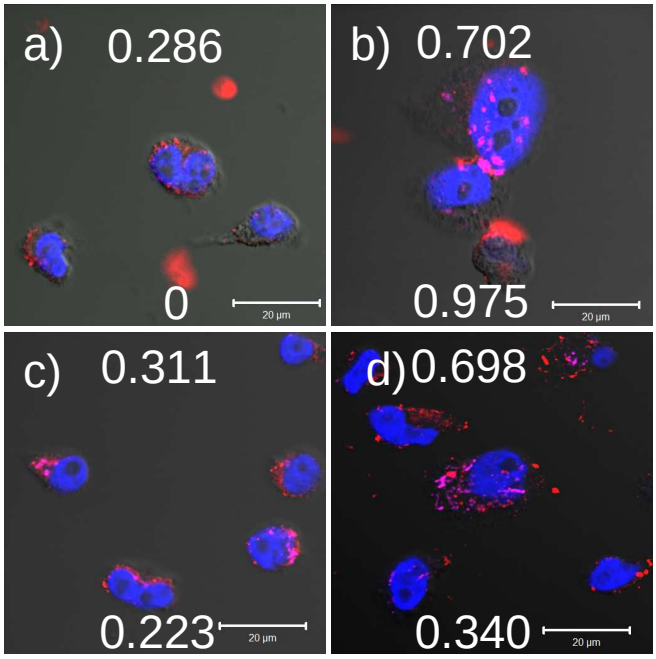

Figure 4.2) Nuclei isolated from HeLa cells 24 hours after transfection. Cells were transfected with (a) pDNA only; (b) JetPEI (PEI); (c) T4, (d) Glycofect (G4). Colors represent the following: magenta = Cy5-labeled pDNA; blue = DAPI-labeled nucleus; red = rhodamine-labeled dextran. Scale bar = 20 µm. Numbers in the upper portion of the images represent the colocalization data as determined by Manders coefficients between rhodamine-labeled dextran and DAPI-labeled nuclei. Numbers in the lower portion represent Manders coefficients between Cy5-labeled pDNA and DAPI-labeled nuclei. Note how nuclei isolated from PEI-treated cells (b) exhibit higher rhodamine-DAPI and Cy5-DAPI colocalization compared to G4 and T4, indicating increased nuclear envelope permeability and increased pDNA nuclear import, respectively.

From the colocalization data between rhodamine-labeled dextran and the DAPI-stained nuclei, we observe higher dextran accumulation in the nuclei isolated from PEI and G4-treated cells compared to cells treated with pDNA and T4. Whether this increased nuclear envelope permeability is a result of direct polymer permeabilization or a result of apoptosis initiation is unclear, so future studies were done in cell-free systems. We also see increased pDNA fluorescence inside of the nucleus in nuclei isolated from PEI-treated cells compared to cells treated with the PGAAs. To further evaluate the impact of the number of hydroxyl groups on nuclear trafficking and uptake, cells were transfected with FITC-labeled T4 and G4. The nuclei were isolated from transfected cells and imaged as described above. We were unable to see any FITC signal with the commercially-labeled JetPEI FluoF in fixed nuclei, but were clearly able to see FITC-labeled T4 and G4 in the nuclei. It is interesting to note that at some sites of polyplex-nuclear envelope interaction, we observe nuclear envelope ruffling as denoted by the arrows in Figure 4.3.

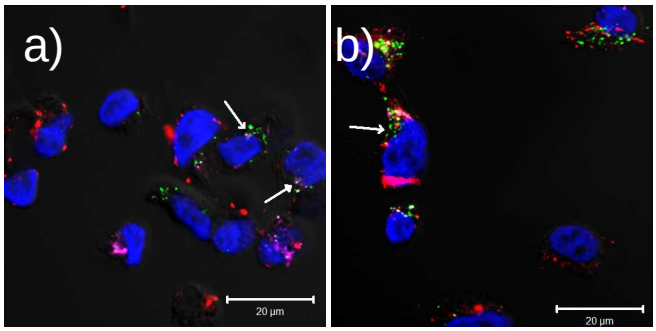

Figure 4.3) Nuclei isolated from transfected HeLa cells 24 hours after transfection. Cells were transfected with (a) T4 or (b) G4. Arrows indicate sites of nuclear envelope ruffling at sites of polyplex-nuclear interaction as determined by DAPI fluorescence. Colors represent the following: magenta = Cy5-labeled pDNA; blue = DAPI-labeled nucleus; red = rhodamine-labeled dextran. Scale bar = 20 µm.

Nuclear envelope permeability in a cell-free system. Based on the higher degree of dextran accumulation in nuclei isolated from PEI-treated cells vs. PGAA-treated cells, it was of interest to us to see whether the polyplexes themselves were responsible for the increased nuclear envelope permeability or if the increased nuclear envelope permeability was a result of apoptosis initiation. To test this, nuclei were isolated from HeLa cells, treated with polyplexes formed with the different polymers for 4 hours, and then a trypan-blue assay was used to determine nuclear envelope permeability. Trypan blue is a small molecule and is able to diffuse through the nuclear pore complex, however, we hypothesized that if the nuclear envelope increased in permeability, more trypan blue would diffuse into the nucleus and therefore the nuclei with compromised nuclear envelopes would appear darker. We did in fact observe darker pixel intensities in nuclei treated with PEI polyplexes compared to nuclei treated with pDNA only (Figure 4.4), indicating that PEI polyplexes are able to induce nuclear envelope permeability in a cell-free system. Furthermore, the trends in pixel intensity illustrated in Figure 4.4 followed the trends observed in Figure 4.2. In Figure 4.2, nuclear envelope permeability as indicated by dextran fluorescence was the highest with PEI, followed by G4, and then T4 and pDNA exhibited similar colocalization between the dextran and nuclei. In the case of the trypan blue assay, mean pixel intensity was highest with T4 and then followed by pDNA > G4 > PEI. It is interesting to note that the polymers able to induce the most nuclear envelope permeability (PEI and G4, Figures 4.2 and 4.4) are also the polymers with the highest transfection efficiency (Figure 4.6).

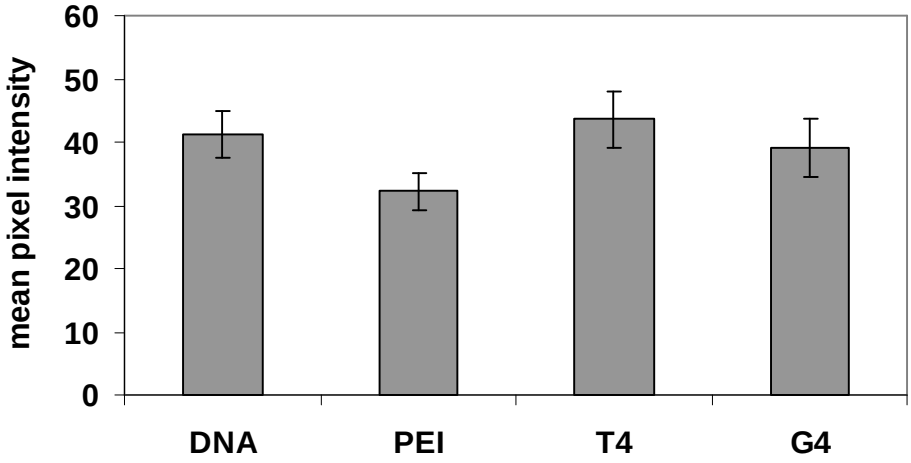

Figure 4.4) Mean pixel intensities of isolated nuclei treated with the indicated polyplexes for 4 hours and then treated with trypan blue. Darker intensities indicate more trypan blue present in the nuclei, indicating increased nuclear envelope permeability. All means are statistically significant from each other ($p < 0.05$, $n \sim 300$) according to the Tukey-Kramer HSD method. Pixel intensities are highest with nuclei treated with T4, and then pixel intensities decrease in the order pDNA (DNA) > G4 > PEI.

Intracellular location of polyplexes. To further study polyplex location during transfection, HeLa cells were transfected with the polymers and fixed 24 hours after transfection (Figure 4.5). It was our hypothesis that perhaps polymer complexation with RNA in the nucleoli could aid in pDNA release, so the nucleoli were labeled with fibrillarin rabbit monoclonal antibody (Cell Signaling Technologies, Inc.). Fibrillarin is a protein involved in RNA processing found primarily in the nucleoli.[33] Our results show little colocalization with pDNA and the nucleoli in whole cells. The mechanism of polyplex dissociation is ongoing in this field. However, due to the fact that pDNA with no nuclear localization signal does not travel to the nucleus, it is believed that polyplex dissociation does occur in or near the nucleus.[34] In fact, Godbey *et. al.* show that both PEI and its pDNA cargo are present in the nucleus 4.5 hours after transfection.[35] We

observed the same trend for the PGAAs T4 and G4; both polymer and pDNA fluorescence were evident in nuclei isolated from transfected cells (Figure 4.1 and Figure 4.3), and many polyplexes seem to still be intact as evidenced by the white pixels in Figure 4.6 that indicate colocalization between polymers and pDNA.

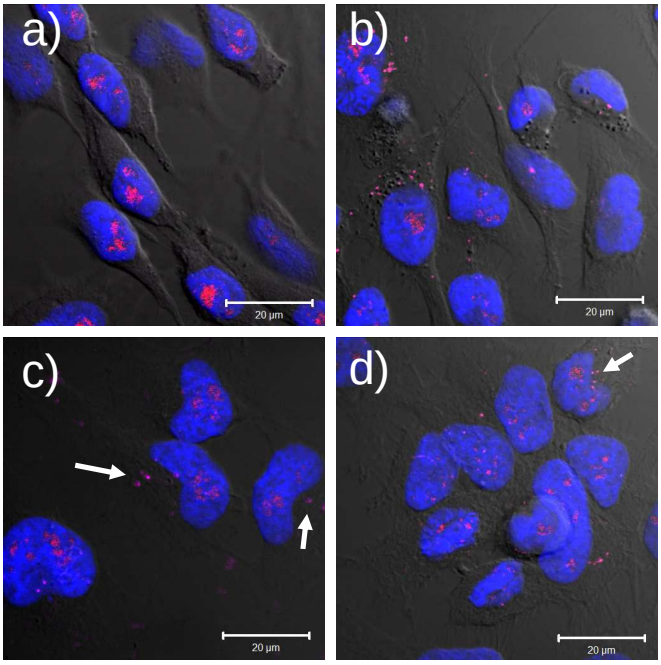

Figure 4.5) HeLa cells transfected for 24 hours with (a) pDNA only; (b) JetPEI (PEI); (c) T4; (d) G4. Polyplexes were formed with Cy5-labeled pDNA. Colors represent the following: magenta = pDNA; blue = nucleus; red = nucleoli. Scale bar = 20 µm. White arrows indicate polyplexes approaching nuclei at the site of nuclear division. We observed little colocalization between the polyplexes (magenta) and the nucleoli (red) at this time point for all polymers tested.

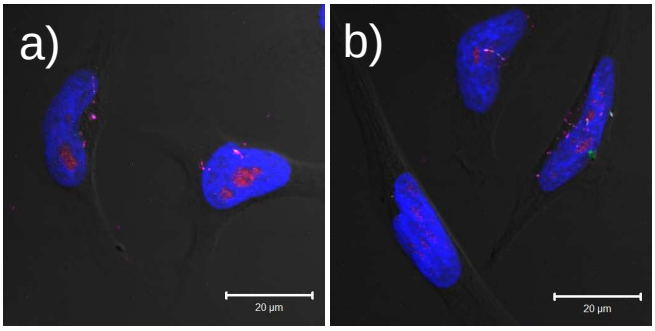

Figure 4.6) Confocal images of HeLa cells transfected with (a) T4 and (b) G4 24 hours after transfection. Colors represent the following: magenta = pDNA; blue = nucleus; red = nucleoli. Scale bar = 20 µm. White pixels indicate colocalization between the polymers (green) and pDNA (magenta).

Traffic inhibition. Based on our confocal microscopy data, it seems that the polyplexes are approaching the nucleus from the side where the microtubule organization center (MTOC) is located during mitosis. This is concluded by observing the shape of the nuclei in Figure 4.5 and is especially apparent in the case of T4 (Figure 4.5 c) and G4 (Figure 4.5 d), where the polyplexes (magenta) are approaching the nuclei at the site of nuclear division as indicated by the white arrows. We hypothesized that the microtubules play a role in polyplex trafficking to some extent, and that perhaps nuclear envelope breakdown during cell division enables polyplexes to enter the nuclei. To test this, cells were treated for 4 hours with the microtubule-disrupting agent nocodazole[36] or treated for 24 hours with the cell cycle inhibitor aphidicolin.[37] The results indicate that for all polymers, disruption of the microtubules for the first 4 hours of transfection leads to statistically significant ($p < 0.05$) lower protein expression (Figure 4.7). It is interesting to note that inhibition of the cell cycle slightly inhibits ($p < 0.05$) gene expression for G4, but not for T4 or PEI (Figure 4.7).

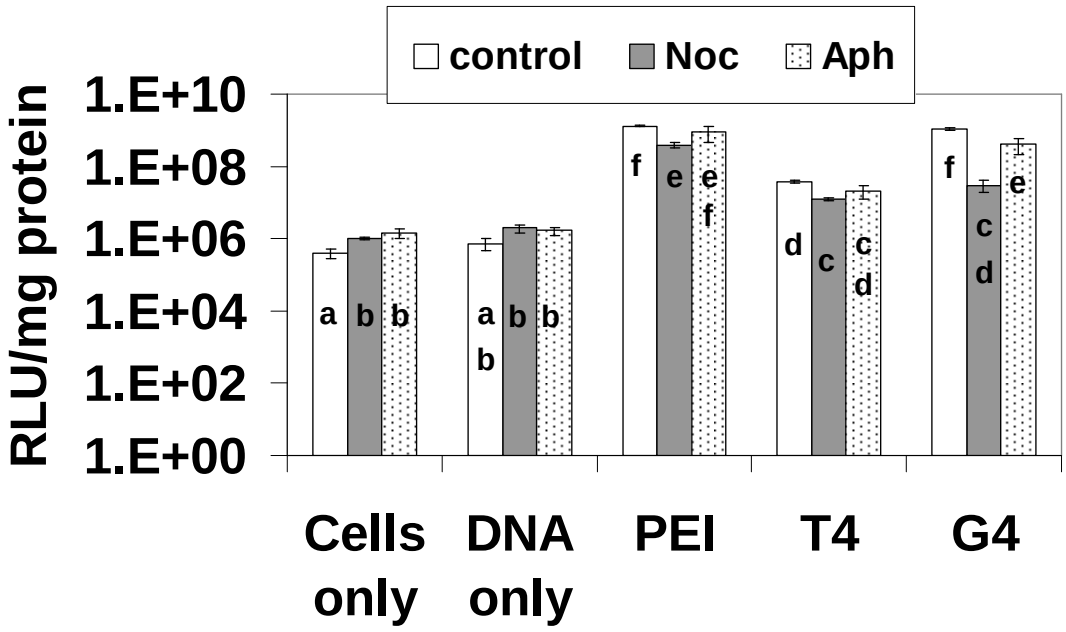

Figure 4.7) Luciferase expression 24 hours after transfection as measured by relative light units (RLU) per milligram of protein in cell lysates. Cells were transfected in the presence or absence of nocodazole (Noc) or aphidicolin (Aph) to determine if microtubule disruption or cell cycle inhibition affected transfection efficiency. Bars with different letters represent means that are statistically significant from each other according to the Tukey-Kramer HSD method ($p < 0.05$, $n = 3$).

Nuclear import in isolated nuclei. To determine whether nuclear import could occur without intracellular machinery, nuclei were isolated from HeLa cells, treated with polyplexes formed with Cy5-labeled pDNA and JetPEI (PEI) at an N/P ratio of 5, T4 at an N/P of 20, or G4 at an N/P ratio of 20. The nuclei and polyplexes were incubated with or without cytosol extract and with or without an ATP-generating system ("energy"). After 4 hours, the nuclei were analyzed for Cy5 fluorescence using flow cytometry. In order to study mechanisms of pDNA nuclear import other than direct nuclear envelope permeabilization, nuclei with higher propidium iodide fluorescence intensity than the cells only and pDNA only controls were not included in these measurements. This was done to minimize the effect on Cy5 fluorescence for pDNA import through increased

nuclear envelope permeability. The results are illustrated in Figure 4.8. From these data, it seems that the PGAAs are more dependent on intracellular machinery than PEI for pDNA nuclear trafficking, as T4 and G4 exhibited Cy5 fluorescence that was no different from the cells only and pDNA only controls (Figure 4.8 a). However, pDNA complexed with PEI was able to associate with the nuclei in this cell free system in all conditions to a significantly higher ($p < 0.05$) extent than the other polyplexes (Figure 4.8 a). The presence of an ATP-generating system had no significant effect on DNA-nucleus association when pDNA was complexed with PEI and added to nuclei in the presence or absence of cytosol. However, it is interesting to note that for PEI the presence of both cytosol and the ATP-generating system resulted in significantly higher ($p < 0.05$) pDNA-nucleus association when compared to PEI polyplexes incubated in the absence of cytosol (Figure 4.8 a).

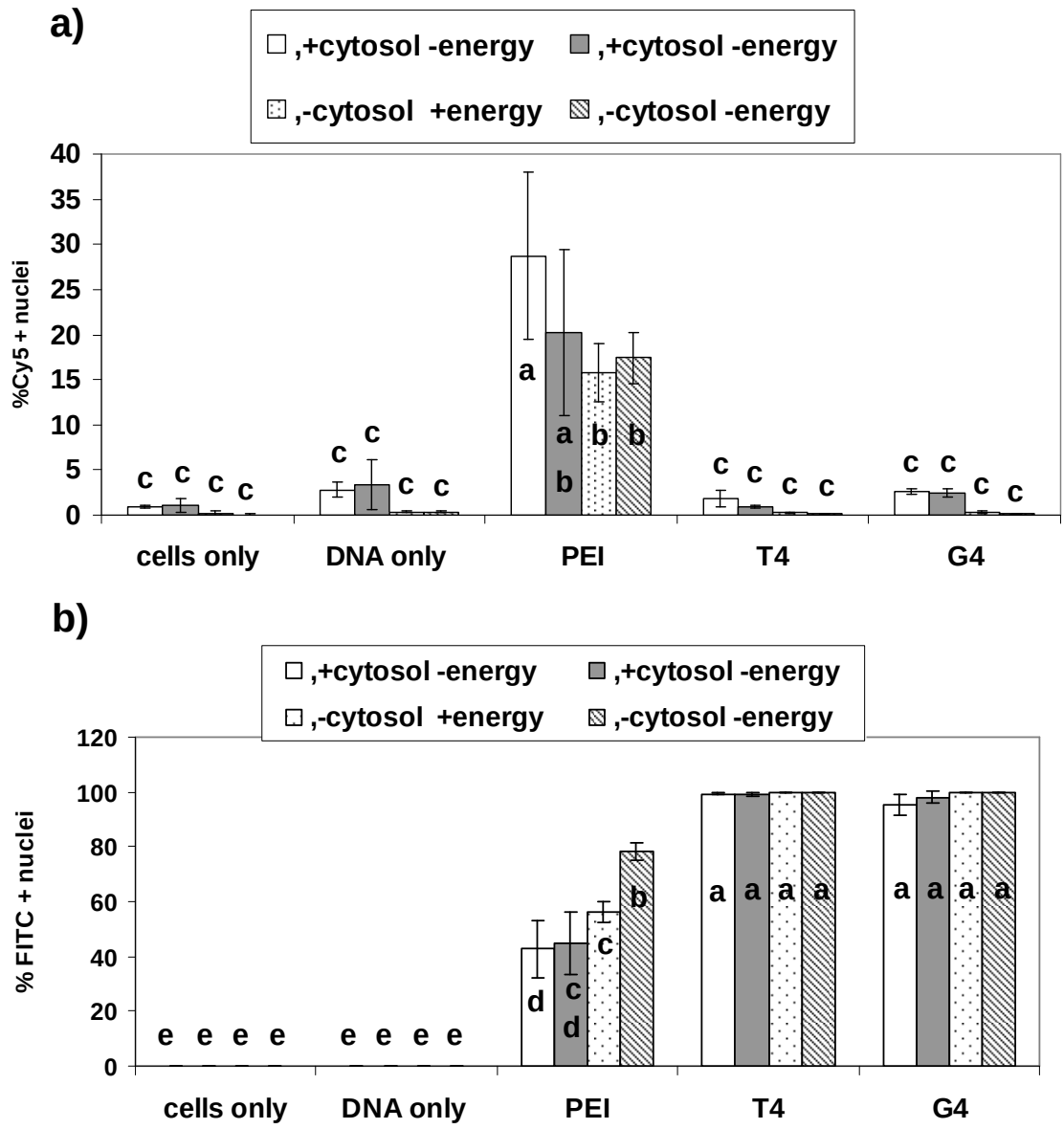

Figure 4.8) Flow cytometry data from nuclei treated with polyplexes formed with different FITC-labeled polymers and Cy5-labeled plasmid DNA. Nuclei were isolated with polyplexes with or without HeLa cytosol extract ("cytosol") and in the absence or presence of an ATP-generating system ("energy"). Nuclei were analyzed for (a) Cy5 fluorescence from the pDNA and (b) FITC fluorescence from the polymers 4 hours after polyplex treatment. Bars with different letters represent means that are statistically significant from each other according to the Tukey-Kramer HSD method ($p < 0.05$, $n = 3$). Bars with matching letters represent means that are not statistically significant from each other.

Furthermore, in all of the polymer-treated nuclei, we saw nearly 100 % of the polymer-treated nuclei were positive for FITC-fluorescence when treated with polyplexes formed with G4 and T4 regardless of incubation conditions, indicating differences in pDNA nuclear association vs. polymer nuclear association (Figure 4.8 b). We also see significantly higher ($p < 0.05$) polymer-nucleus association in the PGAAs compared to PEI (Figure 4.8 b), so it would appear that the sugar moieties in the PGAA repeat units do influence polymer-nucleus interactions. Previous research has shown that the addition of sugar groups to DNA delivery polymers enhances nuclear trafficking and pDNA nuclear import.[38-39] The polymers used in those prior studies had sugar groups hanging from the polymer backbone as pendant groups, while the PGAAs in this current study have the sugars L-tartarate (T4) and galactarate (G4) incorporated into the polymer backbone. It is possible that in free polymers, the sugar groups are more accessible to sugar receptors found on the nuclear envelope[40] compared to polymers joined to pDNA in a polyplex and thus are able to interact with the nucleus even in a cell-free system. It is also possible that nuclear association is dependent on charge. Since the PGAAs were used at a higher N/P ratio of 20 (compared with PEI used at an N/P of 5), there may be more positively-charged moieties able to interact with negatively-charged moieties found on the nuclear envelope and in the nucleus[41-42] in the case of the PGAAs. In addition, many nuclear shuttle proteins that aid in nuclear envelope translocation through the NPCs are negatively-charged.[43] Another potential reason for the differences in polymer-nucleus association between PEI and the PGAAs is the amount of FITC present on the polymers; we know that the PGAAs were labeled using a FITC: polymer ratio of 3:1, but the degree of labeling for JetPEI-FluoF, the labeled PEI used in these studies, is proprietary.

Interestingly, for the PEI polyplex-treated nuclei, FITC positive nuclei were highest in the absence of both cytosol and energy (Figure 4.8 b). This data exhibits nearly an opposite trend from that of the Cy5 positive nuclei in Figure 4.8 a. It would appear, based on these data, that the presence of cytosol increased pDNA-nucleus association for PEI polyplexes while inhibiting PEI-nucleus association. It is possible that the cationic PEI polymer could be interacting with anionic cytosolic proteins, while PEI polyplexes interact to a lesser extent with these proteins and are able to deliver their pDNA cargo to the nucleus. However, if the PGAAs are used at a higher charge ratio, we would also expect them to interact with negatively-charged cytosolic components. The difference in cytosolic interactions of PEI vs. the PGAAs may not only be influenced by the presence of the sugar moiety but also by polymer length; PEI is much longer than the PGAAs (PEI~22,000 Da vs. PGAA~4,000 Da).

From the data shown in Figure 4.8 a, it is evident that there is a high degree of variance in the percent of Cy5 positive nuclei between samples. We hypothesized that there may be more than one mechanism of pDNA nuclear import during polymer-mediated transfection, with one mechanism being direct nuclear permeabilization by the polymers. To further explore this, confocal microscopy on digitonin-permeabilized cells was performed.

Nuclear import in digitonin-permeabilized HeLa cells. In order to determine whether polymer-mediated DNA import into nuclei required cytoplasmic factors, HeLa cells were grown on coverslips to confluency, then treated with DTT and digitonin to permeabilize the cytosol. The nuclei were isolated with or without an ATP-generating system to determine whether plasmid DNA import in the absence of cytosol was energy-

dependent. The nuclei were treated with polyplexes and incubated for 4 hours before being washed, fixed and mounted onto microscopy slides. Confocal microscopy was used to determine colocalization between plasmid DNA and the nucleus. Colocalization (as determined using Manders coefficients) between rhodamine-labeled 2 MDa rhodamine-labeled dextran and DAPI-labeled nuclei was used to assess nuclear membrane integrity. The images for digitonin-treated cells treated with the different polyplexes are shown in Figure 4.9. It was found that there was high variability in the number of dextran-containing nuclei; some nuclei had no dextran fluorescence, while other nuclei had large amounts of dextran fluorescence (results not shown). This is most likely due to a combination of using a detergent-based method to isolate the nuclei and the high rate of mitosis in HeLa cells. For the Cy5 colocalization data, the trends for PEI polyplexes (Figure 4.10) were similar to those observed in the flow cytometry experiment (Figure 4.8 a), with there being significantly more ($p < 0.05$) pDNA nuclear import in the presence of cytosol than in the absence of cytosol. In the case of the PGAA T4, we noticed increased ($p < 0.05$) pDNA import in the presence of both cytosol and energy vs. T4 pDNA import in the absence of both cytosol and energy. In the absence of cytosol, we see a decrease in pDNA import in the absence of energy compared with the presence of energy in the case of G4 polyplexes (Figure 4.10). However, when looking at this Cy5 colocalization data, one notices a large amount of variance between samples. When increasing the amount of samples tested, the standard deviation continued to increase. This led us to believe that more than one mechanism of pDNA nuclear entry was occurring, with one mechanism directly related to the permeability of the nuclear envelope. To test this, colocalization data between dextran and DAPI was plotted against

colocalization with Cy5 and DAPI to see if there was a linear trend between dextran and pDNA uptake. Our hypothesis was that nuclei permeable to dextran would also be permeable to pDNA, and that perhaps differences in pDNA uptake in nuclei that had low amounts of dextran in them could be used to test the energy-dependence of pDNA import.

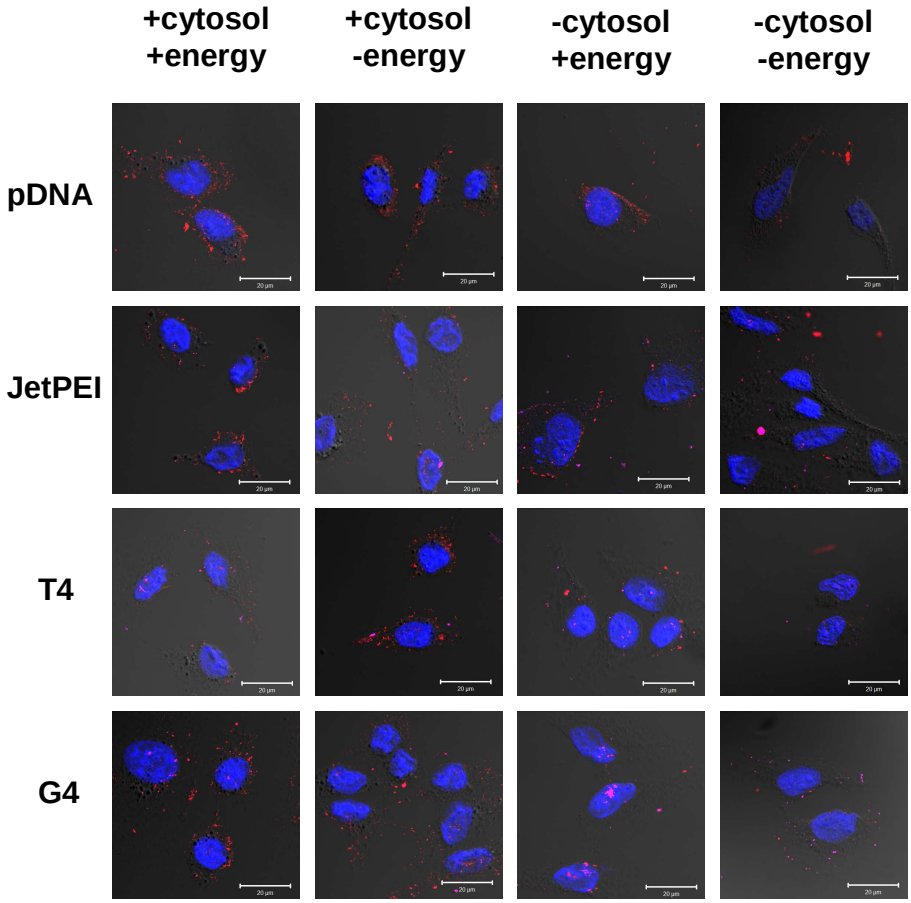

Figure 4.9) Confocal images of digitonin-permeabilized HeLa cells. After permeabilization, the HeLa nuclei were incubated in buffer in the presence or absence of HeLa cytosol extract ("cytosol") and in the presence or absence of an ATP-generating system ("energy"). The nuclei were treated with polyplexes formed with the indicated polymers and Cy5-labeled pDNA for 4 hours before being fixed and imaged. In these images, red represents rhodamine-labeled 2 MDa dextran, blue represents the nuclei, and magenta represents pDNA. Scale bar = 20 µM. Increases of red fluorescence in the nuclei are indicative of increased nuclear envelope permeability, and increases of magenta fluorescence in the nuclei are indicative of increased pDNA nuclear import.

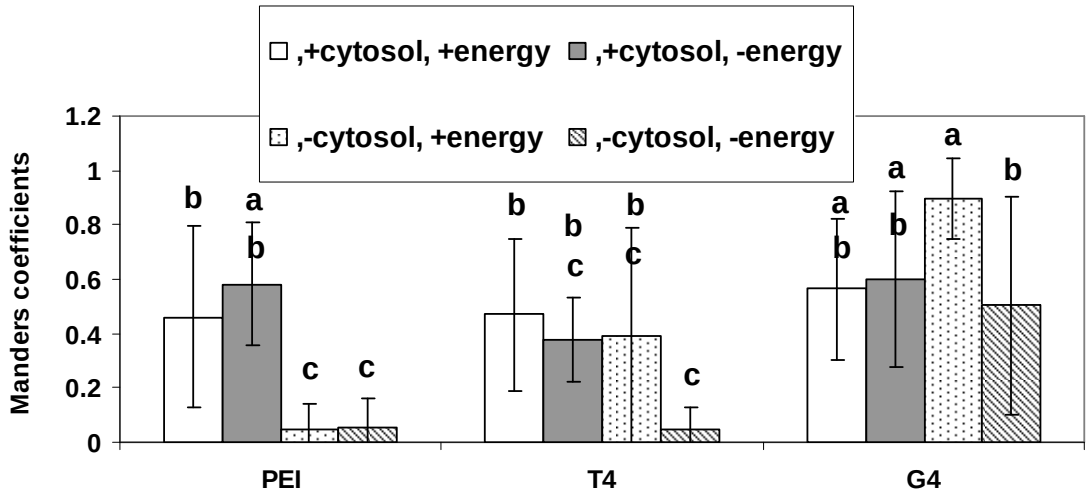

Figure 4.10) Confocal microscopy data. Manders coefficients were used to measure colocalization between Cy5-labeled plasmid DNA and DAPI-labeled nuclei. Data is shown as the mean ± standard deviation for 10 samples. Bars with different letters represent means that are statistically significant from each other according to the Tukey-Kramer HSD method ($p < 0.05$, $n = 10$). No measureable Cy5 fluorescence was found in the nuclei treated with pDNA only or in the cells only controls. Bars with matching letters represent means that are not statistically significant from each other.

When the colocalization data for Cy5 and DAPI is plotted directly against the colocalization data from rhodamine and DAPI (Figure 4.11), we do notice an interesting trend for all of the polymers. It seems that there are different mechanisms of nuclear pDNA import taking place, with one dependent on nuclear permeability (high colocalization between rhodamine and DAPI + high colocalization with Cy5 and DAPI) and another dependent on the presence or absence of cytosol and energy. Different mechanisms of pDNA import occurring would account for the increase in variance as the numbers of samples increase. In Figure 4.11 a, digitonin-permeabilized cells are treated with polyplexes formed with JetPEI (PEI). In the absence of cytosol, we see low colocalization between Cy5 and DAPI (Manders coefficient < 0.4), even when nuclear permeability is increased (Manders coefficient between rhodamine and DAPI > 0.4). In

the presence of cytosol, we do see high Manders coefficients (> 0.4), and a trend between nuclear envelope permeability (high colocalization between rhodamine and DAPI) and pDNA nuclear import (high colocalization between Cy5 and DAPI) becomes evident. Furthermore, when cytosol is present, there seems to be no energy dependence on pDNA import when the pDNA is delivered by PEI, since we see high Cy5-DAPI colocalization even when rhodamine-DAPI colocalization is decreased. In the absence of cytosol, pDNA import seems lower overall in the case of PEI (Figure 4.11 a), further supporting the previous data in Figures 4.8 and 4.10, and no clear trend in energy dependence can be discerned. However, this is not the case when pDNA is delivered by the PGAAs T4 and G4.

In the case of T4 (Figure 4.11 b), we do notice a trend in terms of energy dependence. This is most clear when comparing treatment with T4 polyplexes in the absence of cytosol; overall, in the absence of cytosol and the presence of energy, pDNA nuclear import increases as nuclear permeability increases, which is to be expected. However, in the absence of energy, even at high nuclear permeability (high colocalization between rhodamine and DAPI), we still see low pDNA nuclear import as evidenced by low Cy5-DAPI colocalization (Figure 4.11 b). In the presence of cytosol, the trends in energy dependence are not as dramatic; perhaps this further substantiates that different mechanisms are occurring. It is possible that when delivered by PEI, pDNA exhibits higher nuclear import in the presence of cytosol (Figure 4.11 a), but in the case of the T4, cytosol is not necessary for pDNA import (Figure 4.11 b). However, in the absence of cytosol, we only notice substantial pDNA nuclear import (Manders coefficient for Cy5 and DAPI > 0.4) when the nuclear envelope is permeable (Manders coefficient for

rhodamine and DAPI > 0.4) for the PGAAs (Figure 4.11 b and c). These data support the flow cytometry data in Figure 4.8 a indicating that the PGAAs are more dependent on intracellular machinery than PEI.

The data for G4 polyplexes (Figure 4.11 c) are similar to that of T4 (Figure 4.11 b). Again, as with T4, in the absence of cytosol we do see energy-dependent pDNA nuclear import. However, this trend is not as dramatic in the presence of cytosol. It should be noted that in the presence of cytosol, we notice more data points exhibiting higher Manders coefficients (> 0.4) between rhodamine and DAPI than in nuclei incubated without cytosol. It is possible that there are proteins present in the cytosol that could be disrupting the nuclear envelope to a greater extent than when cytosolic extract is absent from the import buffer. It is also possible that there may be cytosolic proteins involved in pDNA import when the pDNA is complexed with a polymer, similar to the results found by Munkonge *et. al.*[27] In Munkonge *et. al.*'s work, many proteomics techniques were used to identify pDNA "shuttle proteins" that aided pDNA in going from the cytosol into the nucleus. Their research illustrates the fact that certain cytosolic proteins, such as NM23-H2, a c-Myc transcription-activating nucleoside diphosphate kinase, and H2B, a core histone, can highly impact pDNA import into isolated nuclei.[27] These studies as well as our current data illustrate that cytosolic proteins play a role in pDNA nuclear import, even during polymer-mediated pDNA delivery.

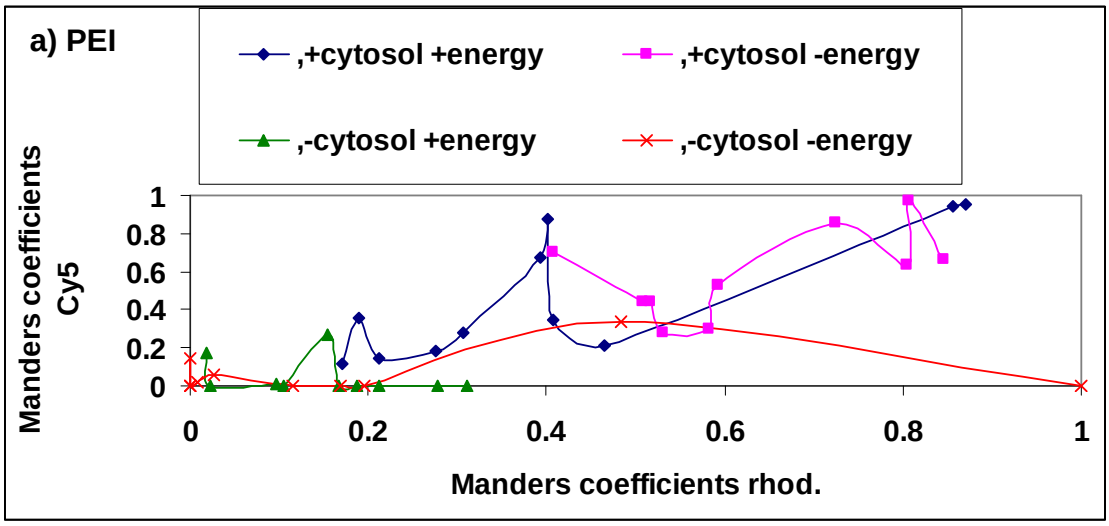
a) PEI
,+cytosol +energy
,+cytosol -energy
,-cytosol +energy
,-cytosol -energy
Manders coefficients Cy5
1
0.8
0.6
0.4
0.2
0
0
0.2
0.4
0.6
0.8
1
Manders coefficients rhod.

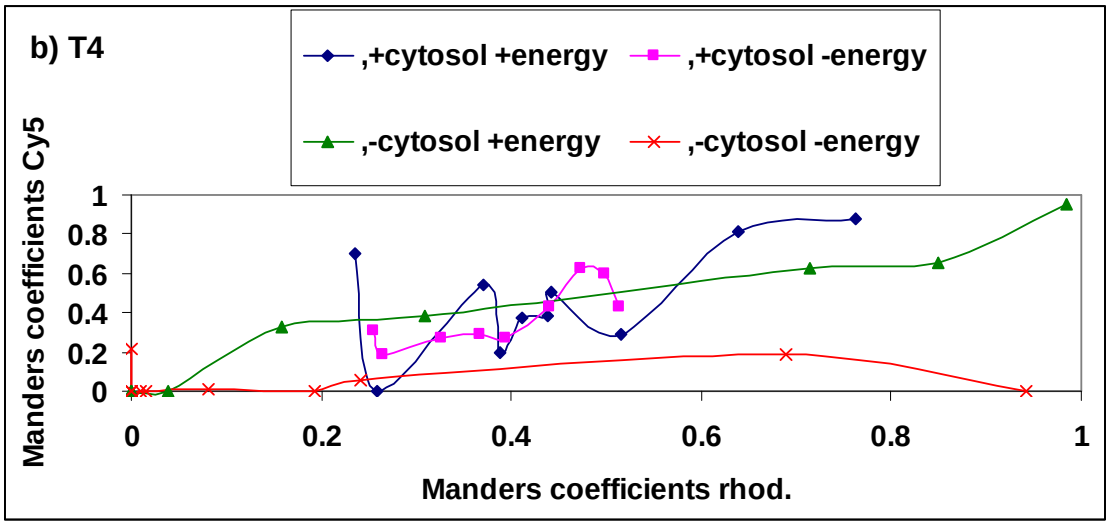
b) T4
,+cytosol +energy
,+cytosol -energy
,-cytosol +energy
,-cytosol -energy
Manders coefficients Cy5
1
0.8
0.6
0.4
0.2
0
0
0.2
0.4
0.6
0.8
1
Manders coefficients rhod.

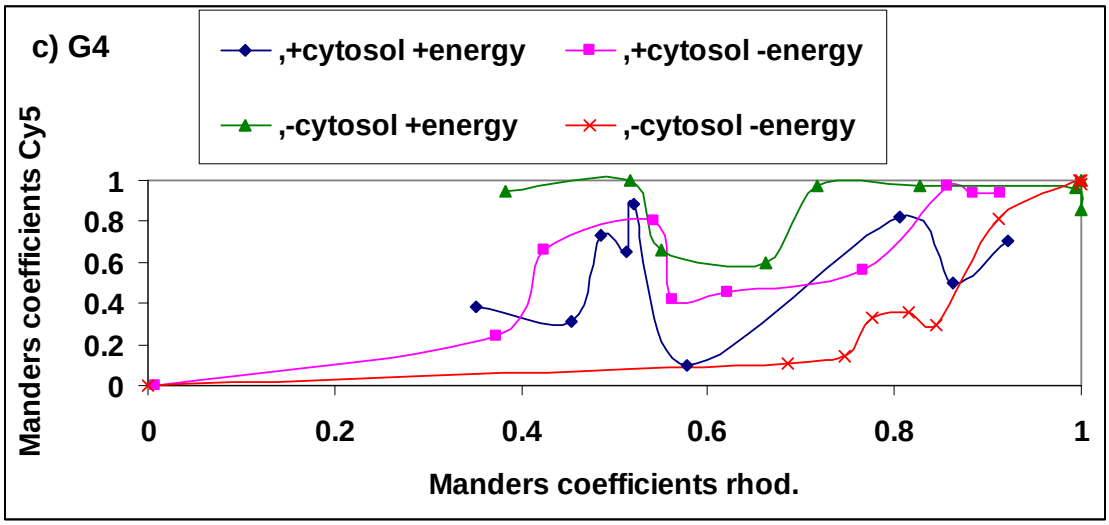
c) G4
,+cytosol +energy
,+cytosol -energy
,-cytosol +energy
,-cytosol -energy
Manders coefficients Cy5
1
0.8
0.6
0.4
0.2
0
0
0.2
0.4
0.6
0.8
1
Manders coefficients rhod.

Figure 4.11) Colocalization data for nuclei treated with (a) JetPEI (PEI) polyplexes; (b) T4 polyplexes; (c) G4 polyplexes. Manders coefficients for Cy5 and DAPI are shown on the y-axis, and Manders coefficients for rhodamine (rhod.) and DAPI are shown on the x-axis. Data is plotted in an effort to discern trends between nuclear envelope permeability and pDNA nuclear import. In the absence of cytosol, the absence of energy results in overall lower pDNA import, unless the nuclear envelope has high permeability (as evidenced by high colocalization between rhodamine-labeled dextran and DAPI-labeled nuclei).

Further analysis of all the polymers is ongoing, but from the present data, we can conclude that nuclear envelope permeability does correlate to pDNA nuclear import, since high dextran-DAPI colocalization corresponds to high Cy5-DAPI colocalization (Figure 4.11). It is unclear whether the nuclei are directly permeabilized by the polymers, however, since nuclei treated with pDNA only and cells only also exhibit high dextran colocalization with the nucleus (data not shown). From the highly variable data in Figure 4.10, it is difficult to make any definite conclusions about the minimal requirements for pDNA import, so this method of plotting nuclear envelope permeability vs. Cy5 uptake (Figure 4.11) proved advantageous by illustrating the link between nuclear envelope permeability and pDNA nuclear import.

Interestingly, we see striking differences in polymer fluorescence between nuclei isolated from whole cells after transfection and polyplexes added to nuclei in a cell-free system. When isolated from transfected cells, we see clear colocalization between the FITC labeled T4 and G4 with the Cy5-labeled pDNA, with punctuate FITC fluorescence (Figure 4.3). However, in the cell-free system, we see less colocalization between the polymer and pDNA, and significant polymer fluorescence in the nucleus, particularly the nucleoli for both T4 (Figure 4.12) and G4 (Figure 4.13). This FITC fluorescence is diffuse through the nucleus, but more predominant in the nucleoli. In the presence of HeLa cytosol extract and the ATP-generating system, we see some aggregates of polymer fluorescence outside of the nuclei (Figure 4.12 a, Figure 4.13 a) that is not present in the

images without cytosol extract (Figures 4.12 and 4.13 b, c and d). These results are intriguing and may indicate that the PGAAs are able to interact with cytosolic proteins, similar to the flow cytometry data observed for PEI (Figure 4.8 b). However, all of the polymers studied exhibited far less pDNA nuclear association in the cell-free system compared to nuclei isolated from transfected cells, indicating an increased presence of free polymer vs. polyplex. This is especially evident with the PGAAs, as evidenced by the flow cytometry data in the cell-free system. In the cell free system, we observe ~ 1 % Cy5-positive nuclei (Figure 4.8 a) compared to ~ 80 % Cy5-positive nuclei isolated from cells transfected with T4 and G4 (Figure 4.1 c). We also observed large differences in pDNA-nucleus association with PEI polyplexes when comparing nuclei isolated from transfected cells (~ 80 % Cy5-positive nuclei, Figure 4.1 c) compared to pDNA-nucleus association in the cell free system (~ 20 % Cy5-positive nuclei, Figure 4.8 a). This indicates that perhaps intracellular machinery does play a role in polyplex trafficking, with more pDNA able to reach the nuclei when the cell is intact. Furthermore, using confocal microscopy to study digitonin-permeabilized cells, we also see little polymer-pDNA colocalization inside of the nucleus with T4 and G4 (Figures 4.12 and 4.13, respectively). We also see ~ 90 % of the nuclei positive for FITC fluorescence, indicating high polymer-nucleus association, in both nuclei isolated from transfected cells (Figure 4.1 c) and nuclei in the cell free system (Figure 4.8 b). The images, as well as the flow cytometry data, indicate that the polymer is able to enter the nucleus without being complexed to pDNA in a cell-free system. It is interesting to note that polymer fluorescence present in the nuclei when the nuclei are isolated from previously transfected cells is punctuate while the polymer fluorescence in the cell-free system is

diffuse. It is possible that in whole cells, free polymer aggregates to other positively-charged moieties present in the cell, but in the cell-free system there is less for the polymer to interact with, so the polymers are able to diffuse to a greater extent in the cell-free system. The fact that we see high polymer fluorescence in the nucleoli makes sense, as the polymer could be electrostatically binding to RNA.

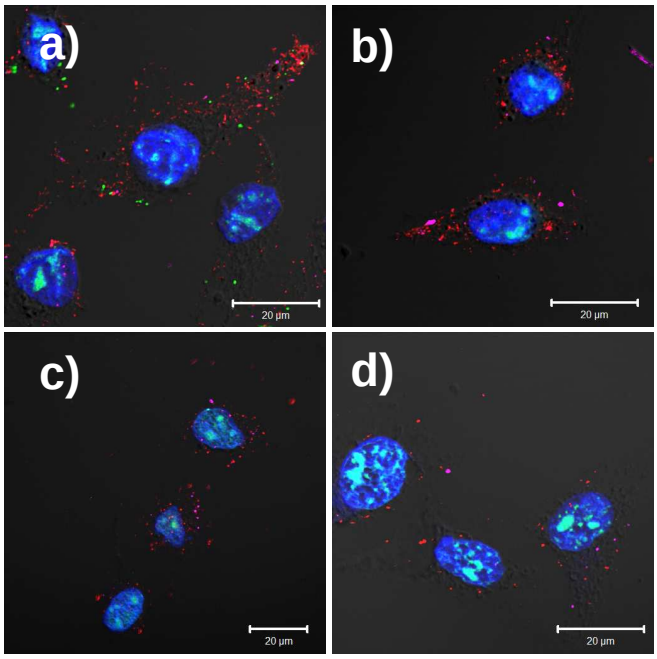

Figure 4.12) Confocal microscopy images of digitonin-permeabilized HeLa cells treated with T4 polyplexes. Cells were incubated in the following import buffers; (a) with cytosol extract and with an ATP-generating system ("energy); (b) with cytosol extract and without energy; (c) without cytosol extract and with energy; (d) without cytosol extract and without energy. Polyplexes were allowed to incubate on cells for 4 hours before cells were washed and fixed. Colors represent the following; red = rhodamine-labeled 2 MDa dextran; green = FITC-labeled T4; blue = DAPI-labeled nucleus; magenta = Cy5-labeled pDNA. Scale bar = 20 µm. Regardless of incubation conditions, polymer fluorescence (green) was present in all nuclei, predominately in the nucleoli.

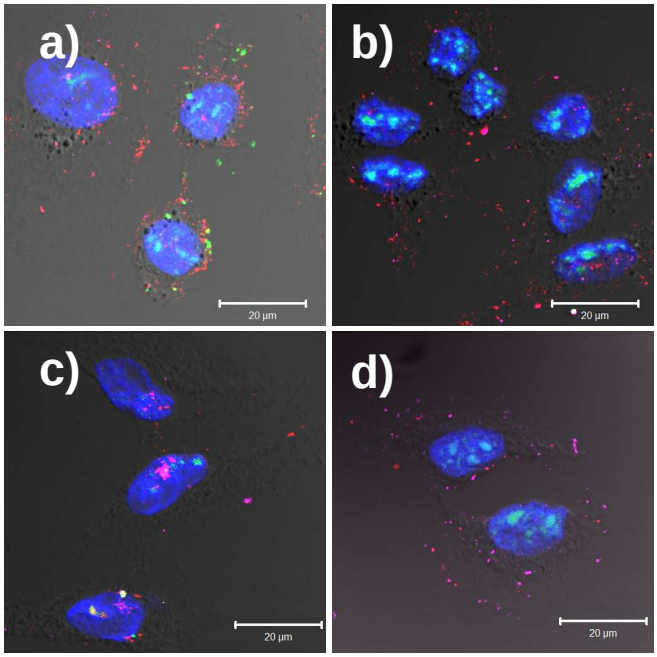

Figure 4.13) Confocal microscopy images of digitonin-permeabilized HeLa cells treated with G4 polyplexes in the following import buffers; (a) with cytosol extract and with an ATP-generating system ("energy); (b) with cytosol extract and without energy; (c) without cytosol extract and with energy; (d) without cytosol extract and without energy. Polyplexes were allowed to incubate on cells for 4 hours before cells were washed and fixed. Colors represent the following; red = rhodamine-labeled 2 MDa dextran; green = FITC-labeled T4; blue = DAPI-labeled nucleus; magenta = Cy5-labeled pDNA. Scale bar = 20 µm. We observed diffuse polymer fluorescence throughout the nuclei, but the brightest polymer fluorescence is evident in the nucleoli.

4.5 Conclusions and Future Goals

Collectively, these data tell us several things about pDNA nuclear import during polymer-mediated DNA delivery. From nuclei isolated 24 hours after transfection, we observe that PEI had slightly higher pDNA nuclear association than the PGAAs (Figure 4.1 a), while the PGAAs exhibited greater polymer-nucleus association (Figure 4.1 b). Further analysis using confocal microscopy revealed that in the case of T4 (Figure 4.2 c) and G4 (Figure 4.2 d), the pDNA was located around the periphery of the nucleus compared to nuclei isolated from PEI-transfected cells (Figure 4.2 b). In addition, the nuclei isolated from PEI-treated cells had higher colocalization between dextran and the

nucleus, indicating increased nuclear envelope permeability. The data from Figures 4.1 and 4.2 indicate that all polymers are able to delivery pDNA to the nucleus within 24 hours after transfection, and that the polymers are able to enter the nucleus to a greater extent than pDNA, as ~ 90 % of the nuclei isolated from transfected cells were positive for FITC fluorescence (Figure 4.1 b). These data are interesting because they illustrate that free polymers may have different mechanisms of nuclear trafficking than polymers complexed with pDNA. Confocal microscopy images taken 24 hours after transfection (Figure 4.5) also confirmed that the polyplexes were indeed reaching the nucleus at this time point. Once we knew that all the polyplexes were capable of reaching the nucleus, we attempted to elucidate how the polyplexes trafficked to the nucleus and subsequently how the pDNA delivered by the polyplexes entered the nucleus.

Our hypothesis was that the polyplexes were able to travel along microtubules, and then enter the nucleus when the nuclear envelope breaks down during mitosis. To test this, cells were transfected in the presence or absence of nocodazole to inhibit microtubule trafficking or in the presence or absence of aphidicolin to halt cell division. Our results indicate that when treated with nocodazole the first 4 hours of transfection, all polyplexes exhibited reduced transfection efficiency (Figure 4.7). However, transfection efficiency was not completely abolished. This could be due in part to the microtubules reassembling after nocodazole was removed, and because there are multiple mechanisms for polyplex-nuclear trafficking occurring. More work is needed in this area and is currently underway in our group. Also, the PGAA G4, but not PEI or T4, had slightly lower ($p < 0.05$) transfection efficiency in the absence of cell division (Figure 4.7). This

could indicate that for G4, cellular division aids transfection by allowing pDNA to enter the nucleus during mitosis.

Next, we wanted to determine the minimal requirements necessary for pDNA import into the nuclei when complexed with different polymers. We also wanted to see if polymer structure affected the mechanism(s) of pDNA nuclear import. For this, we used a cell-free system and isolated nuclei in different buffers; one containing HeLa cytosol extract and an ATP-generating system, one containing HeLa cytosol extract in the absence of an ATP-generating system, one in the absence of cytosol and the presence of the ATP-generating system, and one in the absence of both cytosol and the ATP-generating system. First, in an effort to use a high-throughput method, we isolated nuclei, incubated them in the aforementioned buffers, and treated them with the different polyplexes. After 4 hours, we analyzed the nuclei for Cy5 and FITC fluorescence using flow cytometry. Our results indicate that PEI polyplexes were able to reach the nucleus in all conditions, but more pDNA associated with the nucleus in the presence of both cytosol and an ATP-generating system (Figure 4.8 a). We show no pDNA-nucleus association in the cell-free system when the pDNA was delivered by T4 or G4 (Figure 4.8 a). Interestingly, despite having low pDNA-nucleus association, the PGAAs T4 and G4 exhibited high polymer-nucleus association in all conditions tested (Figure 4.8 b). This indicates that the polymers themselves are able to reach the nucleus without their pDNA cargo. Furthermore, PEI polymers exhibited lower nucleus association in the presence of both cytosol and energy (Figure 4.8 b), contradictory to the Cy5 data for PEI (Figure 4.8 a). Taken together, we can envision different mechanisms occurring for free polymers vs. polyplexes for nuclear trafficking. This is evident in the Cy5 data, where we observe

less Cy5 fluorescence in nuclei from the cell-free system (Figure 4.8) when compared to nuclei isolated from transfected cells (Figure 4.1), indicating that intracellular machinery does play a role in polyplex trafficking. However, intracellular machinery does not necessarily play a role in polymer trafficking for the PGAAs, as there was little difference in the amount of FITC positive nuclei isolated from transfected cells (Figure 4.1 b) vs. nuclei in a cell-free system (Figure 4.8 b). In the case of PEI, we do notice less polymer-nucleus association in the presence of cytosol; this is perhaps indicative of the free polymer interacting with anionic cytosolic components. The reasons why PEI is more affected by the presence of cytosol than the PGAAs remain to be determined and would be an interesting topic for future study in our group.

Using these flow cytometry data, we are unable to tell whether the pDNA is inside of the nucleus or on the nuclear surface. In order to verify that pDNA was being imported into the nuclei and not merely bound to the surfaces of the nuclei, confocal microscopy was used (Figure 4.9). When studying digitonin-permeabilized cells, we noticed high variances in Cy5 fluorescence (Figure 4.10). We hypothesized that perhaps cells with high rhodamine fluorescence, indicating high nuclear envelope permeability, also would exhibit high Cy5 fluorescence. To test this, we plotted the Manders coefficients for rhodamine and DAPI vs. the Manders coefficients for Cy5 and DAPI. This data allowed us to make sense of our highly variable flow cytometry data; it appears that different mechanisms of pDNA import are taking place. It seems that for the PGAAs, in the absence of cytosol there is an energy-dependent mechanism for pDNA import occurring (Figure 4.11 b and c), while in the presence of cytosol there is less energy dependence. The nuclear import of pDNA delivered by PEI (Figure 4.11 a) seems to be more cytosol-

dependent than energy dependent. In all cases, an increase in nuclear permeability did lead to an increase in pDNA nuclear import (Figure 4.11) except for PEI and T4 in the absence of both cytosol and an ATP-generating system. Interestingly, it is the polymers with the highest transfection efficiency (PEI and G4, Figure 4.7) that are able to induce the most nuclear envelope permeability as assessed by dextran permeability (Figure 4.2) and trypan blue permeability (Figure 4.4).

In the future, it would be beneficial to collect more confocal microscopy samples to see if these trends still hold when the sample size is increased. Also, identifying the exact proteins that aid in pDNA nuclear import and determining if polymer structure plays a role in which proteins interact with the polyplexes would be very interesting. This can be done using various proteomics techniques, as explained in the work by Munkonge *et. al*. [27] Also, other methods for protein isolation from the cytosol besides acetone precipitation may be explored, as acetone precipitation may lead to denaturing of the proteins.

Overall, we illustrate that polymer structure can influence the mechanisms of pDNA nuclear import. The presence of hydroxyls in the repeat unit changes the energy requirements and cytosolic requirements for pDNA nuclear entry when compared to PEI. The hydroxyl-containing polymers also exhibited more dependence on intracellular machinery for nuclear trafficking than PEI, as evidenced by the dramatic decrease in pDNA-nucleus association in a cell-free system vs. nuclei isolated from whole cells. We have also illustrated that nuclear envelope permeability impacts pDNA nuclear import, and that nuclei isolated from PEI-transfected cells display greater nuclear envelope permeability than nuclei isolated from T4 or G4-treated cells. It is possible that this

increased nuclear permeabilization is a result of apoptosis being initiated, which we concluded in Chapter 1 happens early during PEI transfection. However, PEI and G4 are also able to induce nuclear envelope permeability in a cell-free system, indicating that the polymers themselves are able to induce nuclear envelope permeability in the absence of apoptosis. Direct nuclear envelope permeabilization presents a possible link between high transfection efficiency and high toxicity observed in many polymer-based DNA delivery systems.

4.6 References

1. Hunter, A. C., Molecular hurdles in polyfectin design and mechanistic background to polycation induced cytotoxicity. *Advanced Drug Delivery Reviews* **2006,** *58*, 1523-1531.
2. Lv, H.; Zhang, S.; Wang, B.; Cui, S.; Yan, J., Toxicity of cationic lipids and cationic polymers in gene delivery. *Journal of Controlled Release* **2006,** *114*, 100-109.
3. Fischer, D.; Li, Y.; Ahlemeyer, B.; Krieglstein, J.; Kissel, T., In vitro cytotoxicity testing of polycations: influence of polymer structure on cell viability and hemolysis. *Biomaterials* **2003,** *24*, 1121-1131.
4. Boussif, O., Lezoualc'h, F., Zanta, M.A., Mergny, M.D., and Scherman, D., A versatile vector for gene and oligonucleotide transfer into cells in culture and in vivo: polyethylenimine. *Proceedings of the National Academy of Sciences of the United States of America* **1995,** *92*, 7297-7301.
5. Godbey, W. T., Wu, K.K., and Mikos, A.G., Poly(ethylenimine)-mediated gene delivery affects endothelial cell function and viability. *Biomaterials* **2001,** *22*, 471-480.
6. Ira, Y., Mely, Y., and Krishnamoorthy, G., DNA vector polyethyleneimine affects cell pH and membrane potential: A time-resolved fluorescence microscopy study. *Journal of Fluorescence* **2003,** *13*, 339-347.
7. Moghimi, S. M., Symonds, P., Murray, J.C., Hunter, A.C., Debska, G., and Szewczyk, A., A two-stage poly(ethyleneimine)-mediated cytotoxicity: implications for gene transfer/therapy. *Molecular Therapy* **2005,** *11*, 990-995.
8. Brownlie, A., Uchegbu, I.F., and Shatzlein, A.G., PEI-based vesicle-polymer hybrid gene delivery system with improved biocompatibility. *International Journal of Pharmaceutics* **2004,** *274*, 41-52.
9. Wong, K.; Sun, G.; Zhang; Dai, H.; Liu, Y.; He; Leong, K. W., PEI-g-chitosan, a novel gene delivery system with transfection efficiency comparable to polyethylenimine *in vitro* and after liver administration *in vivo*. *Bioconjugate Chemistry* **2005,** *17*, 152-158.

10. Twaites, B. R.; de las Heras Alarcón, C.; Lavigne, M.; Saulnier, A.; Pennadam, S. S.; Cunliffe, D.; Górecki, D. C.; Alexander, C., Thermoresponsive polymers as gene delivery vectors: Cell viability, DNA transport and transfection studies. *Journal of Controlled Release* **2005,** *108*, 472-483.
11. Liu, Y., Wenning, L., Lynch, M., and Reineke, T.M., Gene delivery with novel poly(L-tartaramidoamine)s In *Polymeric Drug Delivery Volume I - Particulate Drug Carriers*, Svenson, S., Ed. American Chemical Society: Washington, D.C., 2005.
12. Liu, Y., and Reineke, T.M., Poly(glycoamidoamine)s for gene delivery: Stability of polyplexes and efficacy with cardiomyoblast cells. *Bioconjugate Chemistry* **2006,** *17*, 101-108.
13. Lee, C. C., Liu, Y., and Reineke, T.M., General structure-activity relationship for poly(glycoamidoamine)s: The effect of amine density on cytotoxicity and DNA delivery efficiency. *Bioconjugate Chemistry* **2008,** *19*, 428-440.
14. Liu, Y., Wenning, L., Lynch, M., and Reineke, T.M., Gene delivery with novel poly(L-tartaraminoamine)s. In *Polymeric Drug Delivery Volume I - Particulate Drug Carriers*, Svenson, S., Ed. American Chemical Society: Washington, D.C., 2006; Vol. 923, pp 217-227.
15. McLendon, P. M.; Fichter, K. M.; Reineke, T. M., Poly(glycoamidoamine) vehicles promote pDNA uptake through multiple routes and efficient gene expression *via* caveolae-mediated endocytosis. *Molecular Pharmaceutics* **2010,** *7*, 738-750.
16. Dean, D. A. a. L., A.P., Progress and prospects: nuclear import of nonviral vectors. *Gene Therapy* **2010,** *17*, 439-447.
17. Miller, A. M. a. D., D.A., Tissue-specific and transcription factor-mediated nuclear entry of DNA. *Advanced Drug Delivery Reviews* **2009,** *61*, 603-613.
18. Dean, D. A., Strong, D.D. and Zimmer, W.E., Nuclear entry of nonviral vectors. *Gene Therapy* **2005,** *12*, 881-890.
19. Dean, D. A., Dean, B.S., Muller, S., and Smith, L.C., Sequence requirements for plasmid nuclear import. *Experimental Cell Research* **1999,** *253*, 713-722.
20. Li, S., MacLaughlin, F.C., Fewell, J.G., Gondo, M., Wang, J., Nicol, F., Dean, D.A., and Smith, L.C., Muscle-specific enhancement of gene expression by incorporation of SV40 enhancer in the expression of plasmid. *Gene Therapy* **2001,** *8*, 494-497.
21. Duverger, E.; Pellerin-Mendes, C.; Mayer, R.; Roche, A.-C.; Monsigny, M., Nuclear import of glycoconjugates is distinct from the classical NLS pathway. *Journal of Cell Science* **1995,** *108*, 1325-1332.
22. Hong, S.; Hessler, J. A.; Banaszak Holl, M. M.; Leroueil, P.; Mecke, A.; Orr, B. G., Physical interactions of nanoparticles with biological membranes: The observation of nanoscale hole formation. *Bioconjugate Chemistry* **2006,** *17*, 728-734.
23. Boutin, V.; Legrand, A.; Mayer, R.; Nachtigal, M.; Monsigny, M.; Midoux, P., Glycofection: The ubiquitous roles of sugar bound on glycoplexes. *Drug Delivery* **1999,** *6*, 45-50.
24. Monsigny, M.; Rondanino, C.; Duverger, E.; Fajac, I.; Roche, A.-C., Glyco-dependent nuclear import of glycoproteins, glycoplexes and glycosylated plasmids. *Biochimica et Biophysica Acta* **2004,** *1673*, 94-103.
25. Duverger, E.; Pellerin-Mendes, C.; Mayer, R.; Roche, A.-C.; Monsigny, M., Nuclear import of glycoconjugates is distinct from the classical NLS pathway. *Journal of Cell Science* **1995,** *108*, 1325-1332.

26. Liu, Y.; Reineke, T. M., Hydroxyl Stereochemistry and amine number within poly(glycoamidoamine)s affect intracellular DNA delivery. *JACS* **2005,** *127*, 3004-3015.
27. Munkonge, F. M.; Amin, V.; Hyde, S. C.; Green, A.-M.; Pringle, I. A.; Gill, D. R.; Smith, J. W. S.; Hooley, R. P.; Xenariou, S.; Ward, M. A.; Leeds, N.; Leung, K.-Y.; Chan, M.; Hillery, E.; Geddes, D. M.; Griesenbach, U.; Postel, E. H.; Dean, D. A.; Dunn, M. J.; Alton, E. W. F. W., Identification and functional characterization of cytoplasmic determinants of plasmid DNA nuclear import. *The Journal of Biological Chemistry* **2009,** *284*, 26978-26987.
28. Manders, E. M. M.; Stap, J.; Brakenhoff, G. J.; Driel, R. V.; Aten, J. A., Dynamics of three-dimensional replication patterns during the S-phase, analysed by double labelling of DNA and confocal microscopy. *Journal of Cell Science* **1992,** *103*, 857-862.
29. Manders, E. M. M.; Verbeek, F. J.; Aten, J. A., Measurement of co-localizatin of objects in dual-colour confocal images. *Journal of Microscopy* **1993,** *169*, 375-382.
30. Rasband, W. S. *ImageJ*, U.S. National Institutes of Health: Bethseda, MA, 1997-2009.
31. Munkonge, F. M.; Amin, V.; Hyde, S. C.; Green, A.-M.; Pringle, I. A.; Gill, D. R.; Smith, J. W. S.; Hooley, R. P.; Xenariou, S.; Ward, M. A.; Leeds, N.; Leung, K.-Y.; Chan, M.; Hillery, E.; Geddes, D. M.; Griesenbach, U.; Postel, E. H.; Dean, D. A.; Dunn, M. J.; Alton, E. W. F. W., Identification and functional characterization of cytoplasmic determinants of plasmid DNA nuclear import. *J Biol Chem* **2009,** *284*, 26978-26987.
32. Hagstrom, J. E.; Ludtke, J. J.; Bassik, M. C.; Sebestyen, M. G.; Adam, S. A.; Wolff, J. A., Nuclear import of DNA in digitonin-permeabilized cells. *Journal of Cell Science* **1997,** *110*, 2323-2331.
33. Newton, K.; Petfalski, E.; Tollervey, D.; Caceres, J. F., Fibrillarin is essential for early development and required for accumulation of an intron-encoded small nucleolar RNA in the mouse. *Molecular and Cellular Biology* **2003,** *23*, 8519-8527.
34. Bieber, T.; Meissner, W.; Kostin, S.; Niemann, A.; Elsasser, H.-P., Intracellular route and transcriptional competence of polyethylenimine-DNA complexes. *Journal of Controlled Release* **2002,** *82*, 441-454.
35. Godbey, W. T.; Wu, K. K.; Mikos, A. G., Tracking the intracellular path of poly(ethylenimine)/DNA complexes for gene delivery. *Proc Natl Acad Sci U S A* **1999,** *96*, 5177-5181.
36. Barua, S.; Rege, K., The influence of mediators of intracellular trafficking on transgene expression efficacy of polymer-plasmid DNA complexes. *Biomaterials* **2010,** *31*, 5894-5902.
37. Chida, K.; Sueyoshi, R.; Kuroki, T., Efficient and stable gene transfer following microinjection into nuclei of synchronized animal cells progressing from G1/S boundary to early S phase. *Biochemical and Biophysical Research Communications* **1998,** *249*, 849-852.
38. Roche, A. C.; Fajac, I.; Grosse, S.; Frison, N.; Rondanino, C.; Mayer, R.; Monsigny, M., Glycofection: facilitated gene transfer by cationic glycopolymers. *Cellular and Molecular Life Sciences* **2003,** *60*, 288-297.
39. Monsigny, M.; Midoux, P.; Mayer, R.; Roche, A. C., Glycotargeting: influence of the sugar moiety on both the uptake and the intracellular trafficking of nucleic acid carried by glycosylated polymers. *Biosci. Rep.* **1999,** *19*, 125-132.

40. Monsigny, M.; Rondanino, C.; Duverger, E.; Fajac, I.; Roche, A. C., Glyco-dependent nuclear import of glycoproteins, glycoplexes and glycosylated plasmids. *Biochimica et Biophysica Acta* **2004,** *1673*, 94-103.
41. Gagliardi, L. J., Electrostatic considerations in nuclear envelope breakdown and reassembly. *Journal of Electrostatics* **2006,** *64*, 843-849.
42. Mazzanti, M.; Bustamente, J. O.; Oberleithner, H., Electrical dimension of the nuclear envelope. *Physiological Reviews* **2001,** *81*, 1-19.
43. Colwell, L. J.; Brenner, M. P.; Ribbeck, K., Charge as a selection criterion for translocation through the nuclear pore complex. *PLOS Computational Biology* **2004,** *6*, 1-8.

Chapter 5 : Modification of Polymers for Gene Delivery

Based on the manuscripts "A polycation scaffold presenting tunable 'click' sites: Conjugation to carbohydrate ligands and examination of hepatocyte-targeted pDNA delivery" from Lee, C-C; Grandinetti, G; McLendon, P.M.; and Reineke, T.M. *Macromolecular Bioscience* **2010**, *10*, 585-598.

"Cationic glycopolymers as in vitro gene delivery agents for stem-cell therapy" from Kizjakina, K.; Bryson, J.M.; Grandinetti, G.; and Reineke, T.M., in preparation.

"Diblock glycopolymers promote colloidal stability of polyplexes and effective pDNA and siRNA delivery in physiological salt and serum conditions" from Smith, A. E.; Sizovs, A.; Grandinetti, G.; Xue, L.; and Reineke, T.M. *Biomacromolecules*, in press.

5.1 Abstract

There is currently a wide variety of polymer-based gene delivery vehicles in use today. However, very little is known about the mechanisms of polymer-based transfection. As discussed in the previous chapters, modifications in polymer structure can have large impacts on their efficacy as gene delivery vehicles. Here, we explore a variety of polymer structures and the effects structure has on different parameters, including transfection efficiency, cellular uptake, and toxicity. In this chapter, we present

a polymer scaffold that can be modified relatively easily for the incorporation of different targeting groups. We also study the effect polymer structure has on cellular uptake using a library of polymers containing different amounts of primary amines. Furthermore, the effect of adding PEG groups on the transfection efficiency and toxicity of trehalose-containing polymers is explored. We also discuss using fluorescently labeled polymers as well as lanthanide-chelated polymers to further elucidate the intracellular events occurring during transfection. Our results show that different linker lengths between polymers and galactose affect hepatocyte transfection efficiency, but different end groups on trehalose-containing polymers do not significantly influence transfection efficiency. We also illustrate that the amount of primary amines present in a polymer affects cellular uptake and pDNA release. In addition, we illustrate the use of a terbium-chelated polymer to further probe pDNA release from polyplexes.

5.2 Introduction

One of the main advantages of polymer-based delivery vehicles have vs. viral vehicles is the ease with which they can be tailored to meet specific needs. Polymers can be modified to improve targeting, increase transfection efficiency in serum, and allow for the addition of certain groups to aid visualization. In this chapter, several examples of polymer modification and their biological effects are presented.

Previous discussion has focused on the poly(glycoamidoamine)s (PGAAs) and poly(ethylenimine) PEI. These polymers display high transfection efficiency in a variety of cells, allowing them to work as *in vitro* transfection reagents but may hinder their use in therapy due to their non-specificity. In order to target certain cell types, polymer

chemists are able to incorporate various groups into the polymers. Many examples of tumor-targeting cationic polymers exist, including the incorporation of transferrin into polycationic polymers to target transferrin receptors,[1-2] the incorporation of folic acid to target folate receptors,[3-4] and various antibodies.[5-6] Furthermore, polymers have also been targeted to specific organs, including the brain[7] and heart.[8] Our goal was to develop a system that could easily be modified to incorporate a variety of targeting groups. To test this system, we have chosen to incorporate β-D-galactose in our polymer backbones (Figure 5.1) to target hepatocytes. Numerous groups have targeted liver cells by incorporating β-D-galactose or lactose residues in their polymers to target the asialoglycoprotein receptors (ASGPrs) on hepatocytes. Several studies have shown that the binding affinity of β-D-galactose to the ASGPrs depends on the carbohydrate density and geometry.[9-10] The effect the degree of carbohydrate substitution and spacer length has on transfection efficiency and cytotoxicity are illustrated herein, using polymers synthesized by Dr. Chen-Chang Lee.[11] For the studies presented herein, three polymer series were used; the Ma-1-3-Gal series, the Ma-1-6-Gal series, and the Ma-1-9-Gal series. The Ma-1-3-Gal polymers have linker length of 3 carbons between the galactose and the polymer ("y" in Figure 5.1). The Ma-1-6-Gal polymers have a linker length of 6 carbons and the Ma-1-9-Gal polymers have a linker length of 9 carbons between the galactose and the polymer ("y" in Figure 5.1). Within each series, the polymers differ in the degree of carbohydrate substitution, and the percentage of carbohydrate substitution is present in the polymer names. For example, Ma-1-3-Gal-40 has 40 % carbohydrate substitution, and Ma-1-3-Gal-18 has 18 % carbohydrate distribution. In order to test the specificity of the polymers to ASGPrs, the glycoprotein asialofetuin (ASF) was used as a

competitive inhibitor for this receptor.[12] To further test specificity, polymers containing glucose (Ma-1-3-Glu-10), mannose (Ma-1-3-Man-22), and no sugar (Ma-1) were also studied, these sugars should not be inhibited by ASF if they are going through the ASGPrs, which are specific for galactose.[11]

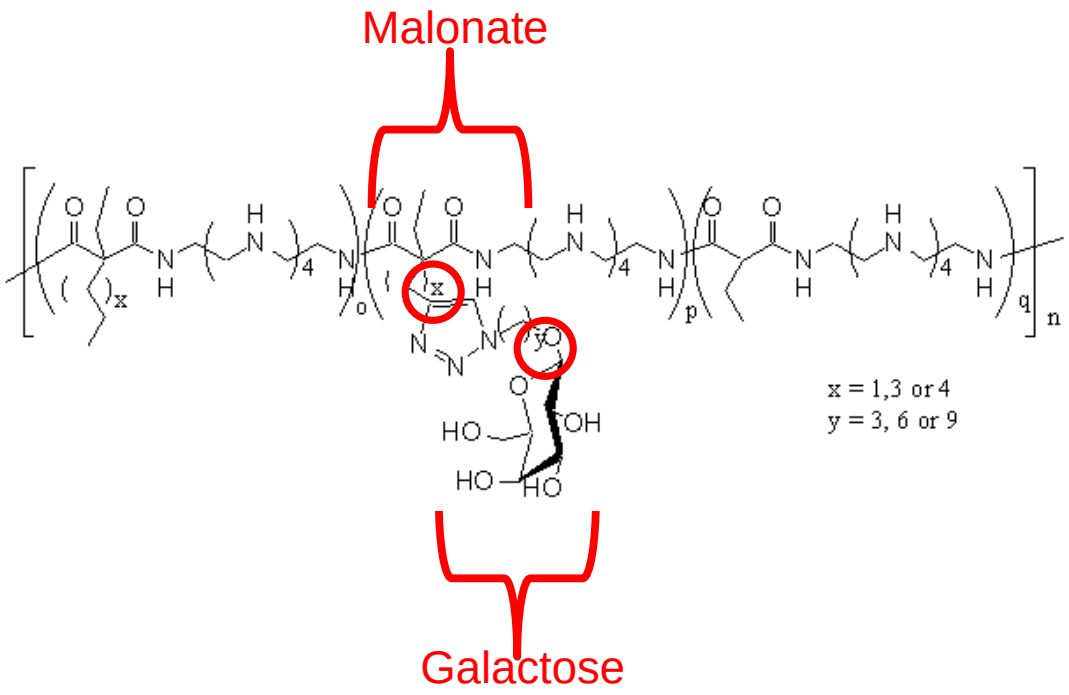

Figure 5.1) Structure of a polymer scaffold incorporating galactose as a proof-of-concept targeting ligand. Polymer structures studied herein differed in the length of the linkage between the galactose and the polymer (y). The polymers were synthesized by Dr. Chen-Chang Lee, and the polymer structure illustration in this figure was provided by Dr. Chen-Chang Lee.

In addition to targeting groups, another therapeutically relevant method for polymer-based nucleic acid delivery is *ex vivo* transfections. An *ex vivo* transfection is where primary cells are transfected outside of the body, and then later implanted into the body. Many researchers are studying ways to improve polymer-based *ex vivo* transfections, but a combination of low transfection efficiency and high cytotoxicity is a severe limitation in this field. Recently, researchers have used carbohydrate-oligoamine polymers in an

attempt to develop polymers with high transfection efficiency and low cytotoxicity in serum-containing media.[13] However, for many of these polymers, transfection efficiency in progenitor cells (cells able to be induced to differentiate into specific cell types) remains low. Recently, our group has developed a library of trehalose-oligoethyleneamine polymers that have proven to be effective at transfecting two clinically relevant cell lines; neonatal human dermal fibroblasts (HDFn) cells, important due to their ability to be induced into pluripotent stem cells,[14] and rat mesenchymal stem cells (RMSCs). Mesenchymal stem cells are used in tissue engineering, hematopoietic support, and immunoregulation.[15] Trehalose-oligoethyleneamine polymers containing either 4 (Tr4), 5 (Tr5) or 6 (Tr6) secondary amines in their polymer repeat unit were synthesized, and it was found that Tr4 exhibited the highest transfection efficiency in these cell types. To further explore structure-function relationships, the effects of different end groups on Tr4 on transfection efficiency and cytotoxicity were tested, these polymer structures can be found in Figure 5.2. Tr4 C has triphenyl (trityl) end groups, and Tr4 D has azide end groups.

One widely-used polymer in therapeutics is poly(ethylene glycol) PEG. PEG has been shown to reduce interactions with serum proteins,[16] improve circulation time *in vivo*,[17] and has the additional benefit of being approved by the Federal Drug Administration.[17-18] Recently, Davis *et. al.* have used PEGylated carbohydrate-containing polymers for the first human clinical phase I trial for targeted siRNA delivery to solid tumors,[19] illustrating the potential of these polymers for therapeutic use. A polymer chemist in our group, Karina Kizjakina, has added PEG to Tr4 polymers in an effort to improve their transfection efficiency in cells normally difficult to transfect with

polymer vectors, namely rat mesenchymal stem cells (RMSCs) and human dermal fibroblasts (HDFn). In an effort to obtain information about structure-function relationships, Tr4 polymers were PEGylated with different linkages; Tr4 B uses a carbamate linkage, while Tr4 A uses an amide linkage. The polymer structures can be found in Figure 5.2.

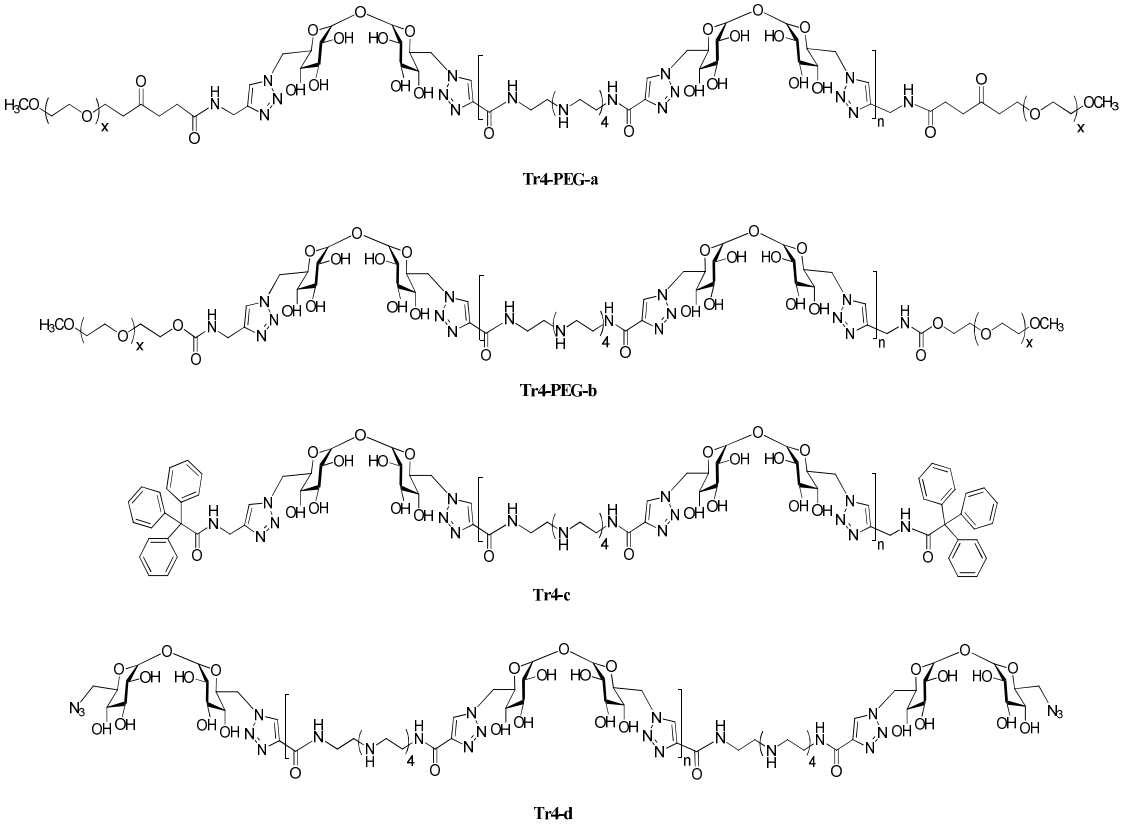

Figure 5.2) Structure of trehalose-containing polymers. Polymers Tr4-PEG-a (Tr4 A) and Tr4-PEG-b (Tr4 B) differ in the lengths of the PEG chains on the ends of the polymers. Polymers Tr4-c (Tr4 C) and Tr4-d (Tr4 D) were synthesized in order to study the effects of different polymer end groups. This figure was produced by Dr. Karina Kizjakina, and synthesis of these trehalose-containing polymers was also performed by her.

As previously mentioned, in order to be therapeutically relevant, polymers must be able to transfect cells in serum-containing media. To achieve higher stability in serum, many groups have used hydrophilic poly(ethylene glycol) (PEG), which has become the

gold standard in improving stealth capabilities of polymers *in vivo.* However, PEG has some negative side effects; it can activate the immune system and can illicit cytotoxicity through oxidative by-products.[20-21] In an effort to combat the negative side effects of PEG, our group has synthesized a library of glycopolymers. Synthetic glycopolymers have gained increased interest in recent years because of their hydrophilicity and their ability to achieve targeted functionality by imitating specific biological interactions. One drawback is that it can be relatively complicated to incorporate carbohydrate groups into polymers, and a robust method is needed to create monodisperse polymer libraries. In recent years, polymer chemists have begun using reversible addition-fragmented chain transfer polymerization (RAFT), which can provide more monodisperse polymers without the need for stringent reaction conditions or the use of potentially harmful transition metal catalysts, such as the click-polymerization method used to attach β-D-galactose ligands into our hepatocyte-targeted polymers. To test this RAFT polymerization method, a library of diblock glycopolymers was synthesized. It was our goal to study the effects of incorporating different amounts of 2-deoxy-2-methacrylamido glucopyranose (MAG) to promote colloidal stability and N-(2-aminoethyl) methacrylamide (AEMA) to electrostatically interact with nucleic acids to form polyplexes. Our plan was that the cationic AEMA block would interact with the nucleic acid while the sugar-containing MAG block would be displayed on the surface to promote colloidal stability and delivery of the diblock glycopolymers, as illustrated in Figure 5.3. Three polymers with different lengths of the AEMA block were synthesized; P1 has a block length of 21, P2 has a block length of 39, and P3 has a block length of 48.

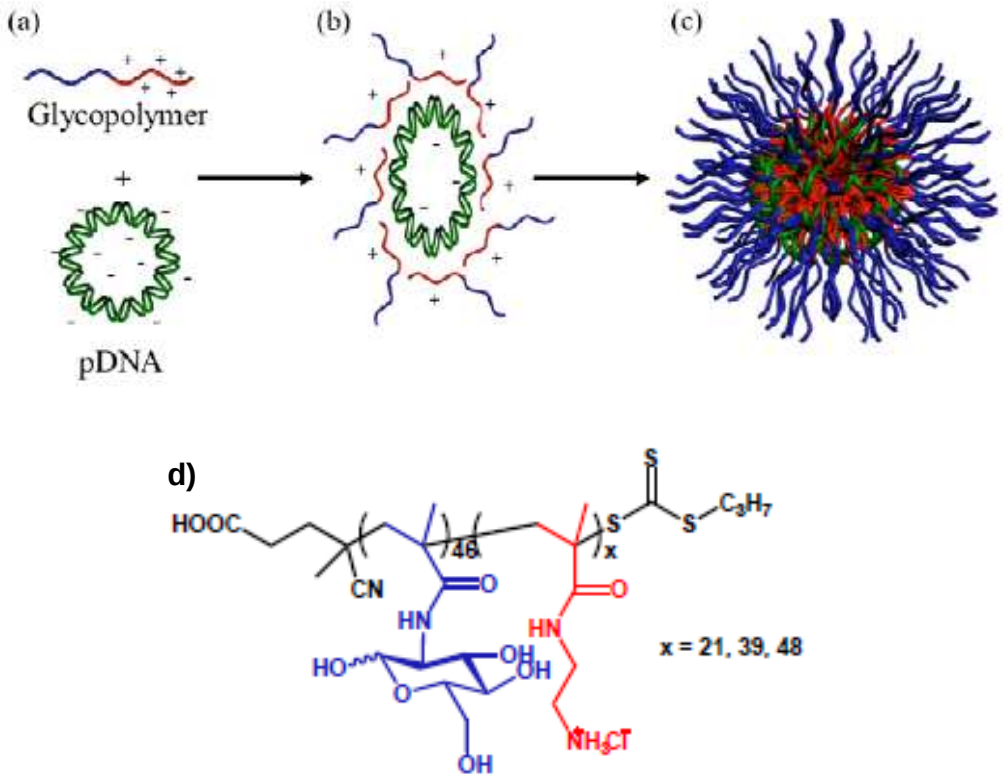

Figure 5.3) Schematic of polyplex formation with diblock glycopolymers and plasmid DNA. (a) The cationic charges on the AEMA block (red) allow the glycopolymer to interact with negative charges on the plasmid DNA (green). (b) Polyplex formation. The MAG block (blue) is expected to be displayed on the outside of the polyplex. (c) The polyplex is formed with the AEMA block and plasmid DNA in the inner core, and the MAG block on the outer surface. (d) Structure of the diblock polymers. The polymers differed in the lengths of the amine block; three different lengths were tested in the current work. This figure was produced by Dr. Adam E. Smith. Synthesis of these polymers was performed by Dr. Adam E. Smith and Antons Sizovs.

The polymers described above where synthesized to elucidate structure-function relationships between polymers and transfection efficiency. In many cases, intracellular mechanisms of polymer transfection are unknown. In an effort to decipher these mechanisms, it would be useful to find a way to track the polymers once they are inside of cells. Many groups have used hydrophobic fluorescent dyes attached to the polymers; however, these dyes can be large in comparison to the polymer and may alter polymer characteristics. Furthermore, labeling polymers is often a non-uniform process and the

labeled polymers are difficult to characterize. Ideally, a molecular tracer would be small enough so as not to interfere with normal polymer function. In an effort to develop a tool for studying the biological mechanisms of gene delivery polymers, our group has synthesized lanthanide-chelated polymers for use as polymer beacons.

Lanthanide metals are small, hydrophilic structures that are resistant to photobleaching, have long luminescent lifetimes, and are relatively nontoxic.[22] Recently, our group has synthesized a europium-chelated polymer to visualize polymer-mediated gene delivery using fluorescence microscopy,[22] illustrating the potential of using this system. To increase the benefits of lanthanide-chelated polymers, we attempted to develop a FRET-based system to observe polyplex unpackaging. For FRET, a suitable donor and acceptor need to be present. Using terbium as the donor, we complexed the terbium-chelated polymers to tetramethylrhodamine (TMR)-labeled pDNA. The emission spectrum for terbium overlaps with the excitation spectrum for TMR, enabling these two fluorophores to be used as a FRET pair.[23] The structure of the terbium-chelated polymers is illustrated in Figure 5.4.

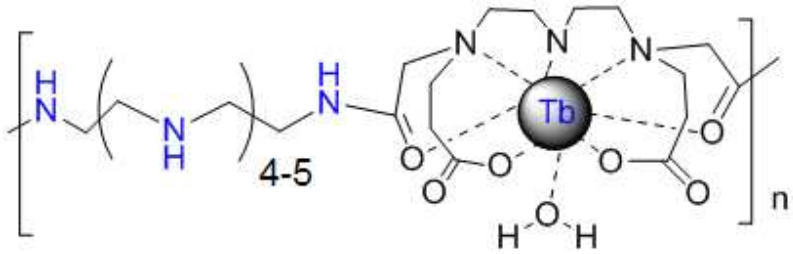

Figure 5.4) Structure of the terbium (Tb)-chelated polymers. The polymers differ in the amount of secondary amines in the repeat unit, with Tb-N4 having 4 secondary amines and Tb-N5 having 5 secondary amines. The degree of polymerization (n) is 20 for Tb-N4, and n = 23 for Tb-N5. Polymer synthesis was carried out by Sneha Kelkar. This figure was provided by Sneha Kelkar.

In the current work, we describe analysis of the quenching of the terbium as a marker of polyplex dissociation, both in solution and *in vitro.*

5.3 Materials and Methods

Asialofetuin (ASF) was purchased from Sigma (St. Louis, MO) and used at a concentration of 1 mg/mL. Plasmid DNA (pDNA) (gWIZ-luc) was purchased from Aldevron (Fargo, ND). Where indicated, pDNA was labeled with Cy5 using a Cy5 *Label*IT® Nucleic Acid Labeling Kit or labeled with tetramethylrhodamine using a TMR *Label*IT® Nucleic Acid kit from Mirus Bio, LLC (Madison, WI) according to manufacturer's protocol.

Cell culture. Human cervical adenocarcinoma (HeLa) cells and Human hepatocellular carcinoma (HepG2) cells were purchased from ATCC (Rockland, MD) and cultured according to specified conditions. Rat mesenchymal stem cells (RMSCs) and human dermal fibroblasts (HDFn) cells were a kind gift from Techulon, Inc. (Blacksburg, VA). Cell culture media and supplements were purchased from Gibco (Carlsbad, CA). Serum-free medium (OptiMEM) was purchased from Gibco (Carlsbad, CA). Plasmid DNA (pDNA) used for luciferase expression assays was gWIZ-luc from Aldevron (Fargo, ND).

Competitive inhibition of the ASGPr receptor. Cells were transfected as previously described.[11, 24] Briefly, HeLa cells were seeded onto 24 well plates at a density of 50,000 cells/well and cultured in Dulbecco's Modified Eagle Medium (DMEM) supplemented with 10 % fetal bovine serum (FBS), 100 Units per mg penicillin, 100 μg / mL streptomycin, and 0.25 μg/mL amphotericin. HepG2 cells were

seeded onto 24 well plates at a density of 100,000 cells/well and cultured in Eagle's Minimum Essential Medium (EMEM) supplemented with 10 % FBS, 100 Units per mg penicillin, 100 μg / mL streptomycin, and 0.25 μg/mL amphotericin. Cells were incubated at 37 °C and 5 % CO_2 for 24 hours before transfection. Polyplexes were formed at an N/P ratio of 5 for all polymers except for G4, which was used at an N/P ratio of 20. Polyplexes were incubated for 1 hour at room temperature before transfection. Prior to transfection, cells were incubated in serum-free media (OptiMEM) with or without 1 mg/mL ASF for 15 minutes at 4 °C. Four hours after transfection, the polyplexes were aspirated off, the cells were washed with 500 μL of phosphate buffered saline (PBS)/well, and 1 mL of supplemented DMEM was added to the HeLa cells and 1 mL of supplemented EMEM was added to the HepG2 cells. The media was replaced with fresh media 24 hours after transfection, and cell lysates were assayed for luciferase activity 48 hours after transfection as previously described.[25] Briefly, cells were lysed 48 hours after transfection, and the cell lysate was analyzed for luciferase activity by adding luciferase substrate (Promega, Madison, WI) to lysates and measuring relative light units (RLU) on a GENios Pro plate reader (Tecan US, Research Triangle Park, NC). Protein content of lysates was measured using a Bio-Rad DC protein assay kit (Hercules, CA).

Transfection of RMSCs and HDFn cells. Prior to transfection, either primary neonatal human dermal fibroblast cells (HDFn, Invitrogen, Carlsbad, CA) or rat mesenchymal stem cells (RMSC, Invitrogen, Carlsbad, CA) were plated on 24 well plates at a density of 100,000 cells per well, with approximately 70% confluency. HDFn cells were incubated in Medium 106, supplemented with 2 % FBS, hydrocortisone (1 μg/mL), human epidermal growth factor (1 ng/mL), basic fibroblast growth factor (3 ng/mL), and

heparin (10 µg/mL), for 24 h at 37 ºC in a 5 % CO_2 environment. RMSC were incubated in Mesanpro RS medium (Invitrogen) supplemented with 2 % FBS. For both cell lines, media was changed 30 minutes prior to transfection. Stock solutions at N/P 20 for each polymer were prepared and diluted to lower N/P ratios (10, 7) so that equal volume of polymer solution (13.33 µL) and pDNA ([pDNA] = 0.075 mg/mL, volume = 13.33 µL) could be combined to form polyplex solution for each well. Cells were transfected in triplicate with a total of 1 µg of pDNA/well. Positive controls - Lipofectamine™ 2000 (Invitrogen, Carlsbad, CA), JetPEI™ (PEI, Polyplus Transfections, Illkirch, France), and G4 (Glycofect™, Techulon Inc., Blacksburg, VA) - were formulated with pDNA based upon their recommended protocols. Polyplexes were incubated for 1 hour at room temperature prior to transfection. Cells were transfected in serum-free medium (OptiMEM) for PEI and G4 and in serum-containing medium for the Lipofectamine and trehalose-containing polyplexes. After transfection, plates were swirled to ensure homogenous solution formation and incubated for 4 h, after which more media (500 µL) was added to each well. Cells were incubated for additional 20 h, followed by a media change and 24 h of additional incubation time. Forty-eight hours after transfection, media was evacuated from wells and cells were lysed in 100 µL Cell Lysis Buffer (Promega, Madison, WI). Cell lysates were deposited on 96-well plates and analyzed for luciferase activity and total protein concentration. Protein concentration was analyzed relative to controls to determine cell viability using a Bio-Rad DC Protein Assay (Hercules, CA) as previously described.[26]

MTT assay. Cells were prepared and transfected as described above for the transfection assay. However, 47 hours after transfection, media was evacuated from each

well and replaced with media containing 3-(4,5-dimethylthiazol-2-yl)-2,5-diphenyltetrazolium bromide (MTT, [MTT] = 0.5 mg/mL) (Invitrogen, Carlsbad, CA). Cells were incubated for an additional 1 hour then washed with PBS and lysed in 250 µL dimethyl sulfoxide (DMSO).

Green fluorescent protein expression. RMSC and HDFn cells were plated into 6 well plates at a density of 500,000 cells/well and allowed to incubate for 24 hours in the conditions described above. Polyplexes were formed using the same methods reported above using a plasmid encoding enhanced green florescent protein (EGFP-C1). Transfection and media change conditions are consistent with those reported above; however, cells were only subjected to complexes at a single charge ratio, N/P=20. After 48 hours cells were trypsinized, washed with PBS twice, and suspended in 500 µL of PBS. Flow cytometry analysis of each sample provided mean florescence intensity as well as the percentage of cells positive for green fluorescent protein (GFP).

For microscopy, cells were plated as described above. The transfection protocol was carried out the same way as for flow cytometry, except 48 hours after transfection cells were washed with PBS and fixed in 4 % paraformaldehyde before being imaged. Cells were imaged using a Nikon TE2000U widefield microscope equipped with a GFP excitation/emission filter set and liquid-cooled CCD camera. Wells were imaged with consistent exposure time and normalized to control backgrounds.

Cellular uptake. HeLa cells were plated into 6 well plates at a density of 250,000 cells/well and transfected in triplicate as previously described.[27] Cells were analyzed for Cy5 fluorescence using a BD FACSCanto II flow cytometer (BD Biosciences, San Jose, CA), and a minimum of 30,000 events per sample were collected.

Confocal microscopy. HeLa cells were seeded onto poly-L-lysine (PLL)-coated coverslips in a 12 well plate at a density of 15,000 cells/well. Cells were incubated in the conditions described above (supplemented DMEM, 37 °C, 5 % CO_2) for 48 hours before transfection to reach confluency. After incubation, polyplexes were formed by adding 50 μL of FITC-labeled P3 to 50 μL of Cy5-labeled pDNA to give 100 μL of polyplex solution at an N/P ratio of 5. The polyplexes were allowed to incubate for 1 hour at room temperature prior to transfection. For transfection, the DMEM was aspirated off, cells were washed with PBS, and 1 mL of serum-free media (OptiMEM) was added to each well. The 100 μL of polyplex solution was then added to each well, giving a total of 1 μg of pDNA/well. Four hours after transfection, polyplexes were aspirated off, cells were washed with PBS, and 1 mL of supplemented DMEM was added to each well. Cells were fixed in 4 % paraformaldehyde at the indicated time points, stained with DAPI (Molecular Probes, Eugene, OR) to label nuclei according to manufacturer's protocol, and mounted onto microscopy slides using ProLong Gold Antifade Reagent (Molecular Probes, Eugene, OR) according to manufacturer's protocol. The slides were allowed to dry overnight in the dark before being sealed with clear nail polish and imaged on a Zeiss LSM 510 META confocal microscope (Carl Zeiss MicroImaging, LLC, Thornwood, NY). Images were taken using a slice thickness of 0.8 μm.

FRET studies. Polyplexes were formed between Tb-N4 and plasmid DNA at the indicated N/P ratios. For polymer only controls, polymer solution diluted to the same concentration as the indicated N/P ratio was added to an equivalent volume of water instead of pDNA. Terbium emission was monitored on a SpectraMax M2 plate reader (Molecular Devices, Sunnyvale, CA) using an excitation wavelength of 380 nm. The

amount of quenching was calculated using the formula ((polymer only RFU – polyplex RFU) / polymer only RFU) * 100.) For the live cell studies, HeLa cells were seeded on to a 6 well plate at a density of 250,000 cells/well, and transfected with Tb-N5 polyplexes formed at an N/P ratio of 20. The transfections were carried out in serum-containing DMEM. Four hours after transfection, media containing the polyplexes was aspirated off, cells were washed with PBS, and cells were imaged on an EVOS fluorescent microscope (AMG, Bothell, WA). Imaging of the terbium polymers was performed using a custom filter cube containing a 380 nm excitation and a 540 nm emission (AMG, Bothell, WA). Fluorescence quantification was carried out by using the software NIH ImageJ,[28] and fluorescence from dead cells was excluded from the measurements.

Statistical Analysis. All data are presented as means ± standard deviations. Statistical analysis of data was done using the software JMP (S.A.S. Institute Inc., Cary, NC). Means were compared using ANOVA followed by the Tukey-Kramer HSD method unless otherwise noted, with $p < .05$ being considered as statistically significant.

5.4 Results and Discussion

Competitive inhibition of ASGPr. Dr. Chen-Chang Lee performed dynamic light scattering (DLS) measurements on polyplexes formed at both 0.01 mg/mL[11] and 0.02 mg/mL (unpublished results). He observed that the hepatocyte-targeted polymers formed smaller polyplexes at the reduced [pDNA], and hypothesized that the smaller polyplex size would allow for more receptor-mediated endocytosis as opposed to non-specific endocytosis. Based on the data in Figure 5.5, we observed that the polymer with a 40% degree of carbohydrate substitution (Ma-1-3-Gal-40) exhibited the greatest competitive

inhibition with ASF at an N/P of 5. Furthermore, at an N/P ratio of 5, the polymer with the highest degree of carbohydrate substitution (Ma-1-3-Gal-40) had the highest transfection efficiency (Figure 5.5 a). At decreased degrees of carbohydrate substitution (18 % for Ma-1-3-Gal-18 and 13 % for Ma-1-3-Gal-13), we observed that ASF had less of an effect on transfection efficiency, however, all polymers exhibited significantly less ($p < 0.05$) luciferase expression in the presence of ASF at an N/P ratio of 5 (Figure 5.5 a). In addition, we see less ASF inhibition at higher N/P ratios (Figure 5.5 b and c) and decreased effect of the degree of carbohydrate substitution upon luciferase expression, most likely due to increased non receptor-specific uptake from the increased charge ratio of the polyplexes. It should be noted here that at an N/P ratio of 10, the polymer with the highest degree of carbohydrate substitution (Ma-1-3-Gal-40) had no significant ($p < 0.05$) decrease in transfection efficiency in the presence of ASF, while the polymers with lower degrees of carbohydrate substitution (Ma-1-3-Gal-18 and Ma-1-3-Gal-13) still had some ASF inhibition. However, these two polymers still exhibited greater ASF inhibition at an N/P of 5 compared to an N/P of 10. These studies guided us to use an N/P ratio of 5 for future studies to minimize non receptor-mediated uptake.

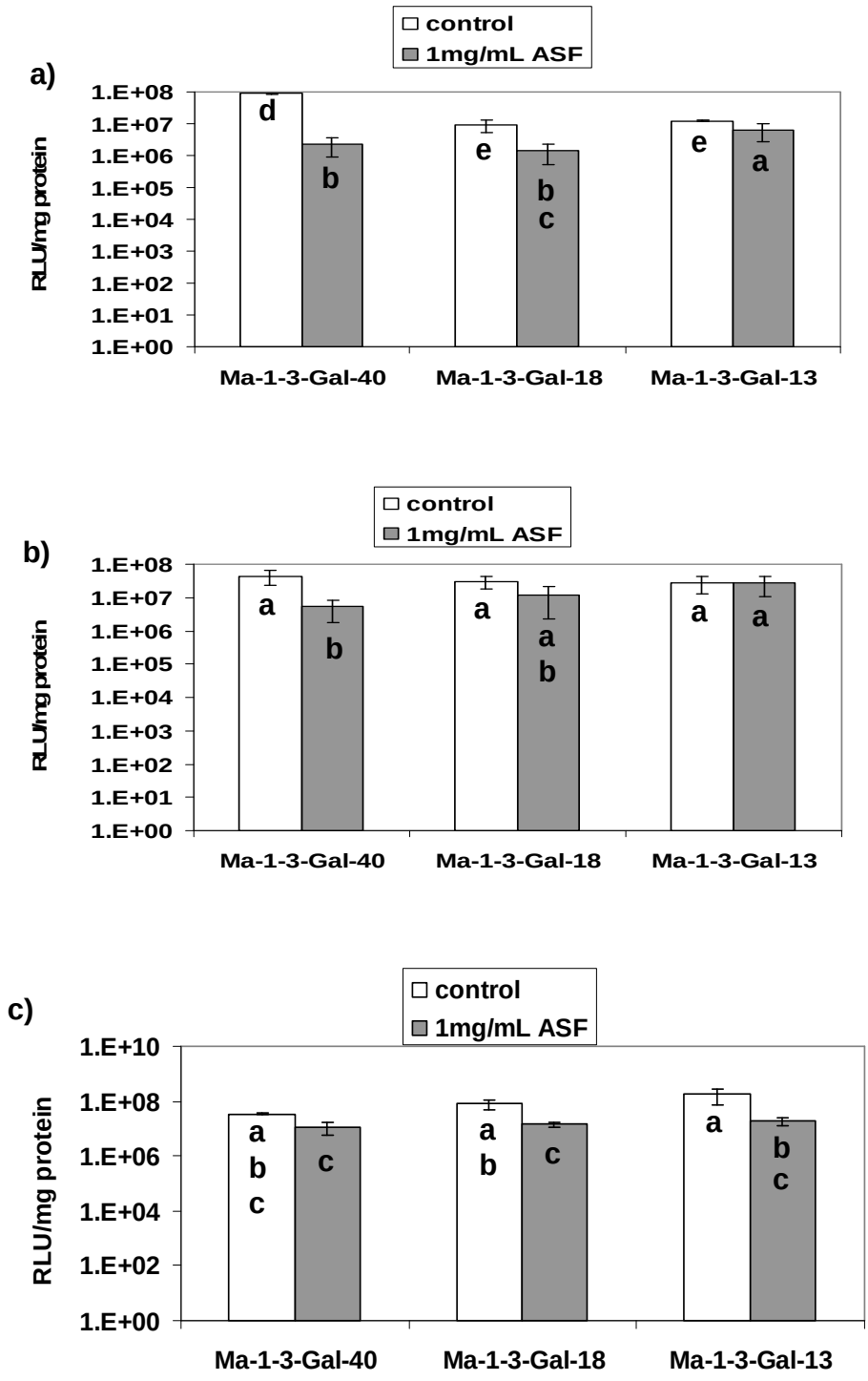

Figure 5.5) Luciferase expression data for HepG2 cells 48 hours after transfection. Cells were transfected in the presence or absence of 1 mg/mL asialofetuin (ASF) at N/P ratios of (a) 5; (b) 8; (c) 10. HepG2 cells were transfected with 0.5 µg pDNA/well. Data are presented as the mean ± standard deviation. Statistical analysis was performed on the log of the RLU/mg protein, and bars with

different letters represent means that are statistically significant ($p < 0.05$) according to the Tukey-Kramer HSD method (n = 2).

Next, in addition to testing the effect the degree of carbohydrate substitution had on transfection efficiency, we also wanted to study the effect that the linker length had on transfection efficiency. In order to determine whether the polymers were exhibiting receptor-mediated endocytosis, flow cytometry was used to study polyplex uptake. These flow cytometry studies were done by Dr. Patrick McLendon.[11] To further study whether inhibiting the ASGPr with asialofetuin (ASF) would have an effect on transfection efficiency, luciferase gene expression assays were performed. The results of transfection in HepG2 cells are shown in Figure 5.6.

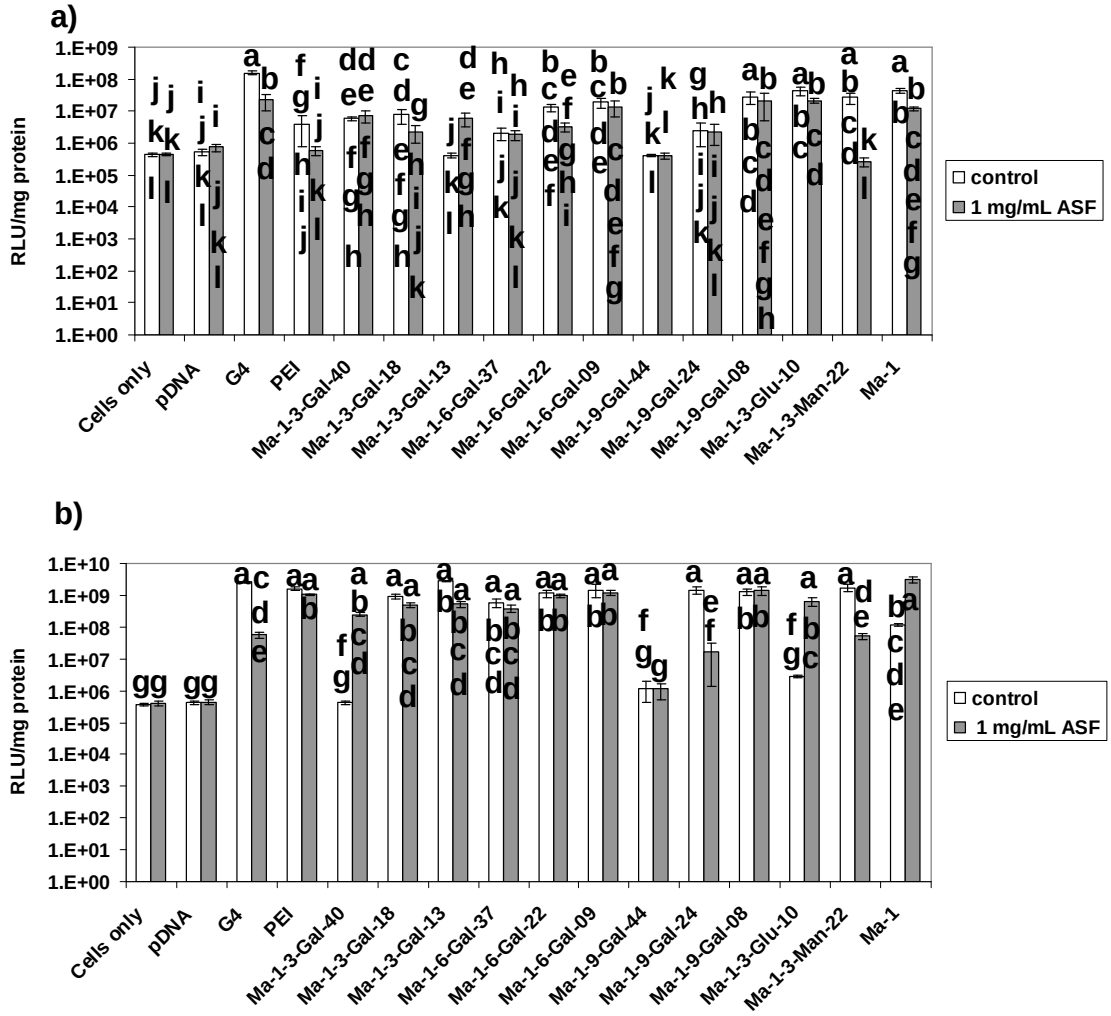

Figure 5.6) Luciferase gene expression as expressed by relative light units (RLU)/mg protein in HepG2 cells 48 hours after transfection. HepG2 cells were transfected in the presence or absence of 1 mg/mL asialofetuin (ASF). Polyplexes were formed at N/P ratios of 5 for all polymers except for G4, which was formed at an N/P ratio of 20. Cells were transfected with (a) 0.5 µg pDNA/well or (b) 1 µg pDNA/well. Data is presented as the mean ± standard deviation of three trials. Statistical analysis was performed on the log of the RLU/mg protein. Bars with different letters represent means that are statistically significant ($p < 0.05$) using the Tukey-Kramer HSD method ($n = 3$). Bars with matching letters are not statistically significant from each other.

We notice some interesting occurrences in this data. First, we notice that the data for the Ma-1-3 series first shown in Figure 5.5 is not evident when polyplexes are formed using a pDNA concentration of 0.02 mg/mL (Figure 5.6 b). In fact, we see a dramatic increase ($p < 0.05$) in transfection efficiency in the presence of ASF for Ma-1-3-Gal-40 when

polyplexes are formed using this pDNA concentration; given the large difference and the fact that there is no luciferase expression observed, it is likely there was an error in transfecting the cells for this data point. We conclude this based on previous data where Ma-1-3-Gal-40 exhibited transfection efficiency using this pDNA concentration (data not shown) and the fact that we do observe luciferase expression in the presence of ASF, which should not be able to increase the transfection efficiency of these polymers if they are being taken up through the ASGPrs. We also observe that the presence of ASF significantly ($p < 0.05$) increases the transfection efficiency of Ma-1-3-Glu-10 and Ma-1 using polyplexes formed at [pDNA] .02 mg/mL (Figure 5.6 b), two control polymers that do not contain galactose and therefore should not be entering through ASGPr-mediated endocytosis. These results are interesting; it is possible that the ASF is inhibiting a less efficient form of endocytosis and influencing the polyplexes to enter the cell in a more efficient way, but more experiments need to be done to determine if this is the case.

We also see significant ($p < 0.05$) ASF inhibition in the case of galactarate-containing G4 and mannose-containing polymer Ma-1-3-Man-22 for both pDNA concentrations (Figure 5.6). We do not expect these polymers to exhibit ASGPr-mediated endocytosis, since there is no galactose on them. Prior research done by Yemin Liu has also shown a slight transfection inhibition of G4 and mannose-containing PGAA M4 in the presence of ASF in HepG2 cells.[29] We are unsure of what causes this; it is believed that asialofetuin is specific for the ASGPr, but perhaps the presence of ASF interferes with other carbohydrate-mediated endocytic pathways. We also observed anomalies in an agglutination assay designed to test the accessibility of the β-D-galactose residues.[11] The anomalies in both ASF inhibition and agglutination experiments may be explained by the

hydrophobic nature of the linker groups; it is possible that the hydrophobic methylene chain folds towards the interior of the polyplex during pDNA complexation, thus inhibiting the ability of the β-D-galactose residues to reach the receptors on the HepG2 cells. It is also possible that in this system, endocytosis could be charge-mediated as well as receptor-mediated. Another potential reason for the discrepancy in data for the Ma-1-3-Gal series is that in the time between the initial ASF inhibition experiments and the later experiments testing a wider range of polymers, the Ma-1-3-Gal polymers may have degraded. To further test the specificity of these polymers, transfections were carried out in HeLa cells, which do not have ASGPrs. The polyplexes were formed using a pDNA concentration of 0.01 mg/mL, and the results are shown in Figure 5.7.

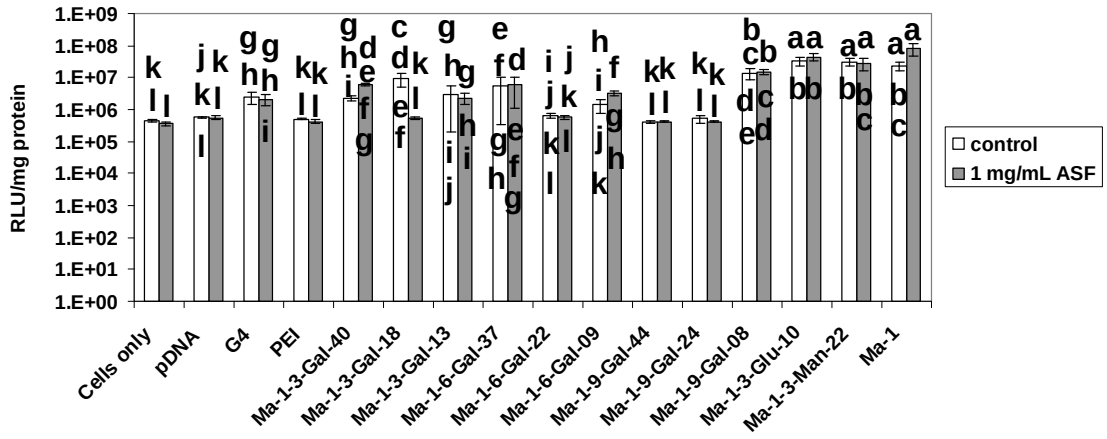

Figure 5.7) Transfection efficiency in HeLa cells. Cells were transfected with 0.5 μg pDNA/well, and luciferase gene expression was assayed 48 hours after transfection. Cells were transfected in the presence or absence of 1 mg/mL asialofetuin (ASF). Statistical analysis was performed on the log of the RLU/mg protein. Bars with different letters represent means that are statistically significant ($p < 0.05$) using the Tukey-Kramer HSD method (n = 3).

Overall, we do notice lower transfection in the β-D-galactose-containing polymers in HeLa cells (Figure 5.7) when compared to HepG2 cells (Figure 5.6 a). Polymers Ma-1-9-Gal-44 and Ma-1-9-Gal-08 failed to transfect HeLa cells at all; the luciferase expression

was not statistically significant ($p < 0.05$) from that of the cells only and pDNA only controls. It is interesting to note the role of pDNA concentration; when forming polyplexes using pDNA at 0.1 mg/mL, we see significant reduction in the efficacy of JetPEI. We also observe no significant ($p < 0.05$) inhibition in the presence of ASF, except in the case of Ma-1-3-Gal-18. This polymer also exhibited reduction in transfection efficiency in the presence of ASF in HepG2 cells. These data and the data in Figure 5.6 suggest that the ASF is also capable of interacting with the polymers themselves in addition to the ASGPrs. In fact, ASF has previously been shown to bind to non-galactosylated proteins such as bovine serum albumin and to monosaccharides such as mannose.[30]

Toxicity of hepatocyte-targeted polymers. It was of interest to us to test the effect of the degree of carbohydrate substitution as well as the linker length on cell viability. We did notice a difference in toxicity profiles when using polyplexes formed at the different pDNA concentrations; at 0.01 mg/mL pDNA (0.5 μg pDNA/well), none of the polymers tested exhibited significant cytotoxicity (Figure 5.8 a) as measured by the amount of protein in cell lysates compared to the cells only control. However, when polyplexes were formed using pDNA at a concentration of 0.02 mg/mL, we do notice a trend in cell viability. In polymers with the shorter linker length (Ma-1-3 series and Ma-1-6 series), cell viability decreases as the degree of carbohydrate substitution decreases (Figure 5.8 b). This trend is reversed in polymers with the longer linker length (Ma-1-9-Gal series); the polymer with the lowest degree of carbohydrate substitution (Ma-1-9-Gal-08) exhibited higher cell viability than polymers with higher degrees of carbohydrate substitution (Ma-1-9-Gal-44 and Ma-1-9-Gal -4) (Figure 5.8 b). All polymers tested

exhibited > 80 % cell viability, and most had toxicity profiles in between those of the two positive controls, JetPEI and G4. This was to be expected, since the carbohydrate content of these polymers is at an intermediate level between G4 and JetPEI.

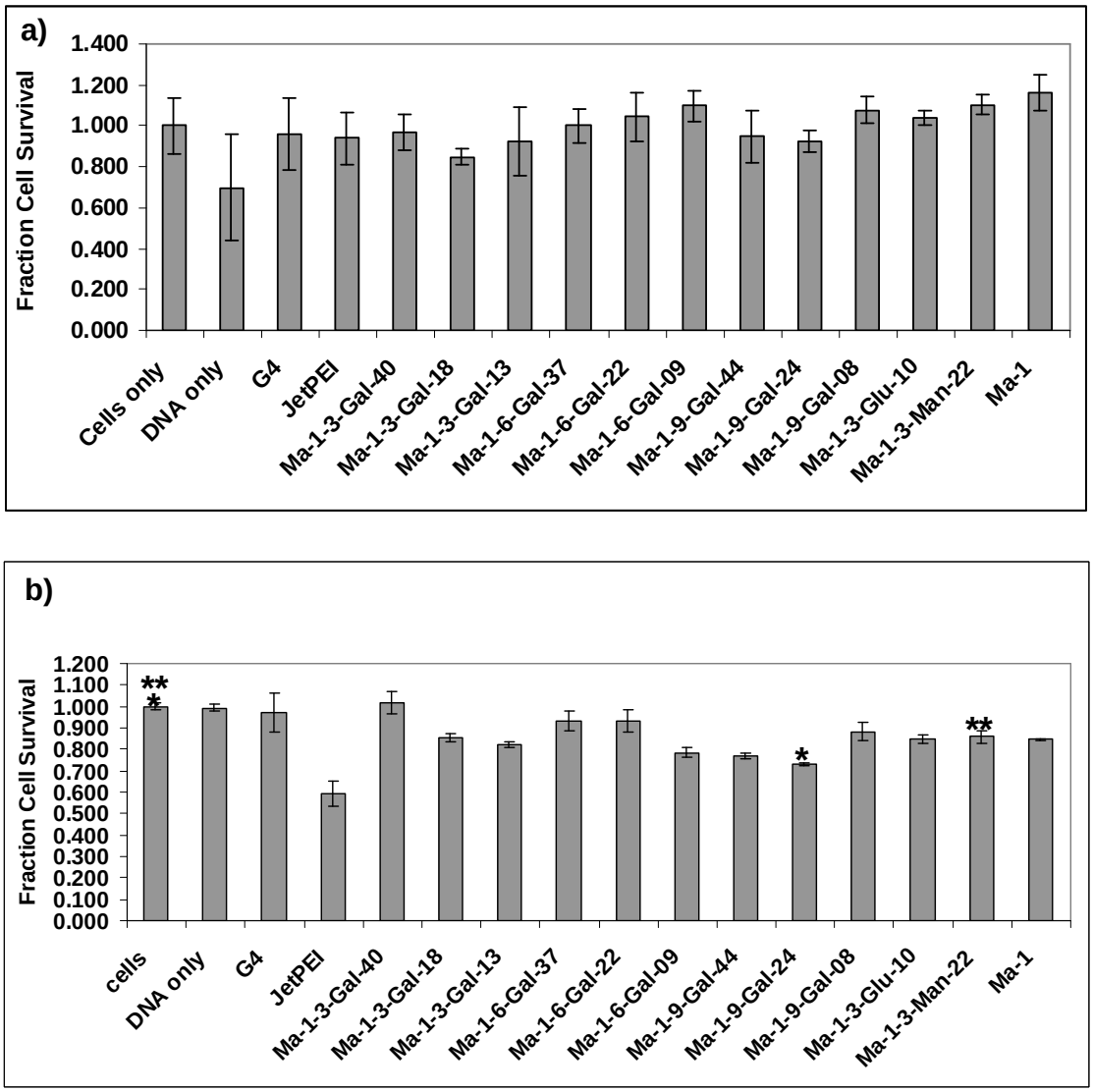

Figure 5.8) Cell viability as measured by the amount of protein in cell lysates. HepG2 cells were allowed to transfect for 48 hours, after which cell viability was measured. All polymers were used at an N/P ratio of 5, with the exception of G4 that was used at an N/P ratio of 20. Cells were treated with (a) 0.5 µg of pDNA/well or (b) 1 µg of pDNA/well. * denotes means that are statistically significant ($p < 0.05$) from each other. ** denotes means that are statistically significant from each other ($p < 0.05$). Statistically analysis was performed using the Tukey-Kramer HSD method ($n = 3$). Means for cell viability data in (a) were not statistically significant from each other according to the Tukey-Kramer HSD method ($n = 3$).

Effect of polymer end group and PEG linkages on transfection efficiency. The hepatocyte-targeted polymer library gave us some insight on how hydrophobic linkages can affect the transfection efficiency profiles of gene delivery polymers. To gain further insight on how polymer structure influences intracellular mechanisms of transfection, polymers containing different end groups were synthesized. The importance of polymer end groups has previously been established.[31-32] Green *et. al.* have demonstrated how polymers can be "tuned" to yield favorable properties by varying their end groups.[33] Here, trehalose-containing polymers ending in either PEG (Tr4 A and Tr4 B), trityl (Tr4 C) or azide (Tr4 D) were tested to determine which would have the highest transfection efficiency in rat mesenchymal stem cells (RMSCs) and human dermal fibroblasts (HDFn cells). To further increase knowledge on structure-function relationships, different linkages for PEG were used; Tr4 A contains an amide linkage, while Tr4 B contains a carbamate linkage. To remain consistent, the molecular weight of the PEGs was kept constant at 5 kDa, and the degree of polymerization for the trehalose polymers is 100. The results for luciferase expression are shown in Figure 5.9.

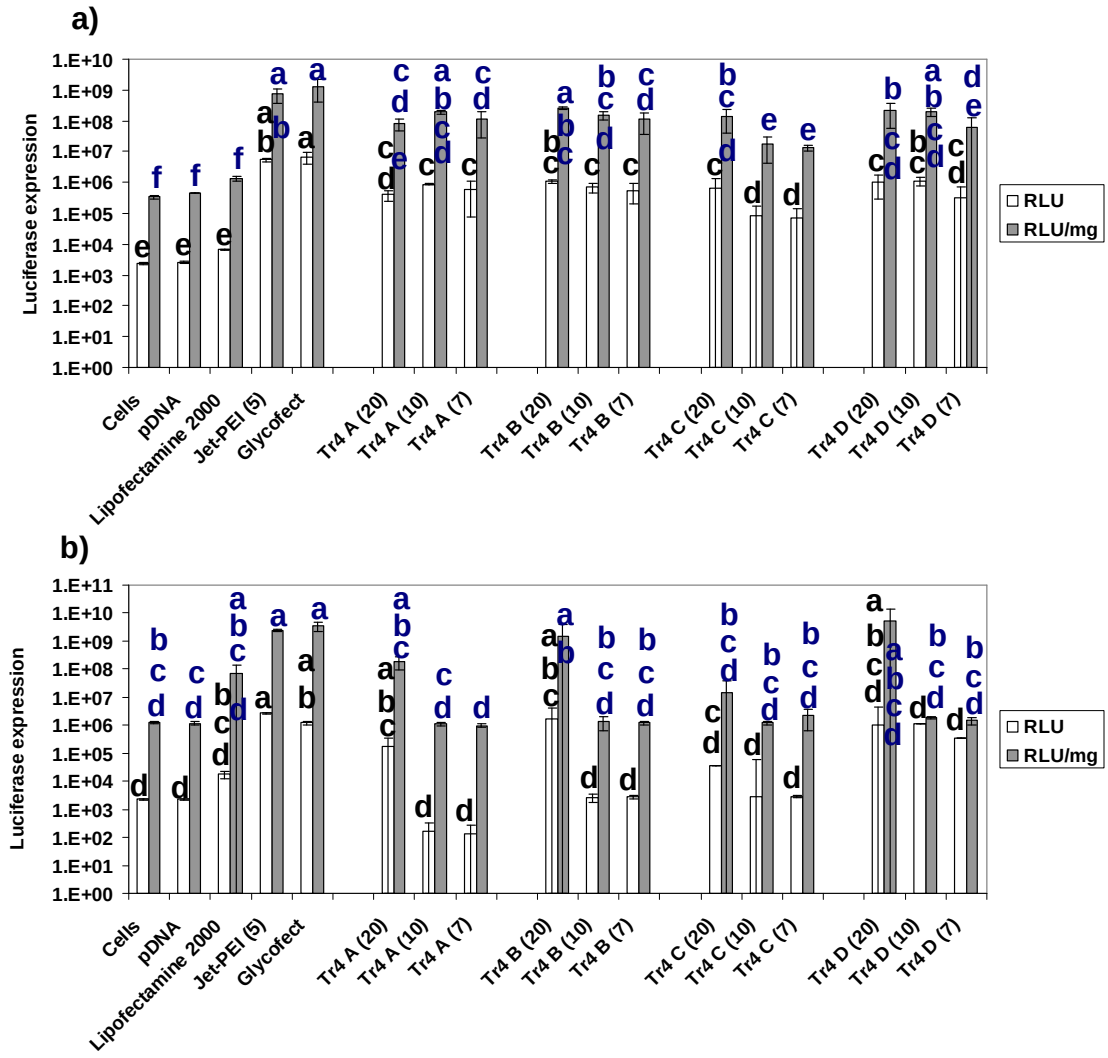

Figure 5.9) Luciferase expression data expressed in relative light units (RLU) and RLU/mg protein. (a) RMSCs and (b) HDFn cells were transfected for 48 hours before the cell lysates were analyzed for luciferase activity. Tr4 polymers were formed at the N/P ratios indicated in parentheses. Positive controls were used according to manufacturer's instructions. Data are presented as mean ± standard deviation. Statistical analysis was performed on the log of the RLU and log of the RLU/mg protein data. Black letters represent statistical analysis for RLU data (white bars), and blue letters represent statistical analysis for RLU/mg protein (gray bars). Bars with different letters are statistically significant ($p < 0.05$) from each other according to the Tukey-Kramer HSD method (n = 3).

In the RMSCs (Figure 5.9 a), the N/P ratio of the Tr4 polymers did not seem to have a significant ($p < 0.05$) effect on transfection efficiency, except in the case of Tr4 C. With Tr4 C, higher N/P ratios resulted in higher luciferase expression in this cell line (Figure 5.9 a). In addition, all polymers had significantly ($p < 0.05$) higher transfection

efficiency than Lipofectamine-2000 in this cell line (Figure 5.9 a). In the HDFn cells (Figure 5.9 b), the PEGylated polymers Tr4 A and Tr4 B reached the transfection efficiency of the positive controls when used at an N/P ratio of 20, while the non-PEGylated Tr4 C and Tr4 D were not statistically significant ($p < 0.05$) from the cells only control. We did not observe any dramatic ($p < 0.05$) effects of PEG linker or on end group type for these transfection efficiency data. To further study how polymer structure affects efficacy, GFP expression was analyzed. This assay differs from the luciferase assay in that it allows us to observe how many cells in a given population were successfully transfected, as opposed to studying enzyme activity in the lysates of transfected cells. Figure 5.10 illustrates the GFP expression data for RMSCs, and figure 5.11 shows GFP expression in HDFn cells. In the GFP experiments, the polymers Tr5 and Tr6 were studied as well. These polymers are identical to polymer Tr4 C (trityl end groups) except they differ in the number of secondary amines in their repeat unit; Tr4 has 4 amines, Tr5 has 5, and Tr6 has 6 amines.

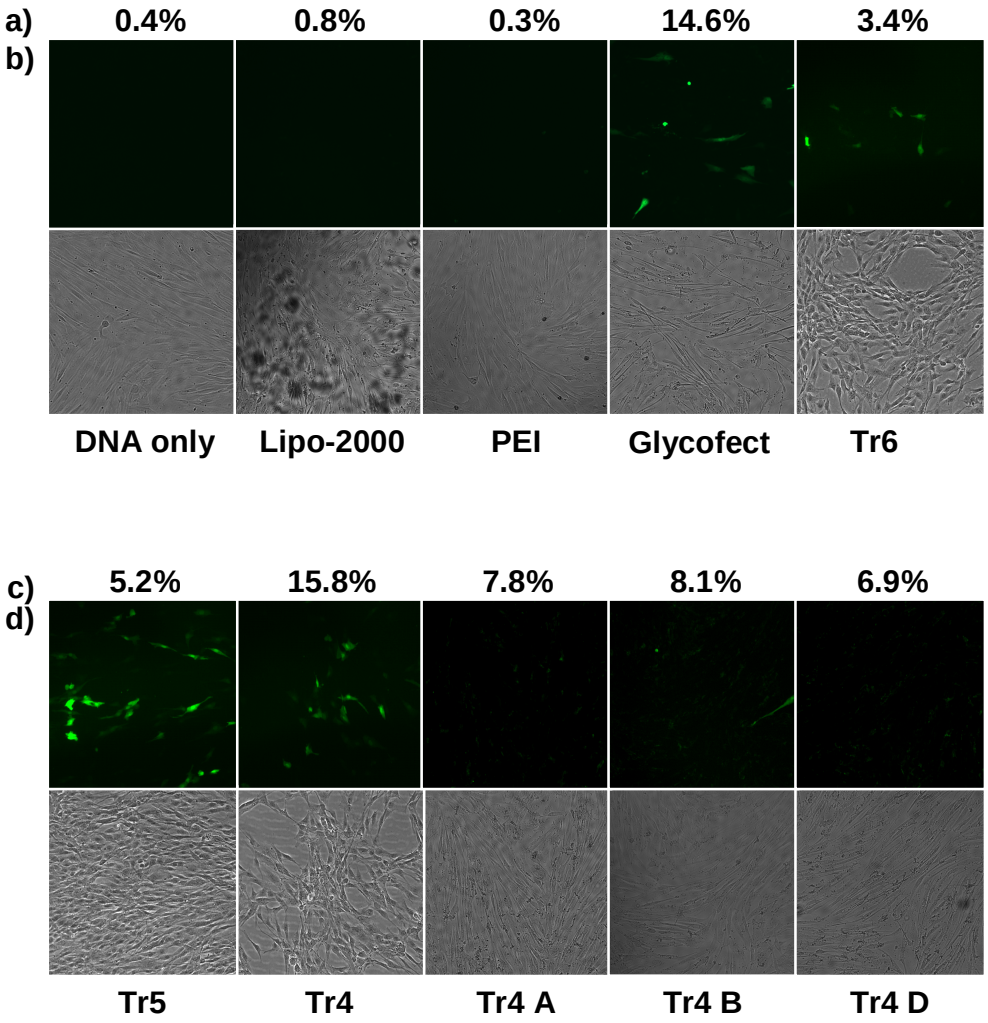

Figure 5.10) Green fluorescent protein (GFP) expression in RMSCs. Cells were analyzed for green GFP expression using (a) and (c) flow cytometry to determine the percentage of cells positive for green fluorescence 48 hours after transfection. Further GFP expression analysis was carried out by (b) and (d) fluorescence microscopy 48 hours after transfection. In this case, Tr6, Tr5 and Tr4 all have trityl end groups, the difference between these polymers is the number of secondary amines in their repeat units (6, 5, and 4, respectively). The trehalose polymers were used at an N/P of 20, while positive control polymers Lipofectamine 2000 (Lipo-2000), JetPEI (PEI), and Glycofect were used according to manufacturer's protocol.

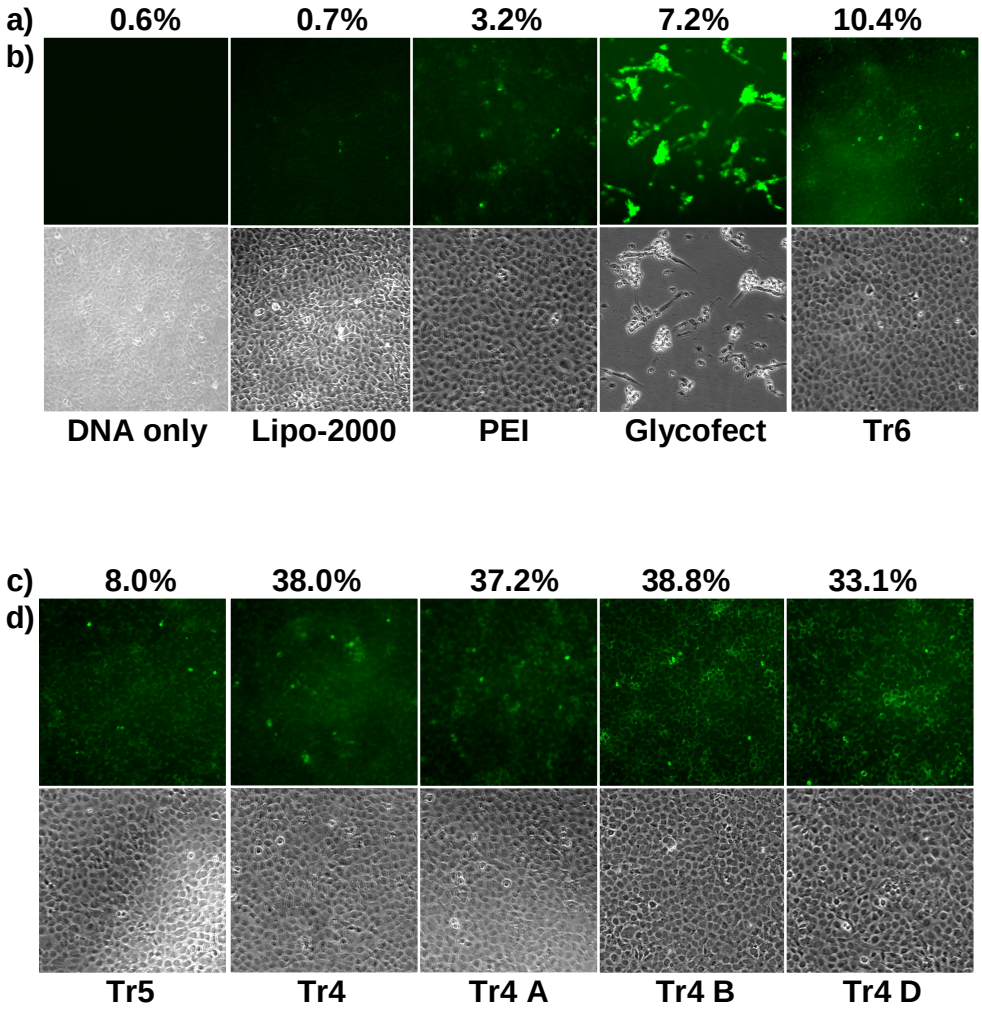

Figure 5.11) Green fluorescent protein (GFP) expression in HDFn cells. Cells were analyzed for GFP expression using (a) and (c) flow cytometry as well as (b) and (d) fluorescence microscopy 48 hours after transfection. In this case, Tr6, Tr5 and Tr4 all have trityl end groups, the difference between these polymers is the number of secondary amines in their repeat units (6, 5, and 4, respectively). The trehalose polymers were used at an N/P of 20, while positive control polymers Lipofectamine 2000 (Lipo-2000), JetPEI (PEI), and Glycofect were used according to manufacturer's protocol.

In the GFP data, we observe a trend in the number of amines; Tr4 exhibits higher gene expression than Tr5 and Tr6. In RMSCs, we do see an effect of the end group; the polymer containing the trityl end group ("Tr4" in Figure 5.10) exhibits higher GFP expression than the PEGylated polymers and the azide-terminated polymer (Figure 5.10 c

and d). The transfection efficiency of Tr4 reached that of the positive control Glycofect (Figure 5.10 a and b) in this cell line.

In HDFn cells (Figure 5.11), the trend of increased transfection efficiency as the number of amines decreases stands, with Tr4 exhibiting higher transfection efficiency than Tr5 and Tr6 (Figure 5.11 a, b, c, and d). In this cell line, the Tr4 polymers out-perform all positive controls. Also, in HDFn cells we do not see as dramatic an effect on polymer end group; all Tr4 polymers performed with nearly the same transfection efficiency. We hypothesized that the increased transfection efficiency of the Tr4 polymers was due to their reduced cytotoxicity in these cell lines. To further explore this hypothesis, assays to test cell viability during trehalose polymer transfection were performed.

Effect of polymer end group and PEG linkages on cell viability. It was of interest to us to determine whether the end group of the polymers would influence cell viability. The results of two different cell viability assays (Bio-Rad DC protein assay and the MTT assay) are shown in Figure 5.12. In RMSCs, all of the Tr4 polymers exhibited ~70% cell viability, with no dramatic effects of end group or PEG linker observed. It was our hypothesis that the incorporation of PEG into these polymers would improve the toxicity profile, but the data in Figure 5.12 a illustrate that this is not the case in this cell line.

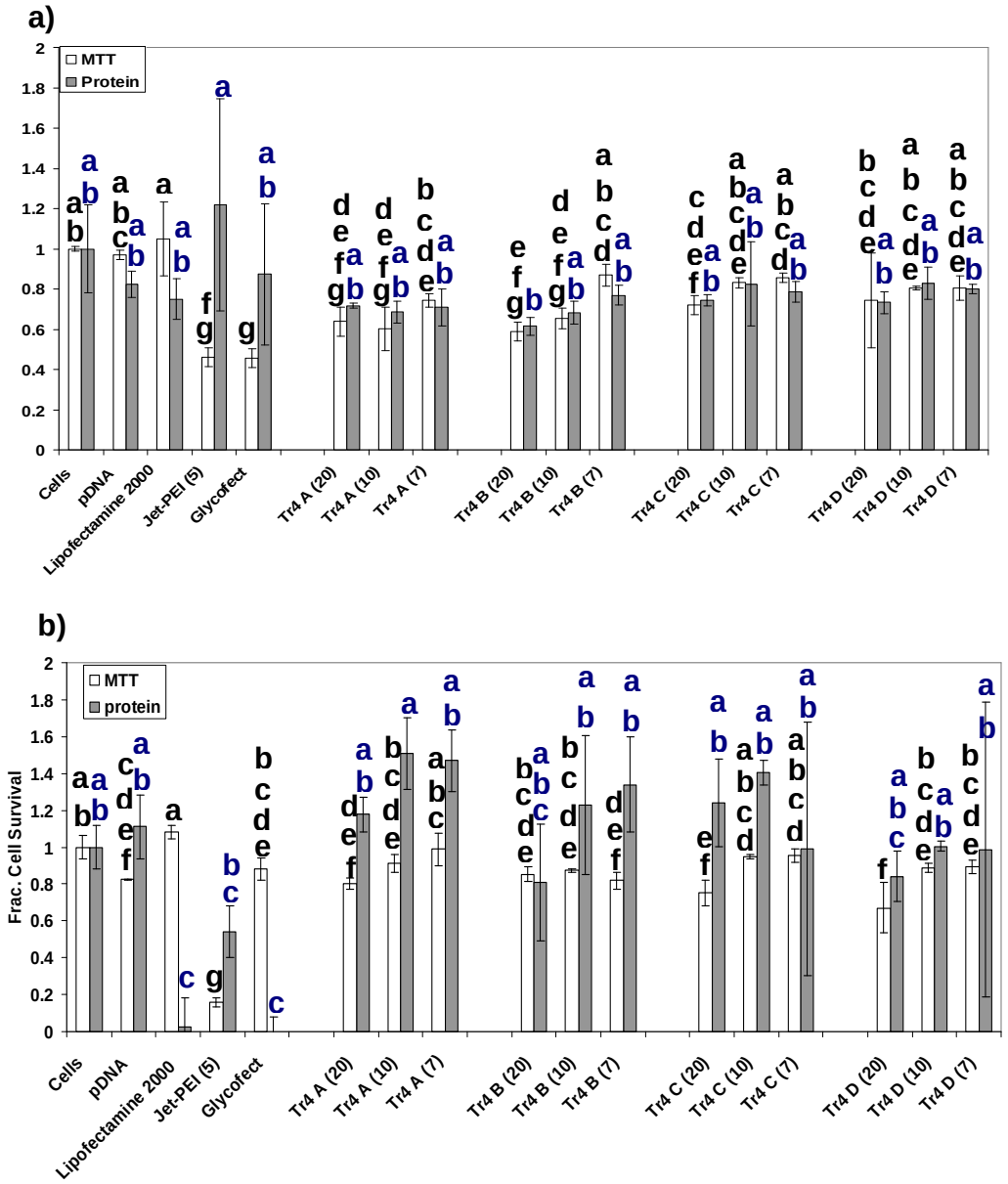

Figure 5.12) Cell viability as measured by protein content present in cell lysates ("protein") and by the MTT assay in (a) RMSCs and (b) HDFn cells. Cells were transfected with the trehalose polymers at the indicated N/P ratios, and cell viability was measured 48 hours after transfection. Data are presented as mean ± standard deviation. Black letters represent statistical analysis for the MTT assay, and blue letters represent statistical analysis for the protein assay. Bars with matching letters are not statistically significant from each other, and bars with different letters represent means that are statistically significant ($p < 0.05$) from each other according to the Tukey-Kramer HSD method ($n = 3$).

In the case of HDFn cells, we see dramatic increases in cell survival in the Tr4 polymers compared to JetPEI, strengthening our hypothesis that the increased transfection efficiency exhibited by the Tr4 polymers in this cell line is a result of increased cell survival during transfection. However, as with the transfection efficiency data and the toxicity data in the RMSCs, we did not see any dramatic effects of polymer end group or PEG linkages on cell viability.

Cellular Uptake of RAFT polymers. In addition to studying the effect of end groups on polymer transfection, it was of interest to us to study the effect of increasing the quantity of primary amines in a polymer upon intracellular uptake. It was our hypothesis that the polymer containing the longest AEMA block (P3) would have the highest uptake, as the presence of more charged groups would increase electrostatic interactions between the polymer and the plasma membrane. Figure 5.13 illustrates the results of the cellular uptake studies.

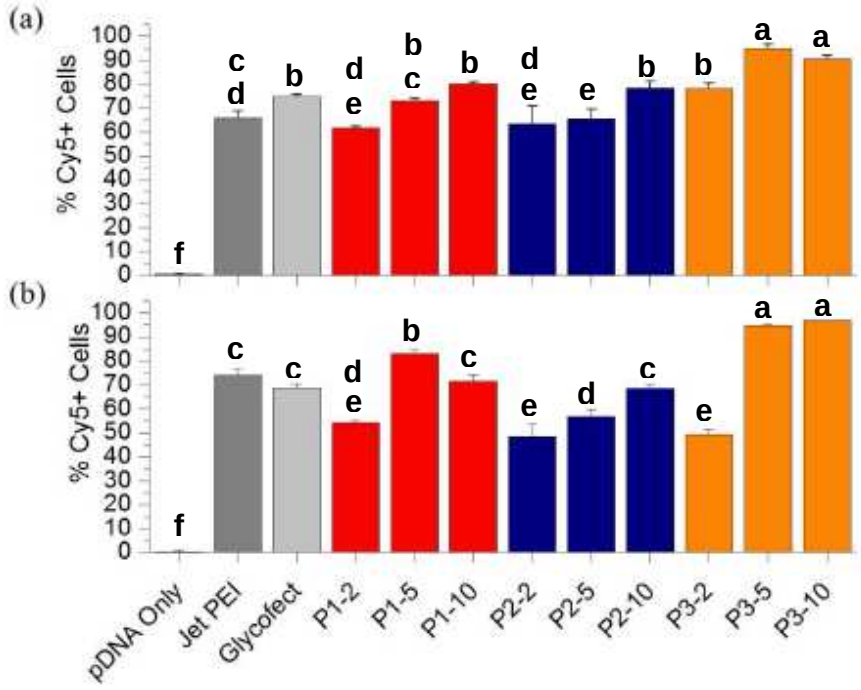

Figure 5.13) Percentage of Cy5 positive HeLa cells transfected with polyplexes formed at N/P ratios 2, 5, and 10 with Cy5-labeled pDNA and P1, P2, P3 in (a) OptiMEM and (b) DMEM. JetPEI and Glycofect were used as positive controls, JetPEI was used at an N/P ratio of 5 and Glycofect was used at an N/P ratio of 60. Cy5 fluorescence was measured 48 hours after transfection. The graphs were provided by Dr. Adam E. Smith. Statistical analysis was done by Giovanna Grandinetti. Data are presented as means ± standard deviations. Bars with matching letters are not statistically significant from each other, and bars with different letters represent means that are statistically significant from each other ($p < 0.05$, $n = 3$) according to the Tukey-Kramer HSD method.

In the absence of serum, we noticed a trend where increasing the N/P ratio increased the amount of Cy5 fluorescence in cells for all of the polymers, with N/P ratios of 10 having significantly higher ($p < 0.05$) uptake than N/P ratios of 2 (Figure 5.13 a). We also noticed this trend in the presence of serum (Figure 5.13 b) for polymers P2 and P3, but for polymer P1, the intermediate N/P ratio of 5 had the highest uptake. There a slight trend in the impact of length of the AEMA block on polyplex uptake, with polymer P3 exhibiting the significantly higher ($p < 0.05$) uptake when comparing the polymers at an N/P ratio of 10. At an N/P ratio of 2, polymer P3 also exhibited the highest polyplex uptake in the absence of serum, but in the presence of serum, there was no significant (p

< 0.05) difference in polyplex uptake at this low N/P ratio. At an N/P ratio of 5, both in the presence and absence of serum, P1 exhibited significantly higher ($p < 0.05$) polyplex uptake than P2, but lower polyplex uptake than P3. Based on these data, we concluded that in the presence of serum, the longer AEMA block increases intracellular uptake compared to polymers with the shorter AEMA block. Interestingly, even though nearly 100 % of the cells are positive for Cy5 fluorescence when treated with polymer P3, this polymer exhibits low transfection efficiency (data not shown). We see a decrease in transfection efficiency as the length of the AEMA block increases at an N/P of 10, with P1 having the highest transfection efficiency in the absence of serum. We hypothesized that the length of the AEMA block was inhibiting polyplex dissociation. To test this, P3 was labeled with FITC and complexed with Cy5-labeled pDNA, and the intracellular location of both the polymer and pDNA were studied using confocal microscopy at different time points.

Polyplex dissociation in cells. In order to decipher why P3 exhibited high uptake but low transfection efficiency, we wanted to determine whether the longer AEMA block was inhibiting pDNA release from the polyplex. Polyplexes were formed using labeled polymer and pDNA, and HeLa cells were transfected in serum-free media and fixed at the indicated time points. The confocal images can be seen in Figure 5.14.

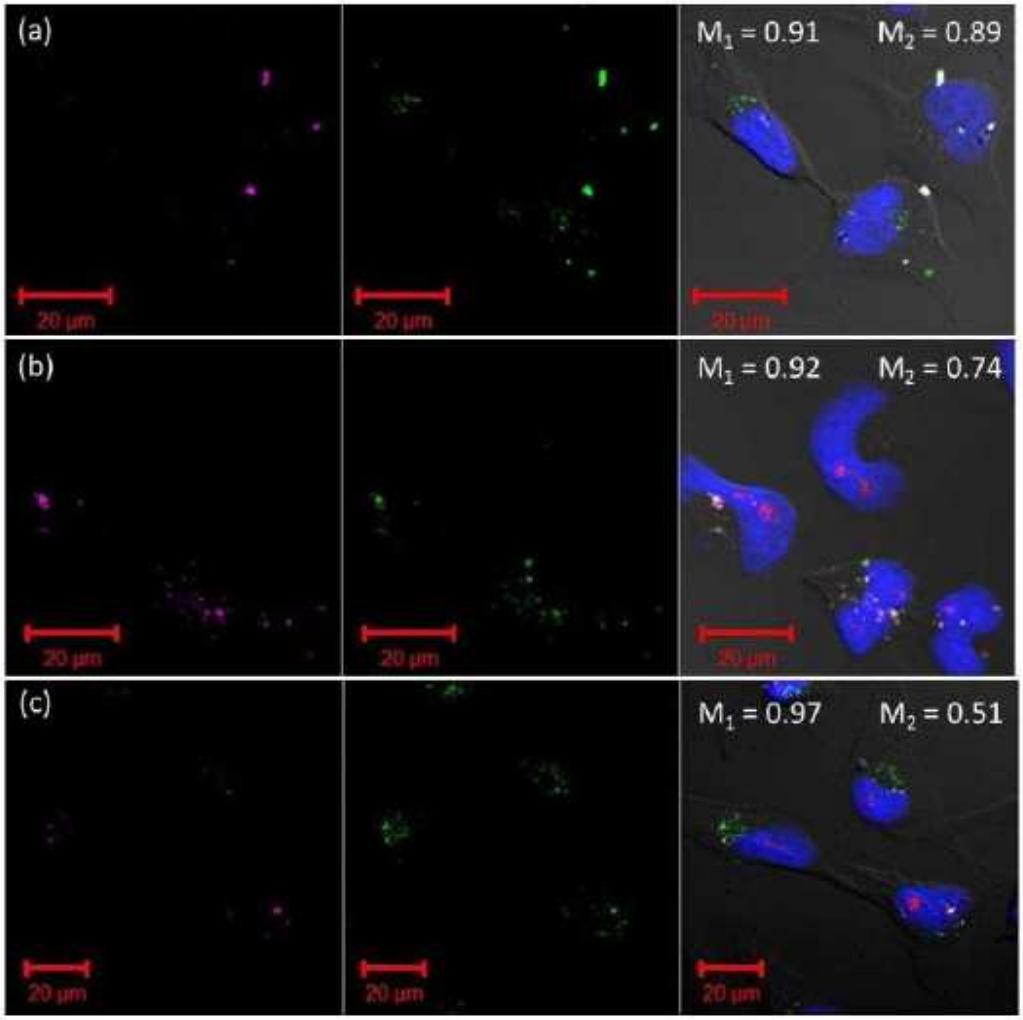

Figure 5.14) Confocal microscopy images of HeLa cells transfected with polyplexes (white) formed between FITC-labeled P3 (green) and Cy5-labeled pDNA (purple). Nuclei (blue) were stained with DAPI. Cells were fixed at (a) 4 hours (b) 24 hours and (c) 48 hours after transfection. Manders coefficients were calculated using the software ImageJ and are shown in the composite images for each time point. M1 = degree of overlap between Cy5-labeled pDNA with FITC-labeled polymer; M2 = degree of overlap between FITC-labeled polymer with Cy5-labeled pDNA. Scale bar = 20 µM.

Manders coefficients between FITC from the polymer and Cy5 from the pDNA were used as previously described[34-35] to determine colocalization between the polymer and pDNA. The Manders coefficients were calculated using the software NIH ImageJ.[28] HeLa cells were fixed 4 (Figure 5.14 a), 24 (Figure 5.14 b) or 48 (Figure 5.14 c) hours after transfection. Over time, the degree of overlap between Cy5 and FITC (pDNA and

polymer) remained high (>0.9). However, the amount of polymer colocalized with the pDNA (M2) decreased over time, going from 0.89 4 hours after transfection (Figure 5.14 a) to 0.51 48 hours after transfection (Figure 5.14 c). This observation confirms our hypothesis that pDNA remains associated with the polymer throughout the 48 hour transfection period, and also indicates that excess polymer may be dissociating from the polyplex over time.

FRET to monitor polyplex formation. The data in Figure 5.14 is interesting, but labeling polymers with hydrophobic fluorescent dyes such as FITC may alter their characteristics. To combat this, smaller lanthanide molecules may be chelated into polymers and their luminescence can be monitored. In addition to aiding elucidation of intracellular trafficking mechanisms, it may also be possible to quantify polyplex dissociation by using Förster Resonance Energy Transfer (FRET). As a proof-of-concept study, polyplexes were formed between a terbium-chelated polymer (Figure 5.4) containing 4 secondary amines in its repeat unit (Tb-N4) and unlabeled pDNA or pDNA labeled with tetramethylrhodamine (TMR). Since terbium and TMR are FRET pairs, we expect to see quenching of the terbium fluorescence when these two fluorophores are close together. As the polyplex dissociated, we expect to see an increase in terbium fluorescence. As a proof-of-concept study, we first had to make sure that the TMR-pDNA was able to quench terbium fluorescence. The results of terbium fluorescence for polyplexes formed at different N/P ratios is shown in Figure 5.15.

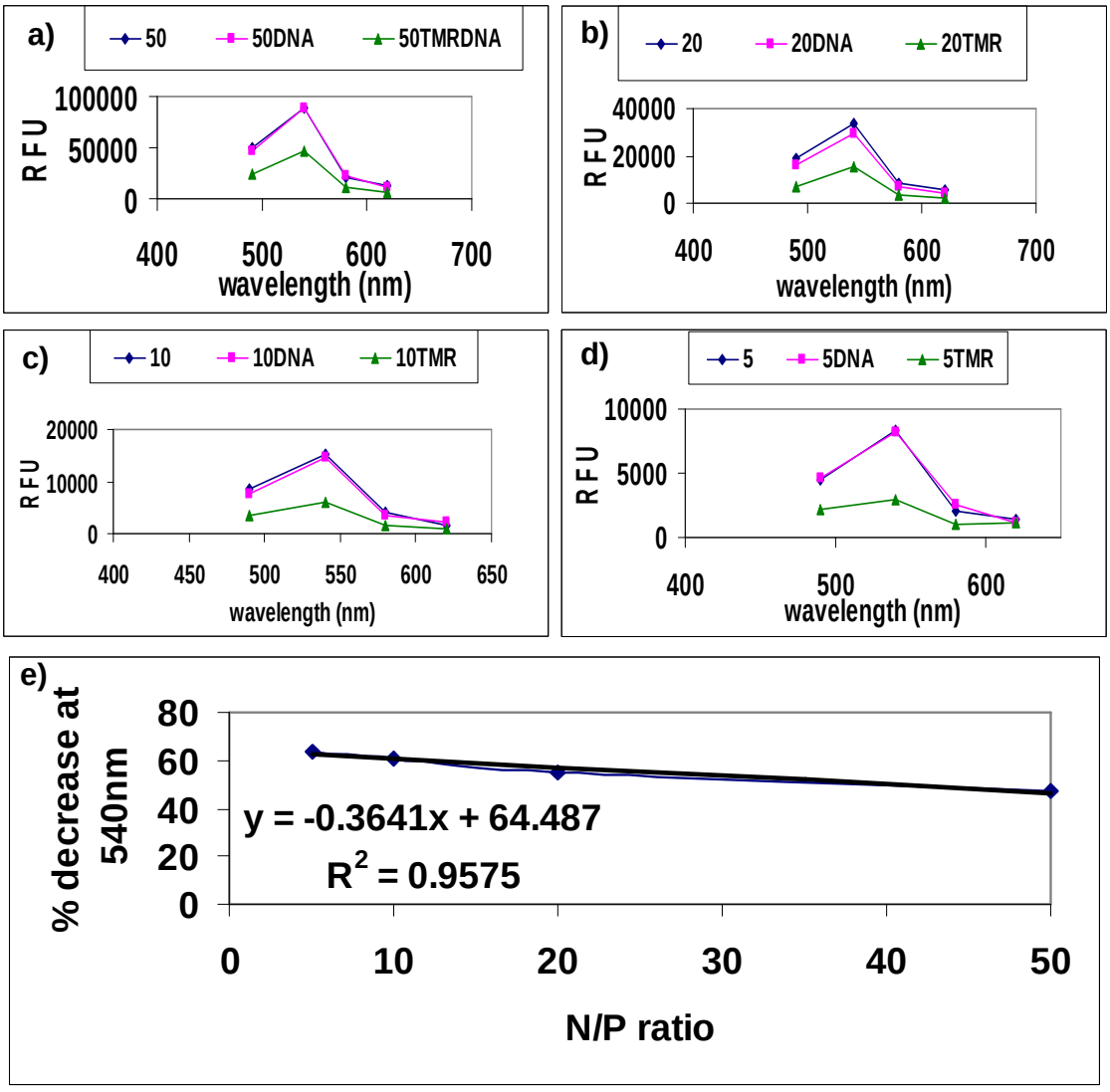

Figure 5.15) Terbium fluorescence at an excitation of 380 nm in the presence or absence of TMR-labeled pDNA. Polyplexes were formed at an N/P ratio of (a) 50; (b) 20; (c) 10; or (d) 5. Lines represent the following: blue = polymer only; magenta = polyplexes formed with unlabeled pDNA; green = polyplexes formed with TMR-labeled pDNA. (e) The percentage of terbium fluorescence quenching as a function of N/P ratio.

We observed quenching of terbium fluorescence at all of the tested N/P ratios (Figure 5.15), and the degree of quenching increased as the N/P ratio decreased (Figure 5.15 e).

We suspect this is due to the greater ratio of fluorescence acceptor (pDNA) to fluorescence donor (terbium). Using this method, we were able to confirm that the TMR-labeled pDNA is able to quench terbium fluorescence, thereby allowing this system to be used for FRET measurements.

Furthermore, we wanted to see if we could observe terbium quenching in polyplexes vs. polymer only *in vitro*. To this end, HeLa cells were transfected with Tb-N5 at an N/P ratio of 20 for 4 hours, and then imaged using fluorescence microscopy. The images for HeLa cells treated with polyplex vs. polymer only can be seen in Figure 5.16 a and b, respectively.

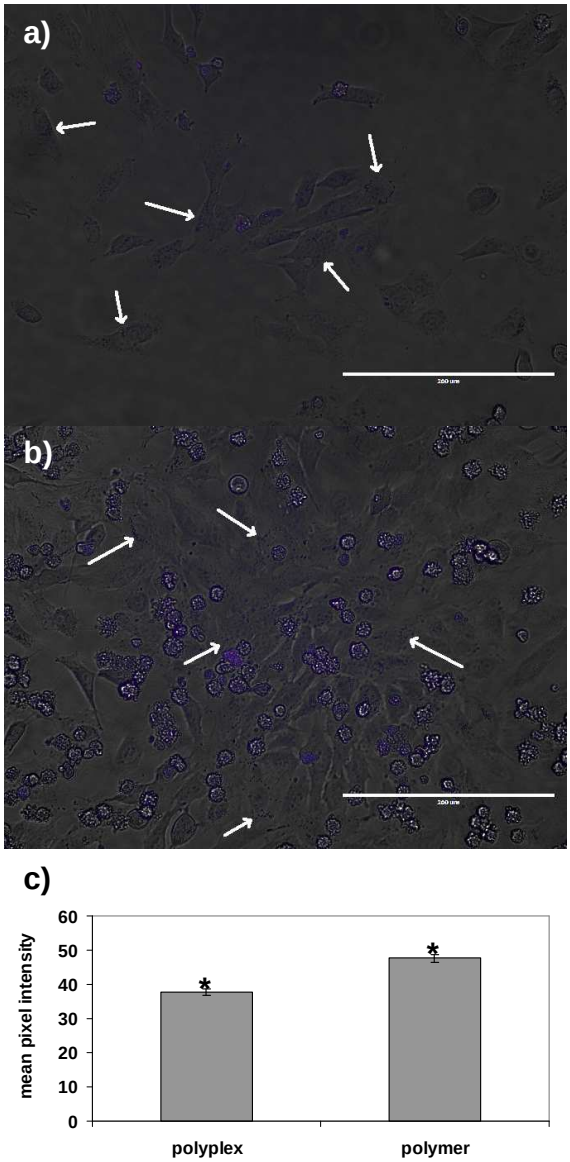

Figure 5.16) Images of HeLa cells treated with (a) Tb-N5 polyplexes at an N/P of 20 and (b) Tb-N5 polymer only at the same concentration as the N/P 20 polymer solution. The cells were imaged using fluorescent microscopy 4 hours after transfection. Arrows denote sites of punctuate polymer fluorescence in cells. Scale bar = 200 µm. (c) Fluorescence intensity from the polymer was quantified using the software ImageJ. Mean pixel intensity data are shown as mean ± standard deviation. Dead cells were excluded from these measurements. *denotes statistical significance ($p < 0.05$, $n = 4$) according to ANOVA followed by the Student's t-test.

From the images in Figure 5.16, it is clear that the polymer only solution (Figure 5.16 b) is more toxic than the polyplex solution (Figure 5.16 a), as evidenced by the increased

amount of dead cells in Figure 5.16 b compared to Figure 5.16 a. For both the polyplex and polymer only-treated cells, we see punctuate fluorescence inside of the cells, perhaps indicative of vesicular transport. We also observe a significant ($p < 0.05$) quenching in terbium fluorescence in the polyplexes vs. the polymer only (Figure 5.16 c), illustrating that terbium quenching can be monitored *in vitro*.

5.5 Conclusions and Future Goals

The work presented in this chapter represents strong collaboration between synthetic chemistry and biochemistry that is a hallmark of Reineke group research. Overall, this chapter seeks to derive relationships between polymer structure and DNA delivery efficacy. Studying how structure impacts the intracellular trafficking mechanisms of polymers would yield insight on how to tailor future polymers to be safe and effective therapeutic tools. There are endless possible polymer structures and in this chapter, we illustrate how seemingly small differences in structure can influence the biological interactions of polymers.

The addition of targeting groups to polymers is a widely used strategy to decrease systemic toxicity *in vivo* and to improve the efficacy of polymer delivery. In this chapter, we describe using β-D-galactose to target ASGPrs on HepG2 cells, and the effect of the degree of carbohydrate substitution and the length of the linker used to join the carbohydrate to the polymer backbone were studied. Although we did not achieve high ASGPr specificity, we did illustrate a polymer scaffold that can be modified to incorporate other targeting groups. Future work including testing the effects of different targeting groups as well as using a hydrophilic linker instead of a hydrophobic one would

be useful to father understand how to make the targeting groups more accessible to their targets.

In addition to targeting groups, another strategy to improve polymers for therapeutic use is to improve their transfection efficiency in serum-containing media. To this end, polymers containing trehalose have been synthesized by our group.[36-37] These polymers exhibited high transfection efficiency in the presence of serum.[38] In order to further improve the efficacy of these trehalose polymers, a new trehalose polymer library was synthesized with an increased number of secondary amine groups in the repeat unit. To further understand structure-function relationships, the effects of PEGylation using different linkers and the effects of different end groups were tested.

In the two cell lines tested, we did not see a dramatic effect of end group on polymer transfection efficiency or cytotoxicity. We did notice that polymers containing a decreased amount of secondary amines in their repeat units had higher transfection efficiency. Future work could be to further study Tr4-based polymers and test the effects of adding targeting moieties to the ends of the polymer.

Another library of diblock polymers was synthesized to test the effects of incorporating longer primary amine blocks into the polymer backbones upon polymer transfection. Contrary to our hypothesis, the polymer containing the longest amine block had the lowest transfection efficiency, in spite of exhibiting the highest cellular uptake. To study why this was occurring, confocal microscopy studies were done to determine whether the presence of many charged groups made it more difficult for pDNA to be released from the polyplexes compared to polymers containing shorter amine blocks.

The microscopy studies confirmed our belief; nearly all of the pDNA present in the cell was colocalized with the polymer, even as long as 48 hours after transfection.

The data from these experiments gave us valuable insight concerning polymer design. Although increasing the amount of primary amines does help cellular uptake, getting into the cell may not be a limiting factor in the transfection efficiency of these polymers. Future work testing the effect of different lengths of the carbohydrate block would be beneficial in furthering knowledge on structure-function relationships.

All of these polymer libraries were created to test the effect of altering polymer structure on transfection efficiency and toxicity. However, many of the intracellular mechanisms occurring during polymer transfection remain unknown, and as discussed in previous chapters, polymer structure can play a large role in what is occurring in the cells during transfection. To further study intracellular phenomena during transfection, it would be useful to not only track where the polymer is at certain time points, but to also monitor polyplex dissociation, which as shown by the data for the RAFT polymers, plays a role in the transfection efficiency of polymers. In order to study this further, the quenching of terbium fluorescence in the presence of TMR-labeled pDNA was used to determine the formation of polyplexes. We have shown that this system works *in vitro*, and future work using unlabeled pDNA as a negative control and testing different time points in the transfection of HeLa cells is currently underway. Furthermore, Sneha Kelkar, a polymer chemist in our group, is currently carrying out studies using increasing salt concentrations to dissociate polyplexes in solution.

Overall, this chapter illustrates the impact polymer structure can have on transfection efficiency. Discovering what makes certain polymers excellent transfection reagents

while other polymers are poor is exciting, and through continued efforts in our group we hope to father elucidate the mechanisms occurring in cells during transfection as well as how polymer structure influences these mechanisms.

5.6 References

1. Bellocq, N. C.; Pun, S. H.; Jensen, G. S.; Davis, M. E., Transferrin-containing, cyclodextrin polymer-based particles for tumor-targeted gene delivery. *Bioconjugate Chem.* **2003,** *14*, 1122-1132.
2. Bartlett, D. W.; Su, H.; Hildebrandt, I. J.; Weber, W. A.; Davis, M. E., Impact of tumor-specific targeting on the biodistribution and efficacy of siRNA nanoparticles measured by multimodality in vivo imaging. *PNAS* **2007,** *104*, 15549-15554.
3. Lu, Y.; Low, P. S., Folate-mediated delivery of macromolecular anticancer terapeutic agents. *Advanced Drug Delivery Reviews* **2002,** *54*, 675-693.
4. Sudimack, J.; Lee, R. J., Targeted drug delivery via the folate receptor. *Advanced Drug Delivery Reviews* **1999,** *41*, 147-162.
5. Song, H.; He, R.; Wang, K.; Ruan, J.; Bao, C.; Li, N.; Ji, J.; Cui, D., Anti-HIF-1α antibody-conjugated pluronic triblock copolymers encapsulated with Paclitaxel for tomor targeting therapy. *Biomaterials* **2010,** *31*, 2302-2312.
6. Thomas, T. P.; Patri, A. K.; Myc, A.; Myaing, M. T.; Ye, J. Y.; Norris, T. B.; James R. Baker, J., In vitro targeting of synthesized antibody-conjugated dendrimer nanoparticles. *Biomacromolecules* **2004,** *5*, 2269-2274.
7. Huang, R.-Q.; Qu, Y.-H.; Ke, W.-L.; Zhu, J.-H.; Pei, Y.-Y.; Jiang, C., Efficient gene delivery targeted to the brain using a transferrin-conjugated polyethyleneglycol-modified polyamidoamine dendrimer. *The FASEB Journal* **2007,** *21*, 1117-1125.
8. Nam, H. Y.; McGinn, A.; Kim, P.-H.; Kim, S. W.; Bull, D. A., Primary cardiomyocyte-targeted bioreducible polymer for efficient gene delivery to the myocardium. *Biomaterials* **2010,** *31*, 8081-8087.
9. Biessen, E. A.; Vietsch, H.; VanBerkel, T. J. C., Cholesterol derivative of a new triantennary cluster galactoside directs low- and high-density lipoproteins to the parenchymal liver cell. *Biochem. J.* **1994,** *302*, 283-289.
10. Sasaki, A.; Murahashi, N.; Yamada, H.; Morikawa, A., Syntheses of novel galactosyl ligands for liposomes and the influence of the spacer on accumulation in the rat liver. *Biol. Pharm. Bull.* **1995,** *18*, 740-746.
11. Lee, C.-C.; Grandinetti, G.; McLendon, P. M.; Reineke, T. M., A polycation scaffold presenting tunable "click" sites: conjugation to carbohydrate ligands and examination of hepatocyte-targeted pDNA delivery. *Macromolecular Bioscience* **2010,** *10*, 585-598.
12. Marks, D. L.; Kost, L. J.; Kuntz, S. M.; Romero, J. C.; LaRusso, N. F., Hepatic processing of recombinant human renin: mechanisms of uptake and degradation. *American Journal of Physiology* **1991,** *261*, G349-G358.
13. Sizovs, A.; McLendon, P. M.; Srinivasachari, S.; Reineke, T. M., Carbohydrate polymers for nonviral nucleic acid delivery. *Top. Curr. Chem.* **2010,** *296*, 131-190.

14. Wernig, M.; Meissner, A.; Foreman, R.; Brambrink, T.; Ku, M.; Hochedlinger, K.; Bernstein, B. E.; Jaenisch, R., In vitro reprogramming of fibroblasts into a pluripotent ES-cell-like state. *Nature* **2007,** *448*, 318-324.
15. Deans, R. J.; Moseley, A. B., Mesenchymal stem cells: Biology and potential clinical uses. *Experimental Hematology* **2000,** *28*, 875-884.
16. Verbaan, F. J.; Oussoren, C.; Dam, I. M. v.; Takakura, Y.; Hashida, M.; Crommelin, D. J. A.; Hennink, W. E.; Storm, G., The fate of poly(2-dimethyl amino ethyl)methacrylate-based polyplexes after intravenous administration. *Int. J. Pharm.* **2001,** *214*, 99-101.
17. Harris, J. M.; Chess, R. B., Effect of pegylation on pharmaceuticals. *Nature Reviews Drug Discovery* **2003,** *2*, 214-221.
18. Joralemon, M. J.; McRae, S.; Emrick, T., PEGylated polymers for medicine: from conjugation to self-assembled systems. *Chemical Communications (Cambridge)* **2010,** *46*, 1377-1393.
19. Davis, M. E.; Zuckerman, J. E.; Choi, C. H. J.; Seligson, D.; Alabi, C. A.; Yen, Y.; Heidel, J. D.; Ribas, A., Evidence of RNAi in humans from systemically administered siRNA via targeted nanoparticles. *Nature* **2010,** *464*, 1067-1070.
20. Knop, K.; Hoogenboom, R.; Fischer, D.; Schubert, U. S., Poly(ethylene glycol) in drug delivery: Pros and cons as well as potential alternatives. *Angew. Chem. Int. Ed.* **2010,** *49*, 6288-6308.
21. Sarkar, D.; Lopina, S. T., Oxidative and enzymatic degradations of L-tyrosine based polyurethanes. *Polym. Degrad. Stab.* **2007,** *92*, 1994-2004.
22. Bryson, J. M.; Fichter, K. M.; Chu, W.-J.; Lee, J.-H.; Li, J.; Madsen, L. A.; McLendon, P. M.; Reineke, T. M., Polymer beacons for luminescence and magnetic resonance imaging of DNA delivery. *PNAS* **2009,** *106*, 16913-16918.
23. Selvin, P. R.; Hearst, J. E., Luminescence energy transfer using a terbium chelate: Improvements on fluorescence energy transfer. *PNAS* **1994,** *91*, 10024-10028.
24. Liu, Y.; Reineke, T. M., Poly(glycoamidoamine)s for gene delivery. Structural effects on cellular internalization, buffering capacity, and gene expression. *Bioconjugate Chemistry* **2007,** *18*, 19-30.
25. Liu, Y.; Reineke, T. M., Hydroxyl stereochemistry and amine number within poly(glycoamidoamine)s affect intracellular delivery. *JACS* **2005,** *127*, 3004-3015.
26. Liu, Y.; Reineke, T. M., Hydroxyl Stereochemistry and amine number within poly(glycoamidoamine)s affect intracellular DNA delivery. *Journal of the American Chemical Society* **2005,** *127*, 3004-3015.
27. McLendon, P. M.; Fichter, K. M.; Reineke, T. M., Poly(glycoamidoamine) vehicles promote pDNA uptake through multiple routes and efficient gene expression *via* caveolae-mediated endocytosis. *Molecular Pharmaceutics* **2010,** *7*, 738-750.
28. Rasband, W. S. *ImageJ*, U.S. National Institutes of Health: Bethseda, MA, 1997-2009.
29. Liu, Y. Synthesis, characterization, and biological evaluation of poly(glycoamidoamine)s as DNA delivery vectors. Univerisity of Cincinnati, Cincinnati, 2006.
30. Kohnken, R. E.; Berger, E. A., Assay and characterization of carbohydrate binding by the lectin discoidin I immobilized on nitrocellulose. *Biochemistry* **1987,** *26*, 3949-3957.

31. Sunshine, J.; Green, J. J.; Mahon, K. P.; Yang, F.; Eltoukhy, A. A.; Nguyen, D. N.; Langer, R.; Anderson, D. G., Small-molecule end-groups of linear polymer determine cell-type gene-delivery efficacy. *Adv. Mater.* **2009,** *21*, 4947-4951.
32. Zugates, G. T.; Peng, W.; Zumbuehl, A.; Jhunjhunwala, S.; Huang, Y.-H.; Langer, R.; Sawicki, J. A.; Anderson, D. G., Rapid optimization of gene delivery by parallel end-modification of poly(β-amino ester)s. *Molecular Therapy* **2007,** *15*, 1306-1312.
33. Green, J. J.; Zhou, B. Y.; Mitalipova, M. M.; Beard, C.; Langer, R.; Jaenisch, R.; Anderson, D. G., Nanoparticles for gene transfer to human embryonic stem cell colonies. *Nano Lett.* **2008,** *8*, 3126-3130.
34. Manders, E. M. M.; Stap, J.; Brakenhoff, G. J.; Driel, R. V.; Aten, J. A., Dynamics of three-dimensional replication patterns during the S-phase, analysed by double labelling of DNA and confocal microscopy. *Journal of Cell Science* **1992,** *103*, 857-862.
35. Manders, E. M. M.; Verbeek, F. J.; Aten, J. A., Measurement of co-localizatin of objects in dual-colour confocal images. *Journal of Microscopy* **1993,** *169*, 375-382.
36. Prevette, L. E.; Lynch, M. L.; Kizjakina, K.; Reineke, T. M., Correlation of amine number and pDNA binding mechanism for trehalose-based polymers. *Langmuir* **2008,** *24*, 8090-1038.
37. Srinivasachari, S.; Liu, Y.; Prevette, L. E.; Reineke, T. M., Effects of trehalose click polymer length on pDNA complex stability and delivery efficacy. *Biomaterials* **2007,** *28*, 2885-2898.
38. Srinivasachari, S.; Liu, Y.; Zhang, G.; Prevette, L.; Reineke, T. M., Trehalose click polymers inhibit nanoparticle aggregation and promote pDNA delivery in serum. *JACS* **2006,** *128*, 8176-8184.

Chapter 6 : Conclusion

Overall, this work sought to illustrate the effect of polymer structure upon the intracellular events occurring during transfection. We have illustrated how polymers can elicit cytotoxicity, and how polymer structure alters cytotoxic profiles. This work has focused on using a variety of *in vitro* methods to elucidate the mechanisms of transfection, and through the careful study of a variety of polymers, several insights have been gained. Hypotheses that were proven or disproven in this work are indicated in bold print.

It is widely known that poly(ethylenimine) PEI is toxic, but the mechanisms as to why it is toxic remain largely unknown. Previous studies have shown that mitochondrial membrane potential (MMP) decreases during PEI transfection. From the work presented in this dissertation, we have learned that colocalization between PEI polyplexes and the mitochondria increase over time. **We hypothesized that PEI may be interfering with mitochondrial membrane pumps, but mitochondrial membrane pumps are still functional long into PEI transfection. We also hypothesized that the decrease in mitochondrial membrane potential could be a downstream event of apoptosis initiation, and we discovered that caspase-9 is activated as early as one hour after PEI transfection. Another hypothesis tested was that activation of the mitochondrial permeability transition pore (MPTP) leads to the decrease in mitochondrial membrane potential, however, our studies show that inhibiting the MTPT from opening did not play a role in the early loss of MMP.** PEI polyplexes have been shown to colocalize not only with the mitochondria, but with the endoplasmic

reticulum as well one hour after transfection, providing several potential cytotoxic mechanisms. **Furthermore, unlike naturally occurring polyamines spermine and spermidine, the increased production of reactive oxygen species (ROS) does not seem to be a major mechanism of cytotoxicity for PEI.**

When hydroxyl groups are added to the backbone of gene delivery polymers, we see changes in the toxicity profiles as well as the transfection efficiency. **We hypothesized that smaller polymers would be less toxic than longer polymers, and our experiments prove this to be true.** We also have displayed that increasing the molecular weight of the polymers increases transfection efficiency, but at the cost of increasing cytotoxicity. **One hypothesis to explain the link between high cytotoxicity and high transfection efficiency is that the more toxic polyplexes are able to directly permeabilize the nuclear envelope, causing toxicity but also providing a way for plasmid DNA to enter the nucleus. The studies herein show that nuclear envelope permeability increases in cells treated with the higher molecular weight polymers, but whether this is caused by direct polymer permeabilization or by apoptosis initiation remained to be seen. To test whether the increased nuclear envelope permeability was due to apoptosis, studies were conducted using isolated nuclei. The polyplexes with the highest transfection efficiency were in fact able to induce more nuclear envelope permeability than less efficient polymers in this cell-free system; in addition, transfection in the presence of an apoptosis-inducing agent did not increase the transfection efficiency for any polyplexes.** Furthermore, we have shown that the presence of hydroxyl groups can influence polyplex size and charge,

which may contribute to the different cytotoxicity profiles observed for hydroxyl-containing vs. non-hydroxyl containing polymers.

In addition, the effect of the number of hydroxyl groups per repeat unit on plasmid DNA (pDNA) nuclear import was studied. **We have shown that the presence of hydroxyls does seem to alter pDNA import mechanisms compared to a polymer containing no hydroxyl groups.** Furthermore, strengthening the link between high transfection efficiency and the ability to permeabilize the nuclear envelope, the polymer containing more hydroxyl groups displayed higher transfection efficiency and induced higher nuclear envelope permeability both in nuclei isolated from transfected cells and in nuclei in a cell-free system. It was also found that without active trafficking provided by intracellular machinery, pDNA delivery to the nucleus is severely hampered. **This pDNA delivery was affected more in the case of the hydroxyl-containing polymers compared with PEI, further strengthening the hypothesis that polymer structure influences intracellular mechanisms.** There also appears to be different mechanisms of pDNA nuclear import occurring when the pDNA is complexed with different polymers; when complexed with the PGAAs T4 and G4, pDNA seems to enter the nucleus in an energy-dependent manner in the absence of cytosol. In the case of PEI, the presence or absence of energy does not affect pDNA import in the absence of cytosol to as great an extent. Interestingly, we noticed that in both the cell-free and in whole cell system, polymers were able to reach the nuclei to a larger extent than pDNA. Polymer-nucleus association was not affected by the absence of energy or cytosol in the same way that pDNA-nucleus association was affected, indicating different nuclear trafficking mechanisms for polymer vs. polyplex may be present. Further studies are necessary to

determine these mechanisms, and may be accomplished using Förster resonance energy transfer (FRET) to monitor the point at which pDNA is released from the polyplex.

Lastly, we illustrate a wide variety of polymers and the effect that their structure has on transfection efficiency and toxicity. We have illustrated how increasing the amount of primary amines in a polymer can impact pDNA release, and also how different linkages used to attach targeting groups to polymers influence transfection efficiency and toxicity. **We also show how FRET can potentially be used to monitor polymer-polyplex dissociation without the need for bulky, hydrophobic fluorescent dyes. Ideally, the work presented in this dissertation will yield insight into the rational design of polymers, and present the impact that seemingly small changes in polymer structure, such as the number of hydroxyl groups in the repeat unit, can have on the intracellular events occurring during transfection.**

The hypothesis carried throughout this dissertation is that polymer structure influences mechanisms of pDNA delivery. Throughout this work, we have proved that seemingly small changes in polymer structure can influence transfection efficiency and cytotoxicity. The work performed herein should serve as a useful guide for the future development of safe, effective nucleic acid delivery vehicles.